NUMERICAL MODELING OF THE GEOMECHANICAL BEHAVIOR OF A CARBONATE PETROLEUM RESERVOIR UNDERGOING CO2 INJECTION

BY

SIKANDAR KHAN

A Dissertation Presented to the

DEANSHIP OF GRADUATE STUDIES

KING FAHD UNIVERSITY OF PETROLEUM & MINERALS

DHAHRAN, SAUDI ARABIA

In Partial Fulfillment of the

Requirements for the Degree of

DOCTOR OF PHILOSOPHY

In

MECHANICAL ENGINEERING

JANUARY 2017

KING FAHD UNIVERSITY OF PETROLEUM & MINERALS

DHAHRAN- 31261, SAUDI ARABIA

DEANSHIP OF GRADUATE STUDIES

This thesis, written by **SIKANDAR KHAN** under the direction of his thesis advisor and approved by his thesis committee, has been presented and accepted by the Dean of Graduate Studies, in partial fulfillment of the requirements for the degree of **DOCTOR OF PHILOSOPHY IN MECHANICAL ENGINEERING**

Dr. Zuhair Mattoug Gasem
Department Chairman

Dr. Yehia A. Khulief
(Advisor)

Dr. Salam A. Zummo
Dean of Graduate Studies

عمادة الدراسات العليا
DEANSHIP OF GRADUATE STUDIES

Dr. Abdullatif A. Al-Shuhail
(Co-advisor)

8/3/17
Date

Dr. Abul Fazal Arif
(Member)

Dr. Mohamed Ali El-Gebeily
(Member)

Dr. Mohamed A. Habib
(Member)

In the name of Allah, the Most Gracious and the Most Merciful

Dedicated

to

My Beloved Parents, Brothers, Sisters,

My wife

And my daughters

ACKNOWLEDGMENTS

All praises are for ALMIGHTY ALLAH, the most merciful and the most beneficent. May peace be upon the prophet Muhammad (PBUH) and on his family. I am thankful to ALMIGHTY ALLAH by giving me good health, strength and courage to complete this work.

I wish to acknowledge the support received from King Fahd University of Petroleum and Minerals (KFUPM) and King Abdul-Aziz City for Science and Technology Carbon Capture and Sequestration Technology Innovation Center (KACST TIC on CCS) at King Fahd University of Petroleum and Minerals (KFUPM) for funding this work through Project No. TIC-CCS- 1.

I am highly indebted to my thesis advisor Dr. Khulief professor department of Mechanical Engineering King Fahd University of Petroleum and Minerals (KFUPM) who has always remained an invaluable source of knowledge and who helped and guide me throughout my thesis. I am highly thankful to my co-advisor Dr. Al-Shuhail for his intense help in this work and to enhance my theoretical background related to geomechanical analysis. I am highly grateful to the committee members, Dr. Arif, Dr. El-Gebeily, and Dr. Habib for giving me their precious time and valuable guidance.

I would like to express my gratitude to my Parents, brothers, sisters, and my wife for their incredible support and guidance during my entire education career. I am thankful to my colleagues at the university specially Sajid Ali, Khwaja Muhammad, Abba Abdulhamid Abubakar, and Usama Siddique for their help, prayers and providing me a good company during my study at KFUPM.

Table of Contents

LIST OF TABLES

LIST OF FIGURES

NOMENCLATURE

$\mathbb{C}$	Elastic tensor
D	depth
f	Body force
F_v	Volume force vector
G	Shear Modulus (Pa)
k_m	Matrix permeability
k_f	Fracture permeability
k_{fc}	Fracture closure permeability,
K	Bulk Modulus (Pa)
Ni	moles of component i per unit block volume
p_m	Matrix pore-pressure (Pa)
p_f	Fracture pore-pressure (Pa)
Q_m	Source term
q	Darcy's velocity vector
S	Storage term
T_j	transmissibility of phase j
t	time

u Displacement components (m)

V grid block volume

y_{ij} mole fraction of component i in phase j

Greek symbol

α Biot's coefficients for matrix

β Biot's coefficients for fractures

ρ Density (kg/m^3)

ψ Function

$\emptyset_f$ Fracture Porosity

ω Flow coefficient

ρ_m molar density of phase m

$\emptyset_m$ Matrix Porosity

σ_{kk} Mean stress = $(\sigma_{11} + \sigma_{22} + \sigma_{33})/3$ (Pa)

τ matrix-fracture transfer

υ Poisson's ratio

∅ Porosity

ξ shape factor

γ specific gravity

σ_{ij} stress tensor

ε_{ij} strain tensor

ε_0 initial value of strain

ε_v Volumetric strain

Superscripts

n old time level

n+1 new time level

Subscripts

f fracture

g gas

i component

j phase

m matrix

o oil

w water

DISSERTATION ABSTRACT (ENGLISH)

Full Name : Sikandar Khan

Dissertation Title : Numerical modeling of the geomechanical behavior of a carbonate petroleum reservoir undergoing CO_2 injection

Major Field : Mechanical Engineering

Date : January, 2017

Sedimentary porous rocks can be used for long-term subsurface containment of CO_2. Before injecting CO_2 to sedimentary reservoirs, it is necessary to perform stability analysis of the reservoir and to estimate the maximum sustainable pore fluid pressures. In this study, numerical modeling techniques are used to analyze the flow of carbon dioxide and the corresponding deformations of the naturally fractured carbonate sedimentary reservoirs in Saudi Arabia. The present investigation extends the previous studies by considering the sorption-based deformation during the injection of the compressed CO_2 fluid into the Arab-D naturally fractured carbonate reservoir. The change in permeability during the injection of CO_2 is evaluated. Starting with the simple case of single-porosity and single-phase flow in the reservoir, the geomechanical and stability analyses were performed for Biyadh sandstone reservoir. The modeling procedure was extended to include the two-phase flow in the geomechanical and stability analysis of the single-porosity reservoir. Using the coupled geomechanical and stability analysis, the safe carbon dioxide injection parameters and the maximum safe occupancy limit have been estimated for the Biyadh sandstone reservoir. In the second stage of this investigation, the geomechanical modeling procedure was applied to the Ghawar naturally fractured

reservoir by considering only single-phase flow. In this context, the stability analysis was first performed for the naturally fractured reservoir, and then followed by a sensitivity analysis to evaluate the sensitivity of the model output to various input parameters. The developed model was further extended for this case to include the two-phase flow. The reservoir geomechanical and stability analyses were performed; firstly for having only an injection well, and secondly for the general case of having both injection and production wells in the system. The safe values for carbon dioxide injection in the Ghawar reservoir have been predicted based on the geomechanical and stability analysis. This investigation addressed, for the first time, the problem of how to reduce the pore pressure build-up and to increase the reservoir storage capacity by varying both the number and arrangement of the carbon dioxide injection wells. The obtained results provided some benchmark solutions, from which more insight into the sequestration process is gained. The injection of carbon dioxide was shown to cause an increase in the reservoir pore pressure; however adding a production well to the sequestration site tends to decrease the overall pore pressure. For the case of the fractured caprock, carbon dioxide leaked into the overburden layers; thus causing the pore pressure to increase in these layers, and subsequently resulting in ground uplift, which can be monitored and utilized to identify the location of the fracture in the caprock. The obtained results demonstrated the significance of changing the number and arrangement of the injection wells and suggested the existence of an optimum arrangement. The occupancy analysis was performed for the reservoir considering the formation volume factor at the depth of the reservoir which shows that the discussed carbon dioxide injection scenarios are at the safe side of the maximum occupancy limit.

DISSERTATION ABSTRACT (ARABIC)

ملخص الرسالة العلمية

الاسم : سكندر خان

عنوان الاطروحة العلمية: النمذجة العددية الجيوميكانيكية للآبار البترولية الكربونية أثناء عملية حقن ثاني اكسيد الكربون

التخصص: الهندسة الميكانيكية

التاريخ : جنورى 2017

بالامكان استخدام الصخور الرسوبية المسامية في الطبقات الارضية العميقة لتخزين ثاني اكسيد الكربون على المدى الطويل. ومن المهم اجراء دراسة تحليلة لاستقرار تلك الخزانات الرسوبية الجوفية قبل حقن ثاني اكسيد الكربون ، وذلك لتقدير أعلى القيم الممكنة لضغط السائل المُخزَن. هذا البحث يتبنى طريقة النمذجة العددية، وذلك لتمثيل تدفق ثاني اكسيد الكربون و تحليل الانهيار الناتج من تصدعات الآبار الرسوبية الكربونية الطبيعيّ في المملكة العربية السعودية. ويتوسع البحث الحالي عن الدراسات السابقة، وذلك بنمذجة الانهيار القائم على الامتصاص أثناء عملية حقن ثاني اكسييد الكربون المضغوط في بئرعرب - د الكربوني المتصدع طبيعيا. ومن ثم يتم تقدير التغير في النفاذية نتيجة لحقن ثاني اكسيد الكربون. ويتدرج البحث ابتداء من ابسط الحالات المحتملة التي تشمل تدفق السوائل أحادية الطور في الآبار ذات المسامية الأحادية، والمتمثلة في إجراء دراسة جيوميكانيكية واستقرارية لبئر بياض الحجري الرملي. وفي المرحلة الثانية ، تم توسيع طريقة النمذجة لتشمل التدفق ثنائي الطور ضمن التحليلات الجيوميكانيكية والاستقرارية للآبار أحادية النفاذية. وتم ايضاً إجراء دراسة ترابطية جيوميكانيكية-استقرارية لبئر بياض الحجري الرملي، وتحديد القيم الآمنه لمعاملات حقن ثاني اكسيد الكربون ، بالاضافة إلى حساب الحد الأعلى الآمن للسعة التخزينية للبئر. وبالتالي تم تطبيق النمذج الجيوميكانيكي المطور في دراسة بئر الغوار ذات التصدعات الطبيعية، في حالة التدفق أحادي الطور ، وتبدأ باجراء دراسة استقرارية للتصدعات الطبيعية في بئر الغوار ، يتلوها دراسة تحليلية دقيقية لتقييم مدى حساسية نتائج النموذج الرقمي لأي تغيرات محدودة في مدخلات المعاملات المختلفة. كما تم تطويع النموذج المطور في هذا البحث لدراسة حقن ثاني اكسيد الكربون في الآبار ذات التصدعات الطبيعية في حالة التدفق ثنائي الطور، وفيها تم اجراء دراسة ترابطية جيوميكانيكة - إستقرارية، أولا في وجود بئر للحقن فقط، وثانيا في

الحالة العامة لوجود كل من بئر للحقن وآخر للإنتاج. وتؤدي نتائج البحث إلى استنباط القيم الآمنة لحقن التصدعات الطبيعية في بئر الغوار اعتمادا على الدراسة الترابطية الجيوميكانيكية-الاستقرارية. كما تم تطوير منهجية جديدة في هذا البحث لتقليل الضغط المسامي المتراكم وزيادة السعة الاستعابية للبئر عن طريق تغي ي عدد وطريقة توزيع آبار حقن ثاني اكسيد الكربون. النتائج المكتسبة اشارت الى بعض الحلول ،من خلال المزيد من الفهم في عملة العزل ،وقد تبين ان حقن ثاني اكسيد الكربون يؤدي الى ارتفاع ضغط المسامي مع ذلك ، اضافة انتاج البئر الى مكان العزل يؤدي الى تقليل الضغط المسامي العام .في حالة تصدع الغطاء الصخري يتسرب ثاني اكسيد الكربون الى الطبقات الاثقل ولهذا السبب يزيد الضغط المسامي في هذه الطبقات ، مما ادى لاحقا الى ارتفاع الارض واللتي مكنتنا من الملاحظة والاستفادة لمعرفة مواقع التصدع في الغطاء الصخري . ايضا النتائج أوضحت أهمية تغيير عدد وترتيب آبار الحقن، كما تنبأت الدراسة بامكانية وجود ترتيب أمثل لآبار الحقن يتحقق عنده تزامن لأقل تراكم للضغط وأعلى سعة تخزينية ممكنة.

CHAPTER 1

INTRODUCTION

1.1 The natural balance of CO_2 in atmosphere

Two elements, namely oxygen and carbon combine to form CO_2. At room temperature, CO_2 is in gaseous form. CO_2 can be converted into liquid phase and can also be frozen into solid phase. The percentage of carbon dioxide is 0.04 % of the air in the atmosphere that we breathe. Carbon dioxide is also present in the drinking and seawater. Carbon dioxide is not toxic, not flammable, and also it does not explode. It has been practically used in some fire extinguishers. During the breathing process, oxygen is inhaled and CO_2 is exhaled into the atmosphere. During photosynthesis process, CO_2 is absorbed by plants and oxygen is released back to the environment. The previous processes combine together to form the carbon cycle, in which the level of CO_2 is kept stable in the environment [1].

During the natural CO_2 cycle, the level of CO_2 is stable, but the excessive burning of fossil fuels produces higher quantities of CO_2, which disturbed its balance in the atmosphere. This excess amount of carbon dioxide needs to be permanently stored in underground sedimentary reservoirs. The annual flow of CO_2 is shown by arrows in Figure 1.1. Mankind produces extra CO_2 , which remains in the environment and contributes to global warming [2].

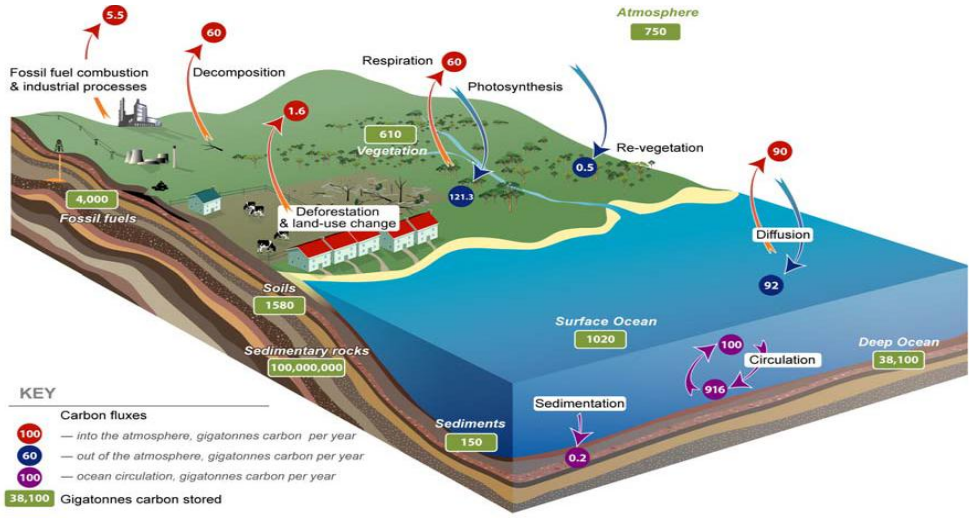

Figure 1.1 The annual flows of carbon dioxide in billion tons [2]

1.2 CO_2 capture and storage

The Carbon Capture and Storage (CCS) is a process, in which CO_2 is captured from the environment, then transferred to the storage area, and finally stored in sedimentary reservoirs. The main purpose of CCS process is to prevent the excessive release of carbon dioxide to the environment [3-5]. The process of CCS will mitigate both the acidification of the oceans and global warming [1]. The three main steps of CCS are given below:

1. Capture of carbon dioxide
2. Transport of the captured carbon dioxide
3. Geological storage of carbon dioxide

1.2.1 CO_2 capture

CO_2 is mostly captured at the points where its quantity is high in the exhaust air like emissions from the industries, fossil fuel energy facilities, natural gas processing, and synthetic fuel plants. CO_2 can also be extracted from the air but it is not so practical. CO_2 is highly concentrated at the point sources already discussed and concentration is reduced

away from the point sources. The coal combustion in oxygen produces almost pure CO_2 that can be directly processed [6-8]. If the captured CO_2 contains excessive impurities then a scrubbing process will be needed. Currently, three types of scrubbing processes are in use as explained below [1, 9, 10, 11]:

1. The post combustion capture process, which is mainly applied to the fossil-fuel burning power plants, in which CO_2 is captured from the flue gases at the power stations.
2. The pre-combustion capture process, which mainly exist the in fertilizer industry, chemical industry, and power production. During this process the partial oxidization of the fossil fuel takes place before the actual process. The oxidization process converts carbon mono-oxide to carbon dioxide and also produces hydrogen gas. The carbon dioxide is captured and hydrogen is used as fuel.
3. The oxy-fuel combustion process, in which the fossil fuel is not burned in air but is burned in pure oxygen environment. The flue gases contain only carbon dioxide and water vapor. Water vapor is condensed and the resulting pure carbon dioxide is transported to storage site for storage. Power plants having oxy-fuel combustion are known as zero emission cycles. This method of carbon dioxide capture is normally used in laboratory work for understanding the carbon dioxide capture process.

1.2.2 CO_2 transport

The transportation of CO_2 is the second step of the CCS process. The transportation can be either through the pipeline or through ships. During the year 2013, 5,800 km of carbon dioxide pipelines were used in United States to transport carbon dioxide to oil production

fields for enhanced oil recovery and storage. The Enhanced Oil Recovery (EOR) means, the recovery of oil due to CO_2 injection to sedimentary depleted oil reservoirs. CO_2 can also be injected in non-oil producing sedimentary reservoirs [2, 12, 13].

1.2.3 CO_2 storage

During the storage process, carbon dioxide is injected in supercritical form in sedimentary reservoirs. Carbon dioxide can be stored at various depths below the earth surface in various depleted hydrocarbon reservoirs. The geochemical trapping mechanisms and the impermeability of cap rock will prevent carbon dioxide from escaping to the atmosphere [1, 14-17]. During geological storage carbon dioxide is injected at a high pressure to the sedimentary porous rocks. Sedimentary rocks can store carbon dioxide for a very long period of time.

Figure 1.2 shows the CO_2 injection process. As shown in Figure 1.2 carbon dioxide should be injected below 800 meters because below this depth it changes to supercritical form with high density as compared to the gaseous CO_2 at the ground level. Carbon dioxide diffuses more in supercritical form as compared to sub-critical form and that's the reason that injecting carbon dioxide in supercritical form increases its storage capacity. The volume of carbon dioxide at various depths is shown in Figure 1.2 by a number compared to the CO_2 volume of 100 at the ground level [1, 18].

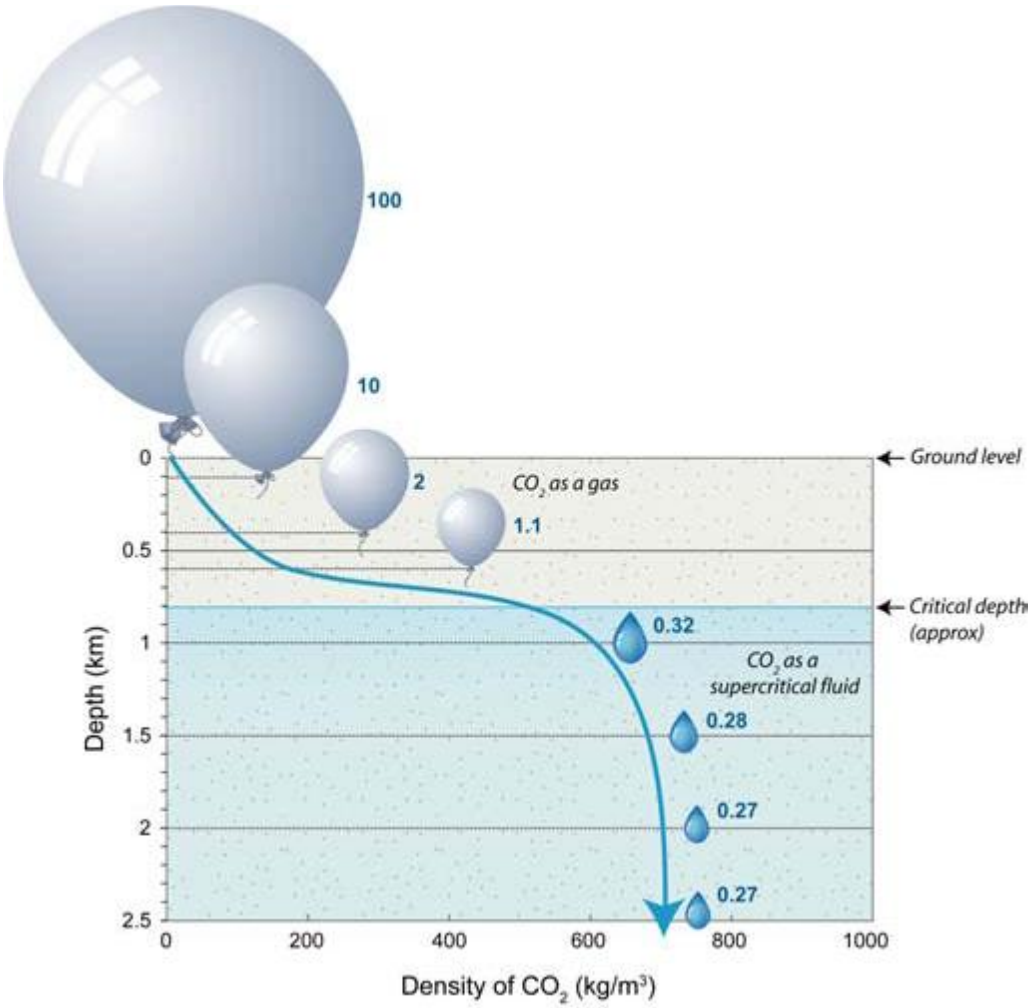

Figure 1.2 Variation in the density and volume of CO_2 at various depths [1, 18]

The injected CO_2 is trapped in the tiny pores of the storage rocks and as the time passes it is dissolved in the water present in the rock formation. It may also react chemically with the rocks and in this way carbon dioxide will be stored even more securely. The stored carbon dioxide will be far from the ground water and will be separated by impermeable layers of rocks [2]. Carbon dioxide is trapped in pores between the white grains of quartz, as shown in blue color in a sandstone storage rock (Figure 1.3).

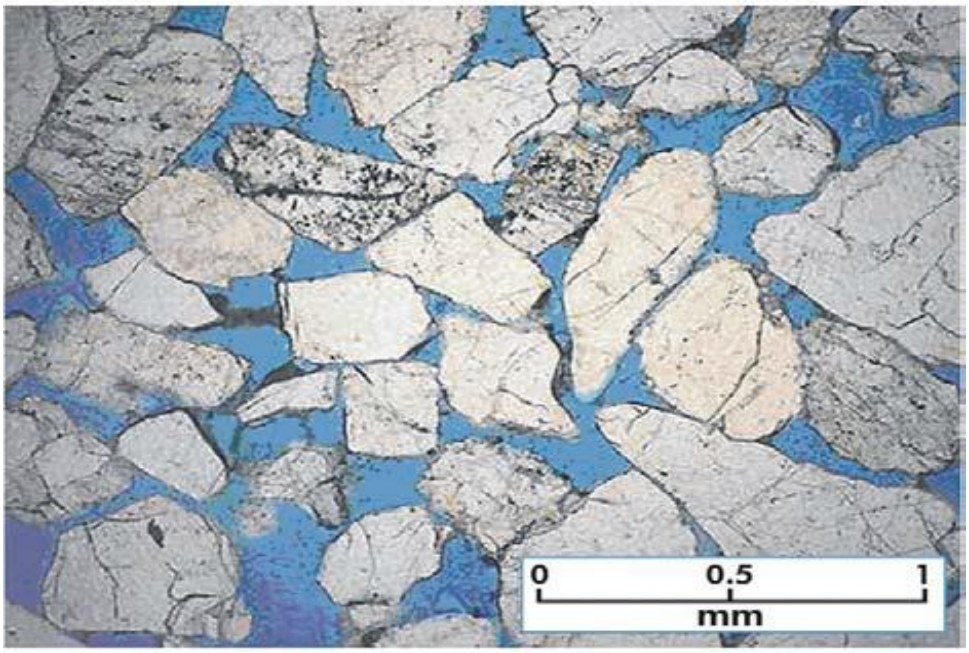

Figure 1.3 Carbon dioxide is trapped in pores with blue color in sandstone [19]

Storage is one of the main components of CCS process and as shown in Figure 1.4, carbon dioxide is captured from the atmosphere, transported to the storage site and at the end stored in the sedimentary reservoirs [2].

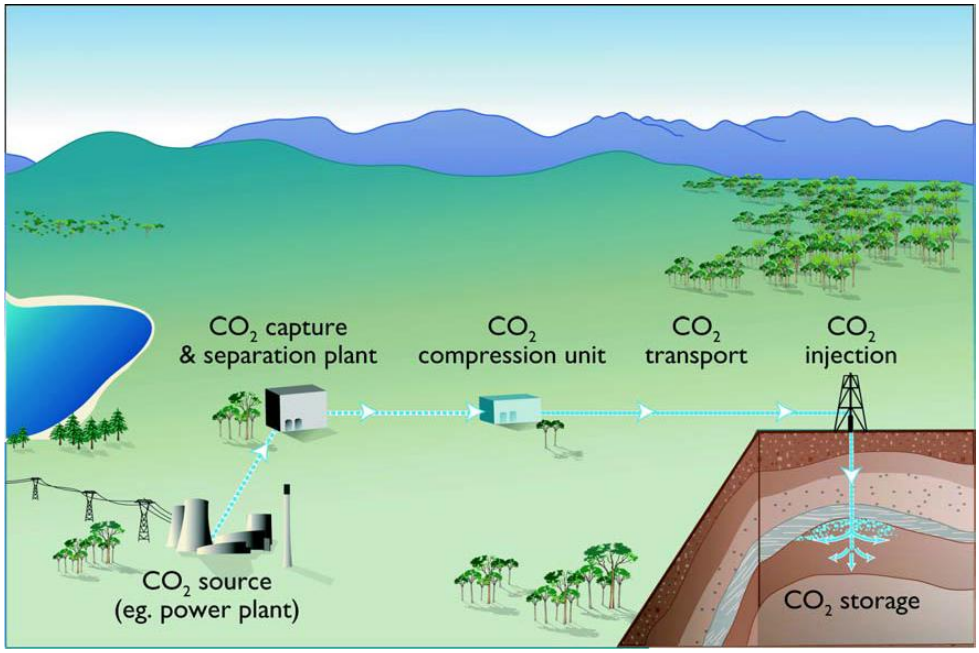

Figure 1.4 The overall process of Carbon capture and sequestration [2]

In United States 30 to 50 million tons of CO_2 is injected in depleted oil reservoirs for enhanced oil recovery [1]. Storing carbon dioxide in depleted oil and gas reservoirs is generally more attractive because the geology of these depleted reservoirs is well known and the enhance oil recovery will offset a part of the storage cost [20-22].

Un-mineable coal seams are also good options for storing carbon dioxide due to high adsorption tendency of carbon dioxide in the coal surface. The amount of carbon dioxide and the pressure with which carbon dioxide will be injected into coal seams depends on the matrix strength of the coal [23-25]. The storing of carbon dioxide releases the already absorbed methane, which will help in offsetting part of the carbon dioxide storage cost [2].

1.3 Various types of sedimentary reservoirs

Some of the important types of sedimentary reservoirs that are used for carbon dioxide sequestration are explained in the following section.

1.3.1 Shale reservoir

The shale has the following properties [19, 26]:

a) has a dark brown color
b) composed of clay and tiny fragments of other minerals, e.g. quartz and calcite
c) behave as excellent seal
d) very rich with sedimentary rocks (almost 42 %)
e) has less porosity as compared to sandstone and carbonate formations
f) classified as single-porosity rock type

Figure 1.5 shows the standard geological symbol for shale reservoir.

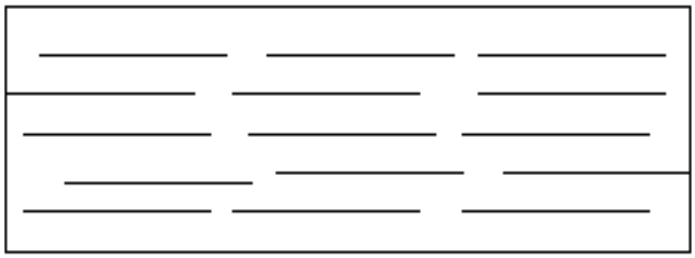

Figure 1.5 Standard geological symbol for shale reservoir [19]

1.3.2 Sandstone reservoir

The sandstone reservoir has the following properties [19]:

a) It is in rusty red color
b) Composed of sand-sized minerals or rock grains
c) The second most abundant (about 37 %) sedimentary rock type of the three main sedimentary rocks (sandstones, shale, carbonates)
d) Sandstone porosity is on the range of 10-30 %
e) Sandstone is considered as single-porosity rock type

Figure 1.6 shows the standard geological symbol for sandstone reservoir.

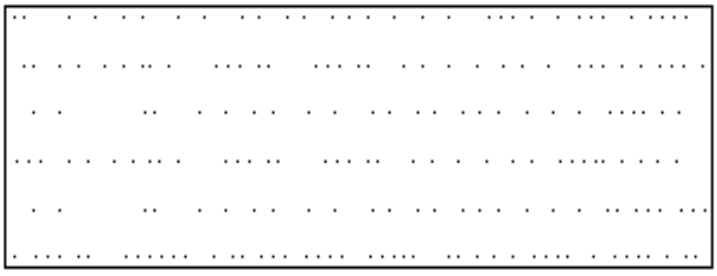

Figure 1.6 Standard geological symbol for sandstone reservoir [19]

1.3.3 Carbonate reservoir

The carbonate reservoir has the following properties [19]:

a) It is in dark gray color
b) Grains are largely the skeletal or shell remains of marine organisms

c) Are the least geologically abundant (about 21%) of the three (shale, sandstones, carbonates), but the highest producer of oil (about 61.5%)

d) Carbonate reservoirs are naturally fractured and having dual-porosity and dual-permeability, one due to matrix and other due to fractures

Figure 1.7 shows the standard geological symbol for carbonate reservoir.

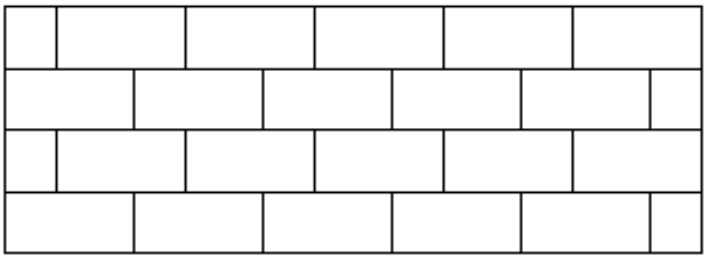

Figure 1.7 Standard geological symbol for carbonate reservoir [19]

1.4 Effective stresses on the reservoir

The increase in pore pressure during carbon dioxide injection process can ultimately cause the failure of the reservoir rock. The effective stress can be related to the pore pressure by the following equation,

$$\sigma' = \sigma - P_f \tag{1.1}$$

The symbol σ' is for the effective stress, P_f (pore-fluid pressure), and σ is for the total stress [27-29]. The effective principle stresses can be resolved into two components (a shear and normal) on the potential failure planes, is shown in Figure 1.8.

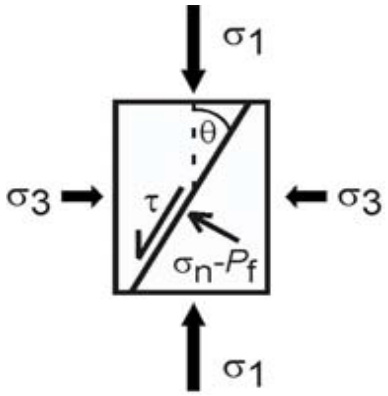

Figure 1.8 Stresses on the fault plane at an angle θ with principle plane [27]

Mathematically the resolved stresses at the fault is given as,

$$\tau = C + \mu\,(\sigma_n - P_f) \tag{1.2}$$

The symbol τ is for the shear stress, μ for coefficient of friction, C is the shear strength of the fault plane, and σ_n is the normal component of the stress on the fault plane [27]. The fault stability can be calculated using equation (1.1) & (1.2), if by some means we are able to find the stresses at the fault surface. Equation (1.2) is basically Mohr-Coulomb failure criteria. The injection of carbon dioxide will decrease the value of the effective normal stress on the fault plane and when the value of the stress decreases to a critical value, the reservoir shear failure is caused.

1.5 Maximum sustainable reservoir pore fluid pressure

In order to achieve reservoir stability during carbon dioxide injection process, the increase in the pore pressure and stresses should be kept below the critical values. Figure 1.9 summarizes the geomechanical analysis for the reservoir and shows that as carbon dioxide is injected into the reservoir, stability analysis should be performed. Based on the initial stress state and reservoir properties, the stability analysis will give the maximum safe values for the pore pressure.

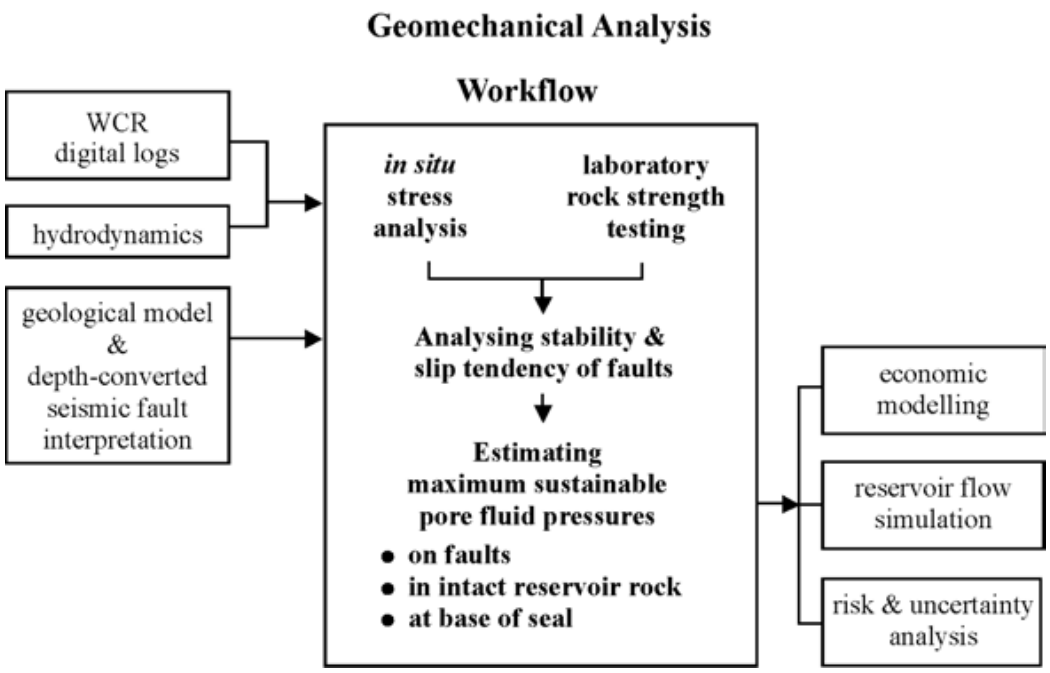

Figure 1.9 A flow chart for the geomechanical analysis [27]

Stresses in the CO_2 storage reservoir can be determined from the drilling data as was done by Streit et al. [27]. Laboratory tests can be used to find the strength of the faults, reservoir and seal rocks. A Mohr-Coulomb failure criterion is one of the methods that can be used for the assessment of fault stability and for the estimation of maximum sustainable fluid pressures during CO_2 injection [30]. The ratio $\tau/(\sigma_n - P_f)$ in equation (1.2) is known as slip tendency, where μ is the Byerlee friction coefficient having values normally from 0.6 to 0.85. As an example, Gibson-Poole et al. [31] presented the geomechanical analysis for the CO_2 storage for various sites of Australia.

1.6 Poroelasticity

In simple modeling strategies for the fault stability assessment and determination of the maximum sustainable pore-fluid pressure, the poroelastic behavior of the porous rock is not considered as shown in equation (1.1). The poroelastic behavior of the porous rock will affect the effective stresses during the CO_2 injection and storage.

For including the effect of the poroelastic behavior of the porous rocks the effective stresses should be calculated from an equation that includes Biot's poroelastic coefficient (α) as given below,

$$\sigma' = \sigma - \alpha P_f \quad (1.3)$$

The Biot's poroelastic coefficient (α) corresponds for the fluid interaction with the rock surface as the fluid flows in the rock. The Biot's poroelastic coefficient (α) has a value less than 1 and is given for various rocks in the literature [32, 33, 34].

1.7 Predicting stress changes during CO_2 injection

The injection of carbon dioxide into the sedimentary reservoir will change both the pore pressure and stress fields in the reservoir. The knowledge of the poroelastic properties for the reservoir rocks is needed for the calculation of the change of the local stresses due to CO_2 injection. The changes in the stresses during carbon dioxide injection will be different from the change in stresses during production process. The process of re-pressurization of the pressure depleted hydrocarbon reservoirs will not have the same pressure/stress coupling as it has during the depletion process [35]. The magnitude of stresses during carbon dioxide injection process is highly dependent on the value of the injection pressure. In an experiment by Hettema et al. [36], injection pressure was varied from 10 to 38 MPa. As the injection pressure was increased, it causes an increase in the magnitude of pore pressure in the reservoir and the values of the stresses are also increased. The values of the stresses decrease during the oil production process due to the decrease in the reservoir pore-pressure [37, 38]. High magnitude of changes in the stresses can cause nonreversible changes to the reservoir structure and can cause failure of the reservoir [39, 40, 41].

1.8 Reservoir stability analysis

The reservoir stability analysis should be performed before injecting carbon dioxide to ensure safe carbon dioxide sequestration process. The stability of the reservoir during carbon dioxide sequestration is a function of the change in the pore pressure and stresses in the reservoir. The value of the pore pressure should not increase than the maximum sustainable value. The maximum sustainable pore pressure is defined as the maximum value of pressure that can be applied to the reservoir without any irreversible geomechanical changes such as reservoir structure failure or fractures reactivation. The stability analysis of the reservoir in this study is performed using the Mohr-Coulomb failure criterion. During the uncoupled geomechanical analysis, the horizontal stresses in the reservoir remains constant and hence the reservoir stability is totally a function of the pore pressure. During the coupled geomechanical reservoir modeling, the increase in the pore pressure causes a decrease in the effective stresses and subsequently an increase in the horizontal stresses and hence the reservoir stability is a function of both pore pressure and stresses in the reservoir.

Both the increase in the pore pressure and pressure depletion can cause failure of the reservoir [27, 30]. As shown in Figure 1.10 (a), the pressure depletion causes the effective stresses to increase and if the effective stresses increases beyond the critical limit, it will cause failure of the reservoir structure. Similarly as show in Figure 1.10 (b), an increase in the pore pressure will cause the effective stresses to decrease and if the effective stresses decreases beyond the critical value, it will cause failure of the reservoir.

(a)

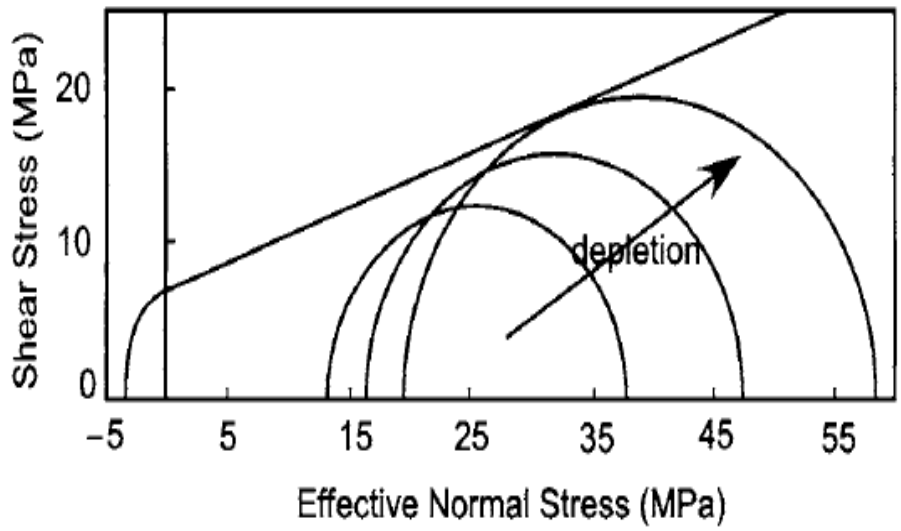

(b)

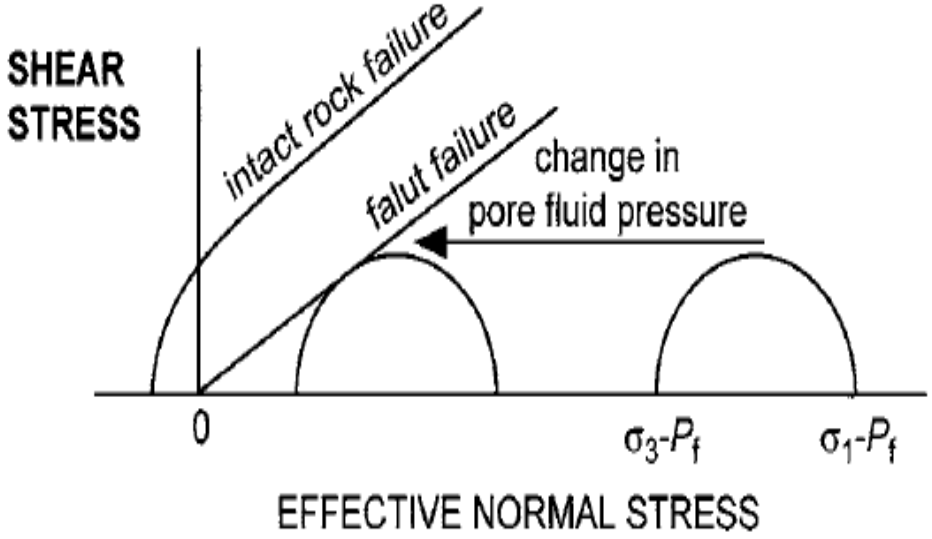

Figure 1.10 Reservoir failure due to change in the pore pressure (a) failure due to pressure depletion (b) Failure due to overpressure

1.9 Research objectives

Most of the oil in the world is produced from the naturally fractured carbonate reservoirs. With the passage of time, the reservoir is depleted from oil and can be used for carbon dioxide sequestration. The current study deals with the numerical modeling of the geomechanical behavior of the naturally fractured Ghawar petroleum reservoir. Before conducting the geomechanical analysis of the naturally fractured Ghawar reservoir, the geomechanical model was used to analyze the single-porosity Biyadh reservoir to validate and verify the developed geomechanical modeling procedure. The objectives of the proposed work are manifested by:

1. Determining the change in the pore pressure of the reservoir during the process of carbon dioxide injection.
2. Calculating the changes in the effective stresses and ground uplift during carbon dioxide injection.
3. Performing stability analysis for the reservoir and predict safe values of the injection parameters.
4. Estimating the safe value of the carbon dioxide occupancy limit for the reservoir.

1.10 Dissertation organization

The basic aim of this research work is to develop a numerical modeling scheme for the geomechanical analysis of a naturally fractured carbonate reservoir undergoing CO_2 injection. Before tackling the complex problem of the geomechanical analysis of naturally fractured reservoir, the developed numerical procedure was applied to the modeling of the geomechanical behavior of a single-porosity sandstone reservoir. The details of all chapters of the dissertation are given below.

- **Chapter 1: Introduction:** This chapter provides introduction of the research topic investigated in this dissertation.
- **Chapter 2: Literature review:** This chapter discusses the literature related to the carbon dioxide injection into the single-porosity and naturally fractured sedimentary reservoirs.
- **Chapter 3: Numerical modeling of CO_2 injection into a single-porosity reservoir:** In chapter 3, starting with the simplest possible case of single-porosity and single-phase flow in the reservoir, the geomechanical and stability analyses were performed for Biyadh sandstone reservoir. In the second stage the modeling procedure was extended and two-phase flow was considered during the geomechanical and stability analysis of the single-porosity reservoir. In this chapter geomechanical and coupled stability analyses were performed for the first time for the Biyadh sandstone reservoir and safe carbon dioxide injection parameters were proposed. Maximum safe occupancy limit was also calculated for the reservoir.
- **Chapter 4: Numerical modeling of CO_2 injection into a naturally fractured reservoir:** Chapter 4 starts with the geomechanical modeling for the Ghawar naturally fractured reservoir by considering only single-phase flow in the reservoir. The coupled stability analysis was also performed for the naturally fractured reservoir. A sensitivity analysis was performed to evaluate the sensitivity of the model output to various input parameters. In the second part of the chapter carbon dioxide injection into a naturally fractured reservoir with water was modeled by considering two-phase flow. The reservoir geomechanical and

stability analyses were performed first for only injection well in the system and then by considering both injection and production wells in the system. Safe values for carbon dioxide injection in the Ghawar naturally fractured reservoir were proposed based on the geomechanical and stability analyses.

- **Chapter 5: Effect of injection well arrangement on CO_2 injection:** In this chapter the effect of injection wells arrangement on the pore pressure buildup and hence on the stability of the reservoir is investigated. Starting with the case of two injection wells, the locations of the wells are changed with respect to the center of the reservoir and their effect on the pressure buildup was monitored. Similar procedure was performed for the cases of having three and four injection wells. Finally, the optimum number of injection wells and their locations are portrayed for the injection site considered in the investigation.
- **Chapter 6: Conclusions and recommendations:** This chapter provides the main findings of the present investigation. The recommendations for the future extensions to this work are also stated.

CHAPTER 2

LITERATURE REVIEW

2.1 Chapter overview

This chapter presents a literature review to establish the state-of-the-art of the various aspects of CO_2 injection to geological reservoirs. Various studies in the literature regarding the modeling of the CO_2 injection and its effects on the mechanical behavior of various types of sedimentary rocks will be reviewed. The first section of this chapter presents various studies from the literature for the CO_2 injection into single-porosity reservoirs like sandstone. In the second section a detail of various studies are presented, in which carbon dioxide is injected into naturally fractured reservoirs.

2.2 Various studies from the literature

The numerical modeling of the geomechanical behavior of the naturally fractured reservoir undergoing carbon dioxide injection is the main objective of the current study. Before the complex numerical modeling of the naturally fractured reservoirs, a detail review should be presented for the relatively geologically simple single-porosity reservoirs. Modeling single-porosity reservoir is easy compared to naturally fractured reservoirs due to the fact that the flow and deformation equations are applied only to the matrix medium in the single-porosity reservoirs. For naturally fractured reservoirs carbon dioxide flow is considered both in the matrix and fractures. The following sections present the various studies for modeling the single-porosity and naturally fractured reservoirs.

2.2.1 Injection of CO_2 into a single-porosity reservoir

A geomechanical modeling was performed for Krechba field at In Salah, Algeria during carbon dioxide injection [42]. At Krechba field one million tons of CO_2 per year over a period of five years was injected at a depth of 1810 meters into a water-filled strata as shown in Figure 2.1. As shown in Figure 2.1, the injection of CO_2 tends to increase the confining pressure inside the reservoir and it helps in the recovery of the gas from the production sites.

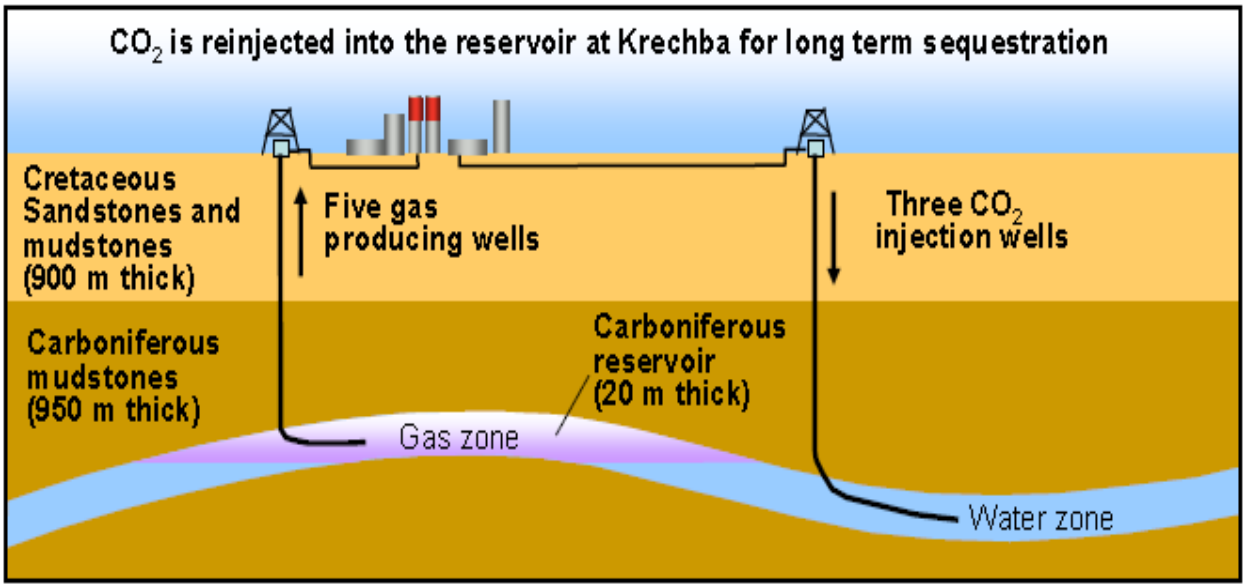

Figure 2.1 Injection of CO_2 at a depth of 1810 meters at Krechba field [42]

A 3D numerical modeling was performed for the selected field with the model dimensions of (10 X 10 X 4 km). The injection zone is a 20 meters thick layer of C10.2 sandstone as shown in Figure 2.2. The geomechanical analysis was performed for the CO_2 injection into the reservoir. A multiphase flow simulator (TOUGH2) was used to model the flow of carbon dioxide in the reservoir and a geomechanical simulator (FLAC3D) was used to determine the change in reservoir stresses with carbon dioxide

flow in the reservoir. The two models are actually fully coupled so a change in the flow pattern will tends to change the stress conditions in the reservoir.

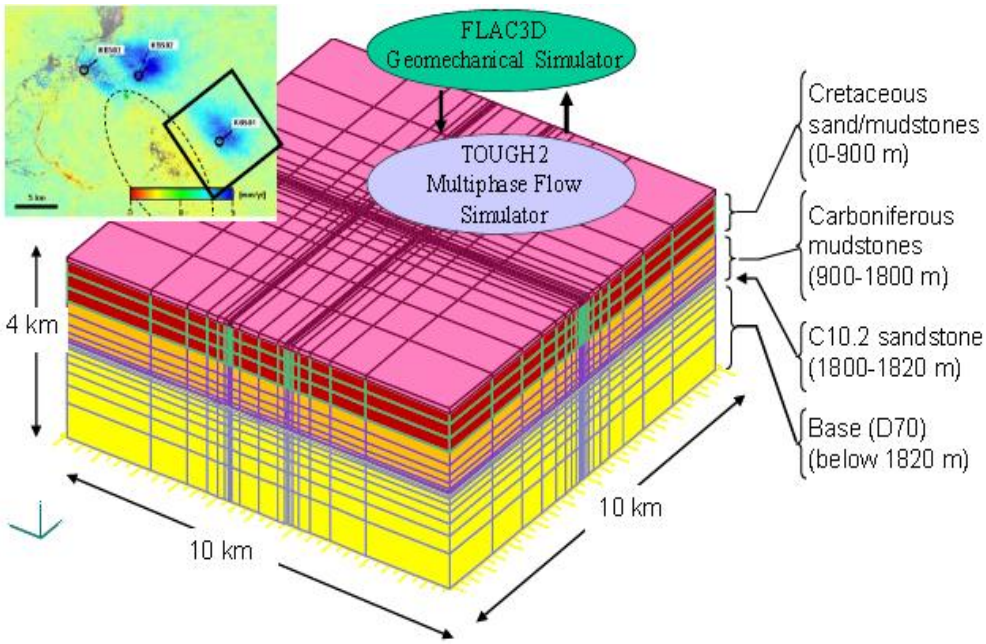

Figure 2.2 A 3D model for the water-filled strata at Krechba field [42]

A new technique, satellite-based inferrometry is utilized to find the ground surface deformation during the five years of injection period of carbon dioxide. The satellite-based inferrometry data shows that during the process of carbon dioxide injection, the ground surface has an uplift of 5 mm per year. The ground uplift was noted to be present for several kilo meters around the point of carbon dioxide injection. Figure 2.3 shows the ground uplift due to the carbon dioxide injection.

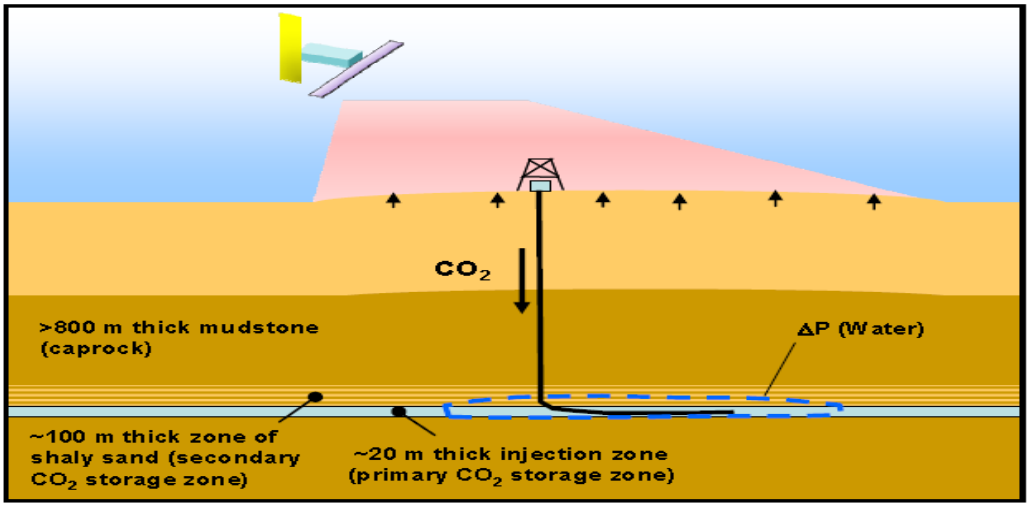

Figure 2.3 Ground uplift at Krechba field due to five years of CO_2 injection [42]

The ground uplift is due to the expansion of the sedimentary reservoir of 20 meter thickness where CO_2 is injected and also due to the expansion of the shaly sand that is with almost 100 meters thickness above the injection zone.

Bustin and Clarkston [43] studied the effect of injection pressure on the storage capacity of a reservoir. They concluded that the injection capacity increases with increase in the injection pressure. As the CO_2 is injected into the sedimentary reservoir, with the passage of time the injection will be decrease due to the deformation of the reservoir matrix [44]. During the carbon dioxide injection the reservoir may fail partially due to the increase of the pore pressure, as well as the change in the minimal horizontal stress [45]. This change in horizontal stresses due to change in pore-pressure is known as pore-pressure-stress coupling [30], in which the increase in the pore pressure tends to alter the stresses in the reservoir. The change in the horizontal stresses has a crucial effect on the failure of the reservoir [46]. The flow of carbon dioxide in a porous medium is a fully coupled geomechanical process that results in the deformation of the reservoir with the passage of time and may further result in the creation of new cracks and reactivation of

already existing cracks in the reservoir [47]. Moreover, carbon dioxide injection into sedimentary reservoirs causes ground vertical uplift that should be taken into account during the selection of a location for carbon dioxide storage. Selection of optimum values of the injection parameters is necessary for safe carbon dioxide storage in sedimentary reservoirs.

Barnes et al. [14] performed numerical modeling for the Mount Simon sandstone reservoir of Holland considering multi phase flow of carbon dioxide and reservoir deformation using STOMP-WCS simulator code. Carbon dioxide was injected at an injection rate of 600,000 metric tons per year for a period of 20 years. The injection reservoir was caped with a low permeability Eau Claire layer that restricts the flow of carbon dioxide into the upward layers. The maximum pressure value during the carbon dioxide injection process remains less than the critical pressure corresponding to the fracture pressure and thus the reservoir remains safe during carbon dioxide injection.

Zhang et al. [48] performed numerical modeling for the carbon dioxide injection into geological carbon dioxide sequestration using TOUGH2 simulator. During their study of carbon dioxide sequestration they concluded that the efficiency of the sequestration process is a function of the injection parameters like carbon dioxide injection rate, and injection pressure.

Yang et al. [49] performed 3D multiphase flow numerical modeling for the Daqingzijing oilfield using a higher order space-time conservation element and solution element method. Simulation results show that the spreading of CO_2 in the reservoir is highly affected by the heterogeneity and variation in the reservoir thickness. During the

20 years of carbon dioxide injection, the results from the numerical simulations show that carbon dioxide spread up to 9 km in radius around the injection point.

Karsten et al. [50] perform numerical modeling for a saline aquifer using TOUGH2 multiphase flow simulator. The numerical simulations investigated the leakage of carbon dioxide through the fault zone. The numerical simulation results show that as CO_2 is injected into the reservoir, the fault permeability will increase with the passage of time and more volume of carbon dioxide will be leaked to the overburden layers.

2.2.2 Injection of CO_2 into a naturally fractured reservoir

Sandrine et al. [51] performed a geomechanical modeling of the Paris basin, and concluded that carbon dioxide injection affects reservoir stability. In their study, the carbonate reservoir was considered as a single-porous structure, wherein the combined effects of the carbon dioxide injection and the long-term sequestration on the fractures were not addressed. It is noteworthy to mention that a carbonate reservoir is a naturally fractured medium, where the activation of fractures often causes leakage of carbon dioxide to the overburden layers.

A geomechanical modeling procedure was also presented by Masoudi et al. [52] for performing stability analysis of the depleted carbonate reservoir at Sarawak basin in east Malaysia. However, the model did not address the flow between the matrix and fractures together with its affect on the pressure buildup and carbon dioxide transport in the reservoir. In another case study for Paris basin by Andre et al. [53], a carbonate reservoir was studied using the SCALE2000 and TOUGHREACT (Multiphase flow simulator). Numerical simulations were carried out for two different cases of carbon dioxide injection, one with carbon dioxide saturated water and a second with pure

supercritical carbon dioxide. The carbon dioxide saturated water results in a greater damage of the reservoir structure as compared to the supercritical carbon dioxide. Supercritical carbon dioxide is more reactive as compared to the subcritical carbon dioxide.

In a study by Chappa et al. [54], for a site located at French Southern Alps, numerical analysis was performed for a fractured shallow carbonate reservoir. The limestone reservoir had a thickness of 15 meters with an area of (30X30 meters). During experimental analysis displacement sensors were used for finding the deformation of the fractured carbonate reservoir during CO_2 injection. The numerical modeling used was based on codes that considered reservoirs as a combination of rigid bodies (rocks) jointed together. The injection pressure of CO_2 tended to move the rocks and these rocks had motion like jointed bodies. 2D analysis was performed with universal distinct element code (UDEC). Cubic law was used to calculate the fluid flow and the reservoir was taken as isotropic. The magnitude of displacement was in good agreement with the experimental outcomes in 2D. For 3D analysis the flow between fractures and matrix and also between the matrix elements ought to be considered in the numerical modeling for better agreement with the output displacement value.

A study of the Arab D limestone was carried out by Fung et al. [55] for Ghawar oil field located in Al-Ahsa Saudi Arabia, in which it was identified that most of the oil sedimentary reservoirs in Saudi Arabia are with dual-porosity. It was further explained that there are actually four modes of porosity, which are named as M, 1, 2, and 3. M stands for macro porosity where as 1, 2, and 3 stand for the three types of micro porosities. The dual-porosity of the combination of M macro porosity and 1 micro

porosity is the dominant mode of dual-porosity in various oil reservoirs of Saudi Arabia. The type M macro porosity has diameter of 58 μm where as the type 1 micro porosity has a diameter of 1.1 μm. So while finding the effects of the injection pressure of CO_2 on the sedimentary reservoir, the dual-porosity modeling of the reservoir is necessary for estimating the strength of the reservoir matrix and its corresponding deformation. The consideration of the dual-porosity will help to find the safe values of the injection pressures of carbon dioxide for specific sedimentary reservoirs.

In another study by Beni et al. [56] for the Minden (Germany), the process of the migration of the injected CO_2 was explained, which further corresponds to three types of trapping mechanisms for carbon dioxide. During the initial periods of injection CO_2 moves toward the top of the storage volume. Then it starts moving in the lateral direction and is partially dissolved in the water present at the reservoir cap rock surface. When carbon dioxide is absorbed by water, it increases the density of water and the CO_2 enriched water starts migrating towards the bottom layer of the reservoir. It takes almost 10,000 years for the CO_2 enriched water to reach the bottom layer. The three types of trapping mechanisms for carbon dioxide are, hydrodynamic, dissolution, and mineral trappings. Initially hydrodynamics trapping is the dominant one, after some time (about 40 years) the dissolution trapping becomes the dominant for some time, and after 100 years the mineral trapping becomes the dominant way of carbon dioxide trapping. The reservoir was composed of limestone and the numerical modeling was performed in TOUGHREACT, which a non-isothermal package used to quantify mixtures of water, CO_2, and NaCl.

Coelho et al. [57] performed a study of the high porosity low permeability limestone. This study was for limestone sedimentary reservoirs present at Campos Basin, Brazil. The mechanical behavior of limestone was studied and it was concluded that due to oil production the rock porosity and permeability exponentially decreases, which may cause the pore to collapse at the reservoir. This problem raises a need to use numerical methods to find the ground subsidence. It was seen that, during the initial stages of fluid withdrawal, elastic deformation occurred in the reservoir matrix. A further increase of strain give rise to pore collapse and after further fluid withdrawal a normal consolidation process occurs due to the rearrangement of the matrix, which decreases porosity and permeability. Figure 2.4 shows the three stages of reservoir deformation.

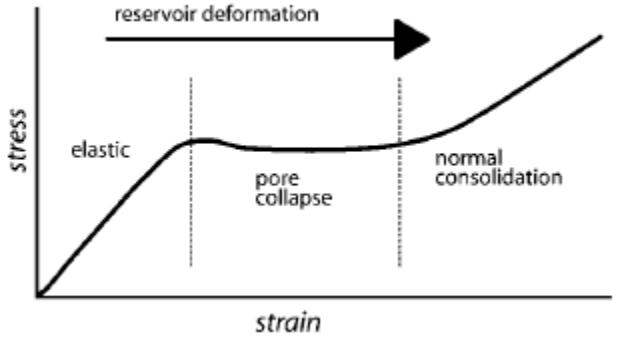

Figure 2.4 Stress-strain curve for a rock under compaction [57]

A study was performed for the Oolitic limestone for the Dogger carbonate reservoirs of the Paris basin [58]. During this study tri-axial tests were performed at the corresponding pressure and temperature of the Dogger carbonate reservoirs to study the mechanical properties of the reservoir during carbon dioxide injection. It was noted that during the carbon dioxide injection, the part that is near to the injection wellbore have dynamic percolation of carbon dioxide and transport of carbon dioxide will not be due to dissolution process. Away from the injection wellbore the transport of carbon dioxide

will be mainly due to the dissolution process. During the process of dynamic percolation the part of the reservoir nearer to the injection point of carbon dioxide is compacted but this compaction is not normally severe.

In a study by Perera et al. [59], for the Sydney Basin coal, Australia, COMET 3 simulator was used to study the storage of CO_2 in coal for various values of the injection pressure, temperature, and moisture contents of the coal matrix. The main aim of this study was to find the ground uplift during the five years of injection period and also to evaluate the effect of various input parameters on the storage capacity of CO_2 in the coal matrix. During the modeling phase a 3D model of (500×500×20 meters) coal layer was modeled at a depth of 1000 meters below the ground level. During the flow modeling carbon dioxide was injected for 10 years through a well of 0.1 meter diameter. Simulations were performed for 4 different scenarios of the process variables i.e. temperature and moisture contents of the coal and injection pressure of carbon dioxide.

It was noted that the capacity of carbon dioxide storage decreases with the increase in temperature of the coal matrix. Similarly the storage capacity decreases with an increase in the moisture contents. The storage capacity increases with an increase in the injection pressure. It means that there is an exponential increase in the storage capacity of carbon dioxide with increasing the injection pressure but there is always an upper value of the injecting pressure, after which the reservoir will be damaged. In this study Mohr column failure criteria is used to evaluate the reservoir damage and the calculation shows that the reservoir will fail at an injection pressure of 19 MPa. The failure analysis in this study shows that the rocks failure because of carbon dioxide injection is normally due to maximum shearing stresses.

It is important to note that for determining the correct values of the pressure, displacement, and stress fields in a naturally fractured reservoir, one may consider the reservoir as a combination of two regimes (i.e. matrix and fractures), such that there is a continuous interaction between the two regimes that allows the confined fluid to move between them [60]. Moreover, the consideration of sorption-induced strains has an effect on the determination of the permeability, porosity and volumetric strain in the reservoir [61].

In this investigation, the Ghawar oil field located in eastern Saudi Arabia, which is the world largest oil field, has been considered. It is a carbonate reservoir with dual-porosity, like most of the sedimentary oil reservoirs in Saudi Arabia. Accordingly, the dual-porosity modeling is necessary for estimating the strength of the reservoir matrix and its corresponding deformation due to the injection of CO_2 at high values of injection pressures. The consideration of the dual-porosity will help to find the safe values of the injection pressures of carbon dioxide for specific sedimentary reservoirs [62].

The literature review attests to the importance of numerical modeling techniques in evaluating stresses and deformations in sedimentary reservoirs in general, and in the naturally fractured sedimentary rocks in particular. In this study, a numerical modeling methodology is invoked for the coupled behavior of the CO_2 injection and the change in the geomechanical behavior of the naturally fractured sedimentary carbonate reservoir, wherein the site of Ghawar Arab-D carbonate petroleum reservoir is considered as a case study from Saudi Arabia. In this investigation, the COMSOL multi-physics modeling software was utilized to couple the CO_2 flow in the naturally fractured media and its corresponding mechanical impact on the reservoir. In this context, a fully coupled non-

linear field equations are written to include the sorption-based deformation of carbonate reservoir during the injection of compressible fluid (CO_2) to the sedimentary reservoir.

The current numerical modeling scheme considers the crucial role of the *in situ* stresses and interaction between fractures and matrix in correctly estimating the deformation and stress fields in the naturally fractured carbonate reservoir during CO_2 injection. The change in the stress-displacement field within the reservoir due to changes in its porosity and permeability as a result of the injected compressible CO_2 has been addressed. Moreover, the present investigation extends the previous studies by considering the sorption-based deformation during the injection of the compressed CO_2 fluid into the naturally fractured carbonate reservoir. The sorption-induced strains and the interaction between matrix and fractures have been evaluated. Moreover, the Mohr-Coulomb failure criterion has been utilized to investigate the stability of the reservoir during the coupled process of carbon dioxide injection into the reservoir and the corresponding change in the stress field.

2.2.3 Existing modeling schemes for geomechanical analysis

Several modeling tools have been utilized for the coupled CO_2 flow and reservoir deformation analyses for both single-porosity and naturally fractured reservoirs. The various case studies from the literature for the single-porosity and naturally fractured reservoirs in the previous sections discuss in detail the various simulators used during the numerical modeling in those studies. In most of the studies in the literature, separate simulators were used for the flow of carbon dioxide and reservoir geomechanical analysis. Using separate tools create new challenges of simulators interfacing because the output from the flow simulator will be used in the deformation simulator and similarly

the output of deformation simulator will be used in the flow simulator in each time interval. Using two simulators also increases the processing time. The equation based modeling option in COMSOL multiphysic solve the above mention problems and also give the flexibility to use recent mathematical models for the flow and geomechanical analysis of naturally fractured reservoirs.

Recently a simulation tool COMET3 was used for carbon dioxide sequestration assessment in Eastern gas shale [63]. The CMG and ECLIPSE simulation tools were also used for modeling the carbon dioxide injection in Devonian gas shale [64]. The Loose staggered-in-time coupling technique can be used to perform efficient geo-mechanical analysis of the reservoir undergoing carbon dioxide injection [65]. Kvamme et al. [66] used improved version of the Ratraso Code Bright (RCB) for saline aquifers. As compared to other methods for modeling the geomechanical behavior during CO_2 injection, this code has an implicit geomechanical module, which can converge even at high injection pressures. In this study the RCB modeling procedure is applied to a 2D example, which confirms the efficient convergence ability of the modeling method.

A geomechanical analysis was performed for Krechba field at In Salah, Algeria during carbon dioxide injection [42]. A multiphase flow simulator (TOUGH2) was used to model the flow of carbon dioxide in the reservoir and a geomechanical simulator (FLAC3D) was used to determine the change in reservoir stresses with carbon dioxide flow in the reservoir. The two models are actually fully coupled so a change in the flow pattern will tend to change the stress conditions in the reservoir. The main problem in using two different simulators for flow and geomechanical analysis is that coupling between the software becomes a big challenge. The same analysis can be performed in

multiphysic software like COMSOL more efficiently due to the fact that COMSOL has both flow and geomechanical simulators within one package. The processing time is much less compared to other strategies using two simulators for the flow and geomechanical analysis. Apart from this, COMSOL has the strength of performing equation based modeling and hence give flexibility to users to use new efficient mathematical models for coupled geomechanical analysis during carbon dioxide injection.

CHAPTER 3

NUMERICAL MODELING OF CO_2 INJECTION INTO A SINGLE-POROSITY RESERVOIR

3.1 Overview of CO_2 injection into single-porosity reservoirs

Before the complex numerical modeling of the naturally fractured reservoirs, a detail numerical modeling procedure is discussed for the relatively simple single-porosity reservoirs. Modeling single-porosity reservoir is easy compared to naturally fractured reservoirs due to the fact that the flow and deformation equations are applied only to the matrix medium in the single-porosity reservoir. In the following sections a numerical modeling procedure for the coupled carbon dioxide flow and reservoir geomechanical analysis is developed first for the single-porosity reservoir with single-phase flow and then for the single-porosity reservoirs with two-phase flow.

3.2 Single-porosity reservoirs with single-phase flow

In the coming sections the process of CO_2 injection into the single-porosity reservoir is discussed. The Biyadh sandstone reservoir in Saudi Arabia is considered as a case study and numerical modeling is performed for carbon dioxide flow and geomechanical analysis of the reservoir. The research work in the following sections presents a first attempt to evaluate the parameters of the safe CO_2 injection process and its feasibility for Biyadh sandstone reservoir. In this context, the flow of the compressible carbon dioxide and its mechanical impact on the porous reservoir matrix is evaluated using COMSOL multi physics software. For an injection period of five years the ground uplift was determined both for locations close to the injection site and at several kilometers away

from the injection site. Using the output displacement variables, the volumetric and principal strains are evaluated. The variation of pore pressure with time, as well as the storage capacity has been evaluated over the entire injection period. Finally the Mohr-Column criterion is used to find the maximum limit injection parameters that can cause failure of the sedimentary reservoir and consequent leakage to the overburden layers.

3.2.1 Governing equations

The mathematical modeling for the fully coupled carbon dioxide flow and reservoir deformation analysis of carbon dioxide injection into sedimentary reservoir consists of two sets of governing equations. The first set of equations deals with the flow of carbon dioxide in the reservoir, while the other set deals with the corresponding deformation of the reservoir. In this section, the equations are defined for the three displacement components, u, v, and w, in addition to the pore pressure. The following section defines the governing equations for the reservoir deformation and carbon dioxide flow in the sedimentary reservoir [67, 68, and 69].

The governing equations for the reservoir deformation are given by

$$-\nabla.\sigma = F_v = \rho_{avg}\, g \tag{3.1}$$

The pore pressure, stress and strain are related as follows:

$$s - s_0 = C:(\varepsilon - \varepsilon_0 - \epsilon_{inel}) - \alpha p_f I \tag{3.2}$$

$$\varepsilon = \frac{1}{2}((\nabla u)^T + \nabla u) \tag{3.3}$$

Here s denotes the stress tensor and s_0 denotes the initial stress values. The flow equations are combinations of mass conservation, Darcy's velocity, and storage model. The mass conservation equation is given by

$$\frac{\partial}{\partial t}\left(\rho_f \varepsilon_p\right) + \nabla.\left(\rho_f q\right) = Q_m \tag{3.4}$$

The Darcy's velocities are given as:

$$q = -\frac{k}{\mu}(\nabla p_f + \rho_f g \nabla D) \tag{3.5}$$

and the storage model is given as:

$$\frac{\partial}{\partial t}\left(\rho_f \varepsilon_p\right) = \rho_f S \frac{\partial p_f}{\partial t} \tag{3.6}$$

Here, S is the storage term. Substituting equations (5) and (6) in equation (4), we get the following equation:

$$\rho_f S \frac{\partial p_f}{\partial t} + \nabla.\rho_f \left[-\frac{k}{\mu}\left(\nabla p_f + \rho_f g \nabla D\right)\right] = Q - \rho_f \alpha \frac{\partial \varepsilon_v}{\partial t} \tag{3.7}$$

Where $\partial \varepsilon_v / \partial t$ is the matrix volumetric strain rate of change. The storage parameter is given by

$$S = \frac{\varepsilon_p}{K_f} + \frac{\alpha - \varepsilon_p}{K_s} \tag{3.8}$$

Where K_f and K_s are the fluid modulus and bulk modus respectively.

3.2.2 Model setup in COMSOL multiphysics

The solution procedure is to use COMSOL multiphysics software to solve the equations of carbon dioxide flow and reservoir deformation. The COMSOL multiphysics software will use the reservoir material properties and carbon dioxide injection parameters as inputs. At the output of the COMSOL software, the values of the pore pressure and ground uplift will be obtained. COMSOL multiphysics software is used to model the carbon dioxide injection into Biyadh sandstone reservoir. In this section, the various input properties required for the modeling process are tabulated along with the description of the modeling procedure adopted in COMSOL. Each geological layer in the overburden,

basement, and the Biyadh sandstone reservoir is modeled in COMSOL such that each layer has a different thickness value. The geological model of Biyadh sandstone reservoir is shown in Figure 3.1. The model constructed in COMSOL representing Biyadh sandstone reservoir with the associated overburden layers and with one injection well is shown in Figure 3.2. In order to accommodate COMSOL requirements the model in Figure 3.1 has been placed layer by layer and only the central part (24-28 km) has been used for modeling. No flow condition is considered at the boundary surfaces of the injection reservoir to calculate the reservoir pore pressure buildup and stability for the severe critical possible condition of the reservoir. With closed boundary conditions the pore pressure buildup will be more compared to the open boundary conditions so the safe values of injection parameters calculated for the closed reservoir will also keep the reservoir safe if open boundary conditions are considered.

The model in Fig. 3.2 has a total of 220,092 degrees of freedom, where each node has four independent variables that represent three displacements in addition to the pore pressure. The modeled reservoir's surfaces have roller constraints, which allow the determination of the vertical ground uplift. Some of the properties of the reservoir and input parameters used in the simulation are listed in Table 3.1 [70, 71, and 72]. The model dimensions and the period of carbon dioxide injection into Biyadh Sandstone reservoir is given in Table 3.2.

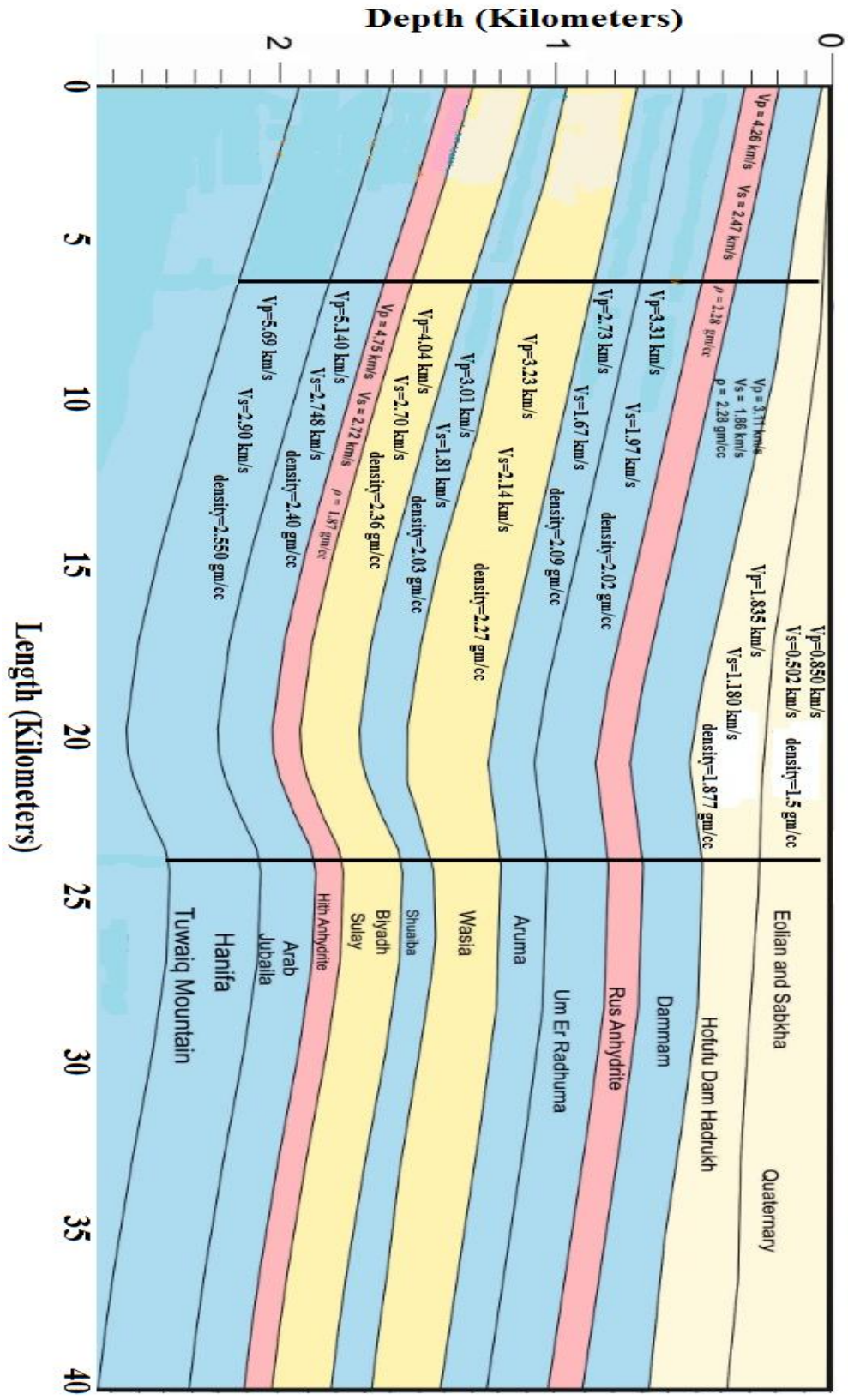

Figure 3.1 Geological model of Biyadh reservoir and various overburden layers [70]

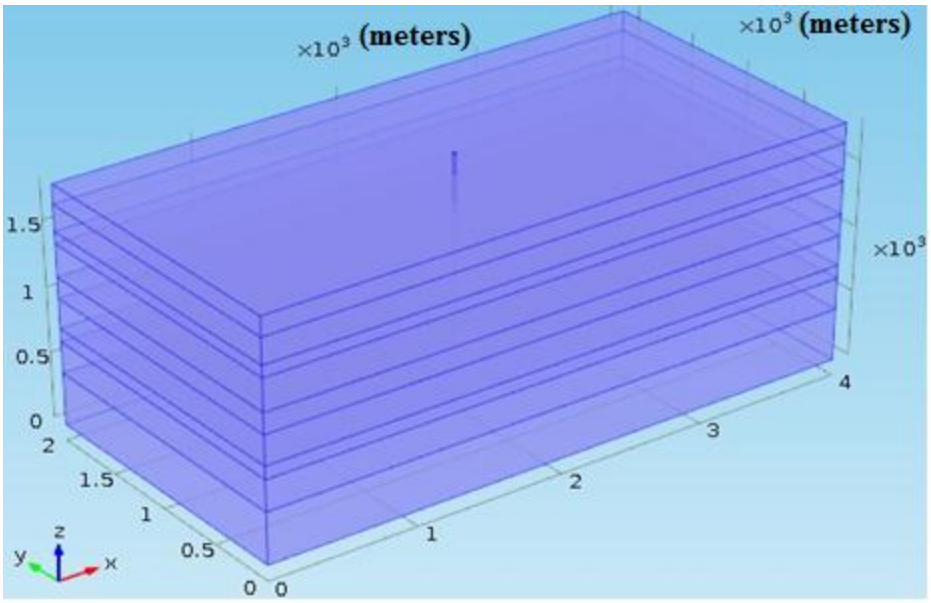

Figure 3.2 Simulation model for the Biyadh reservoir undergoing CO_2 injection

Table 3.1 Formation properties of Biyadh sandstone reservoir [70, 71, and 72]

Model Parameter	**For Reservoir**	**For Caprock**
Rock Density, $\rho(Kg/m^3)$	2360	2030
Young's Modulus, E (GPa)	44.7	18.1
Bulk Modulus, K (GPa)	25.7	9.13
Shear Modulus, G (GPa)	17.2	6.9
Initial porosity, $\emptyset_m$	0.12	0.09
Initial permeability, k_f (10^{-15} m^2)	0.7	0.025
Biot Coefficient, α	0.7	0.4
Dynamic Viscosity, $\mu(10^{-5}Pa.s)$	1.84	1.84
Pressure wave velocity, Vp (m/sec)	4040	3010
Shear wave velocity, Vs (m/sec)	2700	1810

Table 3.2 Overall simulation properties for CO_2 injection into Biyadh reservoir

CO_2 injection period (Years)	10
Overall model dimensions, length×width×height (m)	4,000 X 2,000 X 1,820

3.2.3 Stress regime and pre-stressing of the model

The Biyadh formation is under compressional stress regime according to the world stress map, which tends to produce compressive stresses [73, 74, and 75]. During the coupled carbon dioxide injection and reservoir deformation process, the horizontal stresses change with time. The vertical principle stress is dependent on the density and depths of the overburden layers. If the reservoir is under compressional stress regime, like the one considered in this study, the relationship between the magnitudes of the three principle stresses is such that, $\sigma_1 > \sigma_2 > \sigma_3$, where σ_1 is the maximum horizontal stress (σ_H), σ_2 is the minimum horizontal stress, and σ_3 is the vertical stress caused by the weight of the overburden layers [76, 77, and 78].

3.2.4 Model validation

First, let us start by validating the developed COMSOL multiphysics model. In order to validate the poroelastic modeling in COMSOL, some published carbon dioxide injection scenarios in the available literature have been simulated. The modeling procedure starts with a simple homogenous model for a five-year injection period of carbon dioxide that was solved analytically by Rudnicki [79]. The various input material and simulation properties for the model are listed in Tables 3.3 and 3.4. A single layer 3D simulation model was constructed in COMSOL multiphysics as shown in Figure 3.3. All the

external surfaces are with roller constraint condition except the top surface, which is allowed to move in the vertical direction during carbon dioxide injection.

After an injection period of five years, the spread of carbon dioxide and the corresponding pressure variation is shown in Figure 3.4, wherein the pore pressure is shown to attain higher values closer to the injection well. The change in the reservoir pore pressure is plotted along the length of the reservoir in Figure 3.5, which shows that the pore pressure variation obtained by our numerical model in COMSOL is in excellent agreement with the analytical solution by Rudnicki [79].

The second validation test is for a reservoir having both under burden and over burden layers. In this case, carbon dioxide is injected into a sandstone reservoir for sixty years with both under burden and over burden layers of shale [80]. A multilayer 3D simulation model constructed in COMSOL is shown in Figure 3.6. All the external surfaces have roller constraint condition except the top surface, which is allowed to move in vertical direction during carbon dioxide injection. The input parameters and simulation properties of the model are listed in Tables 3.5 and 3.6.

After an injection period of sixty years, the spread of carbon dioxide and the corresponding pressure variation is shown in Figure 3.7. Both the solution in the literature and in the current study is based on the finite element method. The reservoir pore pressure is plotted in Figure 3.8 for the sixty-year injection period into the sandstone reservoir, which shows that the pore pressure variation obtained from our COMSOL model is in good agreement with the solution reported in [80].

In order to demonstrate that the developed COMSOL multiphysics model for the deep Biyadh sandstone reservoir is representative of the existing field conditions, the

simulated stability results were compared with those reported by Haidary et al. [81]. The stability analysis for the reservoir is strongly dependent on the magnitudes of the pore pressure and horizontal stresses. Haidary et al. calculated the critical values of the horizontal stresses based on micro-frac test data, actual rock failure image logs, and poro-elastic horizontal strain model. Based on the breakout pressure (pressure corresponding to the shear failure of the Biyadh reservoir), the change in the pressure needed for the shear failure of the reservoir was calculated. Using the critical mud weight and the results from Haidary et al. [81], the critical values of the horizontal stresses for the shear failure were calculated.

The change in the pore pressure and horizontal stresses was used to construct a Mohr's circle for the final stress condition of the reservoir. The Mohr's circle based on the work of Haidary et al. in Figure 3.9 shows that the reservoir's shear failure will occur for the corresponding change in pore pressure and horizontal stresses. For the same pore pressure change, the new effective normal stresses were calculated using the geomechanical model in COMSOL multiphysics software. The changes in the pore pressure and horizontal stresses were used to construct Mohr's circle for the new stressed condition of the reservoir based on the geomechanical modeling in COMSOL multiphysics software, as shown in Figure 3.9. The Mohr's circle based on the geomechanical modeling in COMSOL multiphysic software also touches the failure envelope, which shows that the reservoir will be under shear failure if the pore pressure is changed to the value given in Haidary et al. [81]. The Mohr's circles in Figure 3.9 shows that the stability analysis performed using our model for the Biyadh reservoir is in good agreement with the stability analysis performed by Haidary et al. [81].

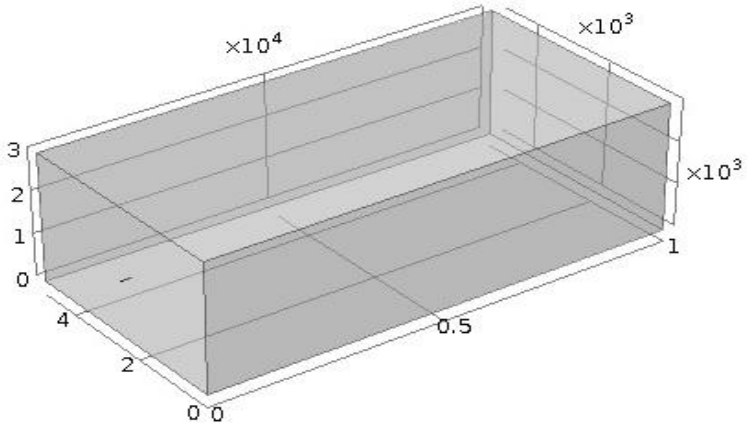

Figure 3.3 Simulation model for CO_2 injection into a single layered sedimentary

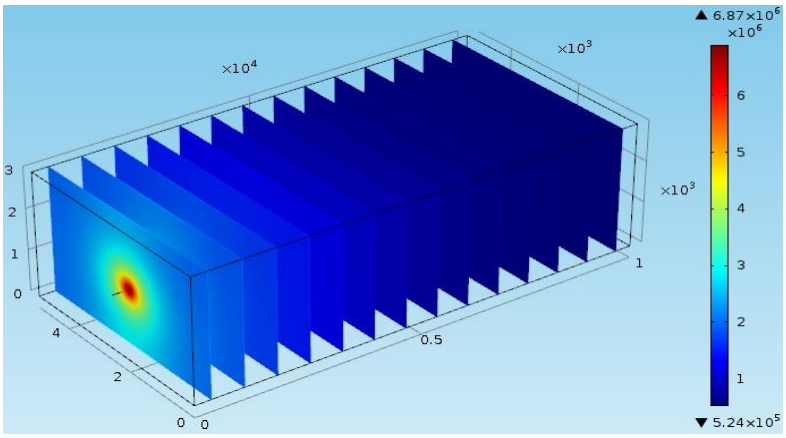

Figure 3.4 The spread of CO_2 and the corresponding pressure variation after five years of CO_2 injection

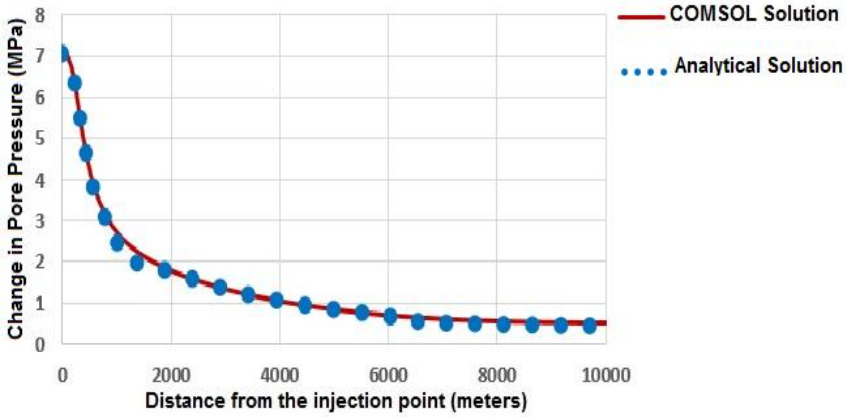

Figure 3.5 Change in the reservoir pore pressure along the length of the reservoir during five years of CO_2 injection

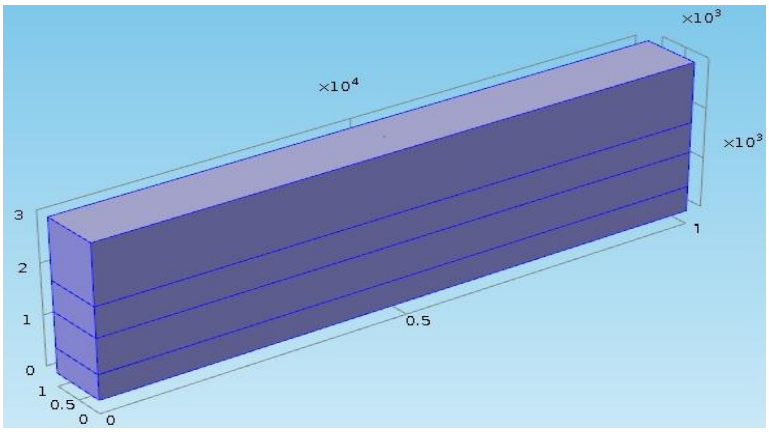

Figure 3.6 Simulation model for CO_2 injection into a multi layered sandstone reservoir

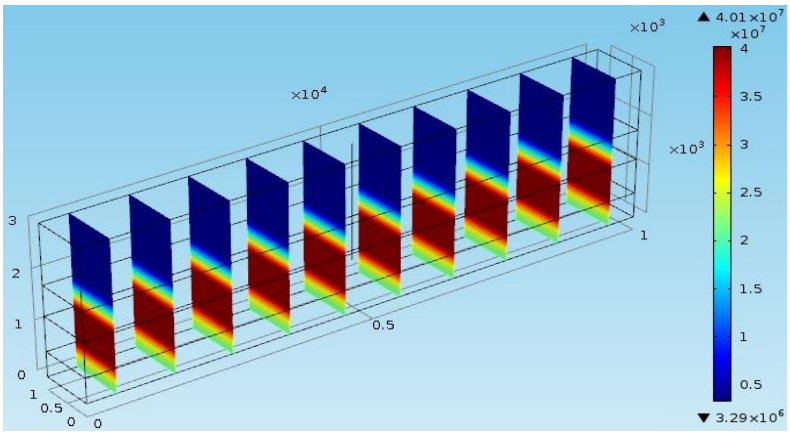

Figure 3.7 The spread of CO_2 and the corresponding pressure variation after sixty years of CO_2 injection

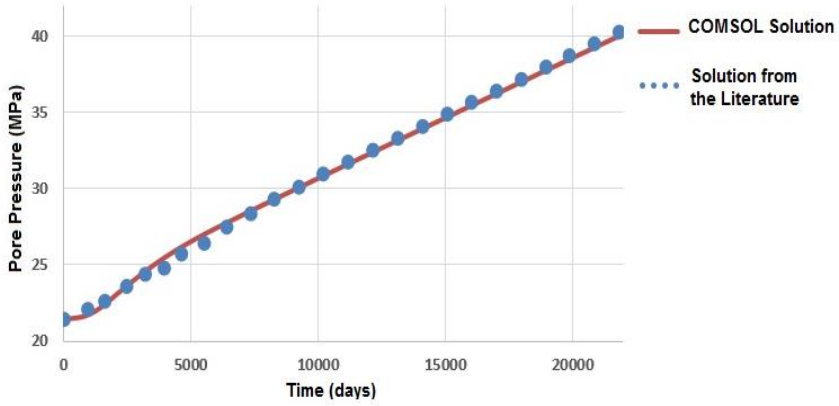

Figure 3.8 The reservoir pore pressure for sixty years of CO_2 injection into the reservoir

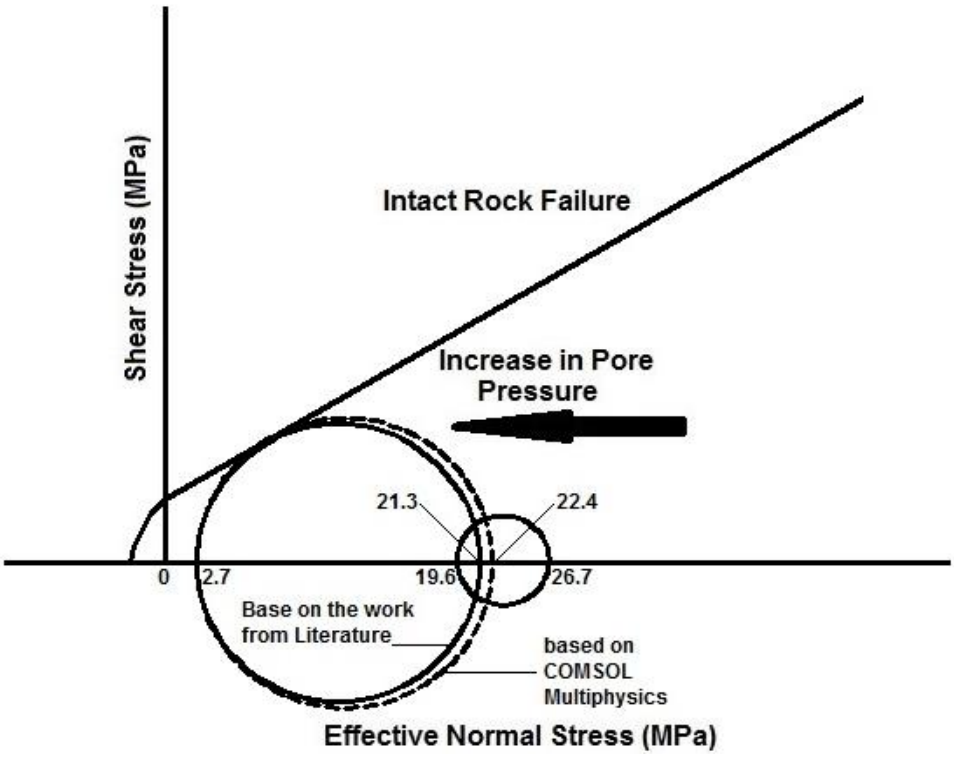

Figure 3.9 Comparison of the stability analysis of COMSOL multiphysic software with the study from the literature

Table 3.3 Various input parameters for the simulation of CO_2 into the single layer model

Parameter	**Value**
Poisson's ratio for the medium	0.25
Density of CO_2, ρ_g (kg/m^3)	1.98
Viscosity of CO_2, μ (Pa s)	1.84×10^{-5}
Density of reservoir material, ρ_r (kg/m^3)	2210
Initial porosity, $\emptyset_0$	0.2
Initial permeability, k_0 (m^2)	9.8×10^{-16}
Shear Modulus, G (GPa)	6.5
Bulk Modulus, K (GPa)	13.3
Biot's coefficient, α	0.7

Table 3.4 Simulation properties for the injection of CO_2 into the single layer model

Rate of CO_2 injection (kg/sec)	40
Period of CO_2 injection (Years)	5
Model dimensions, *length*×*width*×*height*,(m)	10,000 X 5,000 X 3,000
CO_2 injection depth (m)	1700

Table 3.5 The input parameters for the modeling of CO_2 injection into multi layered model

Parameter	**Over burden**	**Top shale**	**Reservoir**	**Basement**
Poisson's ratio for the medium	0.25	0.25	0.25	0.25
Density of rock material, $\rho(kg/m^3)$	2210	2130	2210	2130
Initial porosity, $\emptyset_0$	0.01	0.01	0.20	0.01
Initial permeability, k_0 ($10^{-16}m^2$)	0.098	0.0009	986.9	0.0009
Young's Modulus, E (GPa)	15	15	20	15
Layer Height, $h\ (m)$	1200	600	700	500

Table 3.6 Simulation properties for CO_2 injection into the multi layered model

Rate of CO_2 injection (kTons/year)	207
Period of CO_2 injection (Years)	60
Model dimensions, *length*×*width*×*height*,(m)	10,000 X 1,000 X 3,000
CO_2 injection depth (m)	2300

3.2.5 Results and discussions

3.2.5.1 Critical pore-pressure

Having validated the numerical COMSOL model, one may proceed to investigate the pore pressure variation and its effect on the stability of the Biyadh sandstone reservoir. In this context, the reservoir geomechanical simulation may be performed as uncoupled,

partially coupled, or fully coupled. In this investigation, the reservoir stability analysis is performed using both coupled and uncoupled geomechanical scenarios. During the uncoupled geomechanical modeling, the values of the horizontal stresses remain constant during the pore pressure variation in the reservoir. For the uncoupled geomechanical simulation, it is possible to calculate the value of the critical pore pressure for a reservoir under carbon dioxide injection. The critical pore-pressure is the value that causes failure of the reservoir, reactivates existing fractures or creates new fractures in the reservoir structure. For the intact reservoir with no major faults, the critical pore pressure tends to create new shear fractures that can be calculated as [47, 82]:

$$P_p, \text{critical} - \text{intact} = C_0 \frac{\cos\psi}{1-\sin\psi} + \frac{3\sigma_3 - \sigma_1}{2} \tag{3.9}$$

Where σ_1 and σ_3 are the maximum and minimum principle stresses respectively within the compression stress regime [83]. The pressure P_p is the pore pressure, C_0 is the cohesion, and ψ is the friction angle for the reservoir. If there are pre-existing fractures, then the cohesion is zero and the critical pore pressure is given by

$$P_p, \text{critical} - \text{re} - \text{activation} = \frac{3\sigma_3 - \sigma_1}{2} \tag{3.10}$$

If the value of the pore pressure is increased beyond the value given by equation (3.10), then the already existing fractures tend to get reactivated. The critical pore pressure for the tensile failure of the reservoir is given by

$$P_p, \text{critical} - \text{tensile} = \sigma_3 + T_0 \tag{3.11}$$

where T_0 is the tensile strength of the reservoir. Considering the compressional stress regime, the critical pore pressures for the three cases above are given in Table 3.7.

Table 3.7 Critical pore pressure change at the injection well for the compressional stress regime

Property	Value for the compressional stress regime
σ_1(MPa)	35.70
σ_3(MPa)	28.60
P_p, critical − intact(MPa)	33.71
P_p, critical − re − activation(MPa)	25.05
P_p, critical − tensile(MPa)	31.10

3.2.5.2 Pore-pressure variations and its effects on reservoir stability

The injection of carbon dioxide into the Biyadh sandstone reservoir increases the pore pressure and causes volumetric expansion of the reservoir, which will eventually cause vertical ground uplift. The maximum pore pressure should be within the safe limits to ensure the reservoir stability. Accordingly, optimum values of the injection pressure and injection period should be determined for safe CO_2 sequestration. In this simulation, the injection pressure is varied within the range of 22-26 MPa. CO_2 is injected for ten years at a depth of 1350 meters via one injection well at the center of the reservoir. The following sections discuss the pore pressure variation at various injection pressures and its effects on the vertical ground uplift, as well as stability of the reservoir. The Mohr-Coulomb failure criterion is used to analyze the reservoir stability for the current CO_2 injection scenario, which includes both coupled and uncoupled geomechanical analyses.

3.2.5.3 Pore-pressure variations and its effects on ground uplift

In this study, CO_2 is injected into Biyadh sandstone reservoir. Before the injection, the reservoir was at initial stress and pore pressure conditions. As carbon dioxide injection

has started, the pore pressure started to increase. The increase in the pore pressure is strongly dependent on the injection parameters specially the injection pressure of carbon dioxide. Although, large values of injection pressure maintain a high potential for the flow of carbon dioxide along the reservoir, there exist a maximum value of injection pressure, at which the reservoir maintains its stable condition. After the ten-year injection period, the spread of carbon dioxide and the corresponding pressure variation is shown in Figure 3.10 for different injection pressures. As shown in Figure 3.10, even after the same period of carbon dioxide injection, the pore pressure attains higher values as the injection pressure increases.

The largest value of injection pressure i.e. 26 MPa in this case, is kept lower than the Lithostatic static pressure for the current reservoir to ensure maximum reservoir stability. The pressure variation at various injection periods of carbon dioxide is shown in Figure 3.11 for the maximum safe value (26 MPa) of the injection pressure for the current reservoir. Figure 3.11 shows that the magnitude of the pore pressure increases throughout the reservoir as the injection period increases. The pore pressure variation monitored for various injection pressures at a point near to the carbon dioxide injection well is displayed in Figure 3.12.

During the hydrocarbon production, the pore pressure depletion causes subsidence of the ground surface. Similarly, when carbon dioxide is injected into the reservoir; it increases the pore pressure and causes the ground surface to displace in upward direction. The value of the maximum ground uplift should be monitored during carbon dioxide injection, not only close to the injection well but also farther away up to several kilometers around the injection port. Figure 3.13 shows the ground uplift after ten years

of CO_2 injection at different injection pressures. As shown in Figure 3.13, the ground uplift is maximum just above the injection point and extends for several kilometers around the injection well. Figure 3.14 shows the ground uplift monitored for different injection pressures at a point close to the carbon dioxide injection well.

(a)

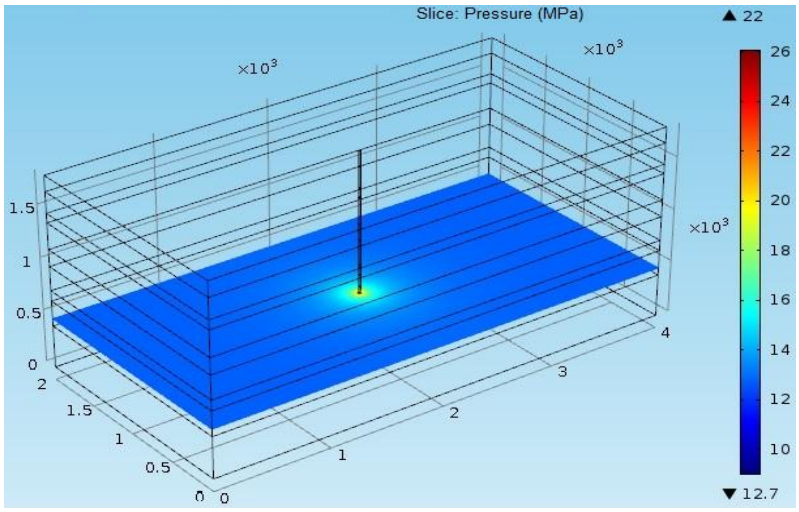

(b)

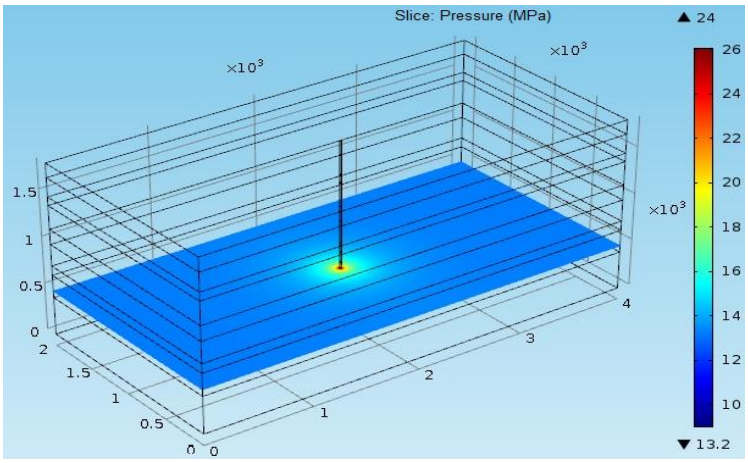

(c)

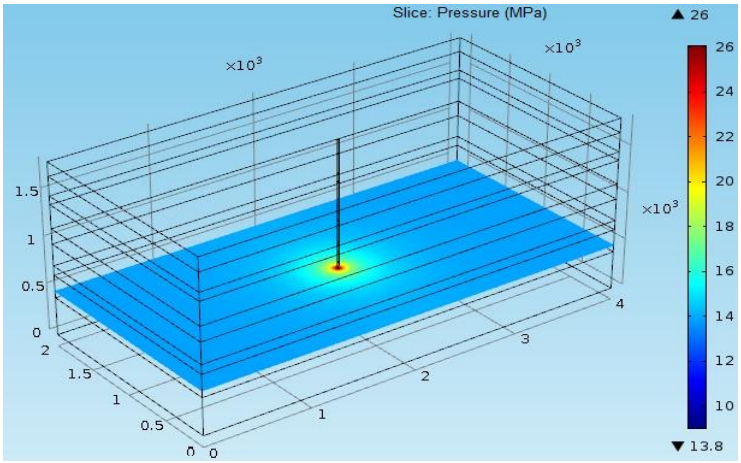

Figure 3.10 The spread of carbon dioxide after ten years of injection period at different injection pressures; (a) 22 MPa, (b) 24 MPa, (c) 26 MPa

(a)

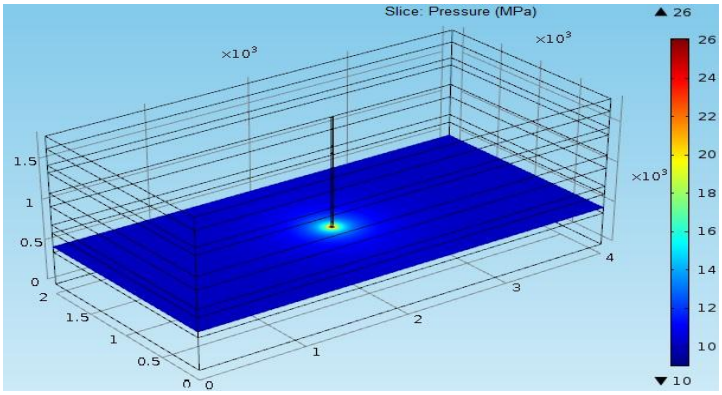

(b)

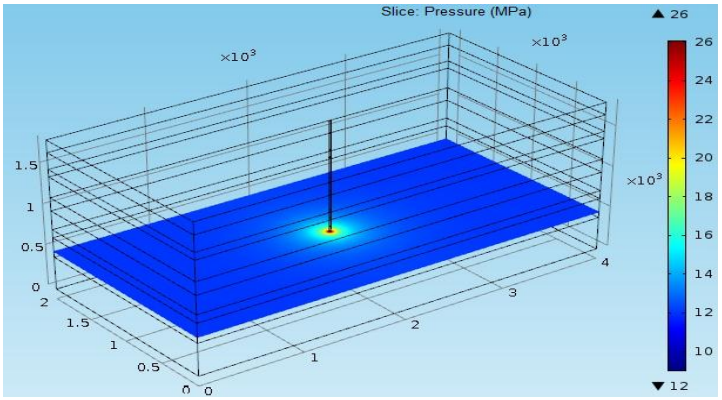

(c)

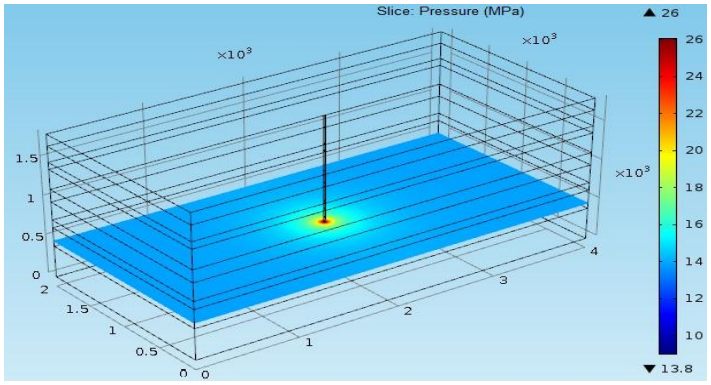

Figure 3.11 The spread of CO_2 and the corresponding pressure variation for different periods of injection; (a) After 2 years, (b) After 6 years, (c) After 10 years

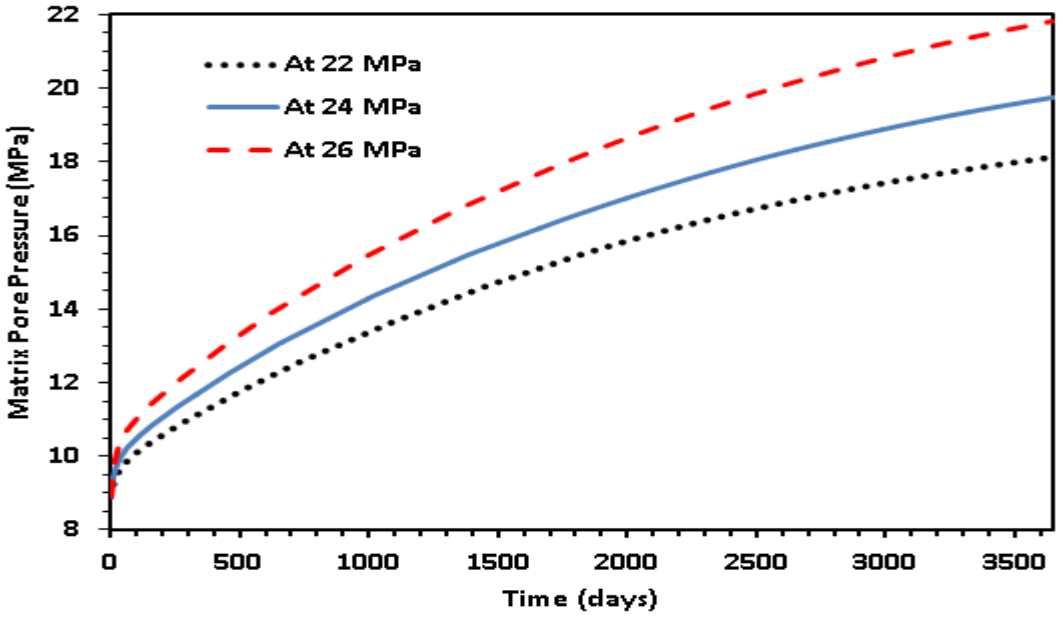

Figure 3.12 The spread of carbon dioxide and the corresponding pressure variation for various periods of injection and at different injection pressures

(a)

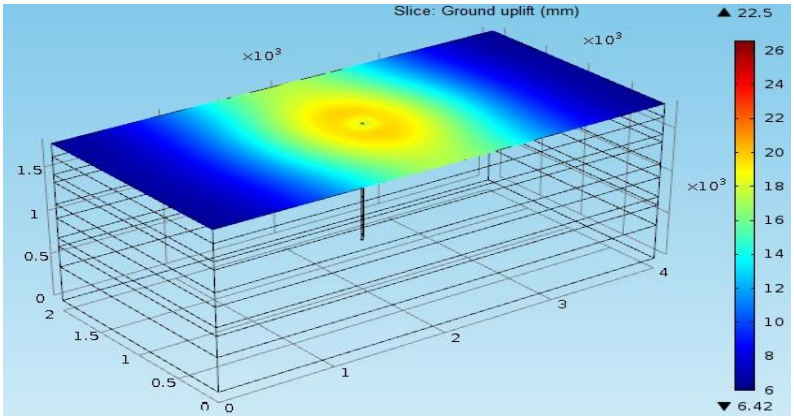

(b)

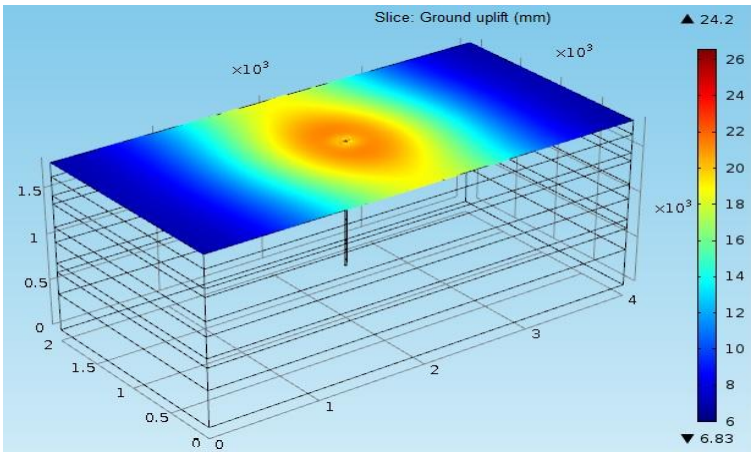

(c)

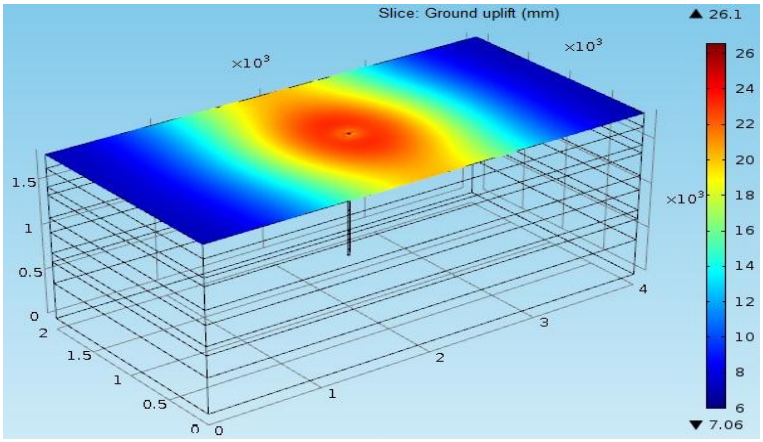

Figure 3.13 Ground uplift after ten years of injection period at different injection pressures; (a) 22 MPa, (b) 24 MPa, (c) 26 MPa

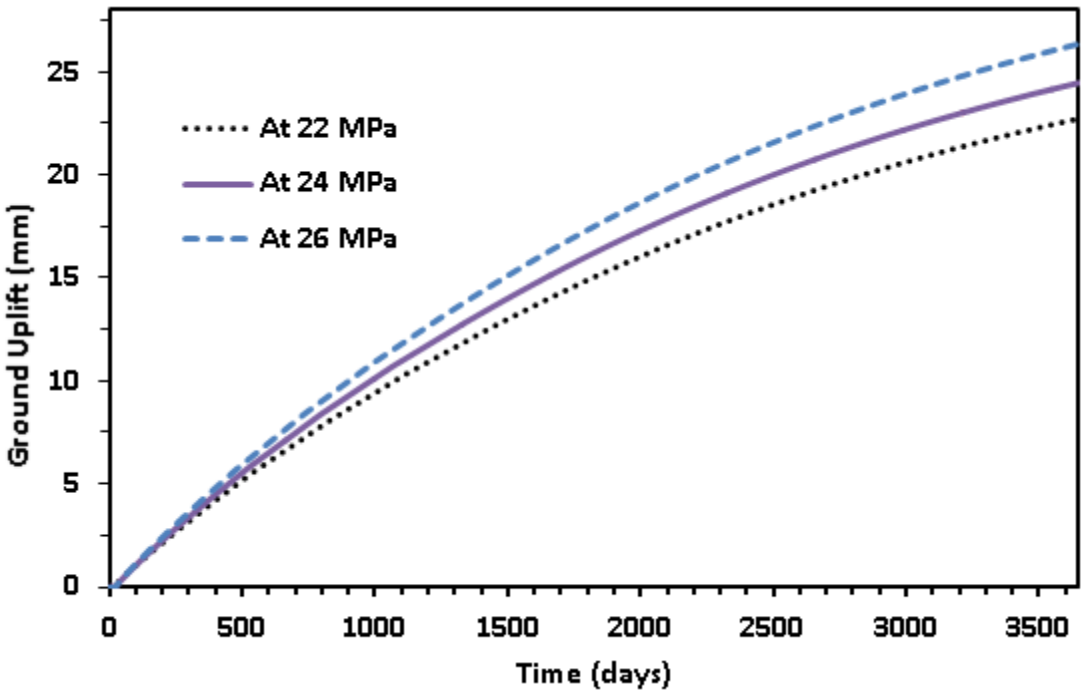

Figure 3.14 The ground uplift for various periods of injection and at various injection pressures

3.2.5.4 Stability analysis of the reservoir

The stability analysis of the reservoir is performed using the Mohr-Coulomb failure criterion. During the uncoupled geomechanical analysis, the horizontal stresses in the reservoir remains constant and hence the reservoir stability is totally a function of the pore pressure. During the coupled geomechanical reservoir modeling, the increase in the pore pressure causes a decrease in the effective stresses and subsequently an increase in the horizontal stresses [30, 84]. As no major fault results from the selected Biyadh sandstone reservoir, the failure envelope for the intact rock type is considered.

For the uncoupled geomechanical analysis of the reservoir, the reservoir stability is only dependent on the pore pressure variations. As shown in Figure 3.12, the maximum pore pressure increase is with an injection pressure of 26 MPa. The increase in the pore pressure causes a decrease in the effective stresses and hence moves the reservoir to a

new stress condition closer to the failure envelope [85]. The dashed circle in Figure 3.15 shows the initial stress condition of the reservoir, while the final stress state at the injection pressure of 26 MPa is represented by the solid circle. The failure envelope and the change in the reservoir stresses shown in Figure 3.15 are in good agreement with the critical pore pressure values given in Table 3.7.

However, for the coupled geomechanical analysis of the reservoir, the reservoir stability is dependent both on the pore pressure variations and also on the change in the horizontal stresses resulting from carbon dioxide injection. As shown in Figure 3.16, the maximum pore pressure and horizontal stresses increase is recorded at the injection pressure of 26 MPa. The dashed circle in Figure 3.16 shows the initial stress condition of the reservoir, while the final state of stress at the injection pressure of 26 MPa is shown by the solid circle. The increase in the pore pressure and horizontal stresses causes the reservoir to shift to a new stress condition closer to the failure envelope.

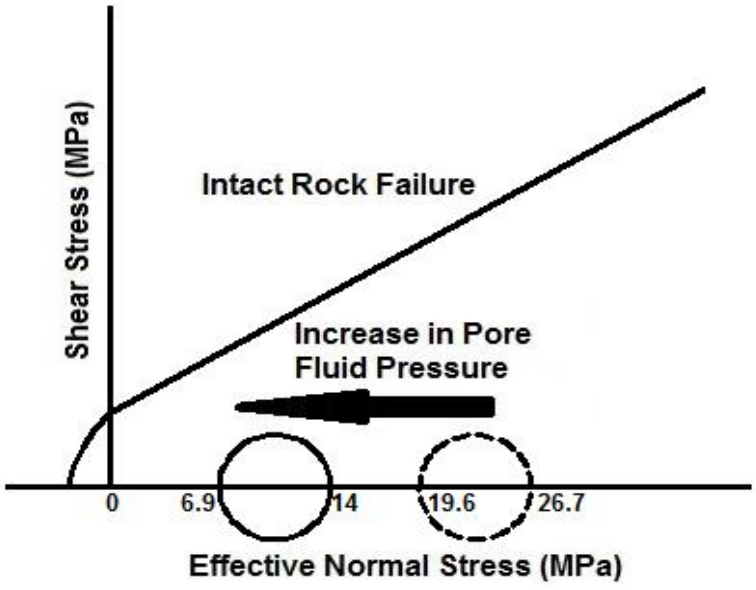

Figure 3.15 Effect of pore pressure variation on the stability of the reservoir for uncoupled geomechanical analysis

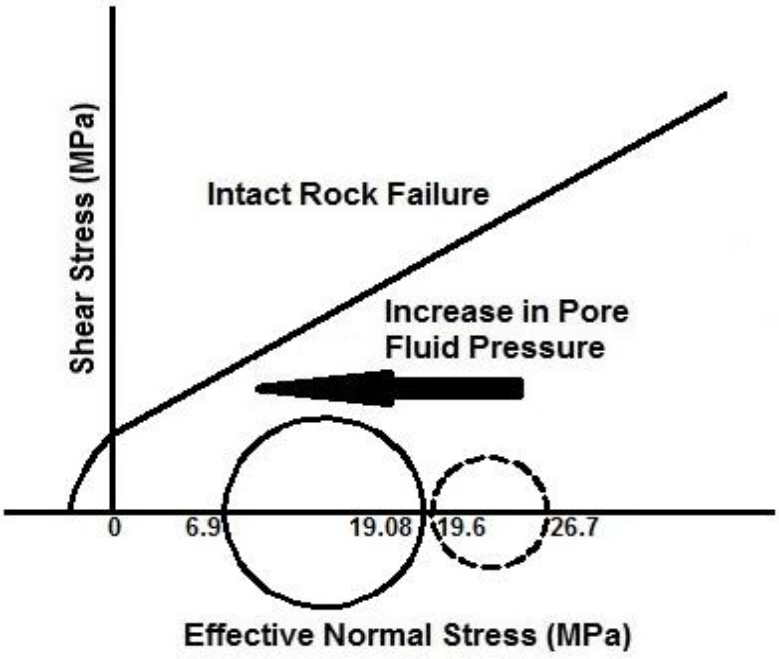

Figure 3.16 Effect of pore pressure variation on the stability of the reservoir for coupled geomechanical analysis

3.2.5.5 Reservoir occupancy

The occupancy of the Biyadh sandstone reservoir is evaluated for a ten-year injection period of carbon dioxide. The initial pore volume for the selected Biyadh sandstone reservoir is $3.072 \text{ X } 10^8 m^3$. Based on the injection scenario given in Tables 3.1 and 3.2, the volume of CO_2 amounts to $2.02 \text{ X } 10^9 m^3$ for the ten years of injection. The value of $2.02 \text{x} 10^9$ m^3 is determined from the mass of carbon dioxide that is injected during ten-year injection period and the density of carbon dioxide. At the depth of 1350 meters, the formation volume factor for the reservoir is 0.00375 m^3/m^3 [86]. For this volume factor at the considered depth, CO_2 is normally stored in a dense state with a volume of $7.57 \text{ X } 10^6 m^3$, which corresponds to occupancy of 2.4 % of the available pore volume. The maximum occupancy value for a closed boundary reservoir was estimated by several

investigators at a maximum of 3% of the total available volume; [68, 87, and 88], which shows that the occupancy of 2.4 % in the current injection scenario with one injection well is within the safe limits.

3.3 Single-porosity reservoirs with two-phase flow

In this section, the single-phase flow modeling in Biyadh reservoir is extended to two-phase flow modeling of CO_2 in the Biyadh reservoir. Two-phase flow is considered during the geomechanical modeling of the reservoir with caprock leakage. Caprock is considered as dual-permeability medium for modeling the carbon dioxide leakage through the caprock. The Barton-Bandis model is utilized to relate the change in the effective stresses to the fracture permeability in the caprock. The Barton-Bandis model was applied only to specific grid blocks that represent fracture in the caprock. The injected carbon dioxide changes the effective stresses on the fracture in the caprock and causes leakage of the stored carbon dioxide. The leaked carbon dioxide will change the ground uplift pattern and hence the modeling procedure in this study will help in finding the exact location and dimensions of the fracture in the caprock from the location and magnitude of the ground uplift. The injected carbon increases the pore pressure, horizontal stresses and causes the vertical ground displacement. The Mohr-Coulomb criterion for the shear failure is used in the study for the stability analysis of the reservoir.

3.3.1 Governing equations

The Biyadh sandstone reservoir contains water and therefore it requires a modeling procedure that can take into account the two-phase flow together with the corresponding deformation of the reservoir. The coupled geomechanical and stability analyses are performed using CMG-GEM software. GEM is an efficient, multidimensional, equation-

of-state (EOS) simulator that provides the flexibility to use custom script files for performing multiphysics operations. GEM was developed by the Computer Modeling Group (CMG) for the geomechanical modeling of single-porosity and naturally fractured reservoirs. GEM can perform efficient dual-permeability modeling by considering fluid flow, not only between the matrix elements but also between the matrix and fractures. One of the advantages of this software is its capability of the simultaneous modeling of the production and injection processes. It can also model the reservoir's post production and post injection responses [89-93].

The iterative coupling method was used in the geomechanics module of CMG-GEM software to perform coupled two-phase flow and reservoir deformation analyses. Due to the iterative coupling method, the flow variable i.e. pressure is first calculated in the parent CMG flow simulator and later sent to the GEM module to calculate the deformation variables such as displacements, stresses, and strains of the reservoir. In the coupled geomechanical modeling by CMG-GEM, the displacement values in each time step are used to calculate the change in the matrix porosity. Using the change in porosity, a new value of the porosity at each grid point is calculated and used for the next time step by the flow simulator [89-93, 94, 95]. The following sections present the equations of the two-phase flow, the deformation of the reservoir, and Barton-Bandis model of carbon dioxide leakage through the caprock [90, 96].

3.3.1.1 Multiphase flow of carbon dioxide through the reservoir

The flow simulator of CMG is a compositional simulator, in which the composition of the phase changes with the change in pressure, and quantity of the injected fluid in the

reservoir. The conservation of mass for the case of CO_2 injection into the reservoir is defined as [69, 80, 89, 97, and 98]

$$\frac{\partial}{\partial t}(\rho_L \emptyset\,(1-\varepsilon_v)S_L) - \nabla.(\rho_L v_L) = Q_L \tag{3.12}$$

where L refers to the phase (either water or carbon dioxide), ρ_L is the density of corresponding phase, $\emptyset$ is the true porosity of the reservoir, ε_v is the volumetric strain in the reservoir due to the injected carbon dioxide, S_L is the saturation, v_L represents Darcy's velocities, and Q_L represents the flow rate. Equation (3.12) relates the changes in deformation of the reservoir and the porosity to the injected CO_2 at a specific flow rate in the reservoir. Due to the deformation of the reservoir, new values of the porosity and volumetric strain are invoked at each iteration step of the coupled model solution. The reservoir porosity ($\emptyset^*$) is a function of both the true porosity ($\emptyset$) and volumetric strain, which is defined by [98]

$$\emptyset^* = \emptyset\,(1-\varepsilon_v) \tag{3.13}$$

where ε_v is the volumetric strain. The new values of porosity, calculated by equation (3.13) will be used by the modeling procedure to find the new values of the pore pressure at each node. The values of the pore-pressure will be used in the deformation equations to find the new values of the effective stresses on the reservoir. Knowing that the current value of porosity at any time step is dependent on the value of the volumetric strain in the reservoir one can use equation (3.13) to write the equation of the conservation of mass as

$$\frac{\partial}{\partial t}(\rho_L \emptyset^* S_L) - \nabla.(\rho_L v_L) = Q_L \tag{3.14}$$

With the current values of porosity in equation (3.14), new values for the pore-pressure can be calculated based on the saturation and capillary pressure of each phase in the reservoir. The relations showing the saturations and capillary pressure of carbon dioxide and water in the reservoir can be stated as [80]

$$S_{water} + S_{carbon\ dioxide} = 1 \tag{3.15}$$

$$P_c(S_{water}) = P_{carbon\ dioxide} - P_{water} \tag{3.16}$$

where S_{water} is the saturation of water, $S_{carbon\ dioxide}$ is the saturation of carbon dioxide. From equation (3.16), the capillary pressure $P_c(S_{water})$ is equal to the difference of the pore pressures corresponding to carbon dioxide and water phases, respectively. Now, utilizing Darcy's law, the Darcy's velocities for phase L are given by

$$v_L = -\frac{k_L}{\mu_L}(\nabla p - \rho_L g) \tag{3.17}$$

where k_L is reservoir's permeability, μ_L is the viscosity, and p is the pore-pressure. At each time step, as CO_2 is injected in the reservoir, the value of the permeability will be updated. New values of the reservoir's permeability are calculated using Kozeny−Carman model from the current values of the porosity as

$$\frac{k}{k_o} = \left(\frac{\emptyset}{\emptyset_o}\right)^3 \left(\frac{1-\emptyset_o}{1-\emptyset}\right)^2 \tag{3.18}$$

where k is the current value of permeability, k_o is the initial reservoir permeability, $\emptyset$ is the current value of the porosity, and $\emptyset_o$ is the initial porosity of the reservoir.

3.3.1.2 Deformation of the reservoir

The pressure-induced deformation of the reservoir causes the displacement field to change. New values of the strain tensor can be calculated using the strain-displacement relationship

$$\varepsilon_{ij} = \frac{1}{2}(u_{i,j} + u_{j,i}) \tag{3.19}$$

where $u_{i,j}$ represent the displacement components and ε_{ij} is the strain tensor and $u_{i,j}$, which is used to calculate the stresses in the reservoir.

Using the constitutive relation of equation (3.20), the stresses in the reservoir can be calculated from the already calculated strains using equation (3.19); e.g. [99-102]. This can be expressed as

$$\sigma_{ij} = 2G\varepsilon_{ij} + \left(K - \frac{2G}{3}\right)\varepsilon_{kk}\delta_{ij} + \alpha p\delta_{ij} \tag{3.20}$$

where σ_{ij} is the stress tensor, G is the shear modulus for the reservoir, K is the bulk modulus, δ_{ij} is the Kronecker delta, and α is the Biot's coefficient. Once we have the new values of pore-pressure and the total stresses, the effective stresses in the reservoir can be easily calculated. The effective stresses in the reservoir can be defined as

$$\sigma_{ij}' = \sigma_{ij} - \alpha p\delta_{ij} \tag{3.21}$$

where σ_{ij}' represent the values of the effective stresses. The effective stresses calculated from equation (3.21) are then used to perform stability analysis of the reservoir.

3.3.1.3 Barton-Bandis model for modeling leakage of carbon dioxide

The carbon dioxide flow equations (3.12-3.18) and the reservoir deformation equations (3.19-3.21) are coupled to give the change in pore pressure, effective stresses, and deformations of the reservoir. The change in the effective stresses is utilized by Barton-

Bandis model to monitor CO_2 leakage during the injection process by calculating the value of fracture permeability from the normal fracture effective stress. The Barton-Bandis model accurately models the change in the fracture permeability by considering an initial value for the fracture permeability at the equilibrium conditions before CO_2 injection. As the effective stresses start to decrease with carbon dioxide injection, the fracture permeability increases. When the effective stresses decreases past the critical value, the fracture permeability becomes very high; thus causing the fracture to open completely and leak the injected carbon dioxide to the overburden layers [91, 92, 97]. As compared to the other models used for calculating the fracture permeability, the Barton-Bandis model can be applied to specific grid blocks to simulate the change in the permeability of a single fracture [60, 103, and 104]. The fracture permeability k_f can be calculated as

$$k_f = k_{fc}\,(e/e_o)^4 \tag{3.22}$$

where k_{fc} is the fracture closure permeability, while noting the following:

$$e = e_o - V_j \tag{3.23}$$

$$V_j = \frac{\sigma_n{}'}{k_{ni} + \sigma_n{}'/V_m} \tag{3.24}$$

$$V_m = e_o \left[1 - \left(\frac{k_{fr}}{k_{fc}}\right)^{1/4}\right] \tag{3.25}$$

where e_o is the initial fracture aperture and e is the current fracture aperture, V_j is the stress to fracture stiffness ratio, $\sigma_n{}'$ is the normal fracture effective stress, k_{ni} is the initial normal fracture stiffness, k_{fr} is the initial fracture permeability and V_m is the minimum fracture aperture.

3.3.2 Model description and input parameters

The CMG-GEM software has been employed for modeling the coupled two-phase flow and deformation of Biyadh sandstone reservoir. In this investigation, the modeling procedure is primarily focused on determining the changes in the pore pressure and ground uplift caused by carbon dioxide injection into the reservoir. The Biyadh sandstone reservoir is located above the Arab Jubaila carbonate reservoir. The geological locations and details of the depths of different geological layers above and below the Biyadh reservoir are shown in Figure 3.1. As shown in Figure 3.17, a simulation model is constructed for Biyadh sandstone reservoir with the injection well located at the center of the reservoir. The three-dimensional layered model of Figure 3.17 represents one under burden layer, a caprock above the Biyadh layer, and six overburden layers.

In this coupled geomechanical modeling procedure, the Biyadh reservoir is treated as a single-porosity structure, while the caprock is modeled as a fractured structure. The dual-permeability modeling in CMG-GEM [89, 92], is performed with the fracture grid blocks activated only in the caprock structure. In this injection process, the fluid transfer takes place only through the matrix blocks and thus the formulation discussed in sections 3.3.1.1 and 3.3.1.2 will be utilized. In this context, the number of grid blocks of the caprock is refined to accurately simulate the fluid flow through the fractures. A total of 19,200 grid blocks are used to construct the model with Cartesian grid type. In the caprock, the Barton-Bandis model is used to calculate the changes in the fracture permeability, while the displacements and pore pressure in the injection zone are calculated at every grid block at each time interval. The injection pressure of 23 MPa was used to inject CO_2 for a period of ten years. All sides of the model were assigned roller

boundary condition to allow motion in the upward direction. Appropriate initial stresses were applied to the reservoir before the onset of carbon dioxide injection. The input parameters used during the modeling are listed in Table 3.8 [60, 70-72, 104-107]. The carbon dioxide injection into Biyadh reservoir represents a case of carbon dioxide injection into a water-filled medium. As CO_2 is injected into the reservoir, it displaces the water in the pores and increases the gas saturation in the vicinity of injection point. In this study the relative permeability curves take into account the reservoir pressure, temperature, and brine salinity [108, 109]. Figure 3.18, shows the permeability curves.

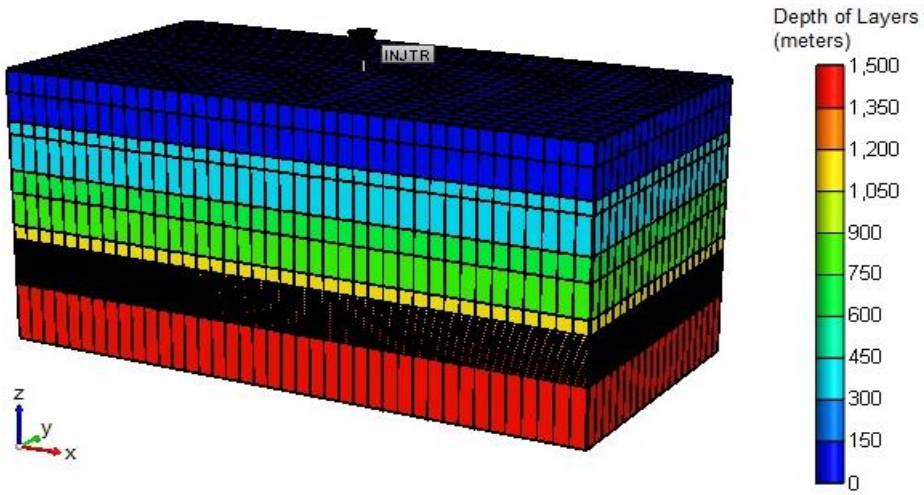

Figure 3.17 Simulation model for Biyadh reservoir with injection well at center of the reservoir

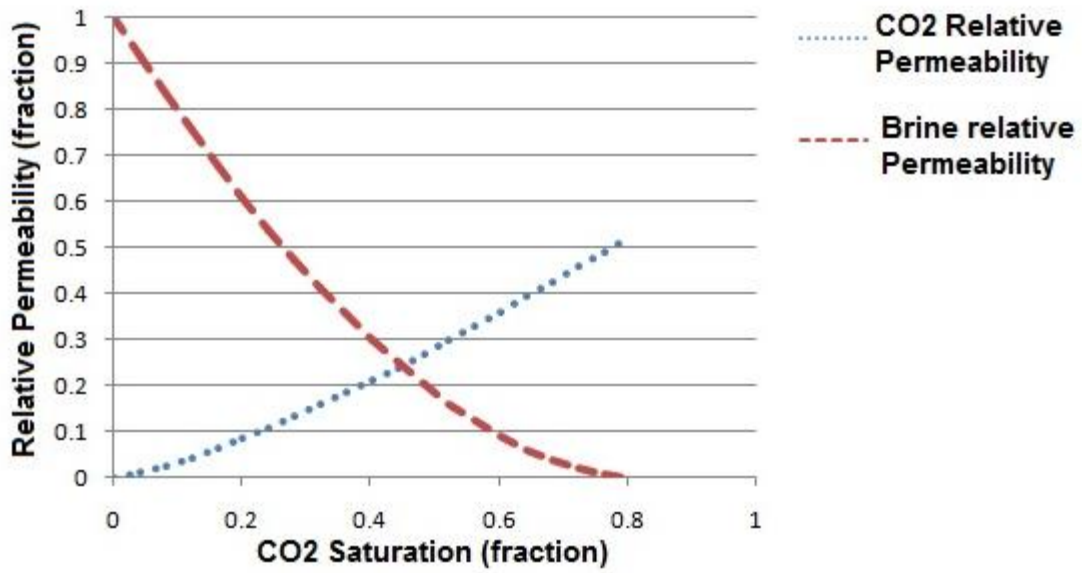

Figure 3.18 Relative permeability curves for CO_2 injection into Biyadh reservoir

Table 3.8 Input parameters for coupled geomechanical modeling of Biyadh reservoir [60, 70-72, 104-107]

Property	**Hofuf Dam Hadrukh**	**Dammam**	**Rus**	**Um Er Radhuma**	**Aruma**	**Wasia**	**Shuaiba**	**Biyadh Sulay**	**Hith Anhydrite**
Layer thickness (m)	150	200	90	250	160	230	100	320	100
Grid top (m)	0	150	350	440	690	850	1080	1180	1500
Rock Density, $\rho(K_g/m^3)$	1877	2289	2280	2020	2090	2270	2030	2360	2960
Young's Modulus, E (GPa)	7	21.43	37.25	21	15.6	27.84	18.1	44.7	42.67
Bulk Modulus, K (GPa)	2.83	11.47	22.8	11.67	7.8	9.82	9.13	25.7	38.2
Shear Modulus, G (GPa)	2.6	8.004	13.91	7.83	5.828	10.4	6.65	17.2	15.932
Initial porosity, $\emptyset_{m0}$	0.2	0.2	0.28	0.24	0.17	0.29	0.09	0.12	0.01
Initial permeability, km0 (10^{-15} m^2)	0.2	0.02	0.25	0.01	0.15	0.2	0.025	0.7	0.00001
Pressure wave velocity, Vp (m/sec)	1835	3110	4260	3310	2730	3230	3010	4040	4480
Shear wave velocity, Vs (m/sec)	1180	1870	2470	1970	1670	2140	1810	2700	2320

3.3.3 Results and discussion

3.3.3.1 Reservoir pore pressure variation with CO_2 injection

The injection of carbon dioxide into the Biyadh reservoir will change both the pore pressure and stress fields. As Biyadh sandstone reservoir is filled with water, the injected carbon dioxide will be stored by displacing water, as well as dissolving into the reservoir's water phase. The increase in the pore pressure primarily affects the reservoir stability if the caprock is not fractured. If the caprock is fractured, then the increase in the reservoir pore pressure tends to activate the already existing fractures in the caprock; thus causing leakage of carbon dioxide into the overburden layers.

A fractured zone is simulated in the caprock to investigate its effect on the pressure response in the reservoir. The fractured zone is simulated by assigning a large value of permeability to the grid blocks in the caprock at a distance of 200 meters from the injection well. The transport of carbon dioxide to the overburden layers is restricted by the impermeable caprock. The simulation results of carbon dioxide saturation are shown in Figure 3.19 for both cases of fractured and non fractured caprock. For the case of non-fractured caprock, carbon dioxide is shown to have been restricted by the caprock to spread only within the reservoir, while for the case of fractured caprock, the carbon dioxide has leaked into the overburden layers.

The pressure response will show the leakage of CO_2 from the reservoir. In Figure 3.20, the pressure response of the reservoir is shown for both cases of the fractured and non-fractured caprock. Pressure buildup is higher in the case of non-fractured caprock and is lower in the case of fractured caprock due to the leakage of the pressurized CO_2 into the overburden layers. The leakage of CO_2 to the overburden layers will increase the local

pore pressure. In the current investigation, carbon dioxide is injected for a period of 10 years. The pore pressure increase due to carbon dioxide injection during this injection period is shown in Figure 3.21. Here, the injection pressure is varied in the range of 23-27 MPa for both fractured and non-fractured cases. It can be concluded from Figure 3.21 that the pore pressure increase is higher when the carbon dioxide flow is restricted by the caprock, and attains a comparatively lower value for the fractured caprock.

It is also important to examine the effect of the location of the fracture zone in the caprock on the magnitude of the pore pressure in the overburden layers. The magnitude of the pore pressure in Wasia overburden layer above the caprock is shown in Figure 3.22 for fractured zone at a distance of 200, 400, and 600 meters from the injection well. It can be observed that the magnitude of the pore pressure reaches relatively higher values as the fractured zone gets closer to the injection well.

(a)

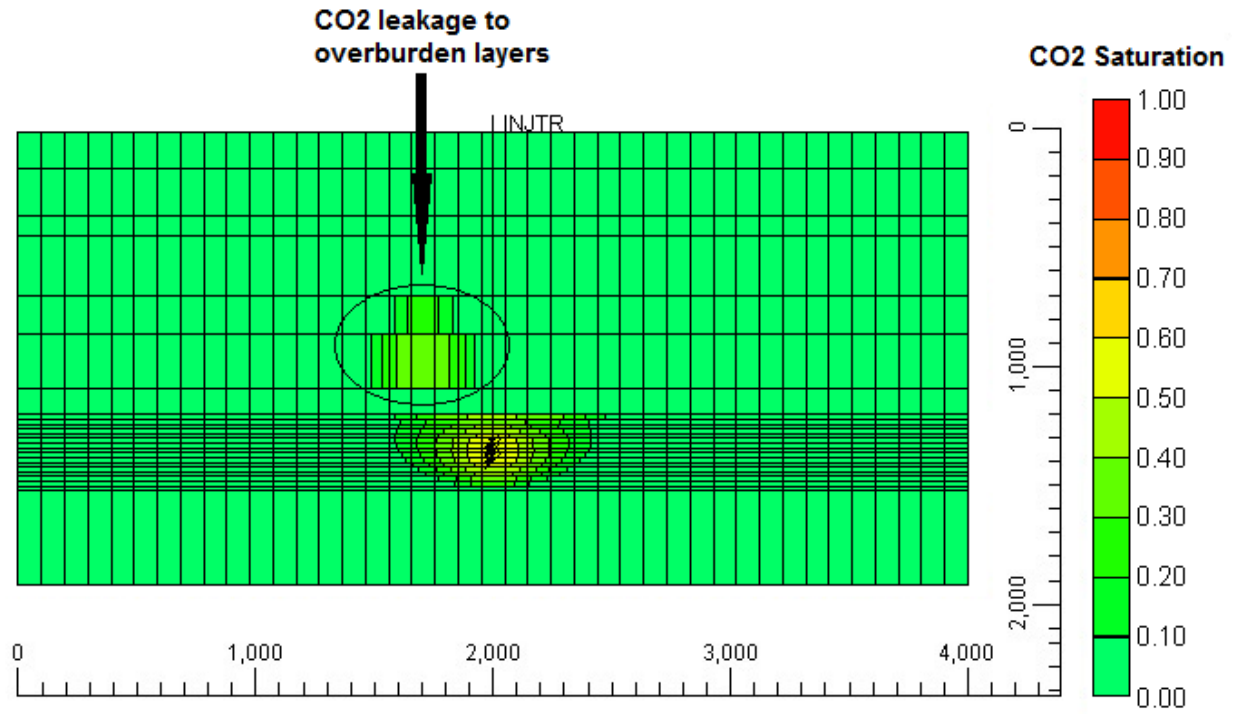

(b)

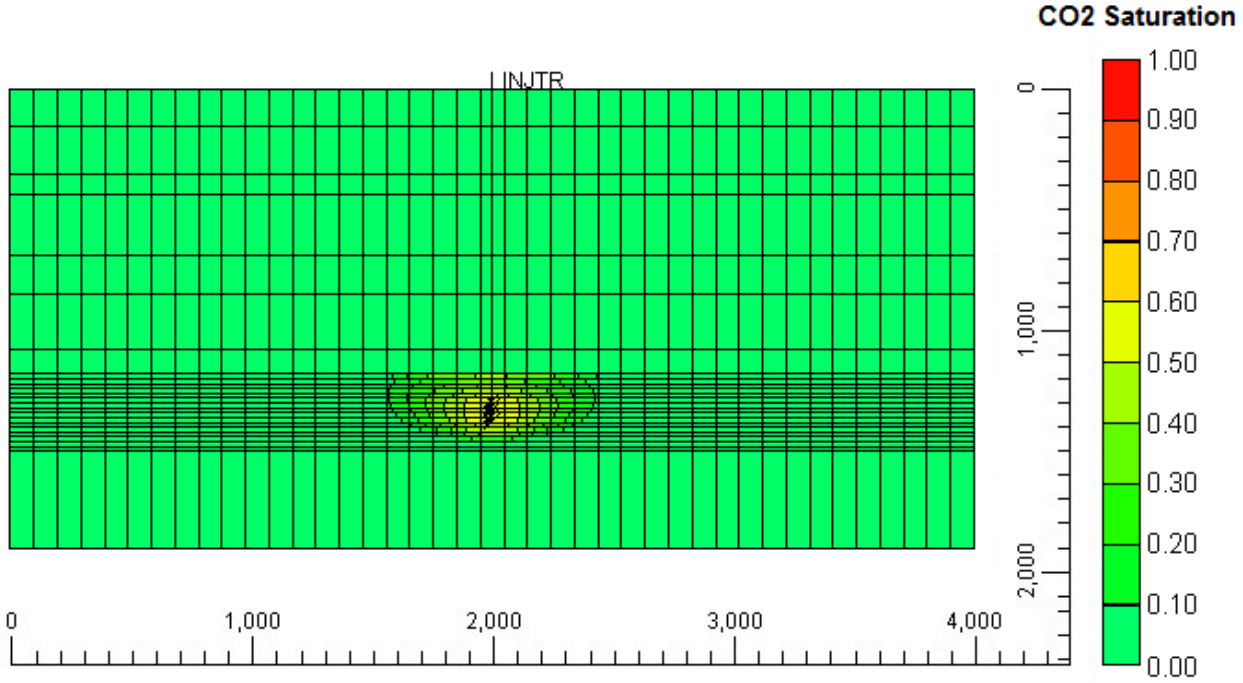

Figure 3.19 Carbon dioxide saturation in the reservoir (a) fractured caprock (b) non-fractured caprock

(a)

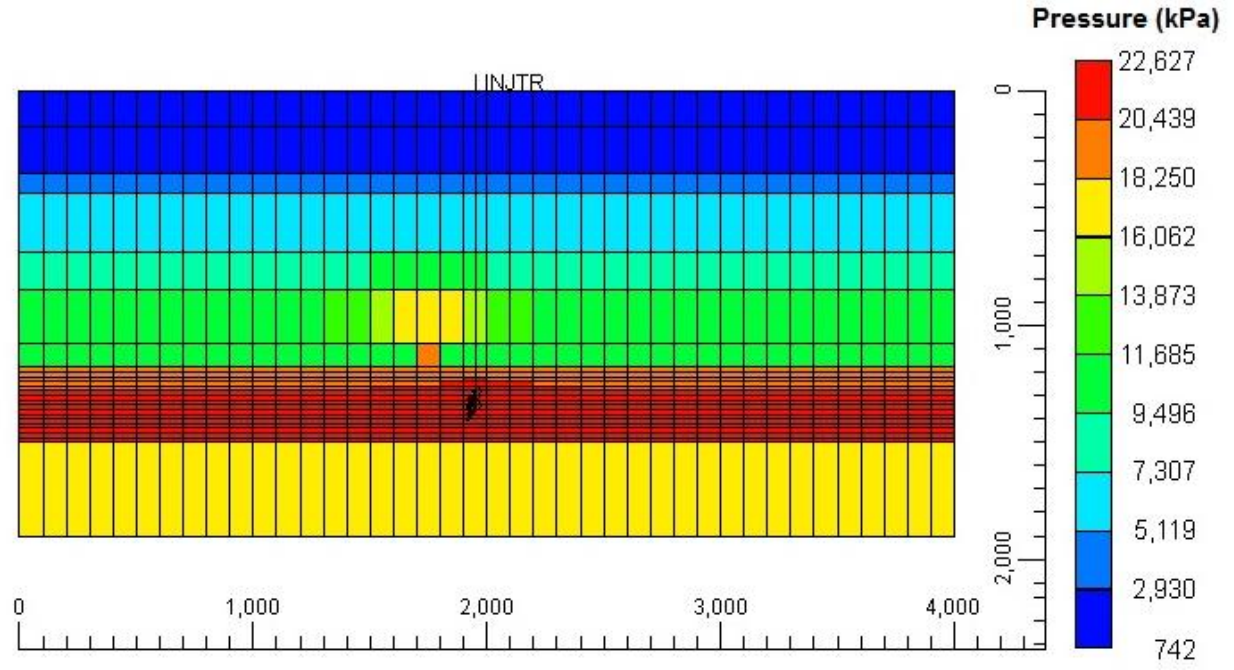

(b)

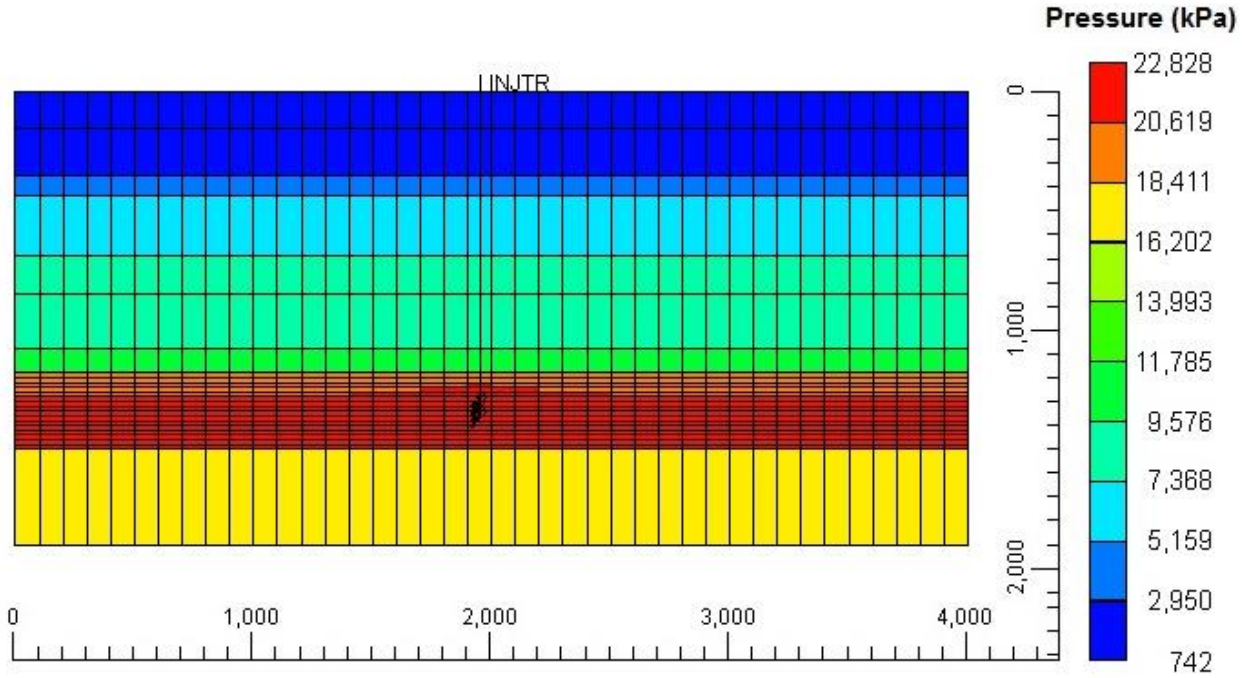

Figure 3.20 Reservoir pressure response during CO_2 injection (a) fractured caprock (b) non-fractured caprock

(a)

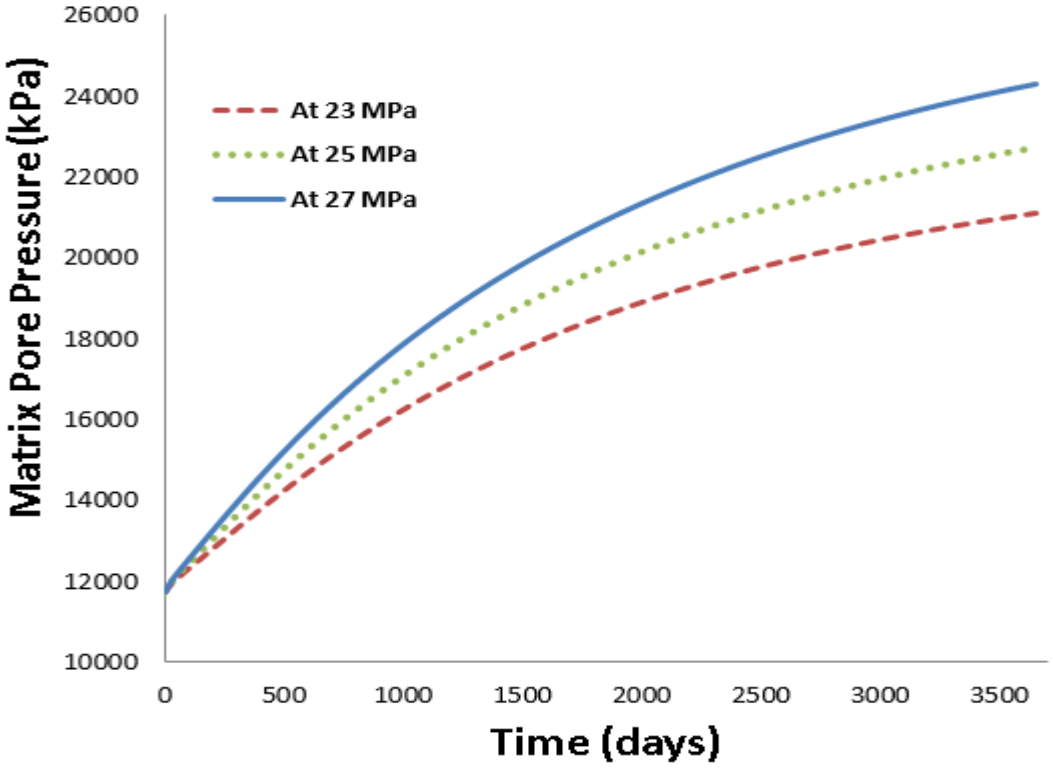

(b)

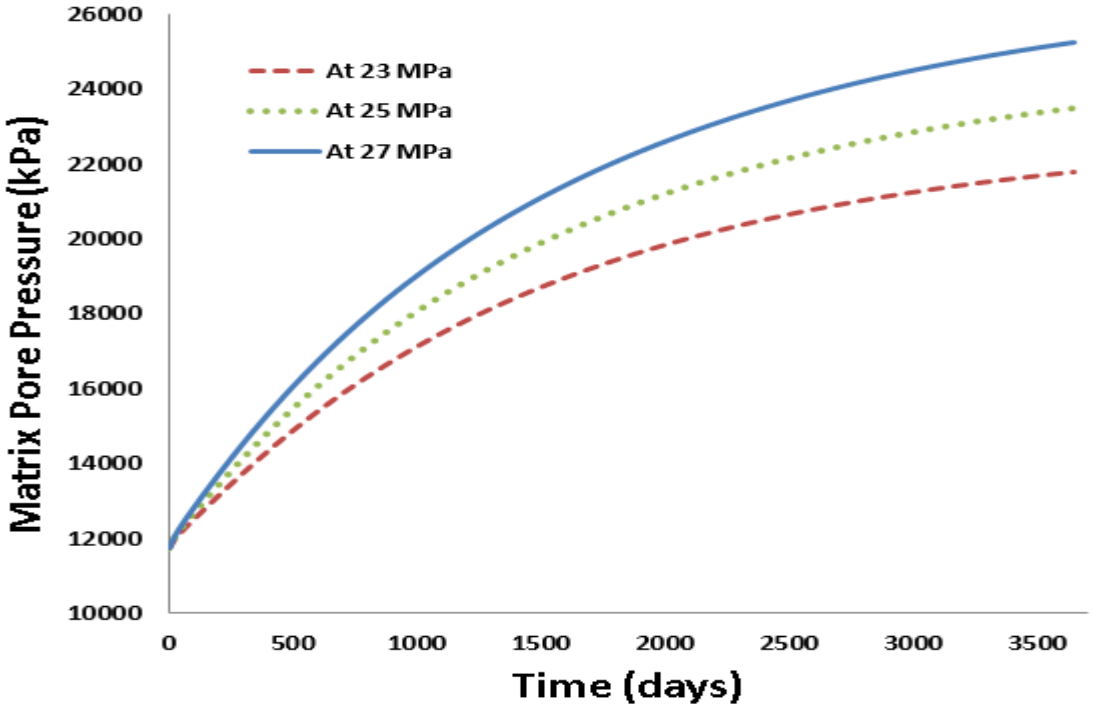

Figure 3.21 Pore pressure variation for 10-year injection period (a) fractured caprock (b) non-fractured caprock

(a)

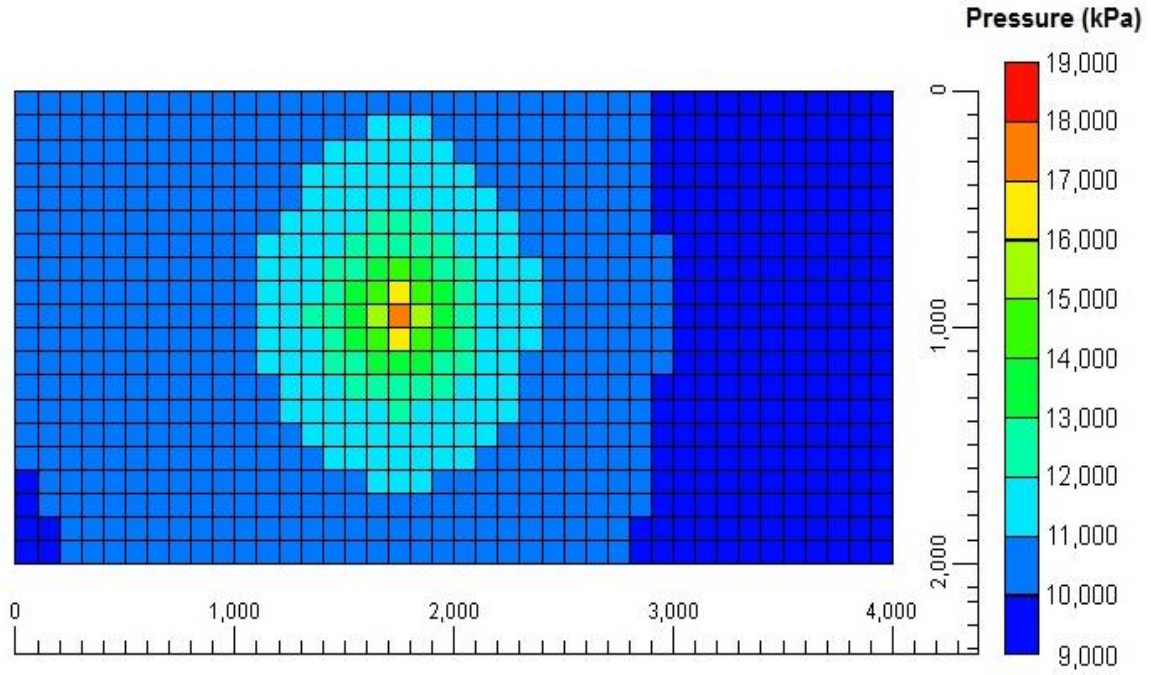
Pressure (kPa)
19,000
18,000
17,000
16,000
15,000
14,000
13,000
12,000
11,000
10,000
9,000
0
1,000
2,000
3,000
4,000
0
1,000
2,000

(b)

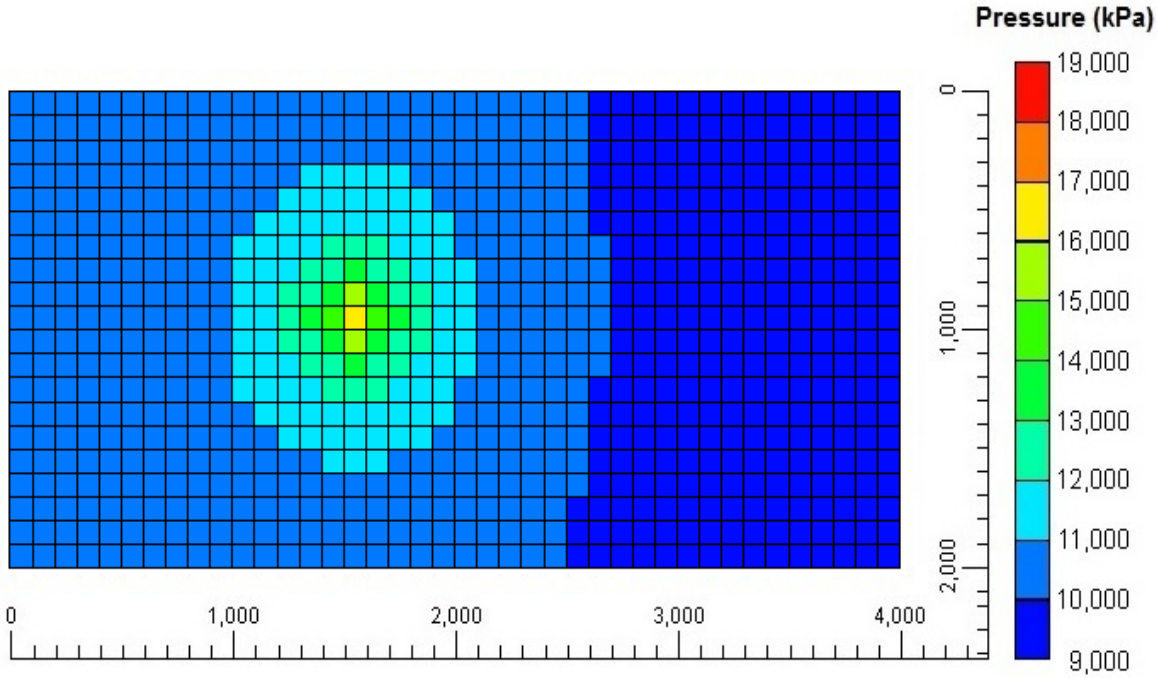
Pressure (kPa)
19,000
18,000
17,000
16,000
15,000
14,000
13,000
12,000
11,000
10,000
9,000
0
1,000
2,000
3,000
4,000
0
1,000
2,000

(c)

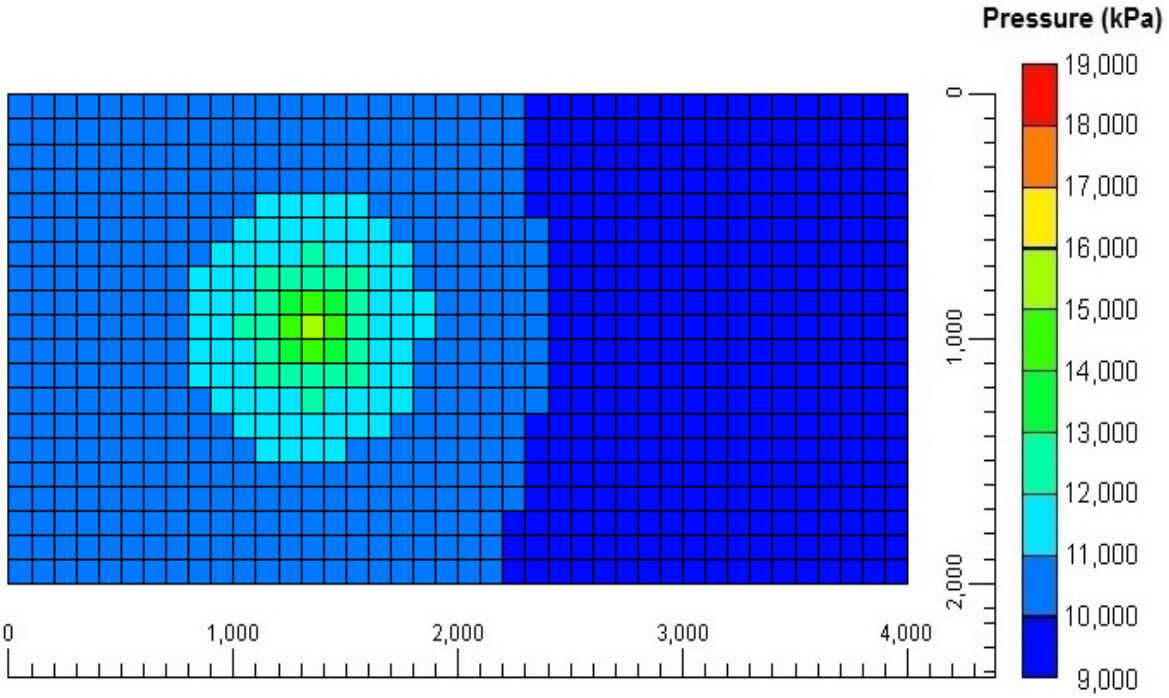

Figure 3.22 The pore pressure in Wasia overburden layer for a fractured zone spaced from the injection well by (a) at 200 meters (b) at 400 meters (c) at 600 meters

3.3.3.2 Ground uplift during CO_2 injection

The pore pressure increase will cause the deformation of the reservoir, thus causing vertical ground uplift. The vertical ground displacement can be calculated from the geomechanical module in CMG-GEM. For both cases of the fractured and non-fractured caprock, the vertical ground displacement was calculated the 10-year injection period at different injection pressures. In Figure 3.23, it can be seen that for the case of non fractured caprock, the ground vertical displacement attains higher values just above the injection point at the center of the reservoir. However, for the case of fractured caprock, the ground vertical displacement is centered above the fractured zone. It is important to state that the increase in the ground vertical displacement just above the fractured zone helps in identifying the location of the fractured zone in the caprock. The effect of CO_2 injection pressure is shown in Figure 3.24 for both cases of the fractured and non-

fractured caprock. As expected, it can be seen that the vertical ground displacement increases as the injection pressure increases.

There is a huge influence of fractured zone permeability on the amount of carbon dioxide leakage to the overburden layers and consequently on the vertical ground uplift. To evaluate the effect of fracture permeability on vertical ground displacement, a fracture zone in the caprock at 200 meters was considered. The influence of the fractured zone permeability on the vertical ground uplift is shown in Figure 3.25, in which the vertical ground displacement above the fractured zone decreases as the permeability of the fractured zone is decreased. Furthermore, one must examine the effect of the fracture zone location in the caprock on the vertical ground displacement. Figure 3.26 displays the vertical ground displacement for a fractured zone located at 200, 400, and 600 meters, sequentially from the injection well. As noted earlier, the magnitude of the ground uplift is higher when the fractured zone is closer to the injection well.

(a)

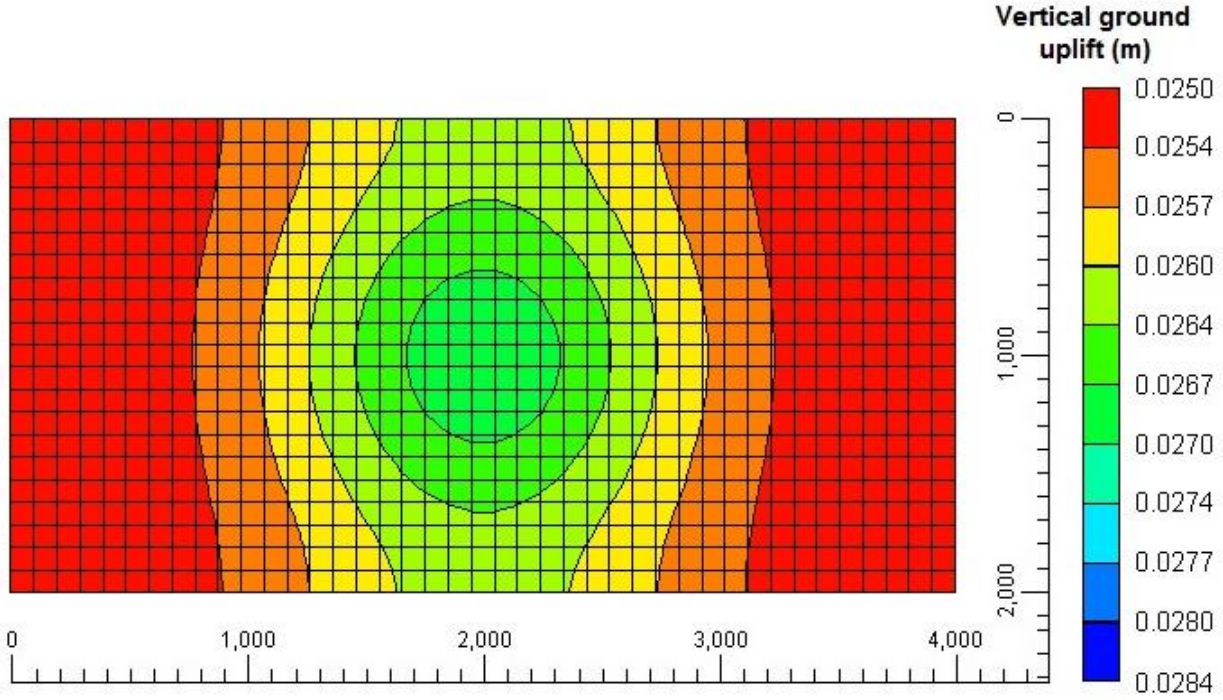

(b)

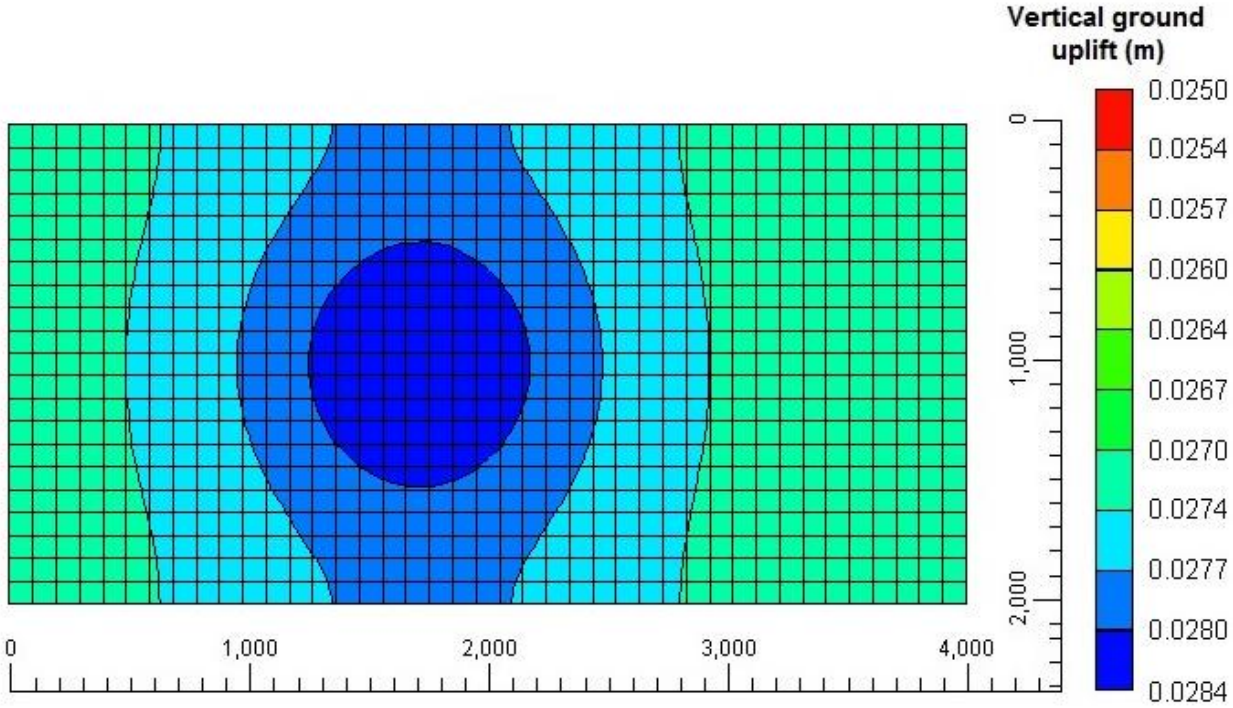

Figure 3.23 Ground vertical displacement for (a) Non-fractured Caprock (b) Fracture at 200 meters from the injection well

(a)

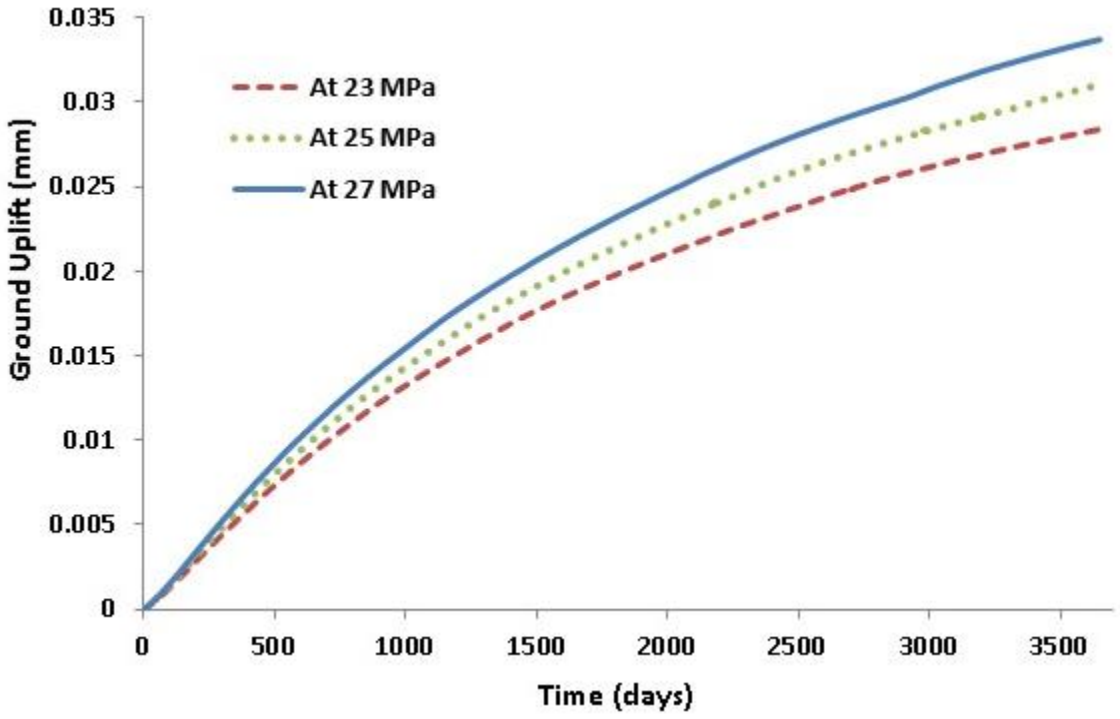

(b)

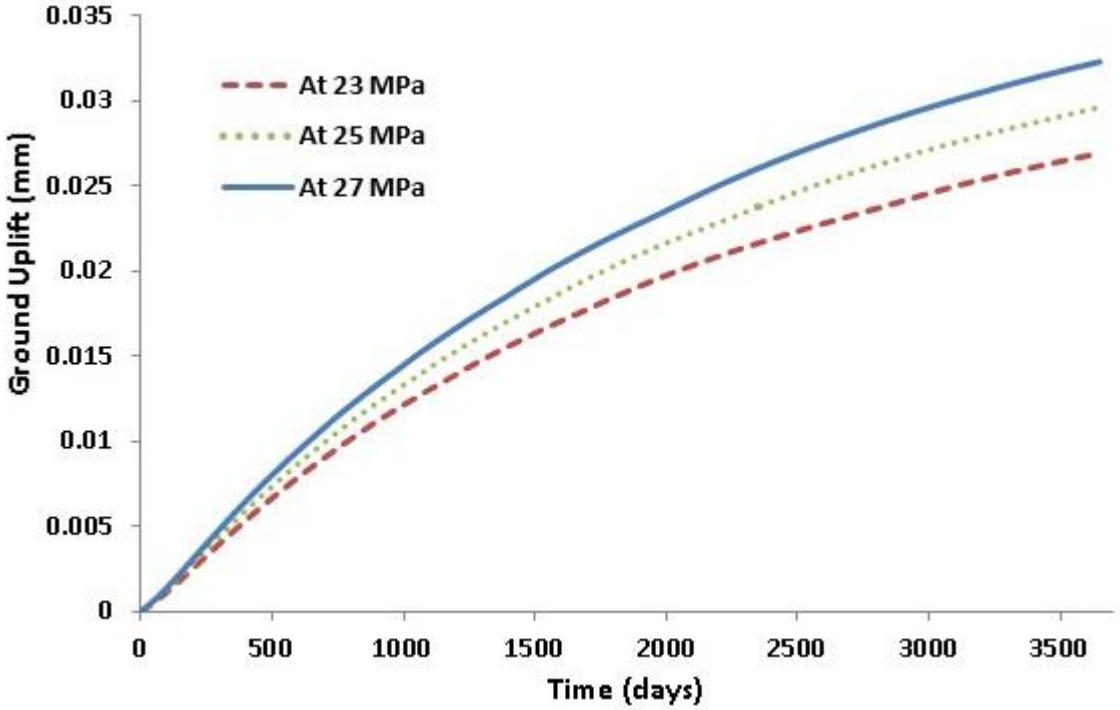

Figure 3.24 Ground vertical displacement during CO_2 injection for 10-year injection period at different injection pressures (a) fractured caprock (b) non-fractured caprock

(a)

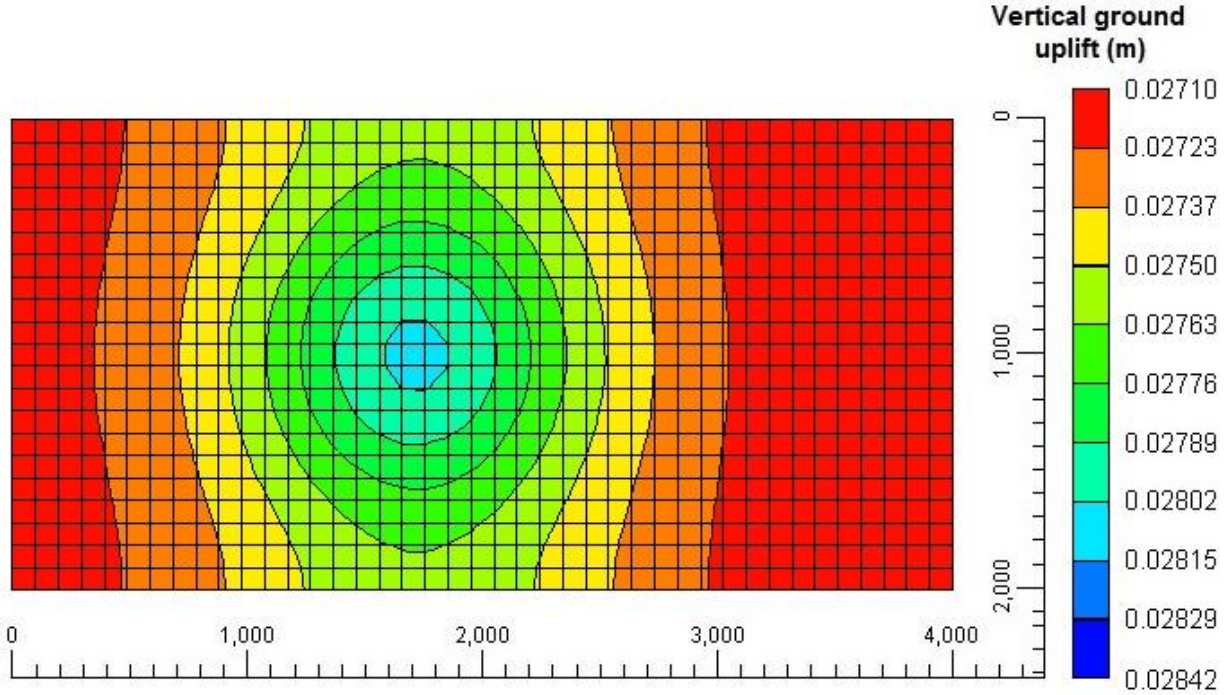

(b)

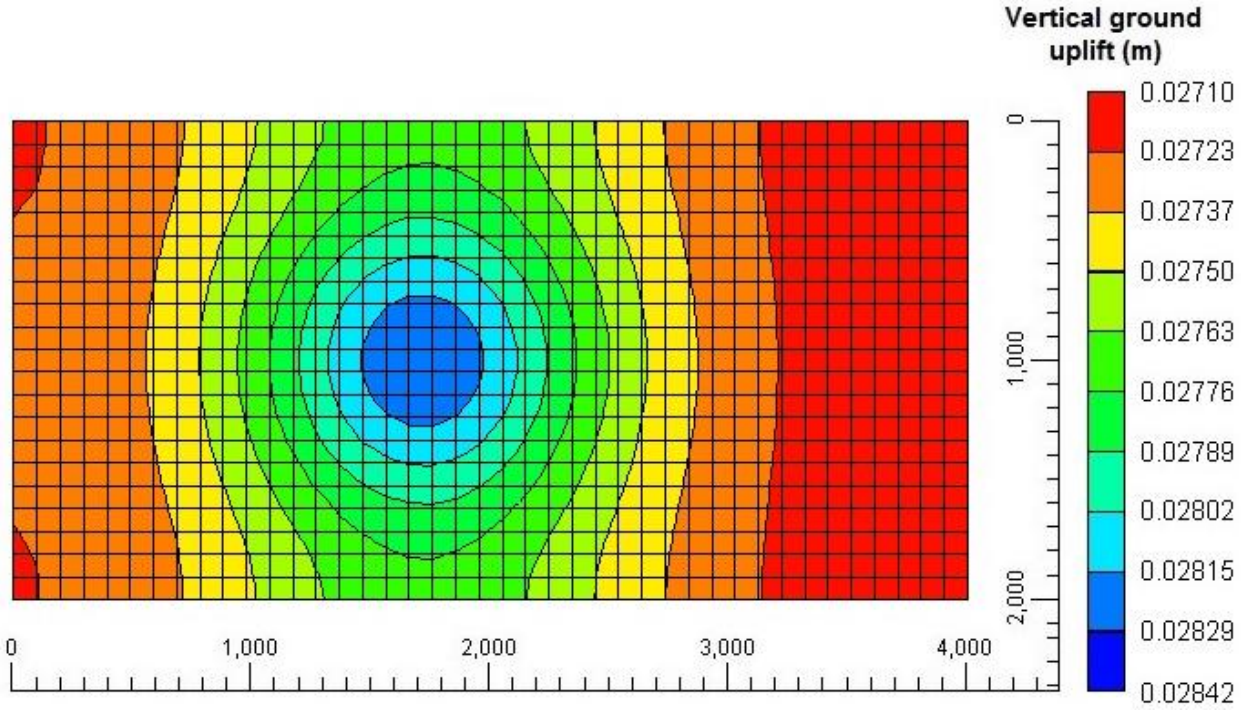
Vertical ground uplift (m)
0.02710
0.02723
0.02737
0.02750
0.02763
0.02776
0.02789
0.02802
0.02815
0.02829
0.02842
0
1,000
2,000
0
1,000
2,000
3,000
4,000

(c)

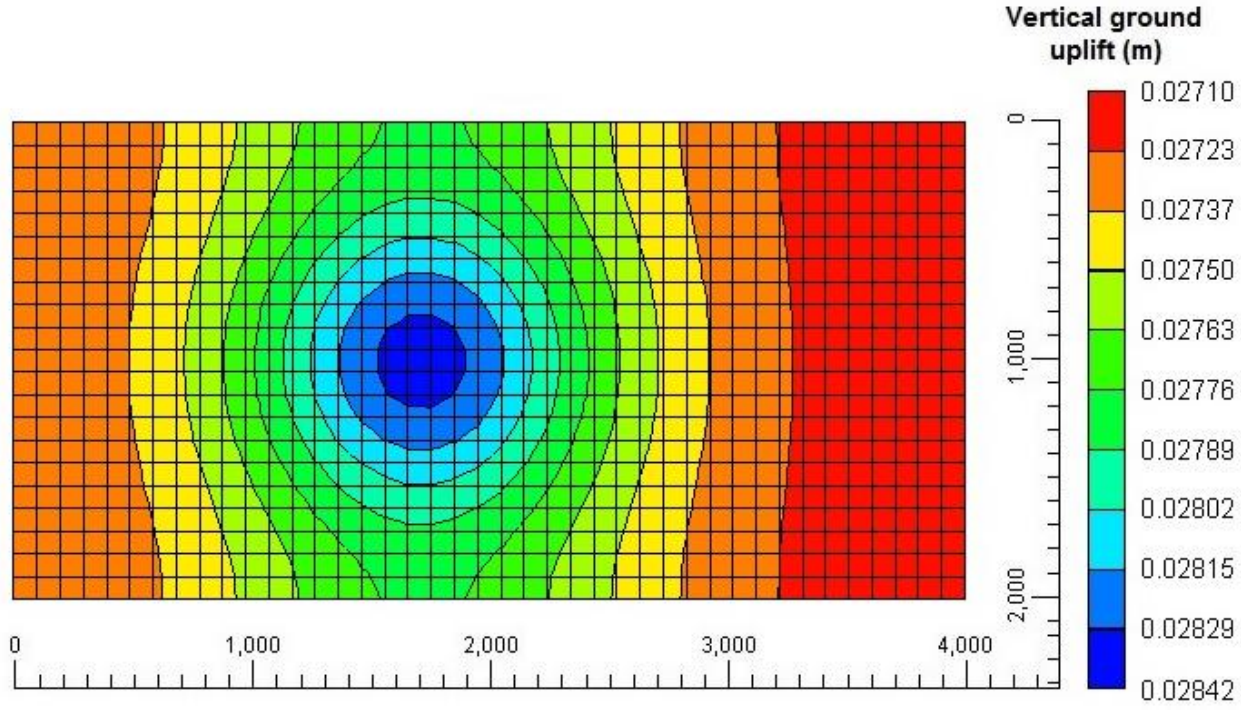
Vertical ground uplift (m)
0.02710
0.02723
0.02737
0.02750
0.02763
0.02776
0.02789
0.02802
0.02815
0.02829
0.02842
0
1,000
2,000
0
1,000
2,000
3,000
4,000

(d)

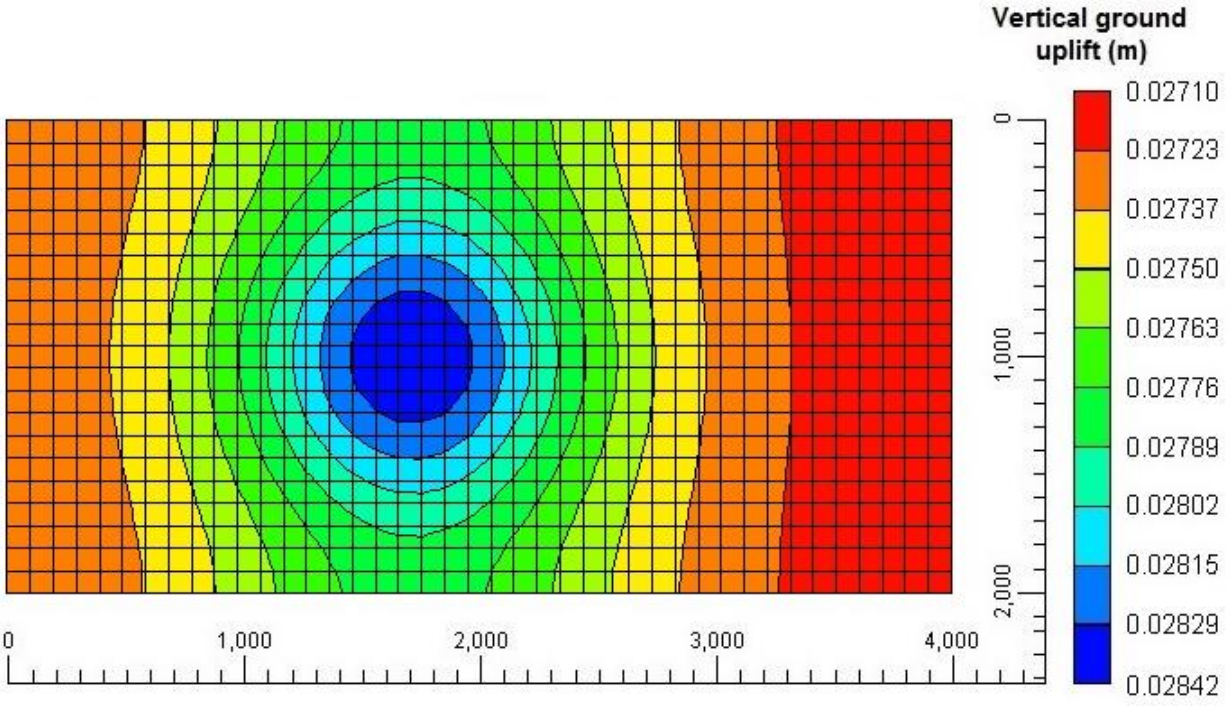

Figure 3.25 Influence of fractured zone permeability on vertical ground uplift (a) 1 mDarcy (b) 25 mDarcy (c) 50 mDarcy (d) 100 mDarcy

(a)

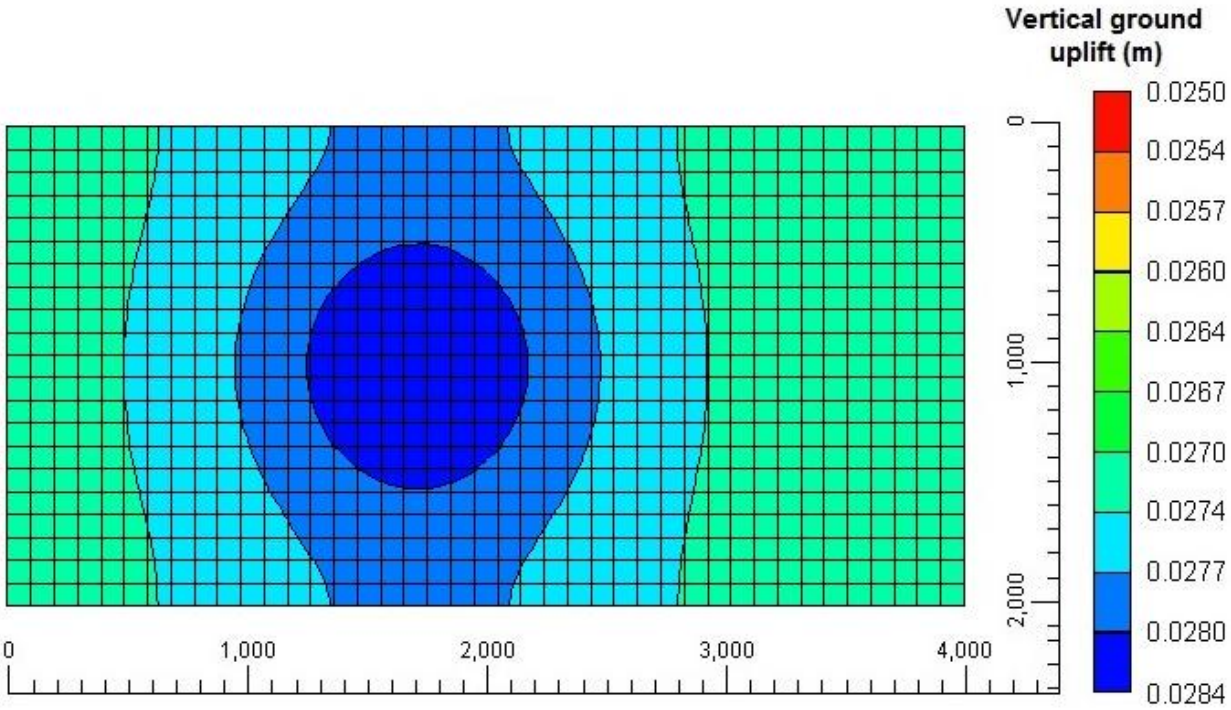

(b)

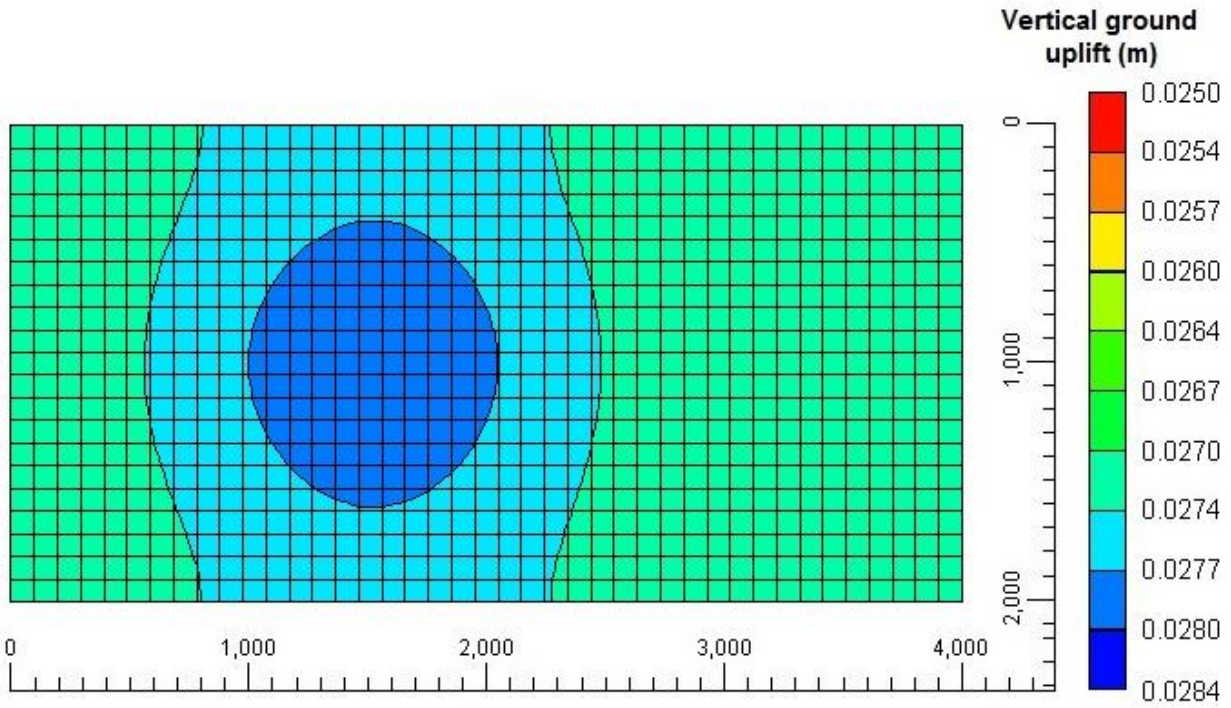

(c)

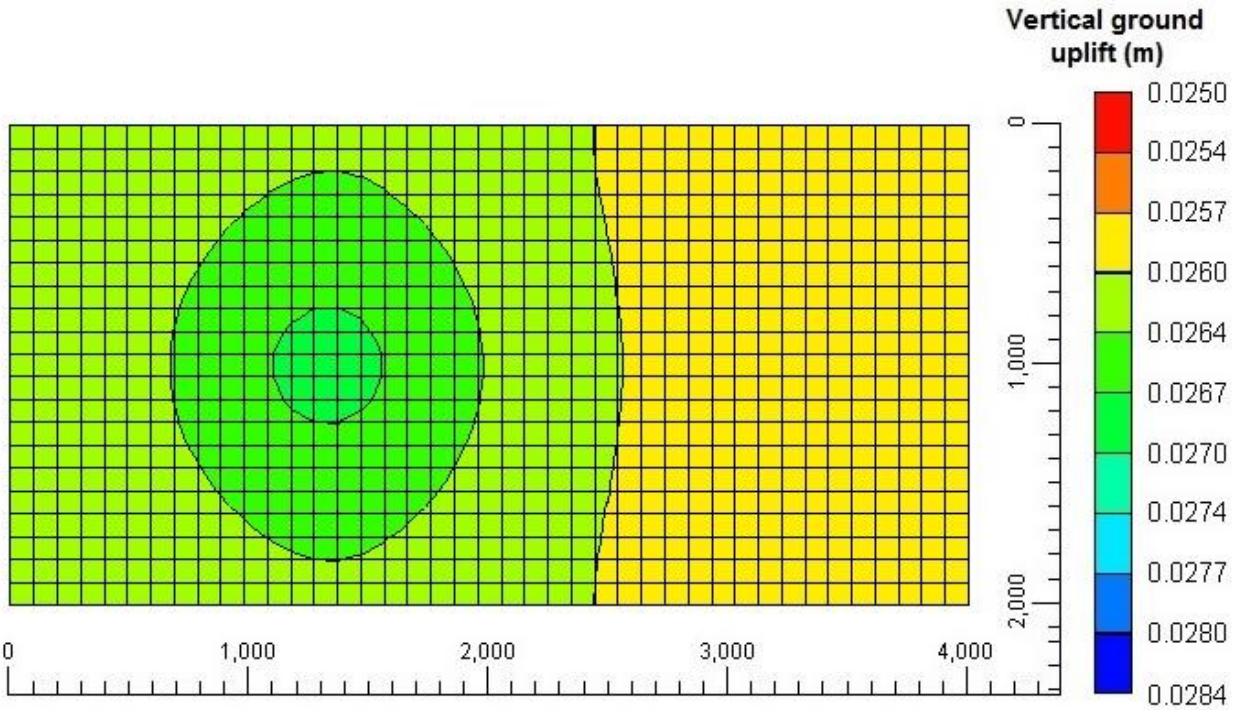

Figure 3.26 The ground uplift for a fractured zone spaced from the injection well by (a) 200 meters (b) 400 meters (c) 600 meters

3.3.3.3 Reservoir coupled stability analysis

In the modeling of CO_2 injection into Biyadh reservoir, a two-phase flow is considered and the geomechanical analysis is invoked to calculate the corresponding deformation of the reservoir. Figure 3.21, shows that the pore pressure buildup assumes higher values in the case of the non-fractured caprock. The reservoir will fail if the pore pressure reaches a critical value [30, 84]. However, in case of fractured caprock, the pressurized CO_2 is leaked into the overburden layers, thus decreasing the value of the pore pressure.

The Mohr-Coulomb failure criterion is utilized to perform the coupled stability analysis of the reservoir during CO_2 injection. As shown in Figure 3.21, the maximum pressure buildup in the reservoir is recorded at the injection pressure of 27 MPa. The failure envelope for Biyadh reservoir is shown in Figure 3.27 for both fractured and non-fractured caprock structure. The dotted circle in Figure 3.27 shows the initial stressed condition based on the initial pore pressure of 11.9 MPa, the minimum principle stress of 29.63 MPa and maximum principle stress of 37.04 MPa. After ten years of CO_2 injection, the final stressed condition shown in Figure 3.27 indicates that the pressure buildup in the case of fractured caprock is not high enough to cause the failure of the reservoir. This is attributed to CO_2 leakage into the overburden layers, which limits the buildup of pressure. Even for high values of pressure buildup during the case of non-fractured caprock, the reservoir is still stable for the 10-year period of CO_2 injection.

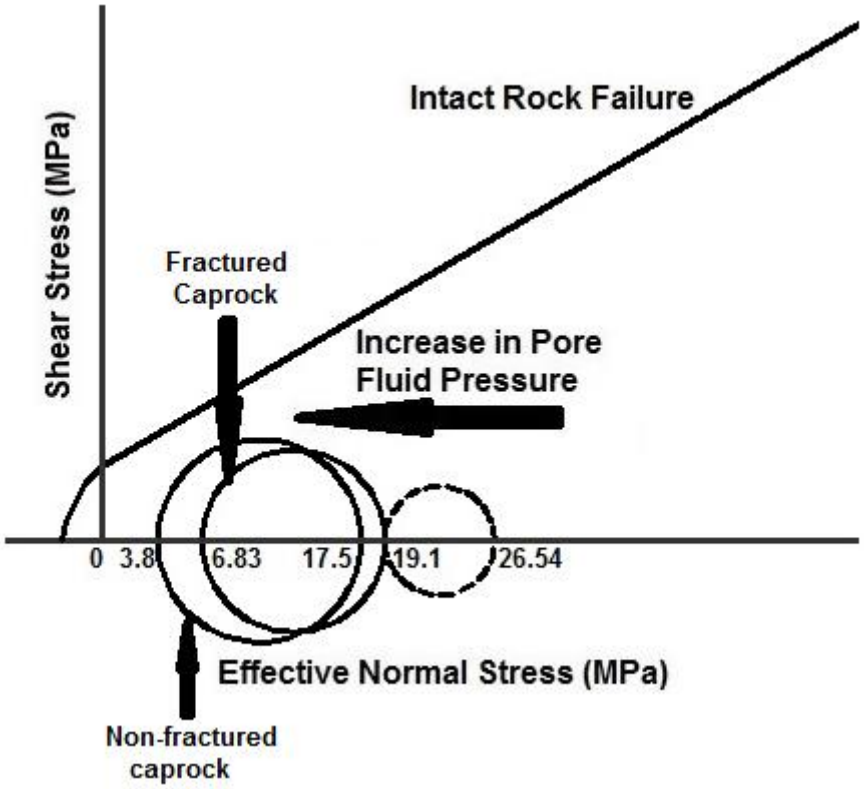

Figure 3.27 Stability of Biyadh reservoir during carbon dioxide injection

This chapter discussed various issues related to the injection of carbon dioxide into single-porosity Biyadh sandstone reservoir with both the single and two-phase flow through the reservoir. The next chapter will discuss the injection of carbon dioxide into naturally fracture Ghawar carbonate reservoir with both single and two-phase flow through the reservoir.

CHAPTER 4

NUMERICAL MODELING OF CO_2 INJECTION INTO A NATURALLY FRACTURED RESERVOIR

4.1 Overview of carbon dioxide injection into naturally fractured reservoir

This chapter starts with discussing the geomechanical modeling of the Ghawar naturally fractured reservoir by considering only single-phase flow in the reservoir. The coupled stability analysis was also performed for the naturally fractured reservoir. A sensitivity analysis was performed in this study to find the critical input parameters. In the second part of the chapter, carbon dioxide injection into the naturally fractured Ghawar reservoir with water in the reservoir was modeled by considering two-phase flow in the reservoir. The reservoir geomechanical and stability analyses were performed first for only injection well in the system and then by considering both injection and production wells in the system. Safe values for CO_2 injection in the Ghawar naturally fractured reservoir were proposed based on the geomechanical and stability analyses.

4.2 Naturally fractured reservoir with single-phase flow

In the coming sections the process of carbon dioxide injection into the naturally fractured reservoir is discussed. The Ghawar naturally fractured carbonate reservoir in Saudi Arabia is considered as a case study and numerical modeling is performed for geomechanical analysis of the reservoir. In this investigation, the COMSOL multi-physics modeling software was utilized to couple the CO_2 flow in the naturally fractured media and its corresponding mechanical impact on the reservoir. In this context, fully coupled non-linear field equations are written to include the sorption-based deformation

of carbonate reservoir during the injection of compressible fluid (CO_2) to the sedimentary reservoir. The current numerical modeling scheme considers the crucial role of the *in situ* stresses and interaction between fracture and matrix in correctly estimating the deformation and stress fields in the naturally fractured carbonate reservoir during CO_2 injection. The change in the stress-displacement field within the reservoir due to the injected compressible CO_2 has been addressed. Moreover, the present investigation extends the previous studies by considering the sorption-based deformation during the injection of the compressed CO_2 fluid into the naturally fractured carbonate reservoir. The sorption-induced strains and the interaction between matrix and fractures have been evaluated. Moreover, the Mohr-Coulomb failure criterion has been utilized to investigate the stability of the reservoir during the coupled process of carbon dioxide injection into the reservoir and the corresponding change in the stress field.

4.2.1 Governing equations for single-phase naturally fractured reservoir

The increase in the pore pressure during carbon dioxide injection causes a change in the effective stresses of the naturally fractured reservoir. This increase in the pore pressure causes a change in the fracture permeability. To include the effect of fractures in the geomechanical formulation for a naturally fractured reservoir, the interaction between the matrix and fracture should be taken into account. Numerical modeling is needed that can relate the pressure build up at the reservoir to changes in the fracture parameters. For naturally fractured reservoirs the mathematical modeling is very complex due to the fact that flow is from two regimes, (i.e. from matrix and fractures [60]. According to Warren and Root, the change in the fracture permeability can be due to the change in the reservoir skeleton stress or it can be a function of the perturbation of the pore pressure.

Hudson and Crampin (1996) [61], used higher-order perturbations in the elastic constants to present a formulation for dual-porosity reservoirs with interconnected cracks. For modeling the flow through the naturally fractured reservoirs, Wu et al. 2010 [103], invoked the same basic assumption of Warren and Root (1963). The carbonate reservoir is modeled by dividing the reservoir into matrix blocks separated by fractures. The fracture aperture (b) and the matrix size (a) change as carbon dioxide is injected into the reservoir, thus changing the reservoir's permeability. The model used by Wu et al. 2010 is adopted in this study for the carbonate reservoir with sufficient different Langmuir constants as given in Table 4.1. The carbonate reservoir is also a naturally fractured reservoir like coal, which can be conceptualized as matrix blocks connected through fractures.

4.2.1.1 Adsorption induced strain and interaction between matrix and fractures

The adsorption of carbon dioxide causes the swelling of the reservoir matrix. The adsorption-induced strain is highly dependent on the matrix pore pressure. The increase in the pore pressure causes the volumetric expansion of the reservoir, which causes a volumetric strain in the reservoir. Volumetric and sorption induced strains are respectively defined as [103]:

$$\varepsilon_v = \frac{\sigma_e^m}{K} + \varepsilon_s \tag{4.1}$$

$$\varepsilon_s = \frac{\varepsilon_L p_m}{p_m + p_L} \tag{4.2}$$

The flow from the fractures to the matrix is a dynamic phenomenon, which depends on the pressure difference between the fractures and matrix. The flow from the fractures to the matrix is given by the following relation:

$$\text{Flow from fractures to matrix} = \omega(p_f - p_m) \tag{4.3}$$

Where ω is a coefficient that takes into account the flow between fractures and matrix. The term ω is given as:

$$\omega = 8\left(1 + \frac{2}{a^2}\right)\frac{k_m}{\mu} \tag{4.4}$$

where k_m is the matrix permeability, a is the matrix element width, and μ is the viscosity of carbon dioxide.

4.2.1.2 Porosity and Permeability of matrix and fractures

The two main factors that affect the permeability and porosity of matrix and fractures are the change in the effective stresses caused by the increase in pore pressure and adsorption induced swelling of the reservoir matrix. The dynamic porosity model for the matrix can be defined as [110]:

$$\emptyset_m = \frac{1}{1+S}[(1 + S_0)\emptyset_{m0} + \alpha(S - S_0)] \tag{4.5}$$

Where

$$S = \varepsilon_v + \frac{p_m}{K_s} - \varepsilon_s \tag{4.6}$$

$$S_0 = \frac{p_{m0}}{K_s} - \frac{\varepsilon_L p_{m0}}{p_{m0} + p_L} \tag{4.7}$$

The permeability can be related to the porosity using the following expression [111, 112]:

$$\frac{k}{k_0} = \left(\frac{\emptyset}{\emptyset_0}\right)^3 \tag{4.8}$$

Upon substituting the porosity model in equation (4.8), the dynamic permeability model for the matrix can be derived as:

$$\frac{k_m}{k_{m\,0}} = \left(\frac{1}{\emptyset_0(1+S)}[\emptyset_0(1+S_0) + \alpha(S-S_0)]\right)^3 \tag{4.9}$$

The subscript "0" is for the initial value of the variables. The porosity for the fracture system is given as:

$$\emptyset_{f0} = \frac{3b}{a} \tag{4.10}$$

The dynamic porosity of the fracture is defined as:

$$\emptyset_f = \emptyset_{f0}\exp\left[\frac{\sigma_e^f - \sigma_e^{f0}}{K_n} - \frac{\sigma_e^m - \sigma_e^{m\,0}}{K_s} - (\varepsilon_s - \varepsilon_s^0)\right] \tag{4.11}$$

The cubic law can be used to find the fracture permeability as [113],

$$k_{f0} = \frac{b^3}{12a} \tag{4.12}$$

The dynamic permeability of the fracture system is defined as

$$k_f = k_{f0}\exp\left[3\frac{\sigma_e^f - \sigma_e^{f0}}{K_n} - \frac{\sigma_e^m - \sigma_e^{m\,0}}{K_s} - (\varepsilon_s - \varepsilon_s^0)\right] \tag{4.13}$$

4.2.1.3 Coupled field equations

The flow of the CO_2 in the sedimentary reservoir tends to increase the pore pressure in matrix and fracture; thus causing a deformation of the reservoir, as well as a change in the reservoir permeability. The increase in the pore pressure will also cause a change in the horizontal stresses in the reservoir. The coupled field equations of the carbon dioxide flow and the reservoir deformations can be written as [103],

$$G\,u_{i,kk} + \frac{G}{1-2\upsilon}\,u_{k,ki} - \alpha\,p_{m,i} - \beta\,p_{f,i} - K\frac{\varepsilon_L p_L}{(p_m+p_L)^2}p_{m,i} + \ f,i = 0 \tag{4.14}$$

Equation (4.14) shows the dependence of the displacement components along the three Cartesian axes on the change of the reservoir pore pressure, which is associated with the carbon dioxide flow. The equations for the CO_2 flow through the sedimentary reservoir are given by

$$\left[\emptyset_m + \rho_{ga}\rho_c\frac{V_L p_L}{(p_m+p_L)^2} + \frac{(\alpha-\emptyset_m)p_m}{(1+S)K_s} - \frac{(\alpha-\emptyset_m)p_L p_m \varepsilon_L}{(1+S)(p_m+p_L)^2}\right]\frac{\partial p_m}{\partial t} \quad + \quad \nabla.\left(-\frac{k_m}{\mu}p_m\nabla.p_m\right) =$$

$$\omega\,(p_f - p_m) - \frac{(\alpha-\emptyset_m)p_m}{(1+S)}\frac{\partial\varepsilon_v}{\partial t} \tag{4.15}$$

$$\emptyset_f\,(1+\frac{p_f\beta}{K_n})\,\frac{\partial p_f}{\partial t} - \emptyset_f\left(\frac{p_f\alpha}{K_s} + \frac{p_L p_m \varepsilon_L}{(p_m+p_L)^2}\right)\frac{\partial p_m}{\partial t} + \nabla.\left(-\frac{k_f}{\mu}p_f\nabla.p_f\right) = -\omega\,(p_f - p_m) -$$

$$p_f\emptyset_f\,(\frac{1}{K_n} - \frac{1}{K_s})\frac{\partial(\frac{\sigma_{kk}}{3})}{\partial t} \tag{4.16}$$

The porosity and permeability of the matrix and fractures change dynamically with the change in pore pressure [110-112]. In this analysis, the cubic law is utilized to find the dynamic fracture permeability.

4.2.2 Modeling scheme in COMSOL multiphysics

The equation-based modeling scheme in COMSOL Multiphysics software has been utilized for the determination of the pressures in matrix and fractures, displacement components, and the corresponding change in the permeability. In the following sections, we explain the detailed modeling scheme for the carbonate reservoir during CO_2 injection.

4.2.2.1 Model description and input parameters

The location of Arab Jubaila carbonate reservoir and the various overburden and under burden layers are shown in Figure 3.1. Using the available geological data [70], a simulation model of CO_2 injection into the Arab Jubaila limestone reservoir was constructed as shown in Figure 4.1. The location of the injection well is at the center of the model as shown in Figure 4.1.

The model has 6548 domain elements with 53,060 degrees of freedom; comprising four independent variables at each node. The independent variables are two displacement components and two pressures (in matrix and fractures). Appropriate boundary conditions are applied to this coupled rock deformation and carbon dioxide flow problem. The in situ stresses are applied to the model. All the boundaries have no flow condition except the injection well. At the injection well the gas entry pressure is set with a constant value of 30 MPa, which can be changed to study the effect of injection pressure variation on injection well stability. The formation properties and various input parameters are listed in Table 4.1, [70, 72, 104-107]. In the current study CO_2 was injected over a period of five years into a reservoir of length equal to 3,000 meters and width equal to 2,000 meters.

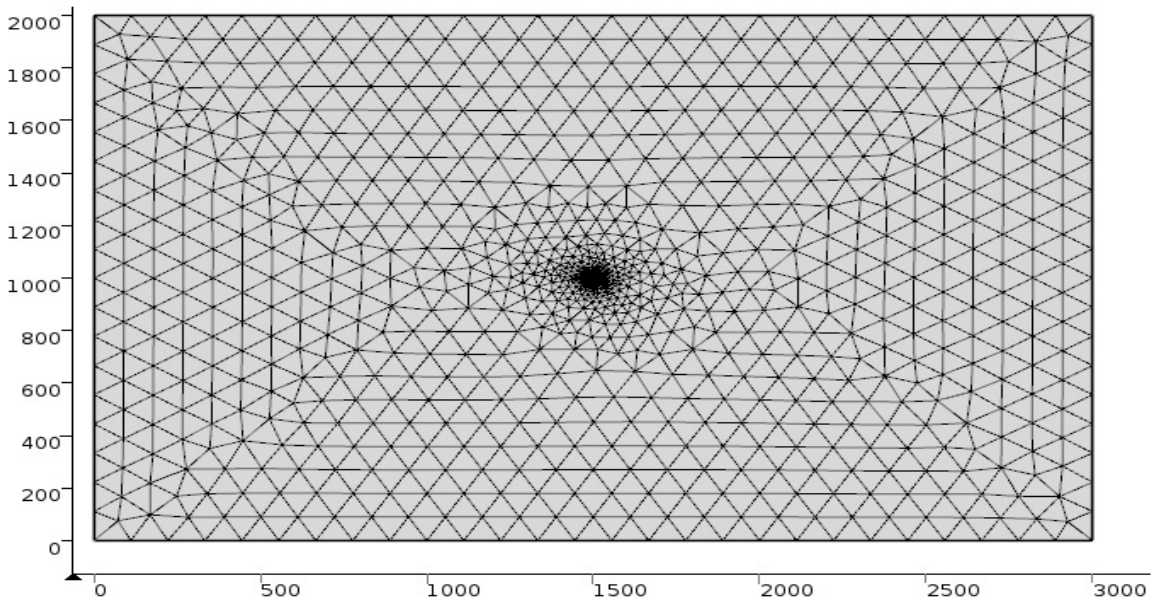

Figure 4.1 Simulation model for the Ghawar Arab-D carbonate petroleum reservoir undergoing CO_2 injection

Table 4.1 Formation properties for the simulation of CO_2 injection in the reservoir ([70, 72, 104-107])

Model Parameter	For Reservoir
Rock Density, $\rho(Kg/m^3)$	2400
Young's Modulus, E (GPa)	48.5
Bulk Modulus, K (GPa)	39.24
Shear Modulus, G (GPa)	18.1
Initial porosity, $\emptyset_m$	0.13
Initial permeability, k_m (10^{-15} m^2)	0.6
Biot Coefficient, α	0.8
Dynamic Viscosity, $\mu(10^{-5}Pa.s)$	1.84
Pressure wave velocity, Vp (m/sec)	5140
Shear wave velocity, Vs (m/sec)	2748
Poisson's ratio (υ)	0.30
Langmuir value for pressure, P_L (MPa)	4.1
Langmuir value for volume, V_L (m^3/kg)	0.01
Langmuir value for volumetric strain, $\boldsymbol{\varepsilon}_L$	0.02
Fracture aperture, b0 (m)	10^{-4}
Matrix size, a0 (m)	0.01

4.2.2.2 Stress regime and pre-stressing of the model

Ghawar oil field is under compressive stress regime as stated by the World stress map [74]. The principal stress direction is compressive, and therefore tends to develop compressive pre-stresses in the Ghawar structure [62]. The pre-stresses in the reservoir structure are due to the gravitational effect and due to the tectonic effects in the 3-dimensional space [76-78]. The three principal directions for the pre-stresses considered are one vertical, and two horizontal directions. For the compressive stress regime, the relationship between these three stresses is given as, $\sigma_H > \sigma_h > \sigma_v$. As the depth increases, the vertical stresses increase due to the weight of the overburden layers. The vertical stress at any depth d is given by

$$\sigma_v = \int_0^d \rho g dz \tag{4.17}$$

For the compressional stress regime, the maximum horizontal stress (σ_H) is the maximum principal stress (σ_1), where $\sigma_1 = \sigma_H = 1.25\sigma_v$. The intermediate principal stress (σ_2) is the minimum horizontal stress (σ_h), where $\sigma_2 = \sigma_h = 1.1\sigma_v$. The minimum principal stress is given by the vertical stress (σ_v). The initial maximum and minimum principal stresses are equal to 46.20 MPa and 36.96 MPa, respectively.

4.2.3 Discussion of results

4.2.3.1 Injection pressure variation

The injection pressure is a key factor during the whole injection process, which controls the infiltration of the injected fluids into the porous reservoir matrix. As the injection pressure increases the pore pressure increases. Therefore, it is necessary to estimate the

safe values for the injection pressure that define the sustainable pore fluid pressures. In the present simulation, the injection pressure for the selected Ghawar carbonate reservoir is varied over the range 30-33 MPa. The simulations are performed using the injection parameters given in Tables 4.1. The spread of carbon dioxide and the corresponding pressure variation are shown in Figure 4.2 for the different periods of injection, wherein the pore pressure increases rapidly during the first three years of carbon dioxide injection and then the rate increases at a slower pace after three years. During the five years of injection, carbon dioxide spreads along the reservoir as shown in Figure 4.2. Since the injection pressure is set at a higher value than the initial pore pressure to facilitate the flow of carbon dioxide into the reservoir, it becomes necessary to evaluate the maximum value of the injection pressure that corresponds to sustainable pore pressures, as explained in the sub-section 4.2.3.2.

The change in volumetric strain in the reservoir is dependent on the change in the effective stresses and sorption-induced strain, which are functions of the matrix pore pressure. The volumetric strain was calculated for various injection pressures and for different periods of injection, as depicted in Figure 4.3. Initially the reservoir is under compression and as the matrix pore pressure increases, the effective stresses starts to decrease and the adsorption induced swelling of the matrix increases. The end effect is an expansion of the reservoir due to the adsorption-induced strains and due to the decrease of the effective stresses with carbon dioxide injection.

One of the key parameters that need to be evaluated after carbon dioxide injection into the reservoir is the change in the permeability of the matrix and fractures, which is highly dependent on the pore pressure change as well as the injection pressure. Moreover,

the adsorption-induced strain affects the value of the permeability. The pressure variation in matrix for a five-year injection period at various injection pressures, and the change in the matrix permeability at various periods of CO_2 injection and with the variation of the matrix pore pressure are shown in Figure 4.4. The permeability of the matrix, for this specific case of carbon dioxide injection increased rapidly at the beginning due to the rapid increase in the matrix pore pressure and the corresponding decrease in the effective stresses; yet with the passage of time, the adsorption induced strains tend to slow down the rate of increase of the permeability. For the five-year injection period, the permeability became almost constant after five years of injection and it start to decrease as the injection period increase. It has been also noted that the adsorption-induced decrease in the permeability is more at higher injection pressures. Moreover, the increase in the matrix pore pressure with carbon dioxide injection causes an increase in the matrix permeability but with the passage of time the adsorption-induced swelling of the matrix causes a decrease in the matrix permeability.

Now, the permeability of the fractures is evaluated. To this end, the pressure variation in fracture for a five-year injection period at various injection pressures, and the change in the facture permeability at various periods of CO_2 injection and with the variation of the fracture pore pressure are shown in Figure 4.5. As compared to the single-porosity medium, the naturally fractured medium; e.g. carbonate reservoir, will also experience pressure variation in the fractures as carbon dioxide injection goes on with time. The pressure variation in the fractures tends to change the permeability of fractures as time passes. The permeability of the fracture, for this specific case of carbon dioxide injection, increased rapidly at the beginning due to the rapid increase in the

fracture pore pressure and the corresponding decrease in the effective stresses; yet with the passage of time, the adsorption induced strains in the matrix tend to slow down the rate of increase of the permeability and with the passage of time the fracture permeability starts to decrease. As demonstrated by the results, the increase in the fracture pore pressure with carbon dioxide injection causes an increase in the fracture permeability but with the passage of time the adsorption induced swelling of the matrix causes a decrease in the fracture permeability.

(a)

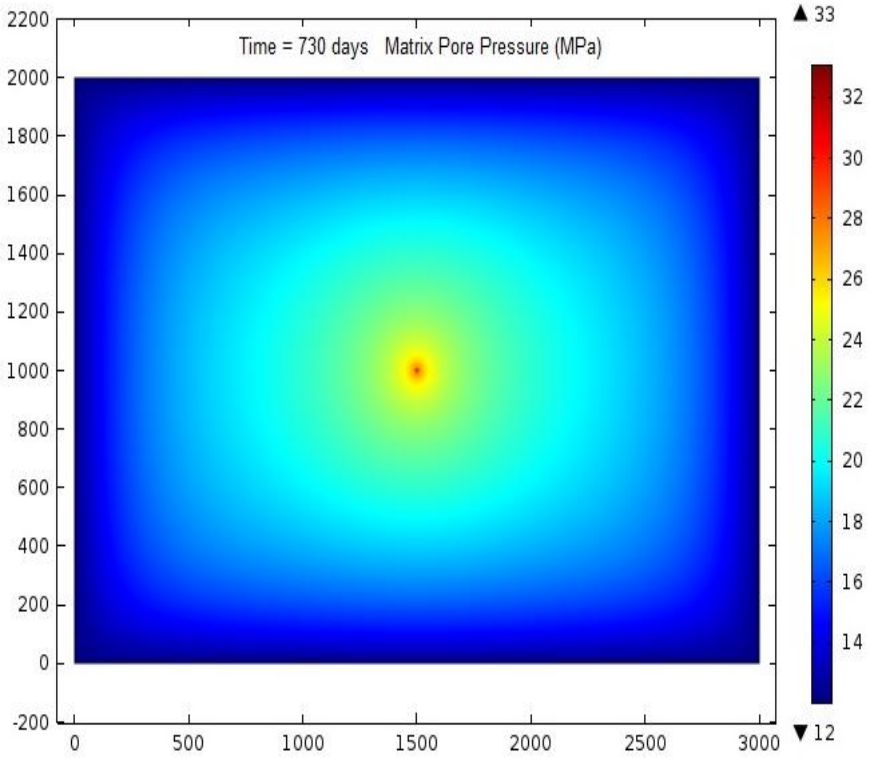

(b)

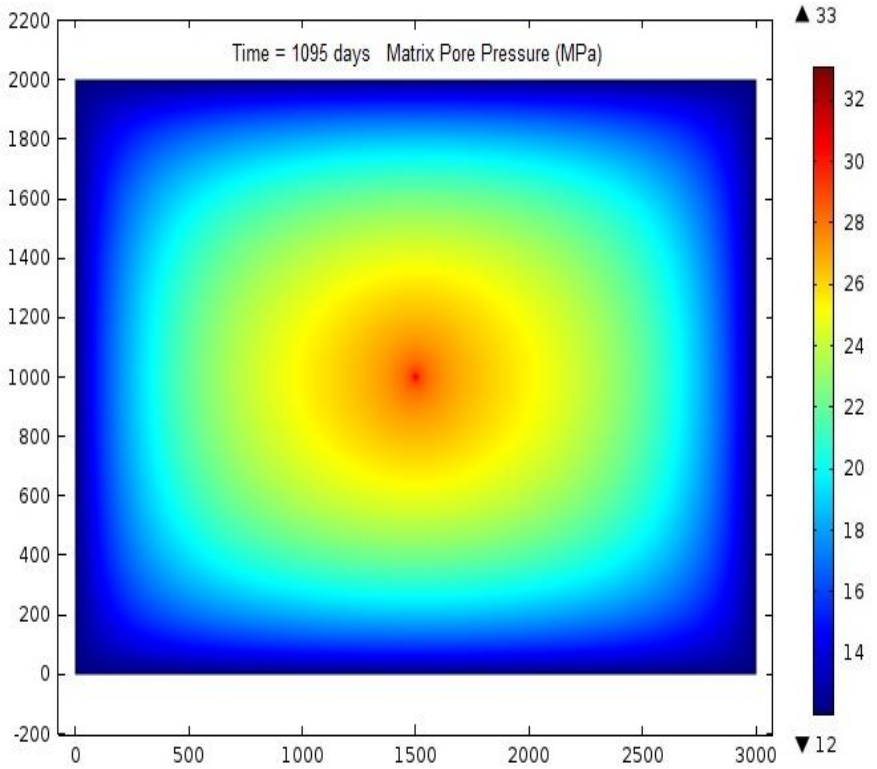
Time = 1095 days Matrix Pore Pressure (MPa)
▲ 33
32
30
28
26
24
22
20
18
16
14
▼ 12
2200
2000
1800
1600
1400
1200
1000
800
600
400
200
0
-200
0
500
1000
1500
2000
2500
3000

(c)

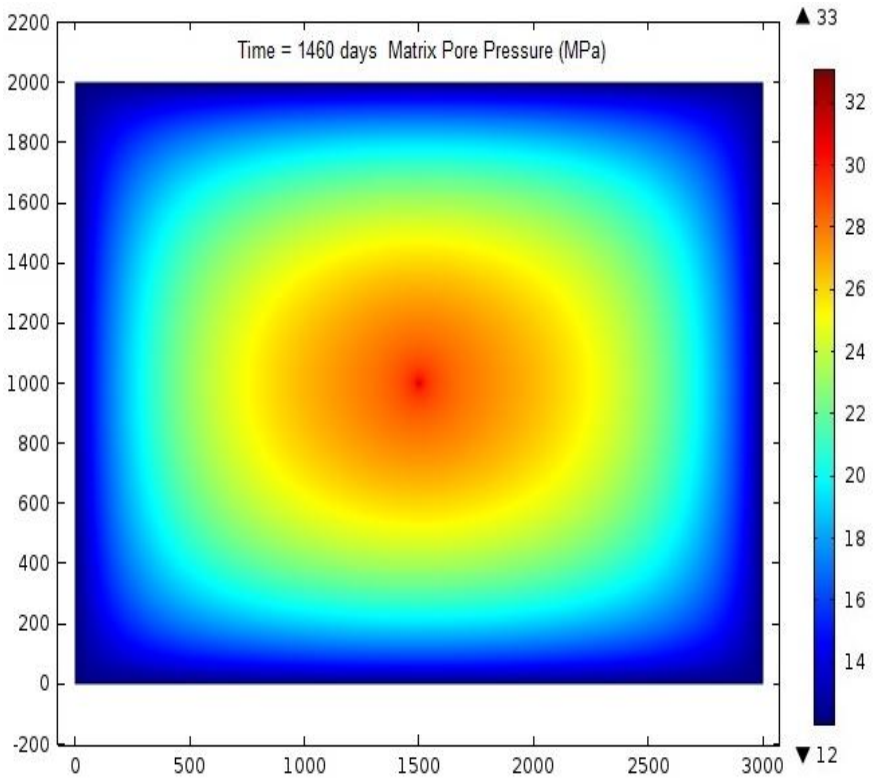
Time = 1460 days Matrix Pore Pressure (MPa)
▲ 33
32
30
28
26
24
22
20
18
16
14
▼ 12
2200
2000
1800
1600
1400
1200
1000
800
600
400
200
0
-200
0
500
1000
1500
2000
2500
3000

(d)

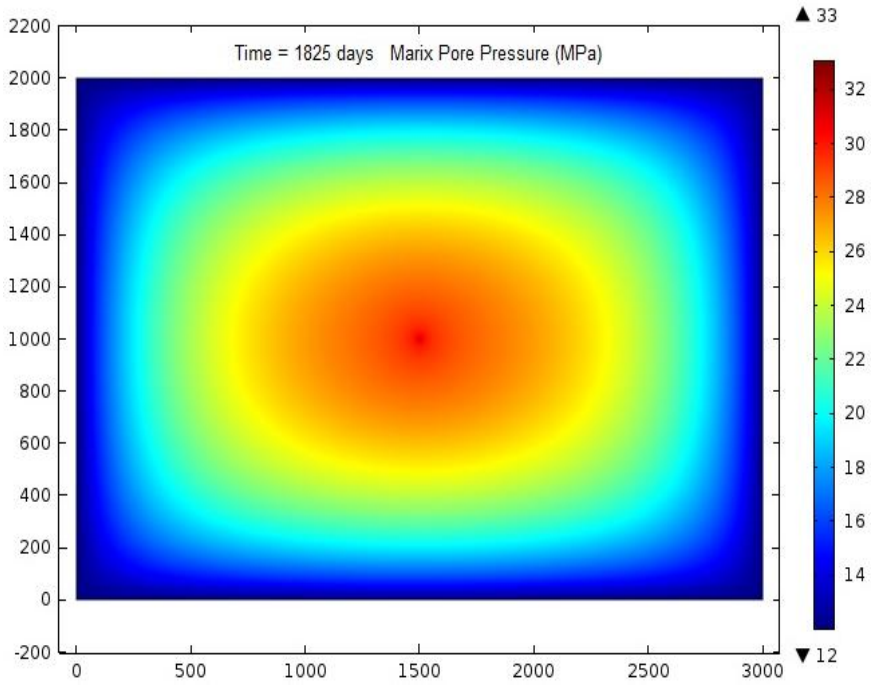

Figure 4.2 The spread of carbon dioxide and the corresponding pressure variation for various periods of injection (a) After two years (b) After three years (c) After four years (d) After five years

(a)

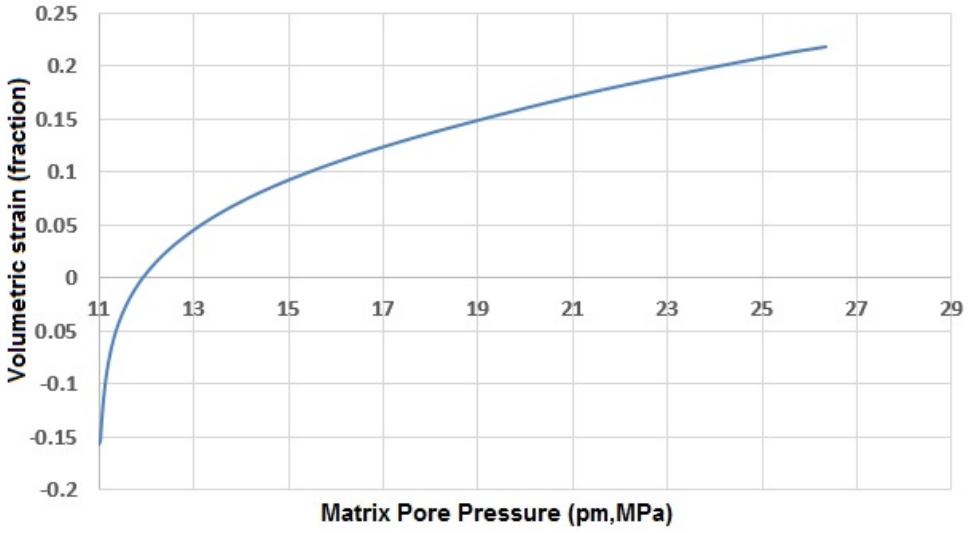

(b)

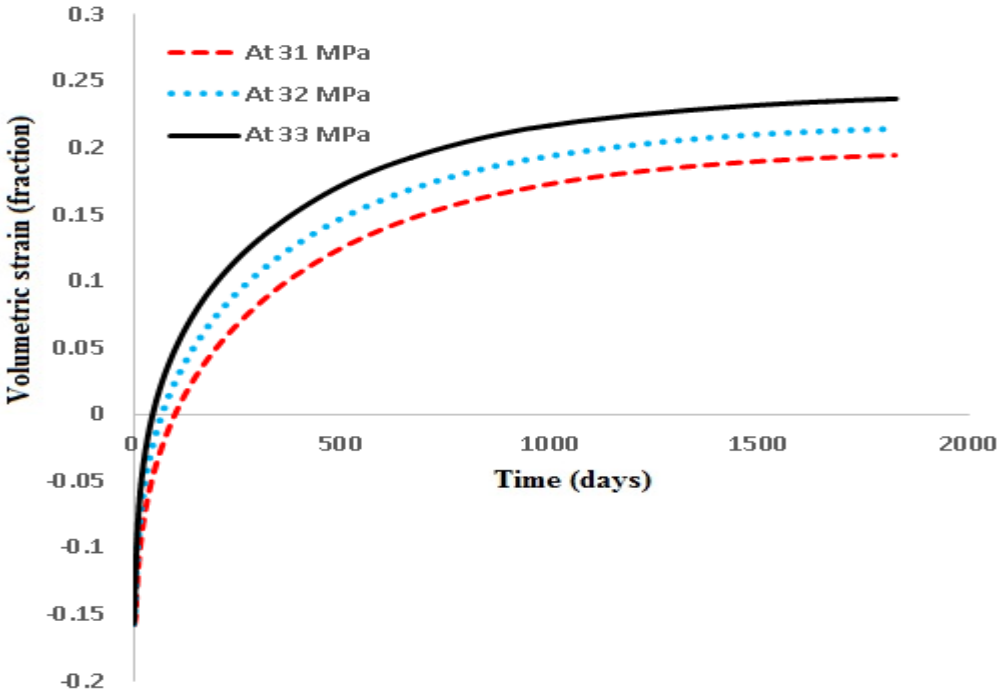

Figure 4.3 (a) The change in volumetric strain with the increase of matrix pore pressure (b) The volumetric strain for a five-year injection period at various injection pressures

(a)

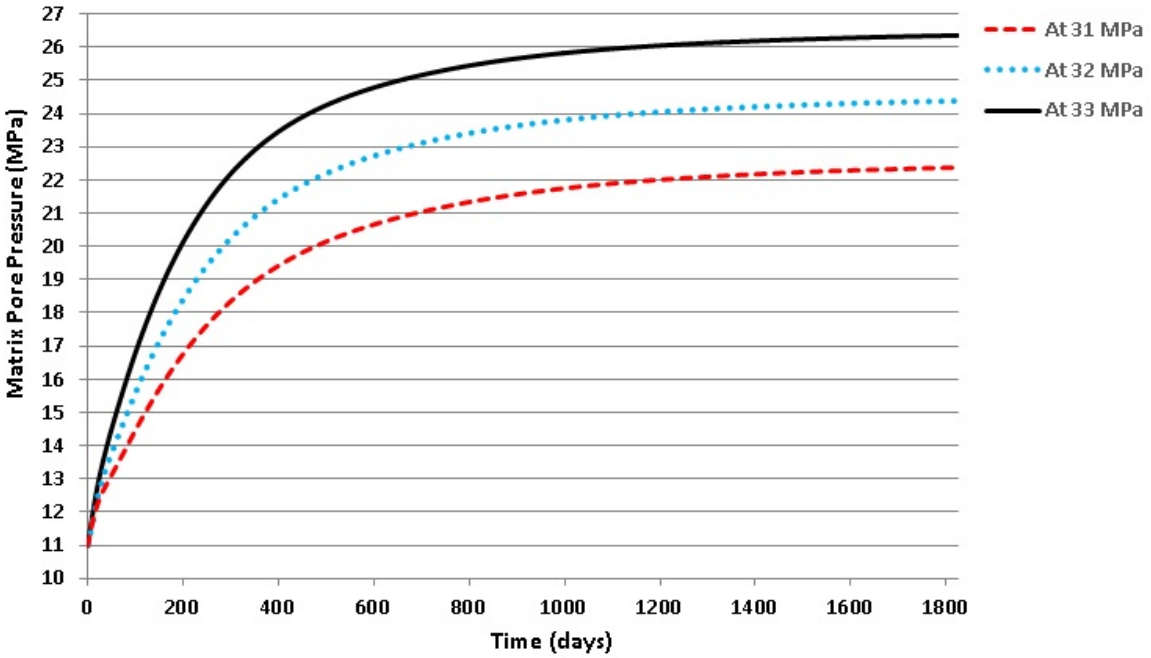

(b)

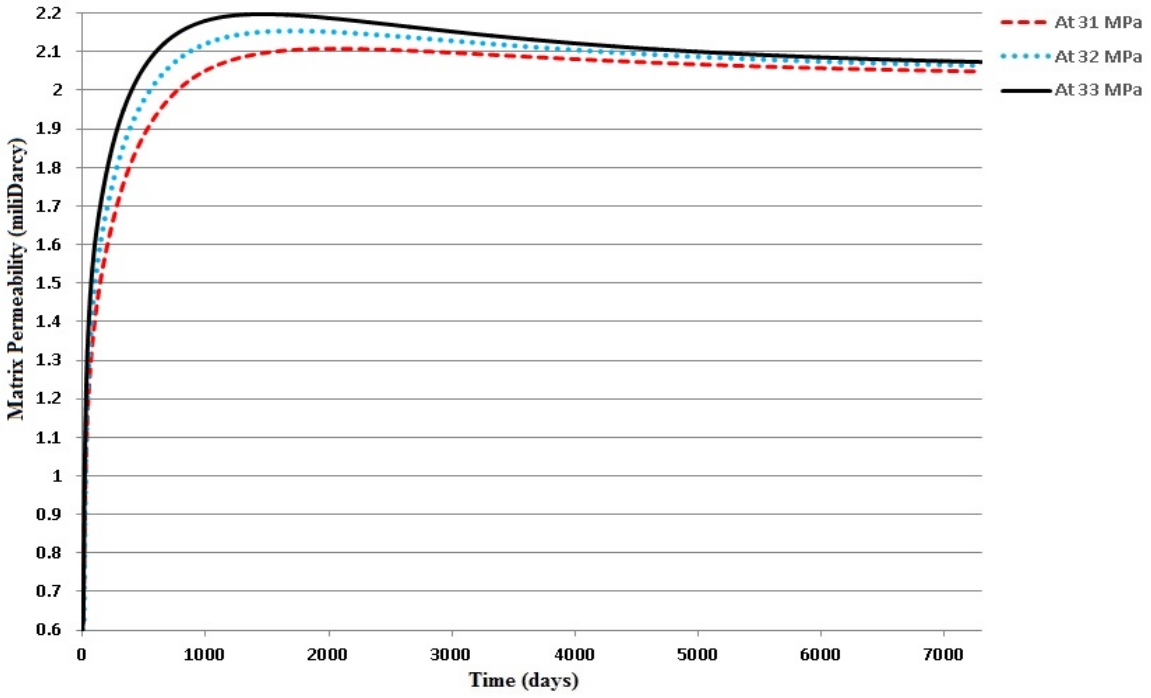

(c)

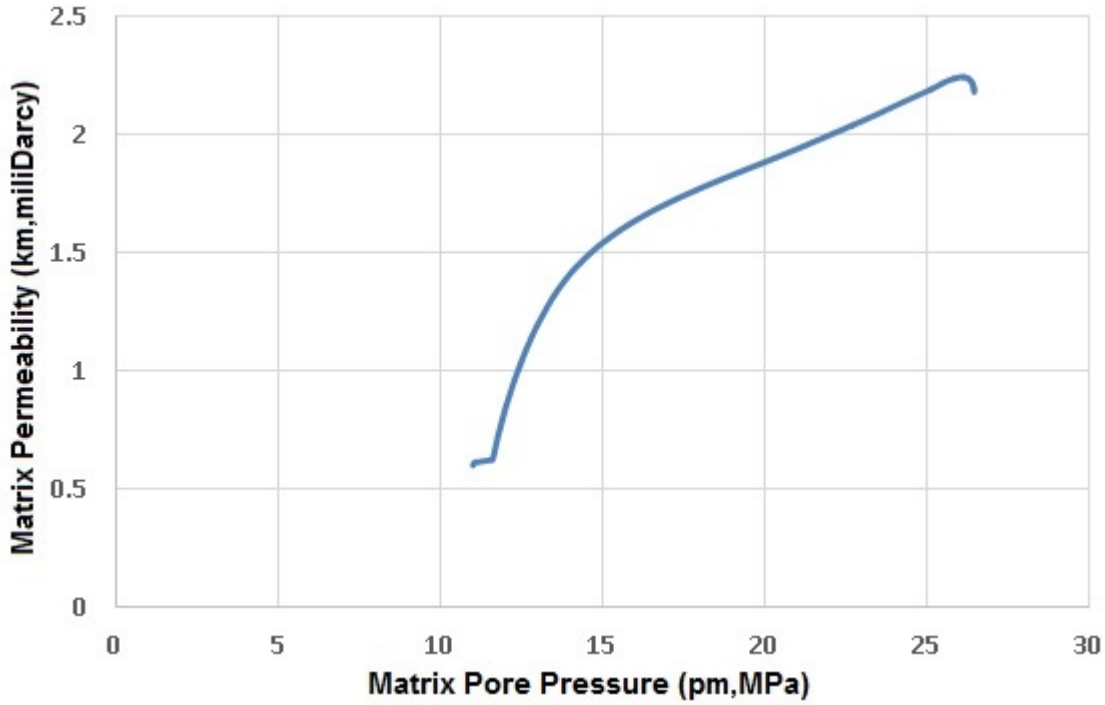

Figure 4.4 (a) Matrix pore pressure for five years of CO_2 injection period at various injection pressures (b) Matrix permeability for twenty various periods of CO_2 injection at various injection pressures (c) Variation of matrix permeability with matrix pore pressure

(a)

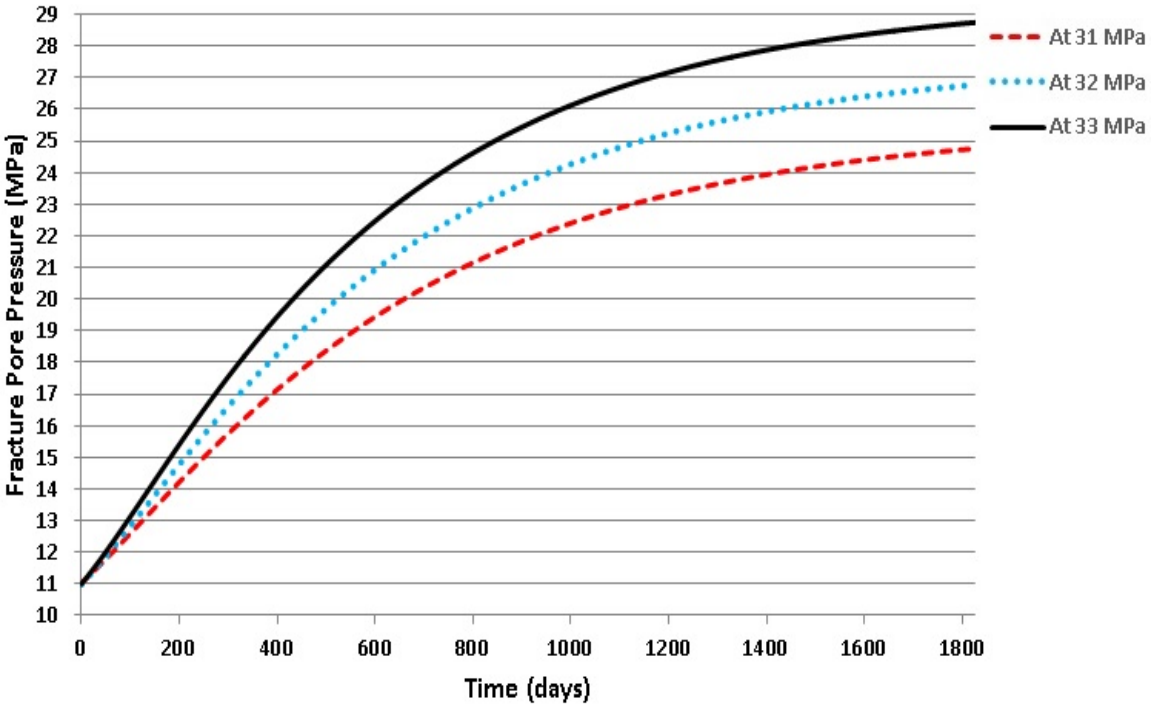
Fracture Pore Pressure (MPa)
Time (days)
At 31 MPa
At 32 MPa
At 33 MPa

(b)

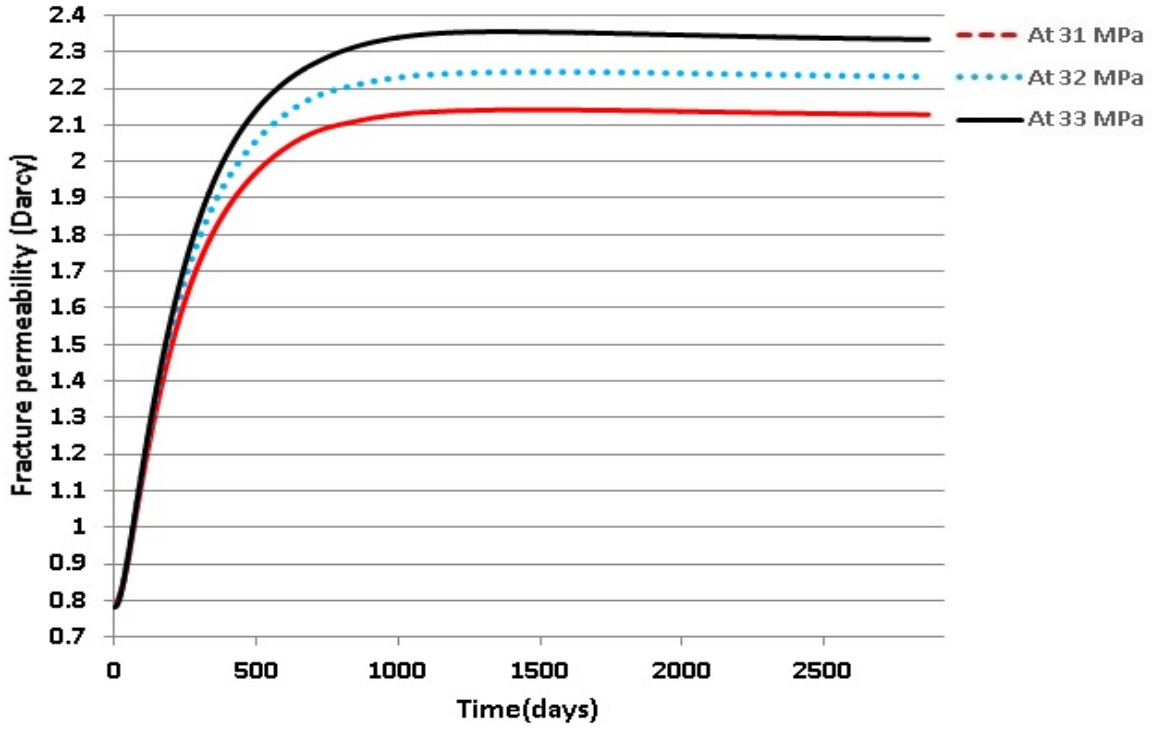
Fracture permeability (Darcy)
Time(days)
At 31 MPa
At 32 MPa
At 33 MPa

(c)

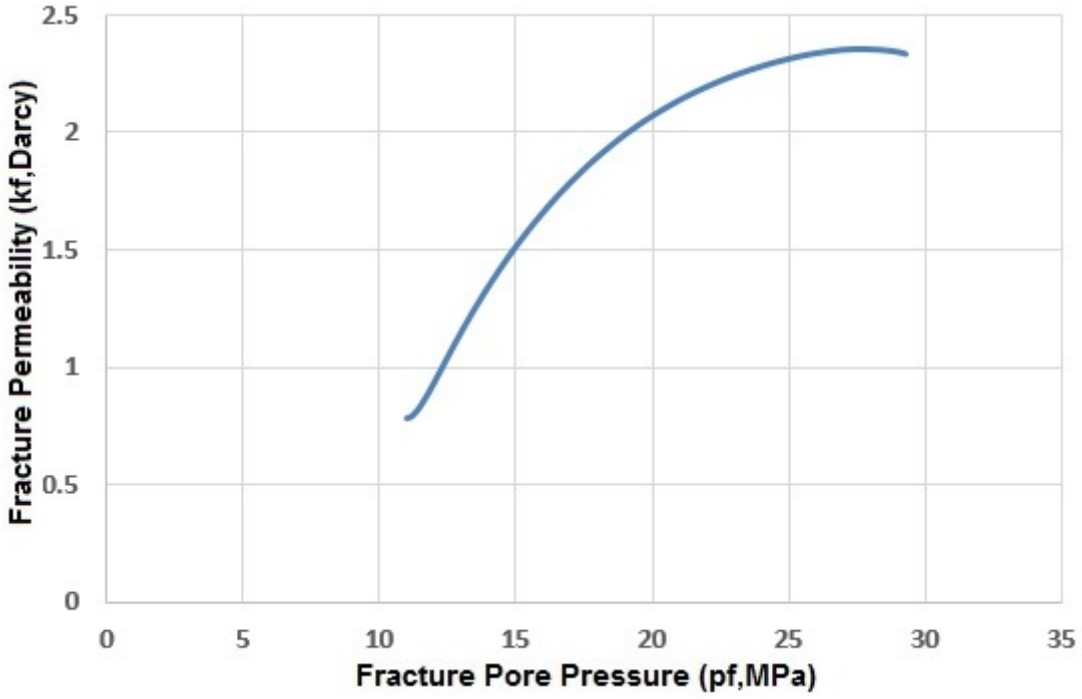

Figure 4.5 (a) Fracture pore pressure for five years of CO_2 injection period at various injection pressures (b) Fracture permeability for various periods of CO_2 injection at with various injection pressures (c) Variation of fracture permeability with fracture pore for various period of CO_2 injection

4.2.3.2 Critical pore-pressure based on the Mohr-Coulomb failure criterion

The maximum sustainable pore pressure is defined as the maximum value of pressure that can be applied to the reservoir without any irreversible geomechanical changes such as reservoir structure failure or reactivation of fractures [82, 83]. The stability of the carbonate reservoir in the compressional stress regime is explained below using the Mohr-Coulomb failure criterion. Using the two-parameter Mohr-Coulomb criterion [30], the failure envelope was drawn for the reservoir and presented in Figure 4.6. The effective normal stresses increase during the reservoir pressure depletion and can cause failure of the reservoir due to the inelastic compaction of the porous matrix. Similarly a decrease in the magnitude of the effective normal stresses may lead to the reservoir

failure if the decrease in the effective normal stress is such that it causes a slip at the fault plane [30].

The stability analysis in Figure 4.6 also takes into account the change in the horizontal stresses due to pore pressure buildup. As the pore pressure is increased it increases the horizontal stresses in the reservoir due to the coupled poroelastic effects. The Mohr's circle diagram of Figure 4.6 shows that as the pore pressure is increased the Mohr's circle becomes larger due to the increase in the horizontal stress and thus the reservoir moves towards the failure envelope. Apparently, as the pore pressure increases to 26.35 MPa, the stress state in the reservoir starts to move towards the failure line, yet the reservoir remains stable at the current injection scenario.

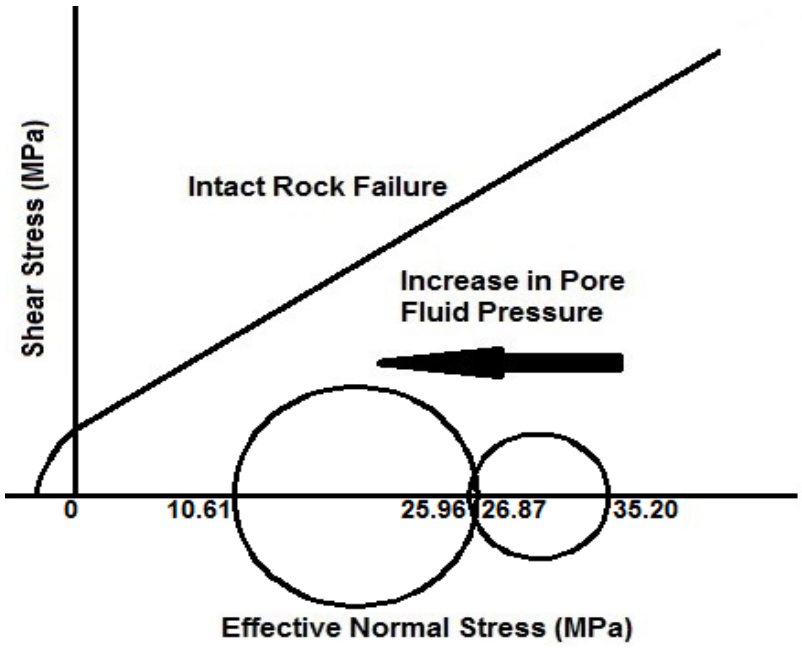

Figure 4.6 Effect of pore pressure variation on the stability of the carbonate reservoir in compressional stress regime

4.2.3.3 Maximum occupancy of the carbonate reservoir

Now, let us calculate the maximum occupancy of the carbonate reservoir. The maximum occupancy of the reservoir was calculated for the injection parameters and injection period considered in this investigation. For the selected reservoir dimensions, the initial pore volume is $1.6926 \text{ X } 10^9 \text{m}^3$. CO_2 is injected at a depth of 1750 meters below the ground level. At this depth and at the reservoir initial pressure, the formation volume factor is 0.00275 m^3/m^3 [86]. The volume of injected CO_2 at the ground level is $2.5252 \text{ X } 10^9 \text{m}^3$ and at the reservoir conditions is $6.94 \text{ X } 10^6 \text{m}^3$; that is occupancy of 0.41% of the available pore volume, which shows that a very small volume of the reservoir is occupied during the five-year injection period. It can be concluded that the carbonate reservoir under the compressional stress regime can safely handle the injection CO_2 through the vertical injection well for an injection period of 5 years. The expected occupancy is 0.41% for the 5 years of injection, which is much less than the maximum occupancy value 3% for reservoirs under the current conditions [30, 87, 88].

4.2.3.4 Model sensitivity analysis

The increase of pore pressure beyond a critical value causes a decrease in the effective stresses, which lead to reservoir failure. A sensitivity analysis is performed to evaluate the sensitivity of the pore pressure to the input parameters of the model. During the sensitivity analysis, the normalized sensitivity coefficients have been calculated for the given model parameters. The normalized sensitivity coefficients (NSCs) are used to evaluate the model sensitivity to each model parameter and specify those model parameters to which the model has high sensitivity [114]. Equation (4.18) can be used to find the normalized sensitivity coefficients, where $\bar{Y}$ is the nominal value for the model

output at a nominal input model parameter $\overline{X}_i$. The variation $\Delta Y$is the change in the model output function with a change of ΔX_i in the input model parameter X_i.The maximum pore pressure after carbon dioxide injection is considered as the function Y, while X_i represent the input model parameters (Modulus of elasticity, initial reservoir matrix permeability, reservoir matrix porosity, Poisson's ratio, and poroelastic constant). The results of the sensitivity analysis are summarized in Table 4.2, wherein the value X+ and X- correspond to $\pm 10\%$ variations, respectively, in the base-value of the input parameter X, while Y+ and Y- show the corresponding values of the output function Y.

The sensitivity analysis has been performed for the input parameters whose values have a greater probability of uncertainty. In this context, the greater the value of NSC for an input parameter, the more sensitive is the model output to that input. As demonstrated in Table 4.2, the calculated value of the pore pressure during carbon dioxide injection is more sensitive to the following input parameters: the initial reservoir permeability, initial reservoir porosity and the poroelastic coefficient. The output values for the pore pressure are tabulated in Table 4.2 for the $\pm 10\%$ variations in the base-values of the dominating input parameters, wherein the corresponding variations in the output pressure values ΔY_i are found to be less than 36.96 MPa (Lithostatic pressure). Accordingly, the probable uncertainty in the input model parameters will not compromise the obtained results pertinent to the stability of the reservoir during carbon dioxide injection; thus attesting to the reliability of the model predictions and the consequent conclusions.

$$\mathrm{NSC_i} = \frac{\Delta \mathrm{Y}}{\overline{\mathrm{Y}}} \frac{\overline{\mathrm{X}}_\mathrm{i}}{\Delta \mathrm{X_i}} \tag{4.18}$$

Table 4.2 Normalized sensitivity analysis results for the model

Parameter	X	X+	X-	Y+	Y-	ΔX_i	ΔY_i	NSC_i
Initial reservoir matrix permeability (km, mDarcy)	0.6	0.66	0.54	24.46 E6	30.23 E6	0.12	5.77 E6	1.094
Poisson's ratio (υ)	0.3	0.33	0.27	27.11 E6	25.96 E6	0.06	1.15 E6	0.218
Initial reservoir matrix porosity ($\emptyset_m$)	0.13	0.143	0.117	25.25 E6	28.55 E6	0.026	3.3 E6	0.626
Modulus of Elasticity (E, GPa)	48.5	53.35	43.65	25.55 E6	27.29 E6	9.7 E6	1.74 E6	0.330
Poroelastic constant (α)	0.8	0.88	0.72	27.44 E6	24.48 E6	0.16	2.96 E6	0.561

3.2.3.5 Validation

In order to validate the dual poroelastic modeling in COMSOL multiphysics, carbon dioxide injection into a naturally fractured medium was simulated. In this case, the model is two-dimensional with pressures in the matrix and factures, while the displacement components along x-axis and y-axis are treated as dependent variables. The governing equations for the naturally fractured medium are utilized to perform the equation-based modeling in COMSOL multiphysics with the corresponding Neumann and Dirichlet boundary conditions defined on the boundaries. The ratio of the horizontal in situ stresses is kept at 1.5. At the injection well, the pressure is kept at 8 MPa and all other surfaces are free of any flow conditions. The input properties for the model are listed in Table 4.3. The simulation model for the fractured medium and the pore pressures variations are shown in Figure 4.7. The pore pressure variations are in good agreement with the reported simulation results available in the literature [103], thus validating the modeling scheme adopted in this investigation.

Table 4.3 Various input parameters for the simulation of CO_2 into fractured medium [103]

Parameter	Value
Young's modulus of the fractured medium, E (MPa)	2713
Young's modulus of the fractured medium grain, E_s (MPa)	8143
Density of CO_2, ρ_g (kg/m^3) at standard condition	1.98
Viscosity of CO_2, μ (Pa s)	1.84×10^{-5}
Langmuir value for pressure, P_L(MPa)	6.10900
Langmuir value for volume, V_L (m^3/kg)	0.01500
Langmuir value for volumetric strain, ε_L	0.02295
Initial porosity of matrix, $\emptyset_{m0}$	0.02
Initial permeability of matrix, km_0 (m^2)	10^{-18}
Fracture aperture, b_0 (m)	1×10^{-4}
Matrix size, a_0 (m)	0.01
Lateral stress ratio, λ	1.5

(a)

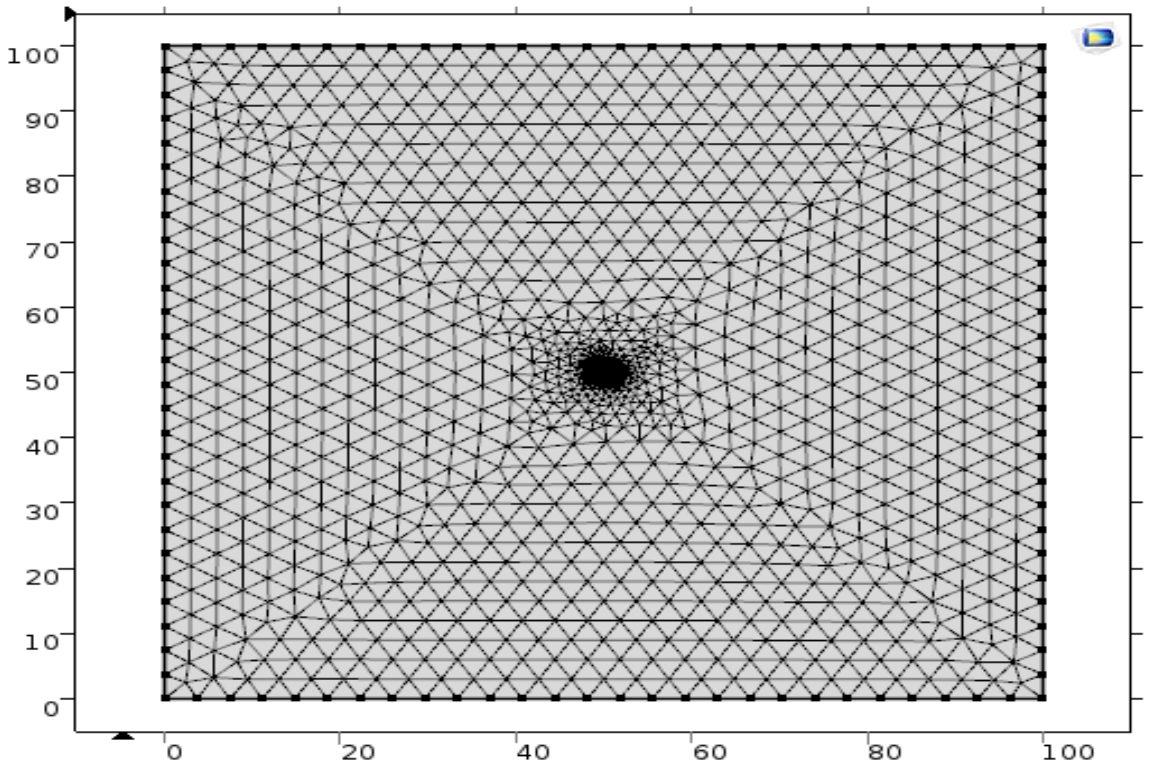

(b)

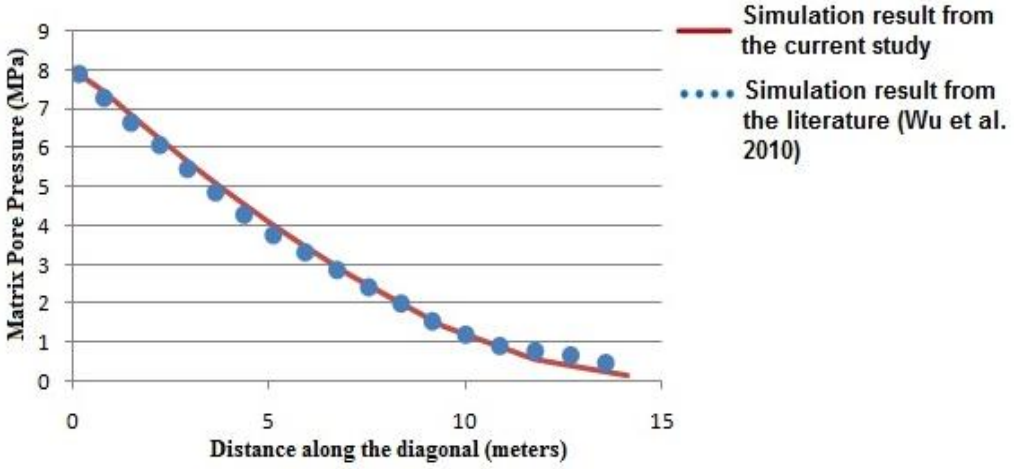

(c)

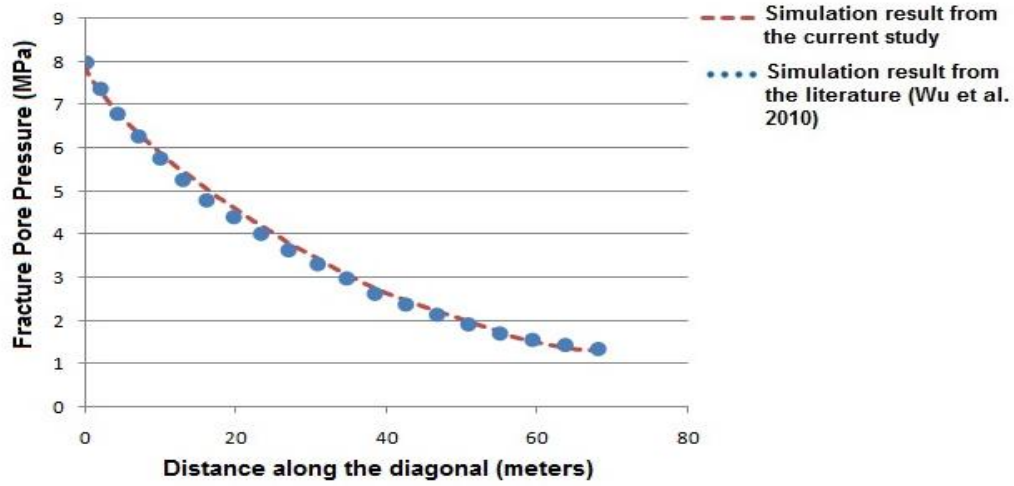

Figure 4.7 (a) Simulation model for carbon dioxide injection into naturally fractures reservoir (b) Change of matrix pore pressure with distance along the diagonal (c) Change of fracture pore pressure with distance along the diagonal

In the next portion of the chapter carbon dioxide flow is considered in naturally fractured reservoir with water as a base fluid. The magnitudes of the pore pressure buildup and ground uplift will be different from the case of single-phase flow.

4.3 Naturally fractured reservoir with two-phase flow

In this section of the chapter, two-phase fully coupled geomechanical analysis is performed using CMG-GEM software to evaluate the safe CO_2 injection parameters for

the Ghawar sequestration site in Saudi Arabia. With two-phase flow in the naturally fractured reservoir, the change in the permeability, stresses, ground uplift and pressure is evaluated. In the first part of the section 4.3, CO_2 was injected into the naturally fractured reservoir with the injection well at the reservoir center. Huge increase in the reservoir pore pressure and ground uplift was noted in this specific case. In the second part of section 4.3, CO_2 was injected at an injection well at the center of the reservoir and water production takes place at a production well at a specific distance from the injection well. Using this strategy the pressure increase was less because the increase in the reservoir pressure due to CO_2 injection was mostly accommodated by the decrease of reservoir pressure due to water production at the production well. The reservoir pore pressure and also the ground uplift were monitored for various periods of carbon dioxide injection and at various injection pressures. Finally for the various injection scenarios in the current study stability analysis is performed for the reservoir to have maximum reservoir stability.

4.3.1 Mathematical formulation for flow and deformation during CO_2 injection

The Ghawar Arab-D reservoir used in this study for carbon dioxide sequestration is a naturally fractured reservoir. The change in the fracture permeability during carbon dioxide injection should be modeled during the coupled geomechanical analysis for the reservoir because fractures are the main channels for fluid flow in naturally fractured reservoirs [60, 61, 103, 115-117]. The iterative (two-way) coupling procedure is used by CMG-GEM for the coupling of two-phase flow and reservoir deformation. To model the naturally fractured reservoir in CMG-GEM two systems of grid are used. A primary grid is used for the matrix and a secondary grid system is used for the fractures such that the

two grid systems are related on one to one basis. The fracture permeability is a key factor, which controls the fluid flow along the reservoir or the leakage of the stored fluid through the fractured caprock. CMG-GEM uses Barton-Bandis model to calculate change in fracture permeability with carbon dioxide injection into the reservoir [118-122]. For the naturally fractured reservoir the governing equations for the two-phase flow through the reservoir matrix and fractures, deformation of the reservoir matrix, and the change in the fracture permeability is discussed in the following sections.

4.3.1.1 Two-phase flow in naturally fractured reservoir

The multiphase flow simulator in CMG-GEM considers the naturally fractured reservoir as a combination of two mediums, a matrix system separated by orthogonal fractures in three dimensions. At each node of the reservoir the pressures, saturations, and composition of each phase is calculated. The dual-permeability condition is considered in the reservoir to allow the fluid to transfer between the matrix blocks. The shape factor used in this study is based on the work of Gilman and Kazemi. The fluid transfer between the matrix and fracture is based on the Pseudo-capillary pressure model with corrections to contact areas between phases [92, 118-122]. The dual-permeability formulation for the matrix blocks in the naturally fractured reservoir is defined as [92, 119]:

$$\psi_{im} = \Delta T^{s}_{om}\, y^{s}_{iom} \left(\Delta p^{n+1} - \gamma^{s}_{o} \Delta D\right)_{m} +$$

$$\Delta T^{s}_{gm}\, y^{s}_{igm} \left(\Delta p^{n+1} + \Delta p^{s}_{cog} - \gamma^{s}_{g} \Delta D\right)_{m}$$

$$-\tau_{iomf} - \tau_{igmf} - \frac{V}{\Delta t} \left(N_{i}^{n+1} - N_{i}^{n}\right)_{m} = 0 \qquad i = 1, \ldots, n_{c} \tag{4.19}$$

$$\psi_{n_c+1,m} = \Delta T^{s}_{wm} \left(\Delta p^{n+1} - \Delta p^{s}_{cwo} - \gamma^{s}_{w} \Delta D\right)_{m} +$$

$$-\tau_{wmf} - \frac{V}{\Delta t} \left(N_{n_c+1}^{n+1} - N_{n_c+1}^{n}\right)_{m} = 0 \tag{4.20}$$

Equations 4.19 and 4.20 discuss the flow of carbon dioxide in the matrix blocks of the naturally fractured medium. The term T_j is the transmissibility of phase j. Where j = water or carbon dioxide in the current study. The term y_{ij} denotes the mole fraction of component i in phase j. The symbol p represents the value of the pore pressure. γ_j is the specific gravity of the phase j. D denotes depth in gravity direction. T denotes the matrix-fracture transfer. V denotes the grid block volume. t denotes the time. N_i represents moles of component I per unit block volume V.

The dual-permeability formulation for the fractures in the naturally fractured reservoir is defined as [92, 119]:

$$\psi_{if} = \Delta T^s_{of} y^s_{iof} \left(\Delta p^{n+1} - \gamma^s_o \Delta D\right)_f + \Delta T^s_{gf} y^s_{igf} \left(\Delta p^{n+1} + \Delta p^s_{cog} - \gamma^s_g \Delta D\right)_f$$

$$+ q_i^{n+1} - \tau_{iomf} - \tau_{igmf} - \frac{V}{\Delta t}\left(N_i^{n+1} - N_i^n\right)_f = 0 \qquad i = 1, \ldots, n_c \tag{4.21}$$

$$\psi_{n_c+1,f} = \Delta T^s_{wf} \left(\Delta p^{n+1} - \Delta p^s_{cwo} - \gamma^s_w \Delta D\right)_f +$$

$$+ q_w^{n+1} + \tau_{wmf} - \frac{V}{\Delta t}\left(N_{n_c+1}^{n+1} - N_{n_c+1}^n\right)_f = 0 \tag{4.22}$$

$$\psi_{pf} = \sum_{i=1}^{n_c+1} N_{if}^{n+1} - \phi_f^{n+1} \left(\rho_o S_o + \rho_g S_g + \rho_w S_w\right)_f^{n+1} = 0 \tag{4.23}$$

The term q represents the injection/production rate. ρ_j denotes the density of the phase j and $S_j$denotes the saturation of phase j. The superscript n is for the old time interval and n+1 is for the new time interval. The subscripts i is used for addressing component, j is used for phase, g is used for gas, w is used for water, m is used for matrix and f is used for fracture.

The fluid transfer between matrix and fractures considers both the capillary pressure effect and matrix-fracture fluid transfer contact area corrections. The fluid transfer between matrix and fractures is given as [92, 119]:

$$\tau_{omf} = \xi V \frac{k_{ro}\rho_o}{\mu_o}(p_{om} - p_{of}) \quad (4.24)$$

$$\tau_{gmf} = \xi V \frac{k_{rg}\rho_g}{\mu_g}(p_{om} - p_{of}) + \left[S_{gm} + \frac{\xi_z}{\xi}\left(\frac{1}{2} - S_{gm}\right)\right](\tilde{p}_{cog,m} - \tilde{p}_{cog,f}) \quad (4.25)$$

$$\tau_{wmf} = \xi V \frac{k_{rw}\rho_w}{\mu_w}\left\{(p_{om} - p_{of}) - (p_{cwo,m} - p_{cwo,f}) - \left(\frac{1}{2}\frac{\xi_z}{\xi}\right)\left[(\tilde{p}_{cwo,m} - \tilde{p}_{cwo,f}) - (p_{cwo,m} - p_{cwo,f})\right]\right\} \quad (4.26)$$

Where k_r is the relative permeability, μ_j is the viscosity of the fluid j, $\tilde{p}$ denotes the capillary pressure and ξ is the shape factor. The shape factor used in this study is based on the study of Gilman and Kazemi and is defined as [92, 119, 123]:

$$\text{Shape factor} = \xi = 4\left(\frac{1}{L_x^2} + \frac{1}{L_y^2} + \frac{1}{L_z^2}\right) \quad (4.27)$$

Where L_x , L_y , and L_z denotes the fracture spacing along x-axis, y-axis, and z-axis respectively.

4.3.1.2 Deformation of the naturally fractured reservoir

As carbon dioxide is injected to the naturally fractured reservoir, the pore pressure increases, which causes the deformation of the reservoir. The pressure induced deformation of the reservoir causes stresses in the reservoir matrix. The change in the matrix stresses causes a change in the normal fracture effective stress, which changes the permeability of the fracture after each time step. New values of strains can be calculated from the current values of displacement along the three axes using the strain displacement relationship [98]:

$$\varepsilon_{ij} = \frac{1}{2}(u_{i,j} + u_{j,i}) \quad (4.28)$$

Where ε_{ij} is the strain tensor, and $u_{i,j}$ represents the displacement components. The strain values calculated from equation (4.28) can be used in the constitutive equation to find the values of the stresses [99-102]:

$$\sigma_{ij} = 2G\varepsilon_{ij} + \left(K - \frac{2G}{3}\right)\varepsilon_{kk}\delta_{ij} + \alpha p\delta_{ij} \quad (4.29)$$

Where σ_{ij} is the stress tensor, G is the shear modulus for the reservoir, K is the reservoir bulk modulus, ε_{kk} represents addition of the diagonal strains in the strain tensor, δ_{ij} is the Kronecker delta, and α is the Biot's coefficient.

Once we have the new values of pore-pressure and total stresses, the effective stresses in the reservoir can easily be calculated. The effective stresses in the reservoir are affected when the pore pressure is increase with carbon dioxide injection and is defined as:

$$\sigma_{ij}' = \sigma_{ij} - \alpha p\delta_{ij} \quad (4.30)$$

Where σ_{ij}' represents the values of the effective stresses. The values of effective stresses calculated from equation (4.30) can be used for the stability analysis of the reservoir.

4.3.1.3 Barton-Bandis model for fracture permeability

The Barton-Bandis model is explained in detail in section 3.3.1.3. Only the equations are listed in this section. Using the Barton-Bandis model the fractures permeability can be calculated from the normal fracture effective stress. During the iterative coupling procedure the new value of the permeability at each time interval is calculated using the following equation [119, 120, 122]:

$$k_f = k_{fc}(e/e_o)^4 \quad (4.31)$$

where, k_f is the fracture permeability and k_{fc} is the fracture closure permeability,

$$e = e_o - V_j \tag{4.32}$$

$$V_j = \frac{\sigma_{n'}}{k_{ni} + \sigma_{n'}/V_m} \tag{4.33}$$

$$V_m = e_o \left[1 - \left(\frac{k_{fr}}{k_{fc}}\right)^{1/4}\right] \tag{4.34}$$

Where, e_o is the fracture opening at the start of simulation, V_m is the minimum fracture opening and e is the new value of fracture opening after each time step. The term V_j defines the effective normal fracture stress to fracture stiffness ratio. k_{ni} is the initial normal fracture stiffness and k_{fr} is the initial fracture permeability.

4.3.2 Modeling scheme in CMG-GEM

The multiphase flow simulator CMG-GEM is used in this part of the study for modeling carbon dioxide injection into the naturally fractured carbonate reservoir with water as the local fluid before carbon dioxide injection. CMG-GEM will evaluate the pore pressure increase in reservoir matrix and fractures and the change in fracture permeability due to CO_2 injection into the reservoir. The detailed modeling scheme, which is utilized for the determination of the pressure response, the vertical ground uplift, and the change in the fractures permeability due to CO_2 injection, is explained in this section.

For building a 3 Dimension layered model for Arab Jubaila carbonate reservoir, the location and depths of the various overburden and under burden layers are needed. Using the available geological data [70] as shown in Figure 3.1, a 3 Dimension layered models for Arab Jubaila carbonate reservoir was constructed in CMG-GEM for the two main cases in this study. As shown in Figure 4.8 (a) a 3 D layered model will be used to inject

CO_2 with a single injection well at the reservoir center and in Figure 4.8 (b) the 3 D layered model will be used to inject CO_2 at an injection well at one side of the reservoir and to produce water with a production well at the opposite side of the reservoir. The 3 dimension layered models in Figure 4.8, has one under burden layer, a caprock above the Arab Jubaila carbonate reservoir layer, and eight overburden layers.

The dual-permeability modeling is performed for the Arab Jubaila carbonate reservoir in CMG-GEM. The Barton-Bandis model is used to calculate changes in fracture permeability with CO_2 injection into the reservoir. In this study the Gilman and Kazemi style of formulation is used to describe the flow between the matrix and fractures of the reservoir. As shown in Figure 4.8, the mesh size in the injection reservoir is refined to facilitate the accurate dual-permeability modeling. The Cartesian grid type is used with a total of 12,000 grid blocks. On each grid block the values of pore pressure and displacements will be computed at each time interval. Carbon dioxide is injected at an air entry pressure of 30 MPa for a time period of 5 years. Boundary conditions are applied to the model with the bottom and side boundaries with roller conditions and the top surface is free to move in the vertical direction. In the geomechanical section of CMG-GEM initial stresses were applied to the model. For the dual-permeability modeling in CMG-GEM, the various input parameters needed are listed in Table 4.4 [70, 72, 104-107]. In this portion of the study carbon dioxide is injected into a naturally fractured carbonate reservoir. The target reservoir is saturated with water so injected carbon dioxide will displace the water in the pores and tends to increase the gas saturation near the injection well. The relative permeability curves selected for use in this numerical study is for the

carbon dioxide injection into the carbonate reservoir under the similar reservoir pressure, temperature, and brine salinity conditions [108, 109].

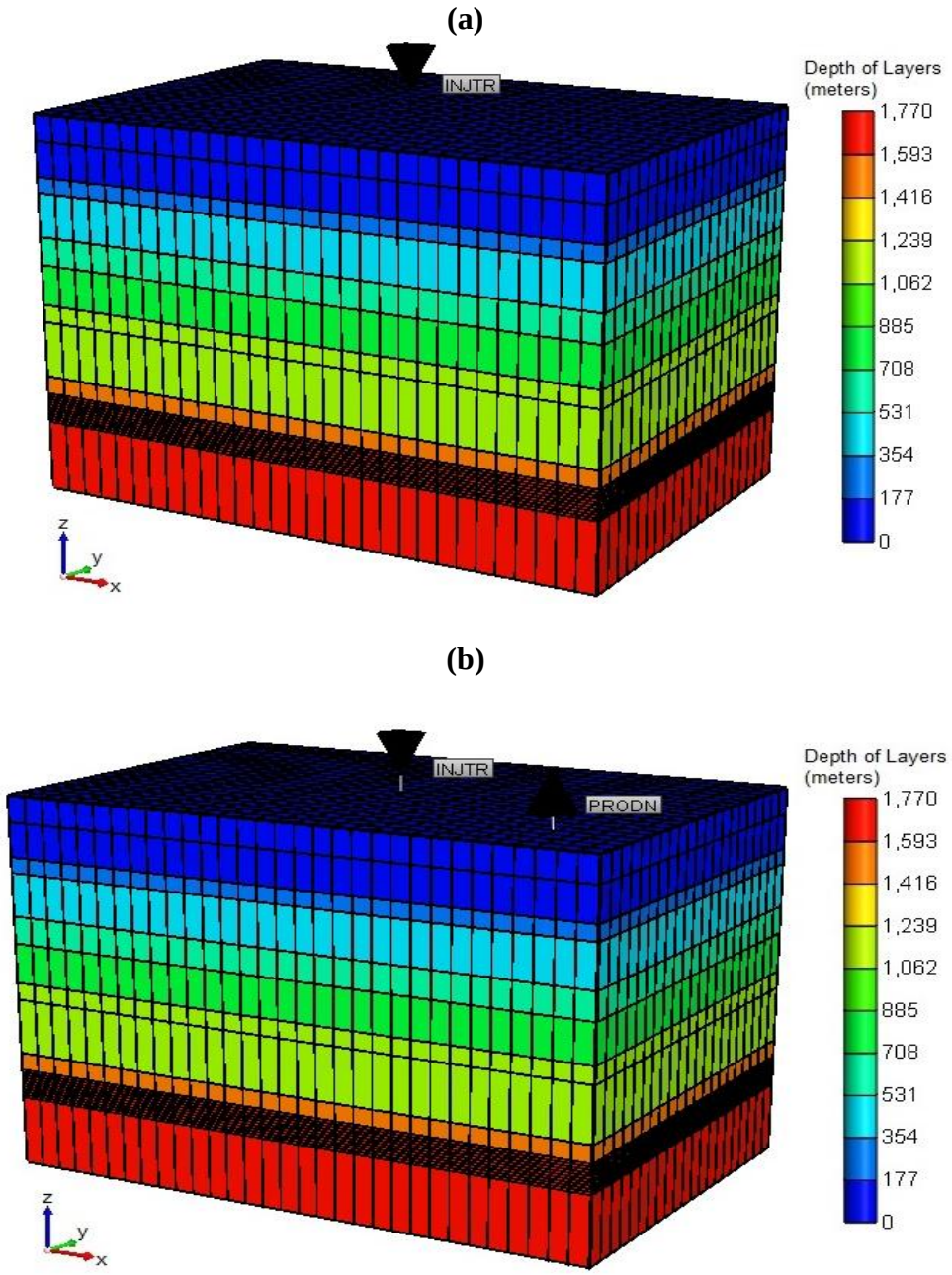

Figure 4.8 (a) Layered model for Arab Jubaila carbonate reservoir with a single injection well at the reservoir center (b) Layered model with CO_2 injection well at one side of the reservoir and producer well at the opposite side of the reservoir

Table 4.4 Various input parameters for the dual-permeability modeling of Arab Jubaila carbonate reservoir [70, 72, 104-107]

Property	**Hofuf Dam Hadrukh**	**Damman**	**Rus**	**Um Er Radhuma**	**Aruma**	**Wasia**	**Shuaiba**	**Biyadh Sulay**	**Hith Anhydrite**	**Arab Jubaila**	**Hanifa, Tuwaiq**
Layer thickness (m)	150	200	90	250	160	230	100	320	100	170	400
Grid top (m)	0	150	350	440	690	850	1080	1180	1500	1600	1770
Rock Density, $\rho(K_g/m^3)$	1877	2289	2280	2020	2090	2270	2030	2360	2960	2400	2550
Young's Modulus, E (GPa)	7	21.43	37.25	21	15.6	27.84	18.1	44.7	42.67	48.5	57.43
Bulk Modulus, K (GPa)	2.83	11.47	22.8	11.67	7.8	9.82	9.13	25.7	38.2	39.24	53.96
Shear Modulus, G (GPa)	2.6	8.004	13.91	7.83	5.828	10.4	6.65	17.2	15.932	18.1	21.45
Initial porosity, $\emptyset_m$	0.2	0.2	0.28	0.24	0.17	0.29	0.09	0.12	0.01	0.13	0.10
Initial permeability, km (10^{-15} m^2)	0.2	0.02	0.25	0.01	0.15	0.2	0.025	0.7	0.00001	0.6	0.2
Pressure wave velocity, Vp (m/sec)	1835	3110	4260	3310	2730	3230	3010	4040	4480	5140	5690
Shear wave velocity, Vs (m/sec)	1180	1870	2470	1970	1670	2140	1810	2700	2320	2748	2900

4.3.3 Numerical modeling results and discussions

4.3.3.1 Reservoir pressure response with CO_2 injection

The injection of carbon dioxide into the naturally fractured carbonate Ghawar reservoir will increase the pore pressure and decrease the effective stresses in the reservoir. The excessive increase in the pore pressure during carbon dioxide injection can cause the failure of the reservoir. The injection of carbon dioxide at high injection pressures will tends to increase the pore pressure of the reservoir, which initiates the necessity of alternative strategies used for keeping the pore pressure below the critical limit. In order

to avoid the excessive increase in the pore pressure during carbon dioxide injection, the strategy used in this study is to use a production well for water production in combination with the carbon dioxide injection well. Removal of the water from the reservoir will tends to lower the reservoir pressure and will provide a potential for the transport of carbon dioxide along the reservoir. Two different injection scenarios are used with production well in the system. During the first case carbon dioxide injection and water production takes place simultaneously for five years. In the second case carbon dioxide was injected for 3 years with the injection well and then the injection of carbon dioxide was stopped and water production was performed for 3 years. At last the water production was stopped and carbon dioxide was injection for 2 years.

The transport of carbon dioxide in the reservoir is a big issue and requires a high pressure potential in the reservoir. The carbon dioxide saturation plots is in Figure 4.9, which shows that with production well in the system, the potential to carbon dioxide flow is high towards the production well. Adding a production well to the carbon dioxide injection and sequestration process tends to decrease the overall pore pressure. It can be seen from Figure 4.10, that the magnitude of pore pressure after five years of carbon dioxide injection is high for injection process with only injection well and no production well. When carbon dioxide injection and water production was carried out simultaneously for five years, the net effect was that the maximum value of the pore pressures was reduced but due to the production process, pressure depletion occurred near the production well. The effect of pressure depletion near the production well will also affect the vertical ground displacements and reservoir stability.

To minimize the pressure depletion another new strategy was followed, in which carbon dioxide was injection for 3 years with no water production during this period. After 3 years, the injection process was stopped and water was produced for 3 years. After 3 years of water production, carbon dioxide was again injected for 2 years. In this strategy the overall injection period of carbon dioxide was 5 years with 3 years of water production. The reservoir pore pressure for both injection strategies of the case of combine injection and production wells is shown in Figure 4.10. It can be seen from Figure 4.10, that the maximum pore pressure value is reduced when water production takes place, but minimum pressure depletion is with the case when water production takes place separately from the carbon dioxide injection.

The pore pressure variation with time is shown in Figure 4.11 for the cases of single injection well and combined injection and production wells. During the case of single injection well the pore pressure increases continuously to a maximum value till the end of injection period. During the case of simultaneous injection and production process the pore pressure increases continuously but the maximum value is less than that of the case of single injection well. During the case when carbon dioxide injection and water production was carried out in series, the output pressure response shows an increase in the pore pressure during the first 3 years of carbon dioxide injection, followed by a pressure reduction during the 3 years of water production, and at the end again an increase in the pressure during the last 2 years of carbon dioxide injection. At the end of the process the final value of the pore pressure is minimum compared to the other injection scenarios.

The bottom hole pressure and location of the production well has great influence on the magnitude of pore pressure in the reservoir. To see the influence of the production well location on the magnitude of the pore pressure, the production well was place at three different locations. The influence of the production well location on the pore pressure is shown in Figure 4.12. It can be seen from Figure 4.12 that when the production well was placed at a distance of 1000 meters from the injection well, the value of the maximum pore pressure was the lowest as compared to the pore pressure values with other two locations of the production well. Placing the production well closer to the injection well reduces the pressure buildup by providing a flow potential for the carbon dioxide by removing water from the reservoir. Even with the nearest location of the production well, the CO_2 saturation plots shows that the injected carbon dioxide will not release with the water production. The reason of not placing the production well nearer from 1000 meters is that the injected carbon dioxide will be mixed with the water and will be pumped out with the produced water. When production well is near to the injection well, the magnitude of the pore pressure decreases but as the production well is moved away from the injection well, the magnitude of the pore pressure is increased.

To see the influence of the production well bottom hole pressure on the magnitude of the pore pressure in the reservoir, water was produced at 3 different bottom hole pressures. The influence of the bottom hole pressure on the magnitude of the pore pressure in the reservoir is shown in Figure 4.13. As shown in Figure 4.13, the lower the bottom hole pressure, the lower is the magnitude of the pore pressure in the reservoir and vice versa. The lower value of the bottom hole pressure corresponds to a high value of pumping potential for the water at the production well and thus creates a high potential

for the carbon dioxide flow towards the production well. The high flow of carbon dioxide prevents the pressure buildup in the reservoir and thus results in lower magnitude of pore pressure in the reservoir.

The injection of carbon dioxide and the production of water from the reservoir cause changes in the pore pressure and in the effective stresses on the reservoir. As shown in Figure 4.14 & 4.15, the maximum decrease in the effective stresses is near the injection well for only injection well in the system. For the cases of combined injection and production, the value of the effective stresses increases near the production well. The variations in the minimum and maximum horizontal stresses during carbon dioxide injection and water production are shown in Figure 4.16 & 4.17 for the corresponding injection and production periods. As shown in Figure 4.16 & 4.17, as the pore pressure increases during the injection of carbon dioxide, the magnitudes of the horizontal stresses are decreased.

(a)

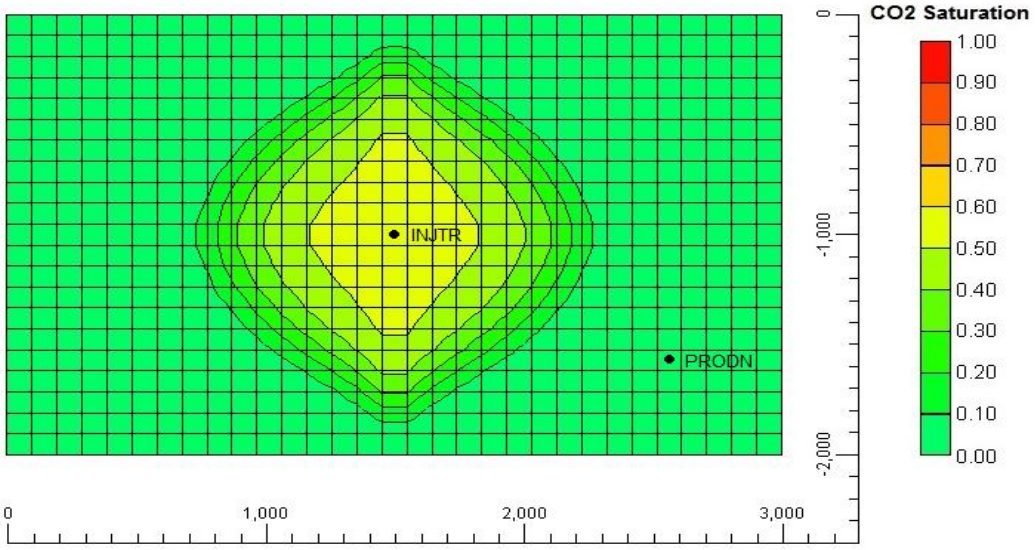

(b)

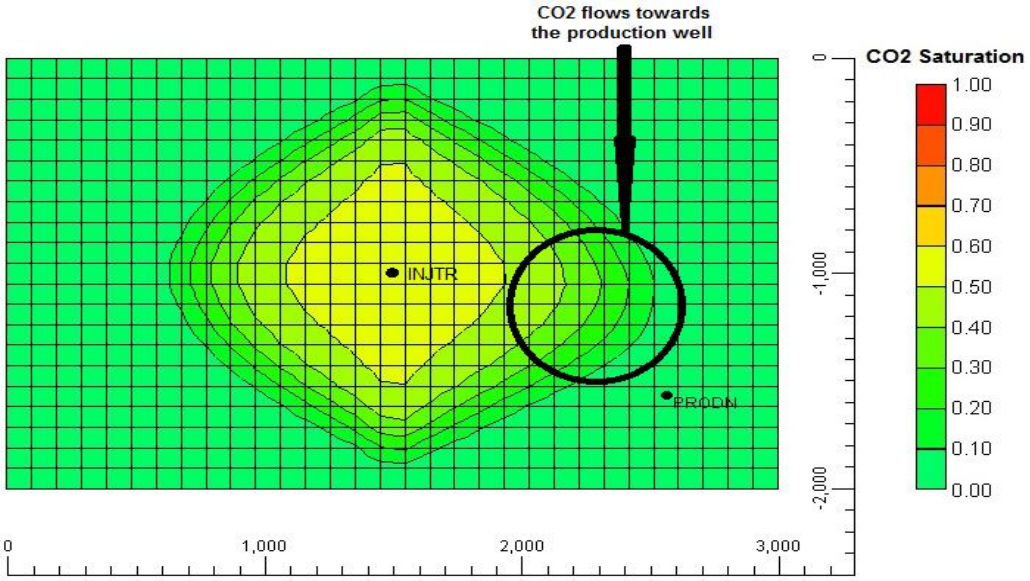

Figure 4.9 Carbon dioxide saturation in the reservoir (a) With only injection well (b) with both injection and production wells

(a)

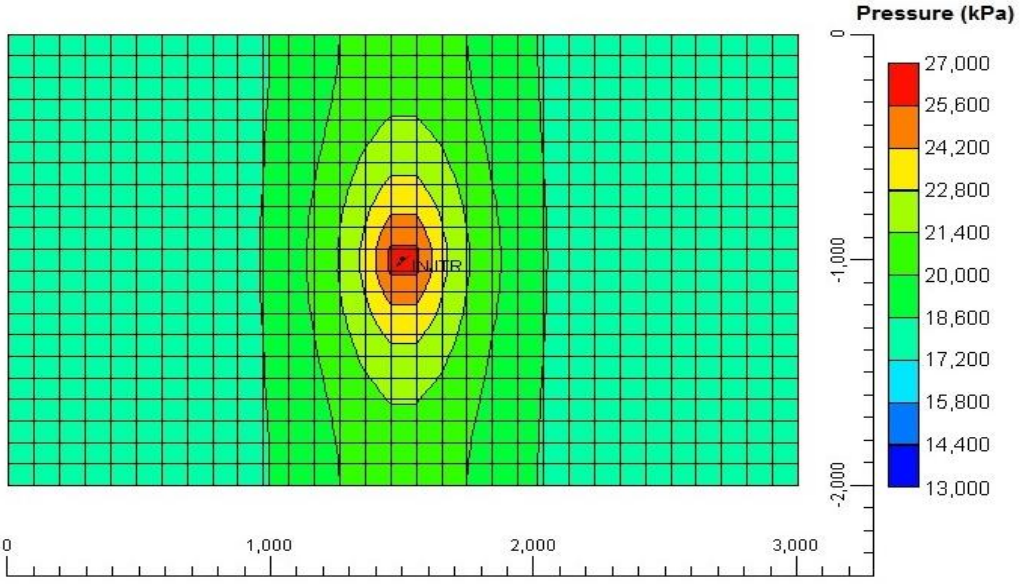

(b)

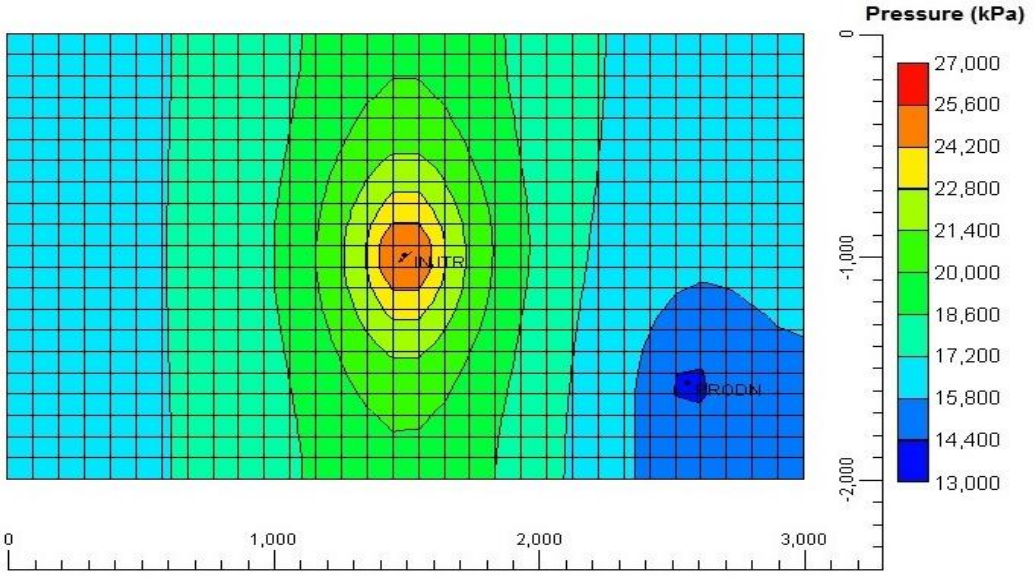

(c)

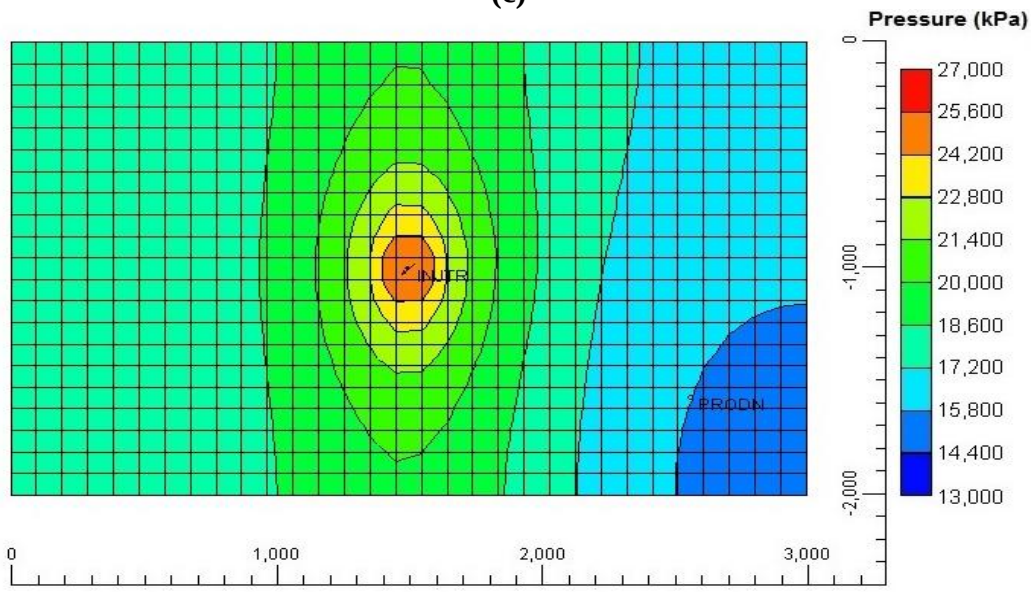

Figure 4.10 Magnitude of pore pressure after CO_2 injection (a) With only injection well (b) with simultaneous injection and production (c) with water production in series with CO_2 injection

(a)

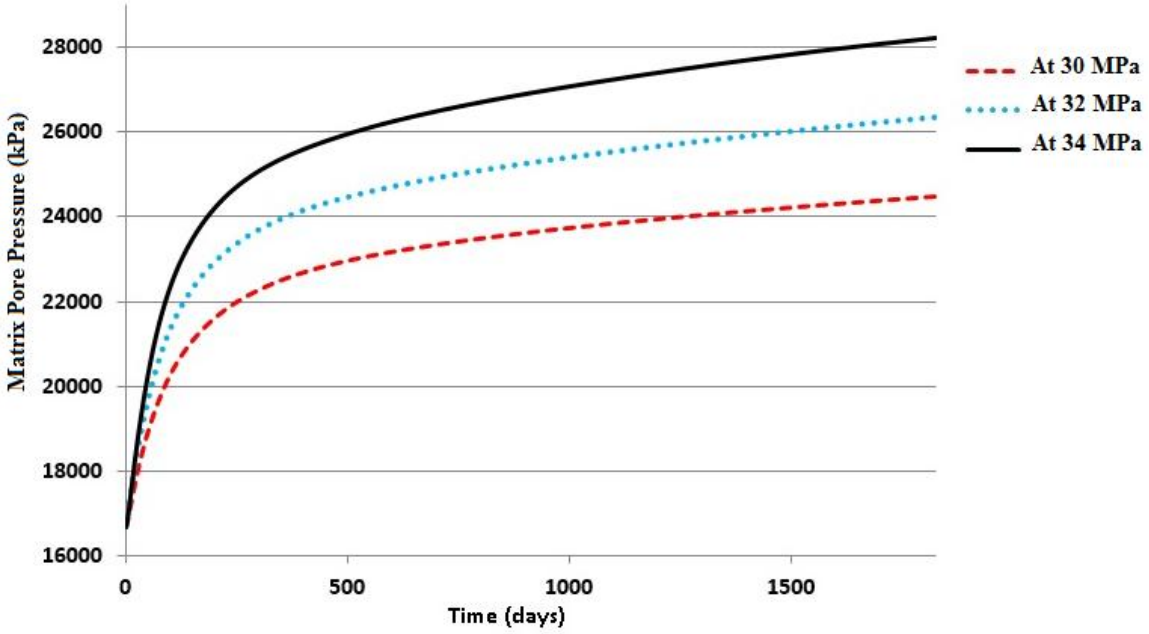
Matrix Pore Pressure (kPa)
28000
26000
24000
22000
20000
18000
16000
0
500
1000
1500
Time (days)
At 30 MPa
At 32 MPa
At 34 MPa

(b)

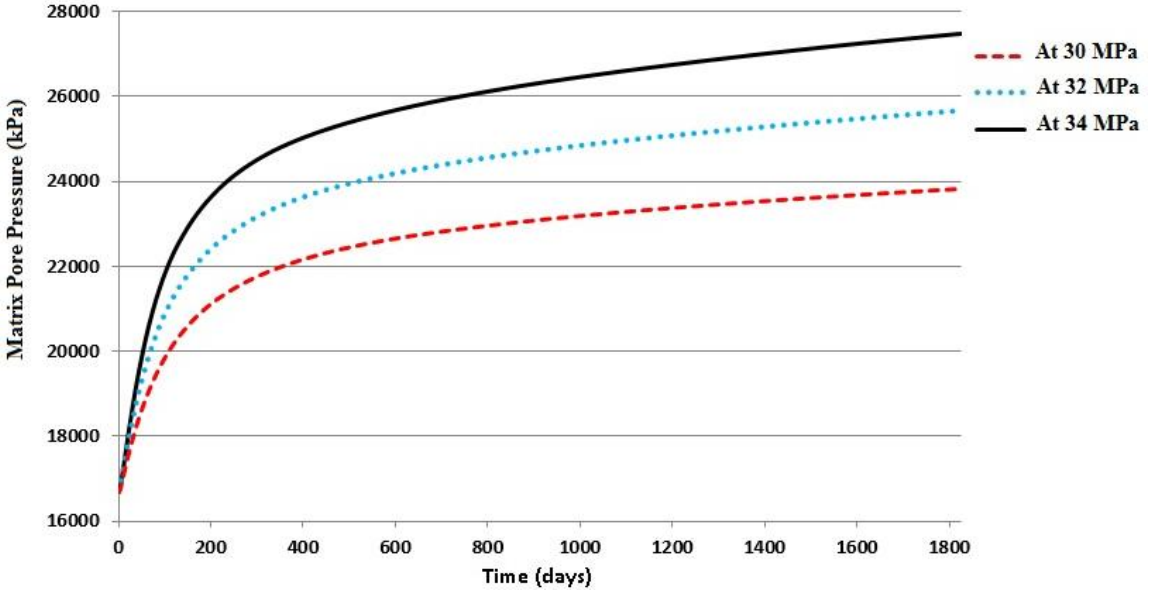
Matrix Pore Pressure (kPa)
28000
26000
24000
22000
20000
18000
16000
0
200
400
600
800
1000
1200
1400
1600
1800
Time (days)
At 30 MPa
At 32 MPa
At 34 MPa

(c)

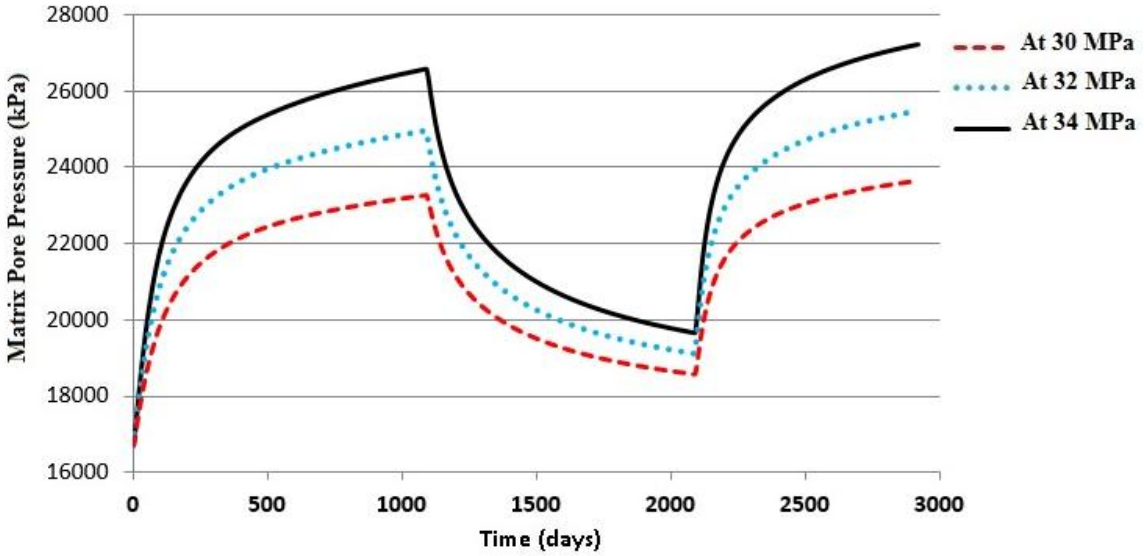

Figure 4.11 Pore pressure variation during CO_2 injection for 5 years of injection period at various injection pressures (a) With only injection well (b) with simultaneous injection and production (c) with water production in series with CO_2 injection

(a)

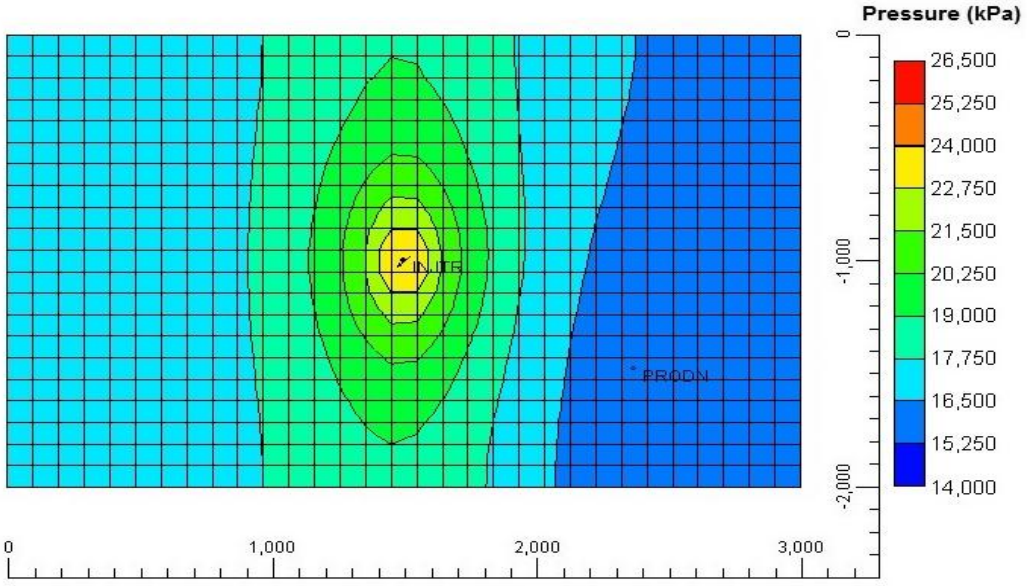

(b)

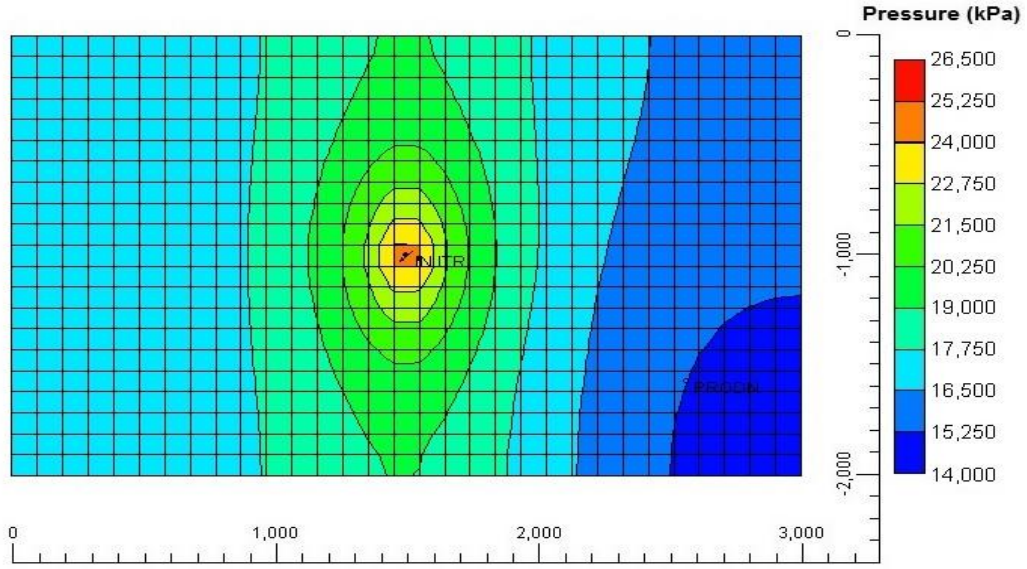

(c)

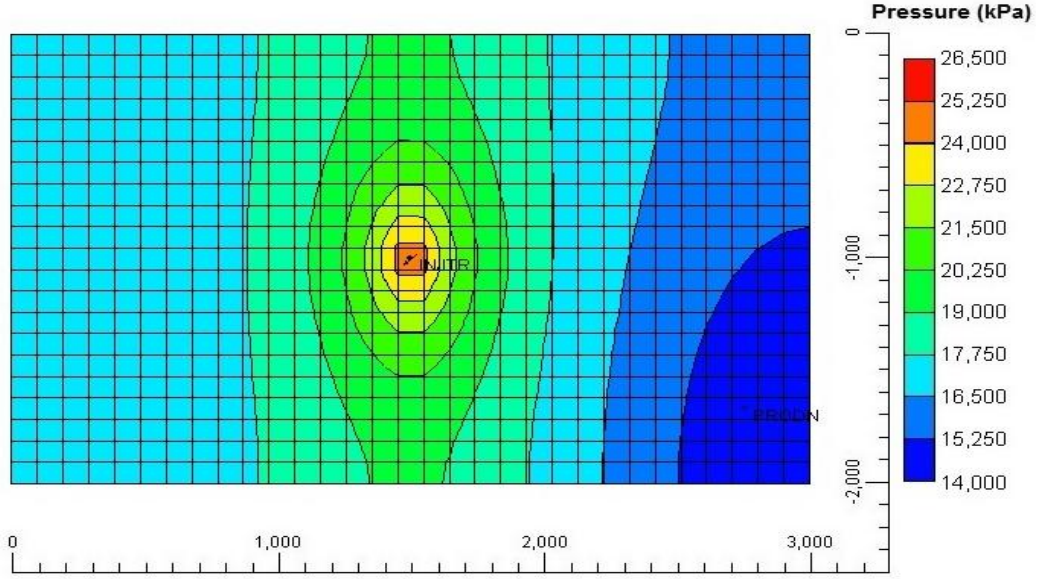

Figure 4.12 Influence of the production well location on the reservoir pore pressure (a) production well placed at a distance of 1000 meters from the injection well (b) production well placed at a distance of 1200 meters from the injection well (c) production well placed at a distance of 1400 meters

(a)

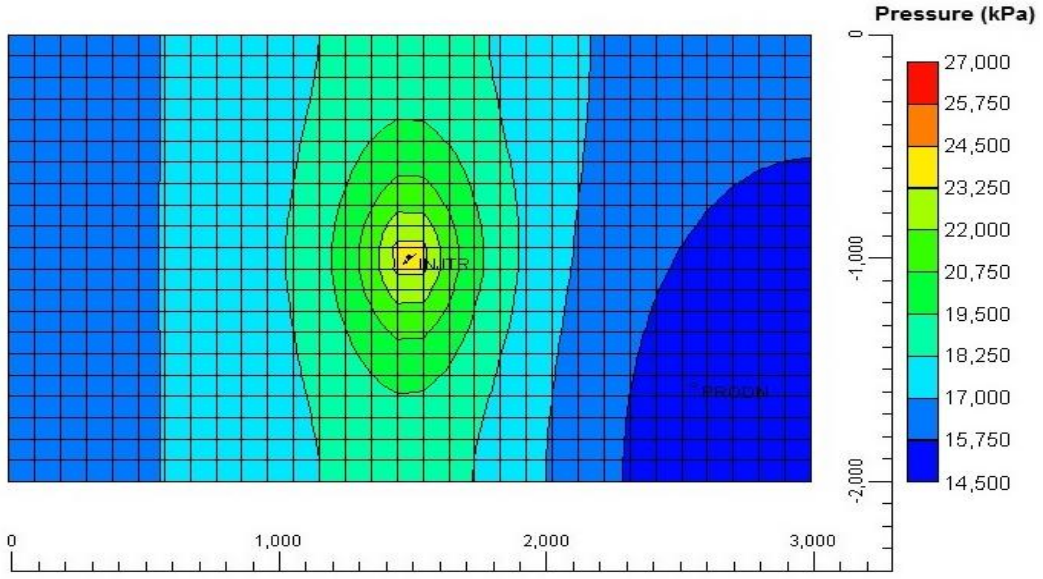
Pressure (kPa)
27,000
25,750
24,500
23,250
22,000
20,750
19,500
18,250
17,000
15,750
14,500
0
-1,000
-2,000
0
1,000
2,000
3,000
INJTR
PRODN

(b)

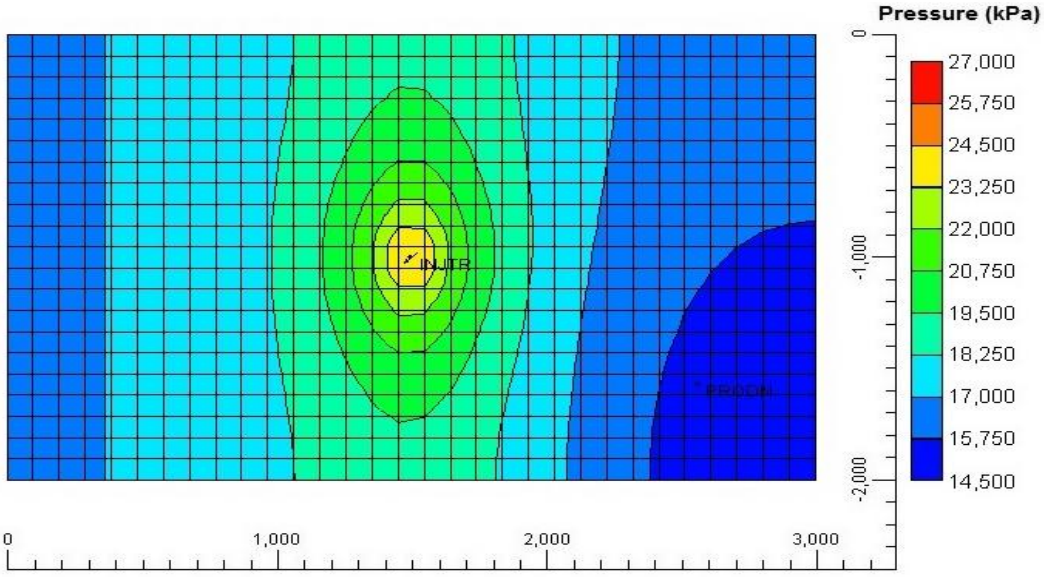
Pressure (kPa)
27,000
25,750
24,500
23,250
22,000
20,750
19,500
18,250
17,000
15,750
14,500
0
-1,000
-2,000
0
1,000
2,000
3,000
INJTR
PRODN

(c)

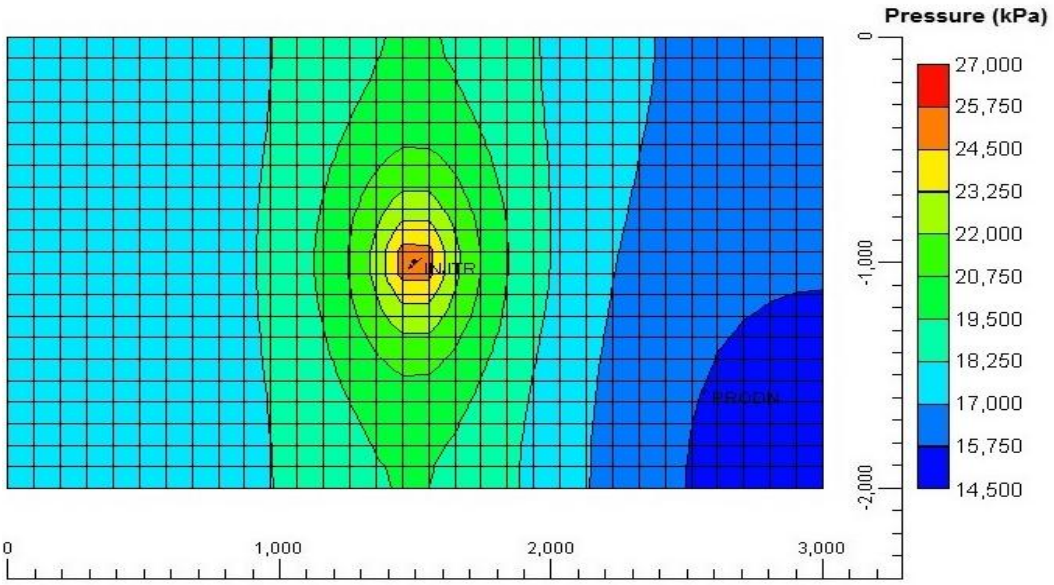

Figure 4.13 Influence of the bottom hole pressure of the production well on the magnitude of the pore pressure in the reservoir (a) Bottom hole pressure of 1000 Pa (b) Bottom hole pressure of 2000 Pa (c) Bottom hole pressure of 3000 Pa

(a)

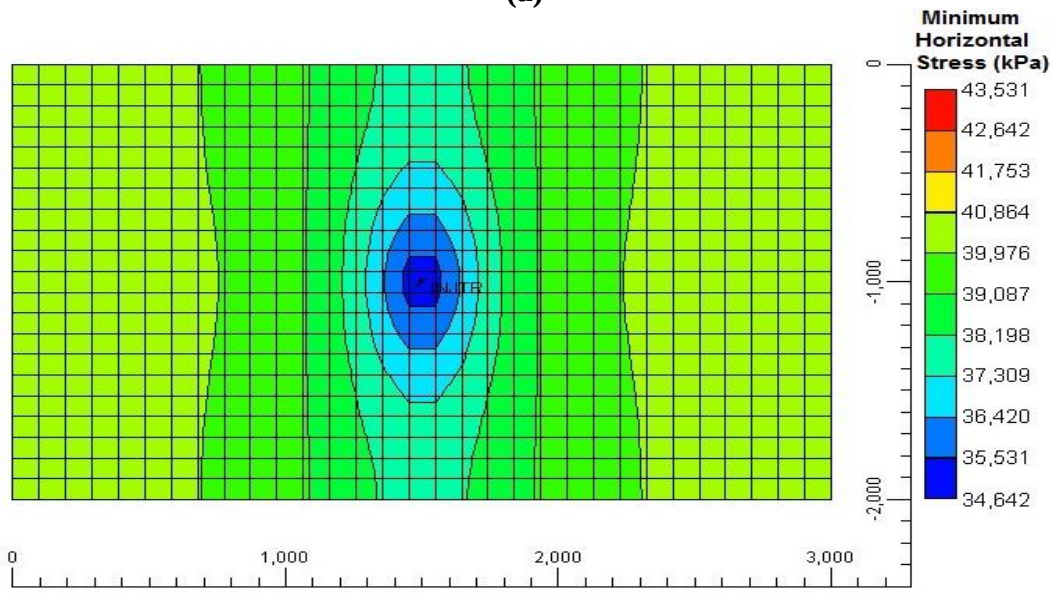

(b)

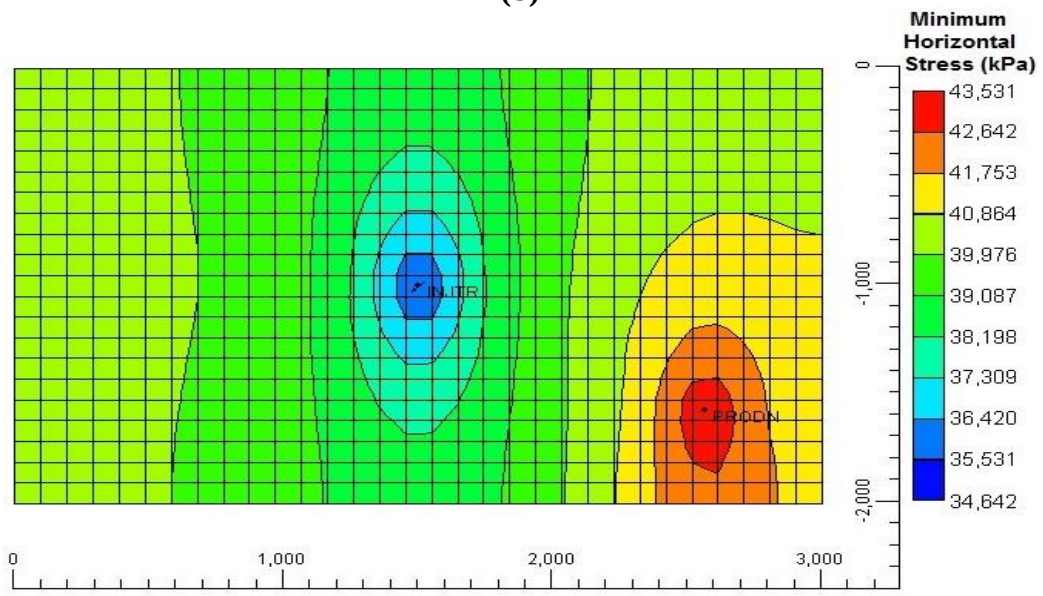

(c)

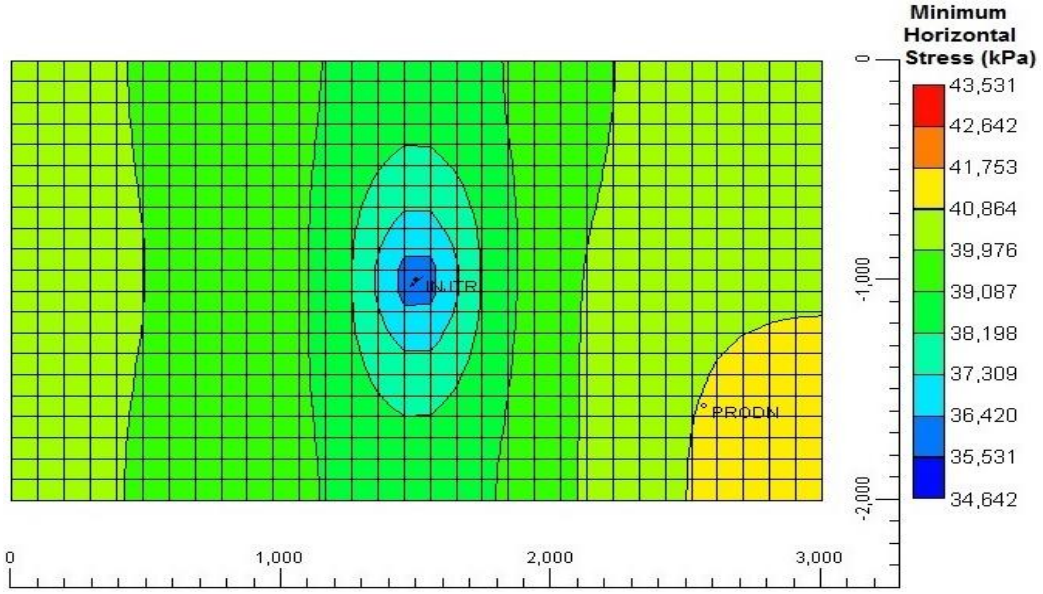

Figure 4.14 Changes in the minimum horizontal stress on the reservoir during carbon dioxide injection (a) With only injection well (b) with simultaneous injection and production (c) with water production in series with CO_2 injection

(a)

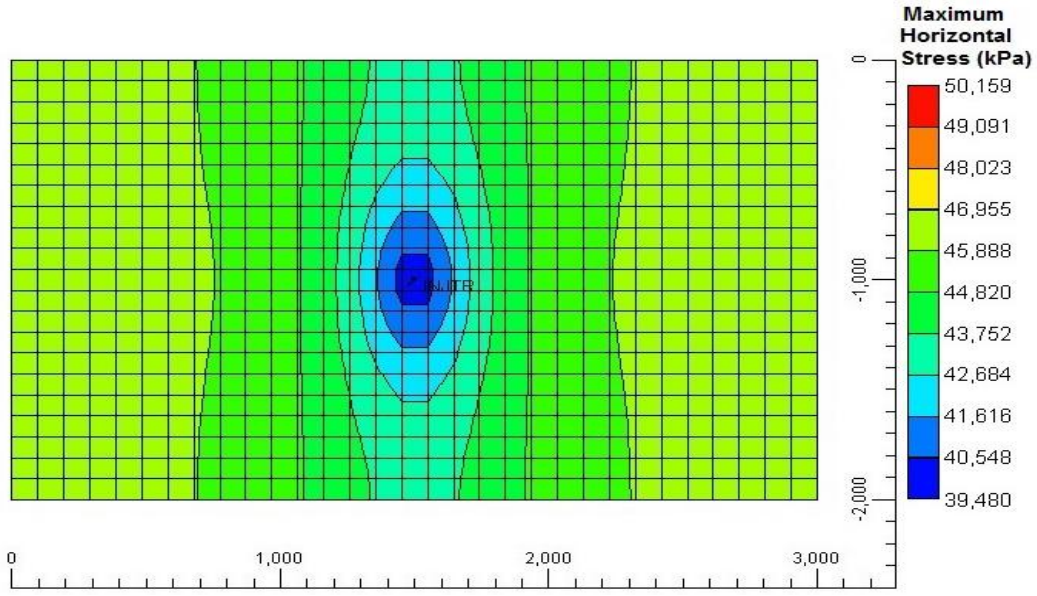
Maximum
Horizontal
Stress (kPa)
50,159
49,091
48,023
46,955
45,888
44,820
43,752
42,684
41,616
40,548
39,480
0
-1,000
-2,000
0
1,000
2,000
3,000
IN_ITR

(b)

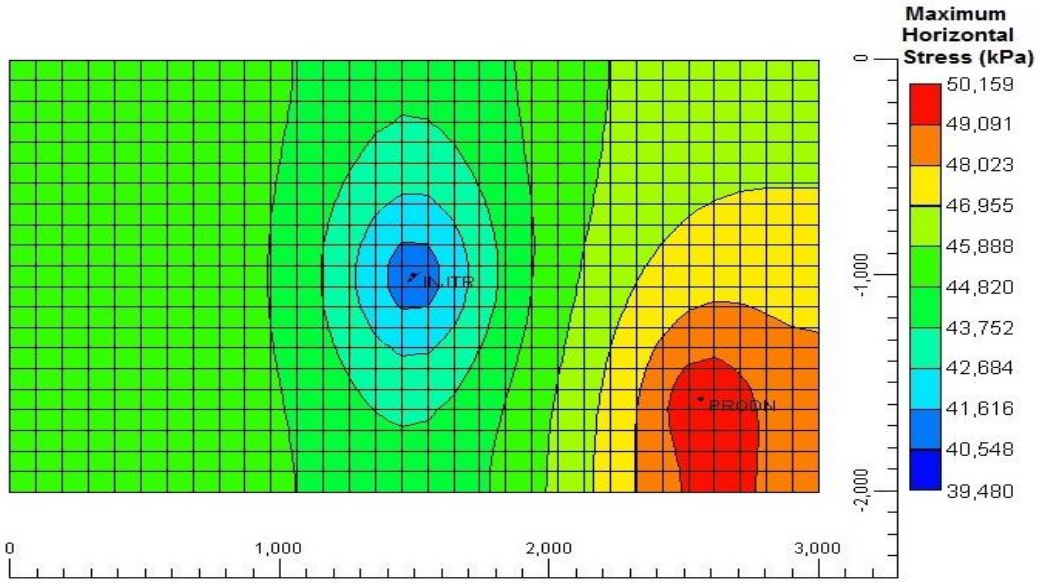
Maximum
Horizontal
Stress (kPa)
50,159
49,091
48,023
46,955
45,888
44,820
43,752
42,684
41,616
40,548
39,480
0
-1,000
-2,000
0
1,000
2,000
3,000
IN_ITR
PROD1N

(c)

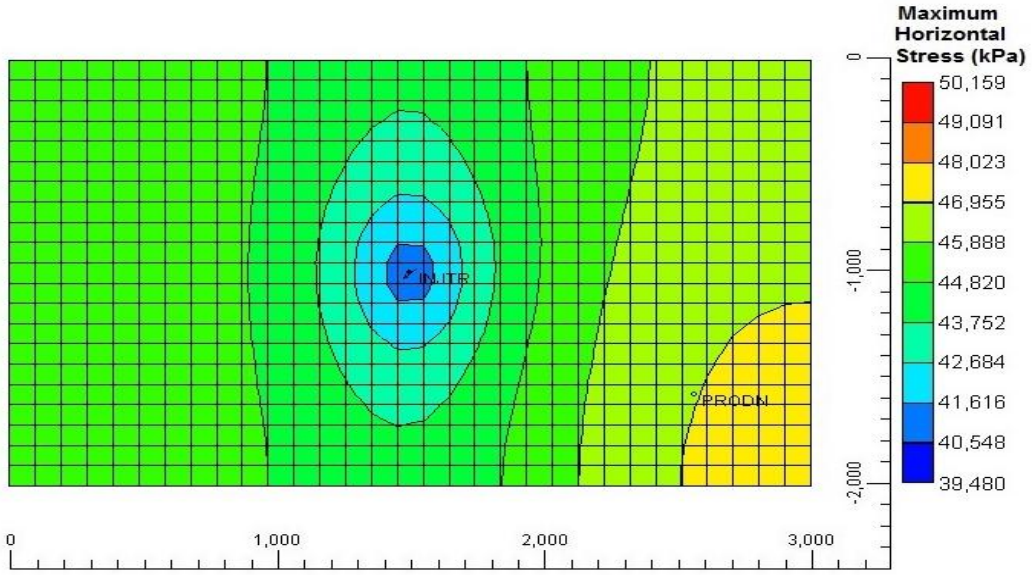

Figure 4.15 Changes in the maximum horizontal stress on the reservoir during carbon dioxide injection (a) With only injection well (b) with simultaneous injection and production (c) with water production in series with CO_2 injection

(a)

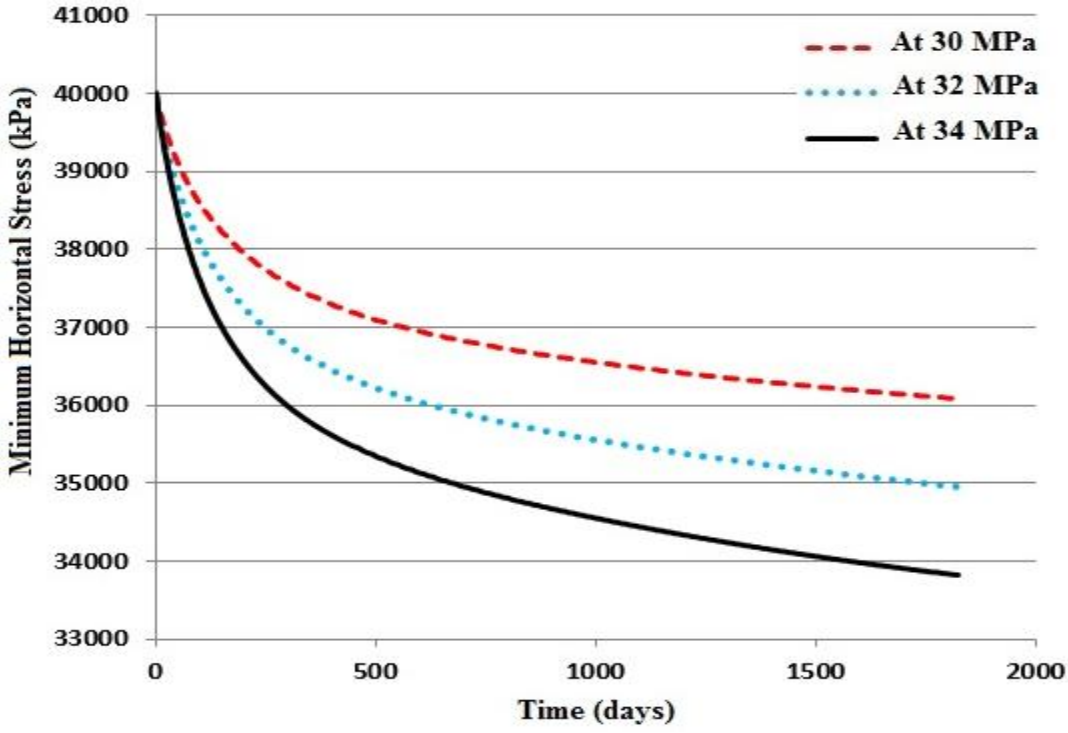

(b)

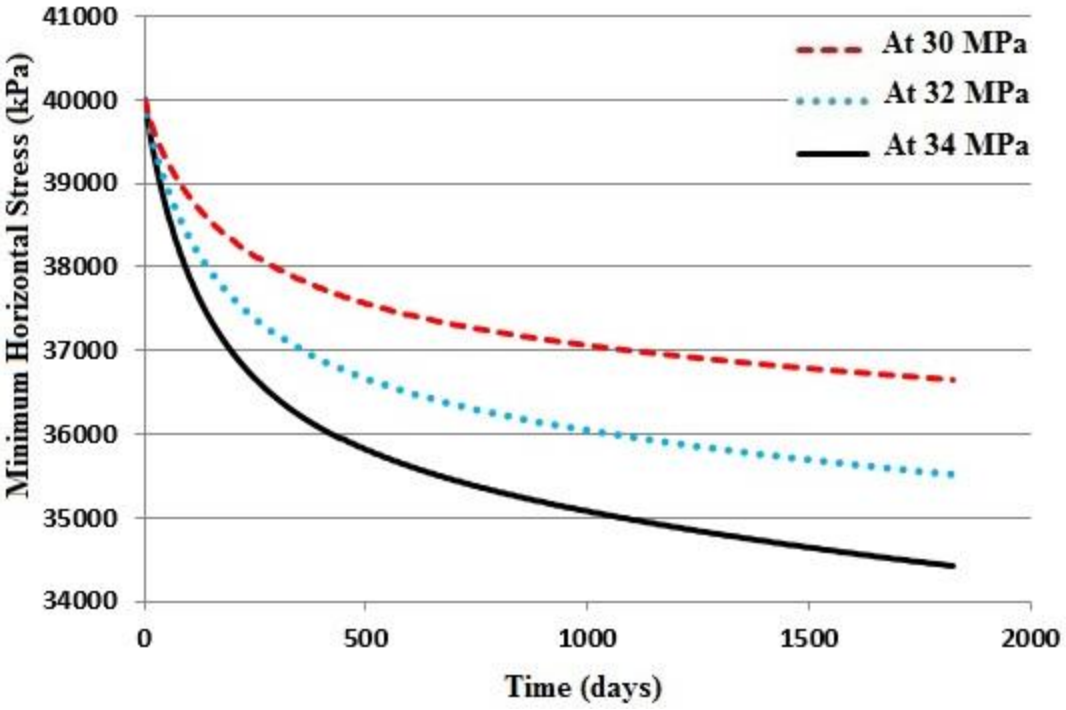

(c)

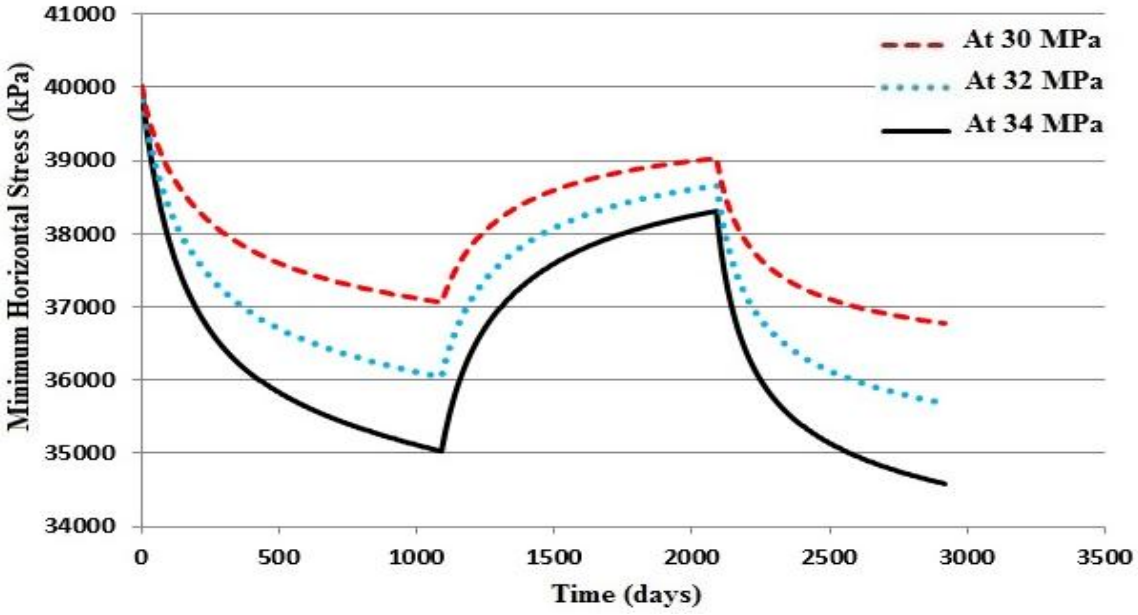

Figure 4.16 Minimum horizontal stress variation during CO_2 injection for 5 years of injection period at various injection pressures (a) With only injection well (b) with simultaneous injection and production (c) with water production in series with CO_2 injection

(a)

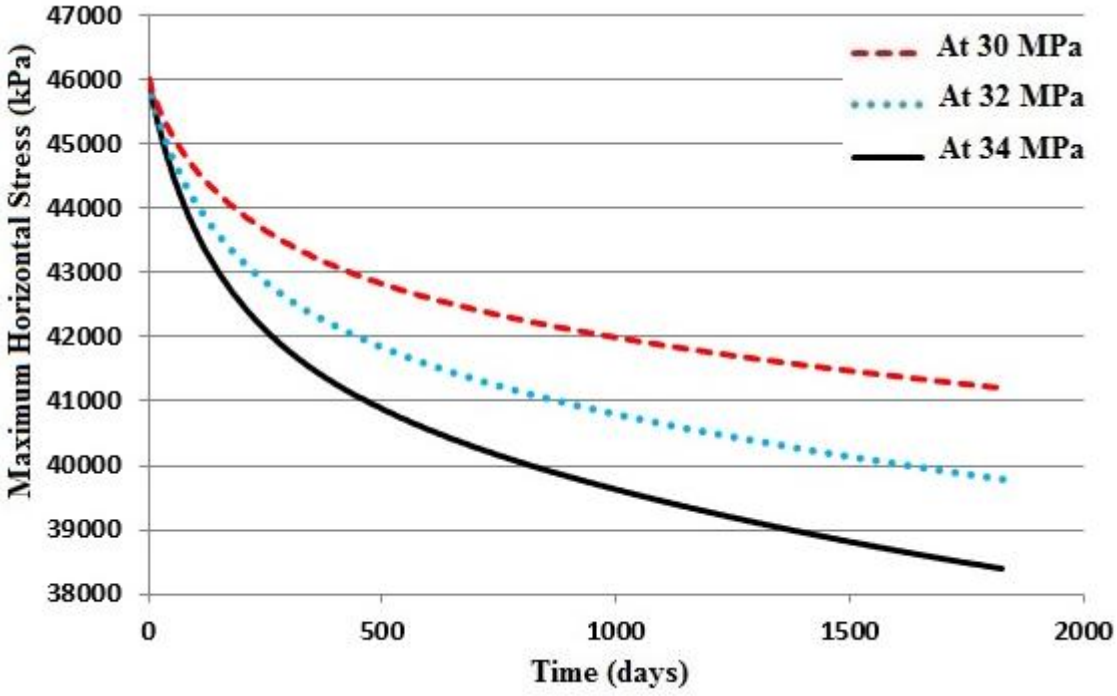
Maximum Horizontal Stress (kPa)
47000
46000
45000
44000
43000
42000
41000
40000
39000
38000
0
500
1000
1500
2000
Time (days)
At 30 MPa
At 32 MPa
At 34 MPa

(b)

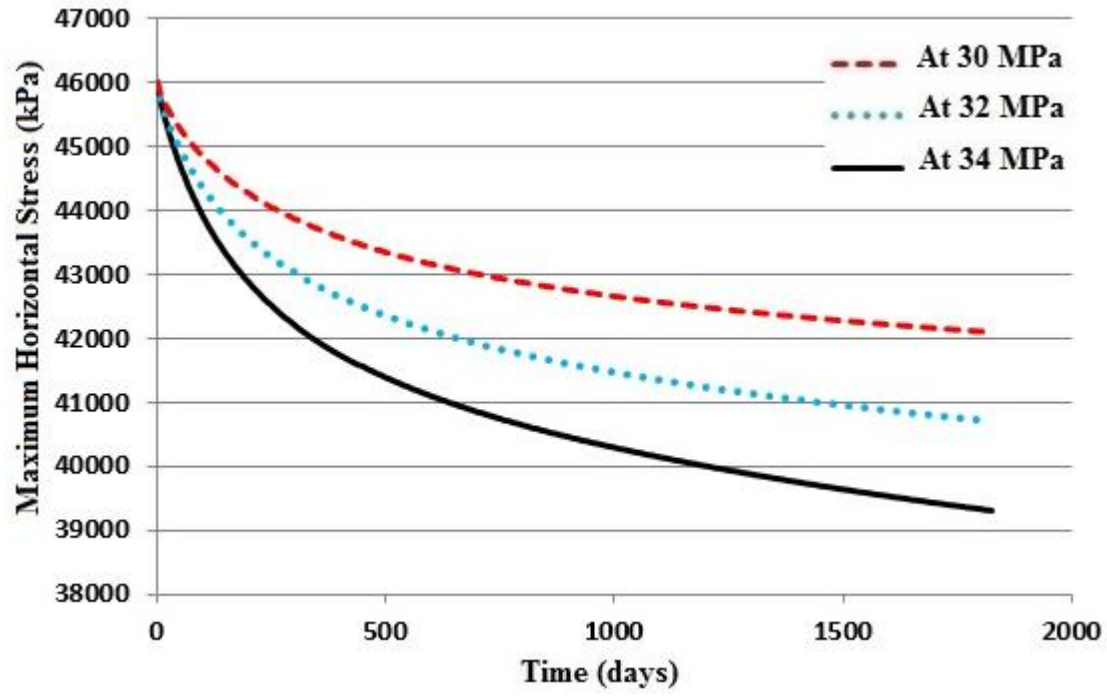
Maximum Horizontal Stress (kPa)
47000
46000
45000
44000
43000
42000
41000
40000
39000
38000
0
500
1000
1500
2000
Time (days)
At 30 MPa
At 32 MPa
At 34 MPa

(c)

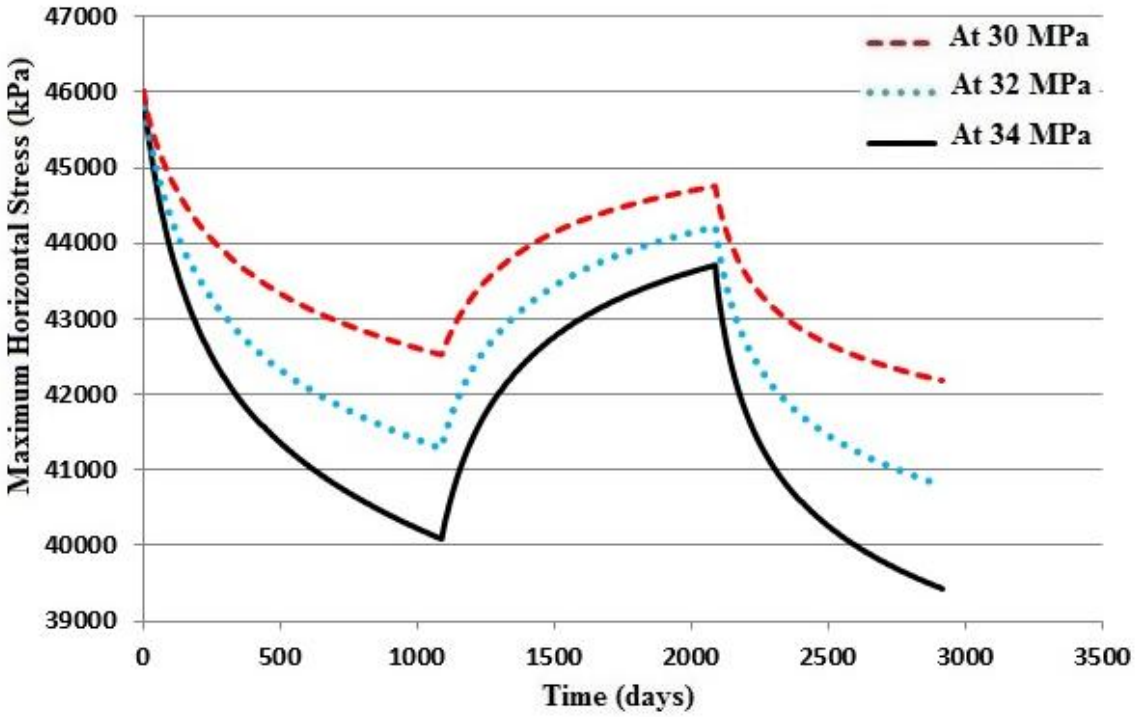

Figure 4.17 Maximum horizontal stress variation during CO_2 injection for 5 years of injection period at various injection pressures (a) With only injection well (b) with simultaneous injection and production (c) with water production in series with CO_2 injection

4.3.3.2 Ground vertical movement during CO_2 injection

The ground vertical displacement is a very key output during the geomechanical modeling of reservoirs undergoing carbon dioxide injection. The geomechanical modeling in this study shows that the pore pressure increase causes the ground uplift and a decrease in the pore pressure causes a subsidence of the ground surface. The ground vertical displacement is shown in Figure 4.18, for the cases of single injection well and combined injection and production wells. As shown in Figure 4.18, for the case of only injection well in the system, the ground vertical displacement is the maximum. Adding the production well to the reservoir helps in reducing the magnitude of ground vertical

displacement. During the simultaneous carbon dioxide injection and water production process although the maximum value of the ground vertical uplift was reduced but the ground surface above the production well has a high value of subsidence due to the pore pressure reduction in the vicinity of the production well. Another strategy was used, in which the water production process was performed after the initial carbon dioxide injection, which helps in limiting the value of ground subsidence above the production well and also reduces the vertical ground displacement above the injection well.

The variation in ground vertical displacement with time is shown in Figure 4.19 for the cases of single injection well and combined injection and production wells. During the case of single injection well, the value of the ground uplift increases continuously to a maximum value till the end of injection period. During the case of simultaneous injection and production process the magnitude of the ground uplift increases continuously but the maximum value is less than that of the case of single injection well. During the case when carbon dioxide injection and water production was carried out in series, the value of the ground uplift increases during the first 3 years of carbon dioxide injection followed by a reduction during the 3 years of water production, and at the end again an increase during the last 2 years of carbon dioxide injection. At the end of the process the final value of the ground vertical displacement is minimum compared to the other injection scenarios.

(a)

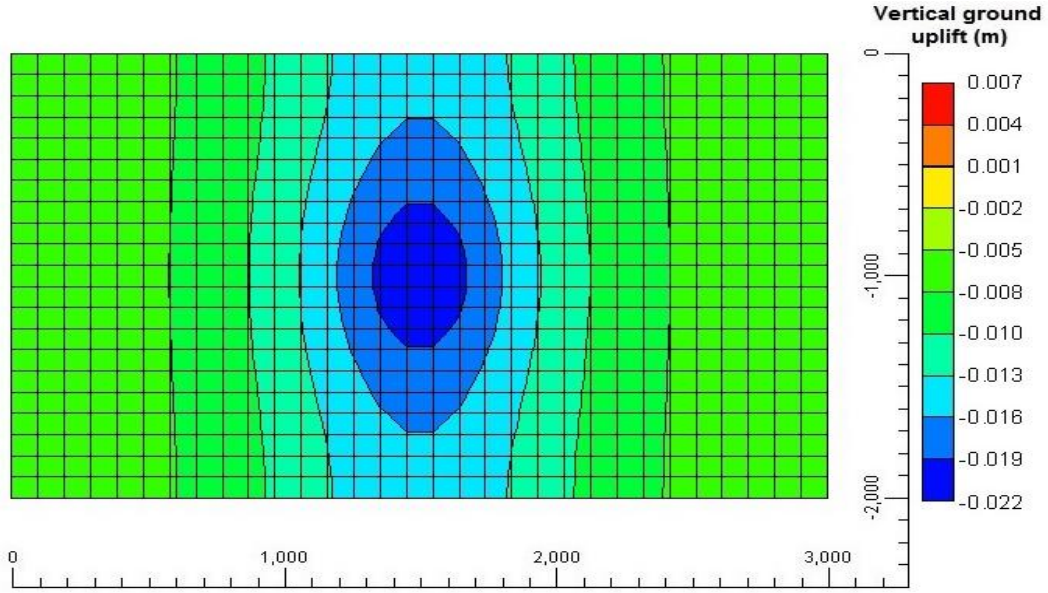
Vertical ground uplift (m)
0.007
0.004
0.001
-0.002
-0.005
-0.008
-0.010
-0.013
-0.016
-0.019
-0.022
0
-1,000
-2,000
0
1,000
2,000
3,000

(b)

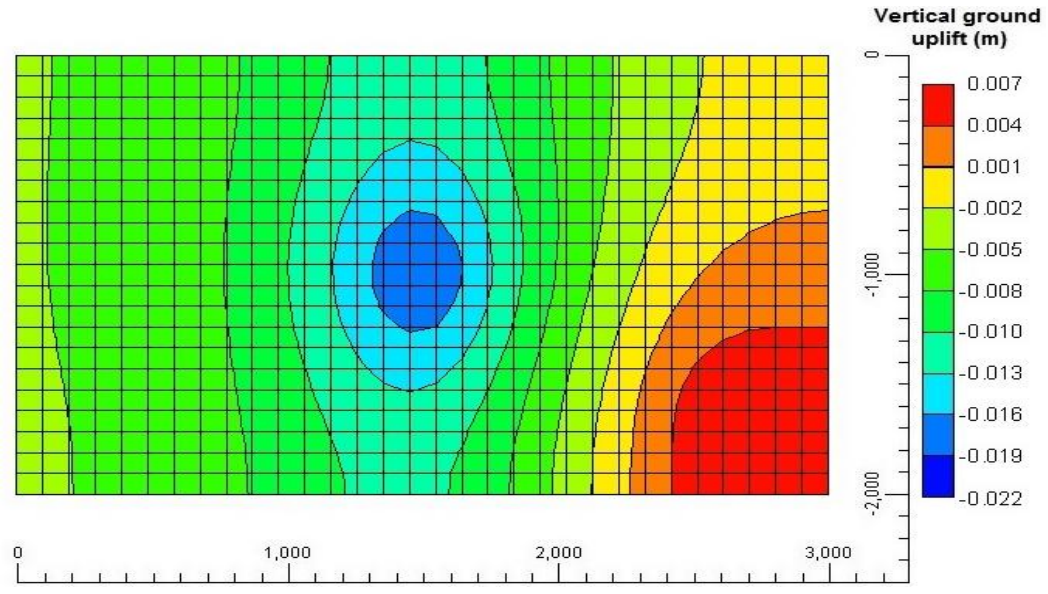
Vertical ground uplift (m)
0.007
0.004
0.001
-0.002
-0.005
-0.008
-0.010
-0.013
-0.016
-0.019
-0.022
0
-1,000
-2,000
0
1,000
2,000
3,000

(c)

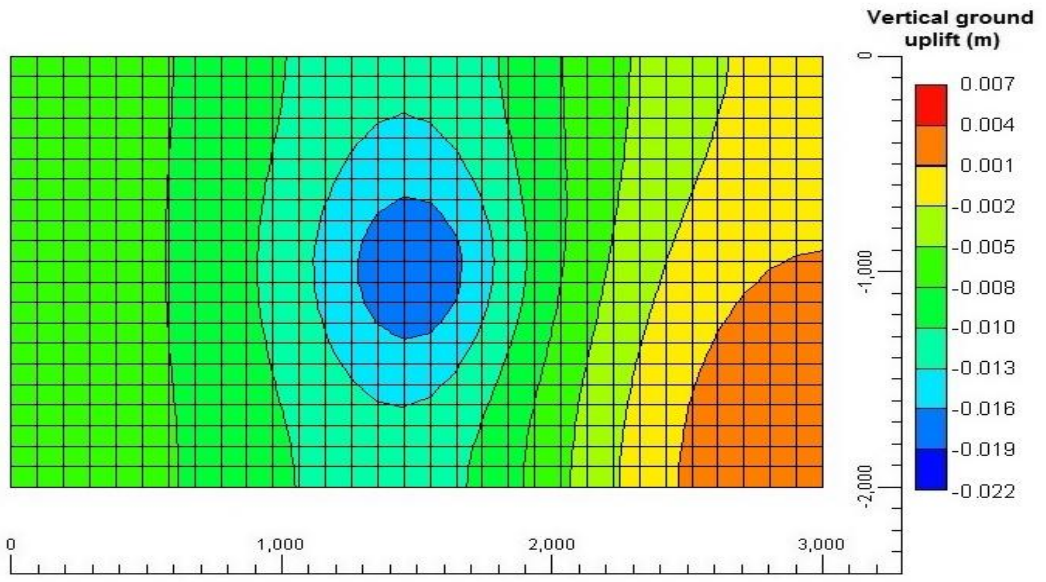

Figure 4.18 Ground vertical displacement after CO_2 injection (a) With only injection well (b) with simultaneous injection and production (c) with water production in series with CO_2 injection

(a)

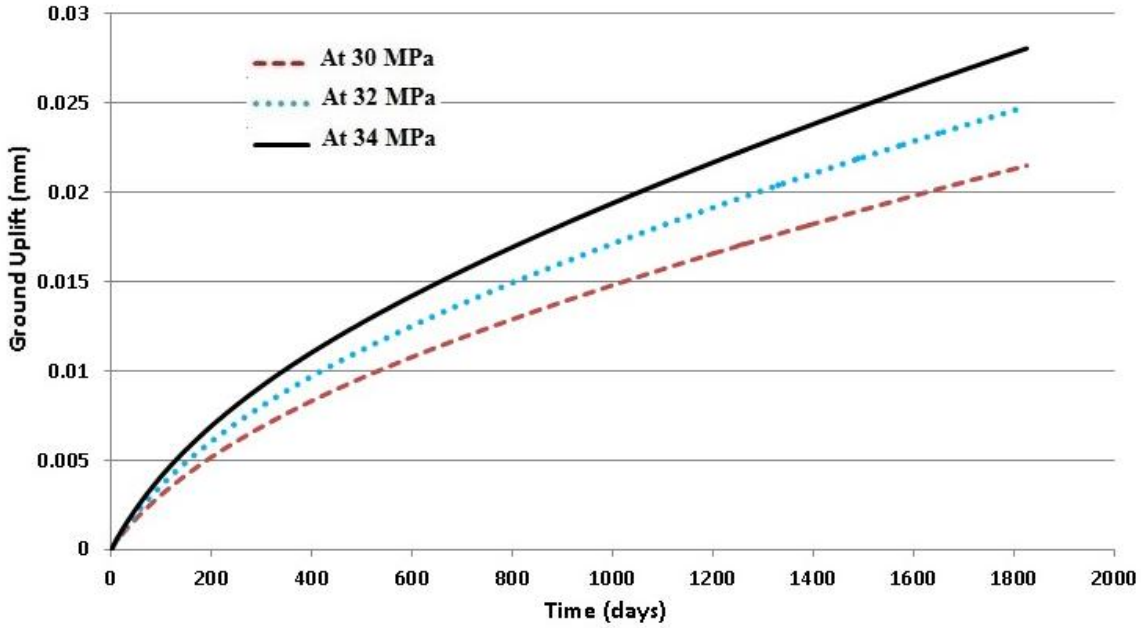

(b)

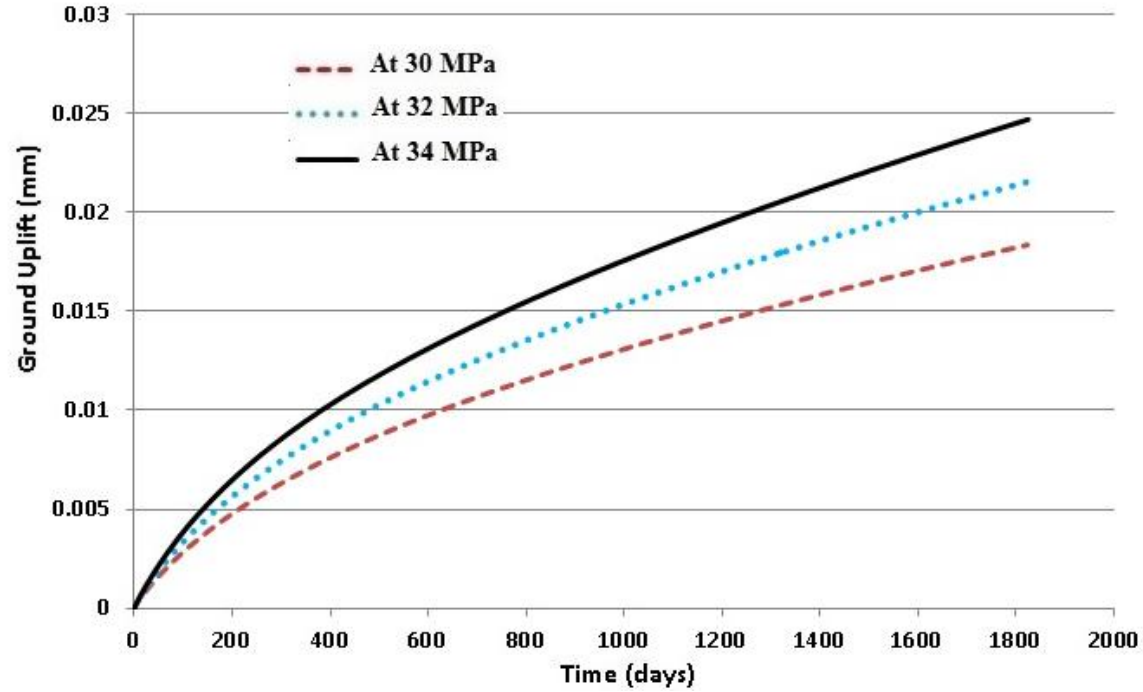

(c)

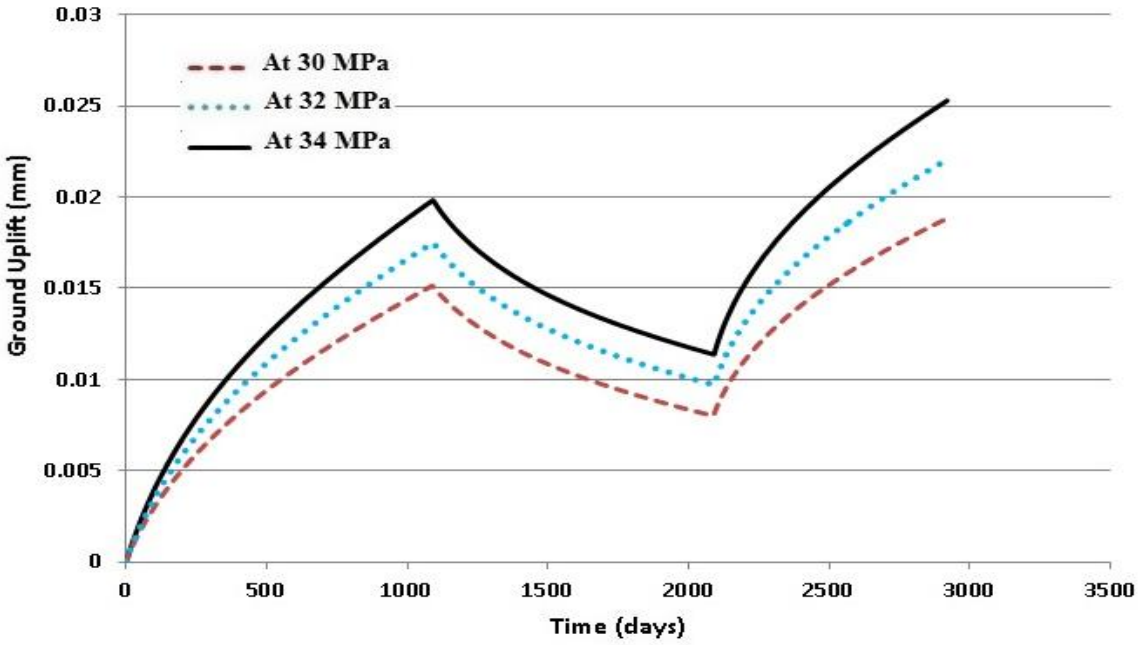

Figure 4.19 Ground vertical displacement variation during CO_2 injection for 5 years of injection period at various injection pressures (a) With only injection well (b) with simultaneous injection and production (c) with water production in series with CO_2 injection

4.3.3.3 Stability analysis for Ghawar reservoir

In the current portion of the study the injection of carbon dioxide into the naturally fractured carbonate Ghawar reservoir is considered with water as a base fluid in the reservoir. Performing the stability analysis for the injection scenarios in this study is very necessary because both carbon dioxide injection and water production are considered in this study. Both the excessive increase in the pore pressure due to carbon dioxide injection and excessive decrease in the pore pressure due to water production can cause the failure of the reservoir structure [30, 84]. Using the Mohr-Coulomb failure criterion the stability analysis was performed for various cases of carbon dioxide injection.

From Figure 4.11, the maximum value of the pore pressure in the reservoir is with the case of only injection well in the system. The failure envelope for the naturally fractured Ghawar carbonate reservoir is shown in Figure 4.20 for the cases of single injection well and combined injection and production wells. The dotted circle in Figure 4.20 shows the initial stressed condition of the reservoir based on the initial pore pressure of 16.5 MPa, minimum principle stress of magnitude 36.96 MPa and maximum principle stress of magnitude 46.20 MPa. After five years of carbon dioxide injection the final stressed condition of the reservoir is shown in Figure 4.20 for the cases of single injection well and combined injection and production wells. Even for high values of pressure buildup during the case of only injection well in the system, the reservoir is still on safe side for five years of carbon dioxide injection.

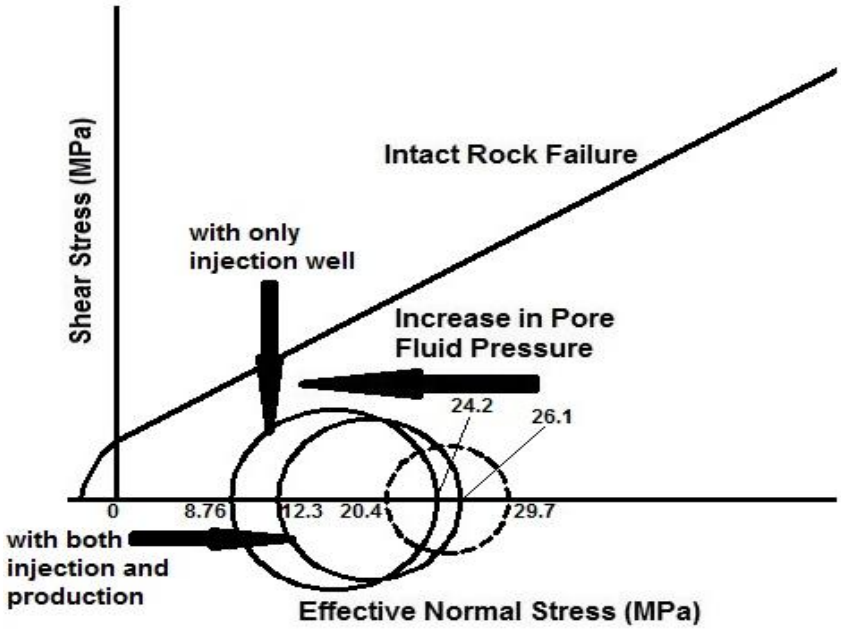

Figure 4.20 Stability analysis for CO_2 injection into the naturally fractured Ghawar reservoir with water as a base fluid

This chapter discusses various issues related to the injection of carbon dioxide into naturally fractured Ghawar carbonate reservoir with both the single and two-phase flow through the reservoir. The next chapter will discuss the injection of carbon dioxide using multiple injection wells and its effects on the storage capacity and stability of the reservoir.

CHAPTER 5

EFFECT OF INJECTION WELL ARRANGEMENT ON CO_2 INJECTION

5.1 Overview of injection wells arrangement

The injection of CO_2 into the reservoir, during long-term subsurface containment of CO_2, increases the pore pressure, as well as the adsorption induced strains. The associated decrease in permeability causes the transport of the injected CO_2 to decrease to a critical value, after which it becomes impossible to transport the injected carbon dioxide to regions of the reservoir far away from the injection well, regardless of its capacity. This problem initiated the need of multiple injection wells. Although increasing the number of injection wells in the reservoir will increase the storage capacity of the reservoir but the injection of huge amount of carbon dioxide will also cause pore-pressure buildup in the reservoir. In the present study a new methodology is developed for reducing the pore pressure build-up and increasing the reservoir storage capacity by varying both the number and arrangement of carbon dioxide injection wells. The effect of injection wells arrangement on the stability of the reservoir is also investigated. Starting with the case of two injection wells, the location of the wells are changed with respect to the center of the reservoir and its effect on the pressure buildup was monitored. Similar procedure was performed for three and four injection wells. At the end optimum number of injection wells and their location was proposed for the injection location in the study.

COMSOL multiphysics software is used to model the reservoir and the overburden layers between the ground surface and the reservoir. Starting from the Arab

Jubaila carbonate reservoir each geological layer is modeled in COMSOL, such that each layer has a different thickness value [70]. Starting with the case of two injection wells, the number of injection wells was increased up to four. The Ghawar Arab D carbonate reservoir with different arrangements of injection wells is shown in Figure 5.1. Each of the models in Figure 5.1 has a total of 276,660 degrees of freedom with five independent variables at each node (two pressures and three displacement components). The two pressure variables are for the matrix and the fracture. For calculation of ground vertical uplift due to carbon dioxide injection, the bottom surface of each simulation model is constrained, the surfaces defined by normal along x and y axes are described by roller boundary conditions, and the top surfaces are left free for each of the simulation model in Figure 5.1. The formation properties and various input parameters are listed in Table 5.1.

(a)

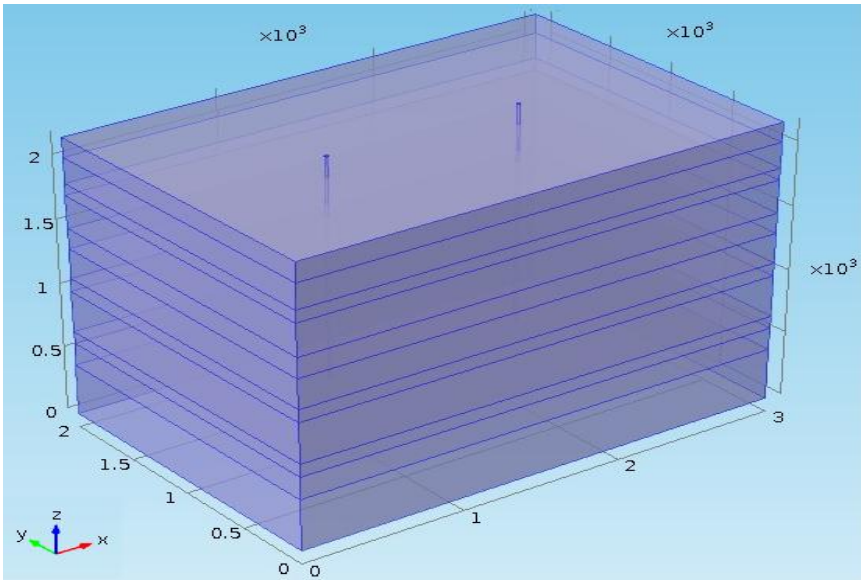

(b)

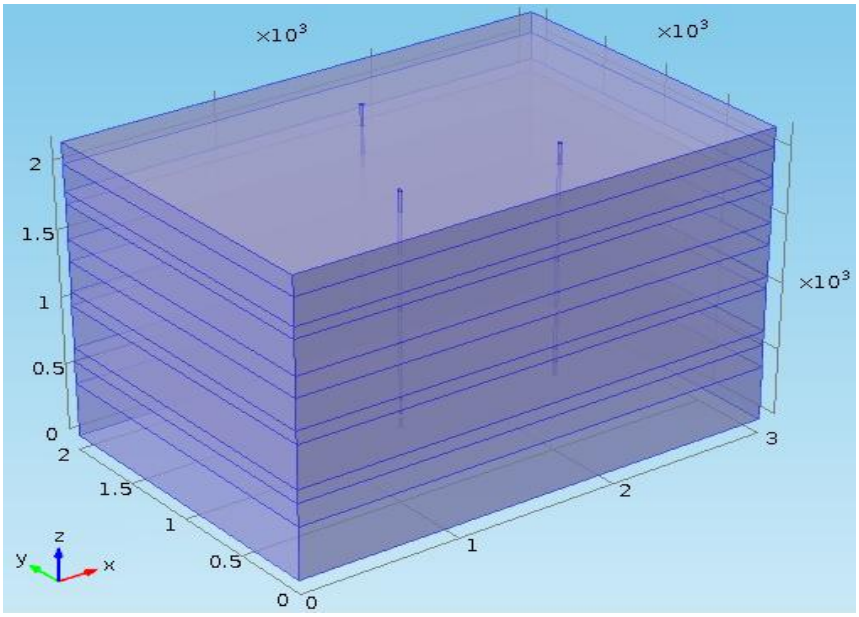

(c)

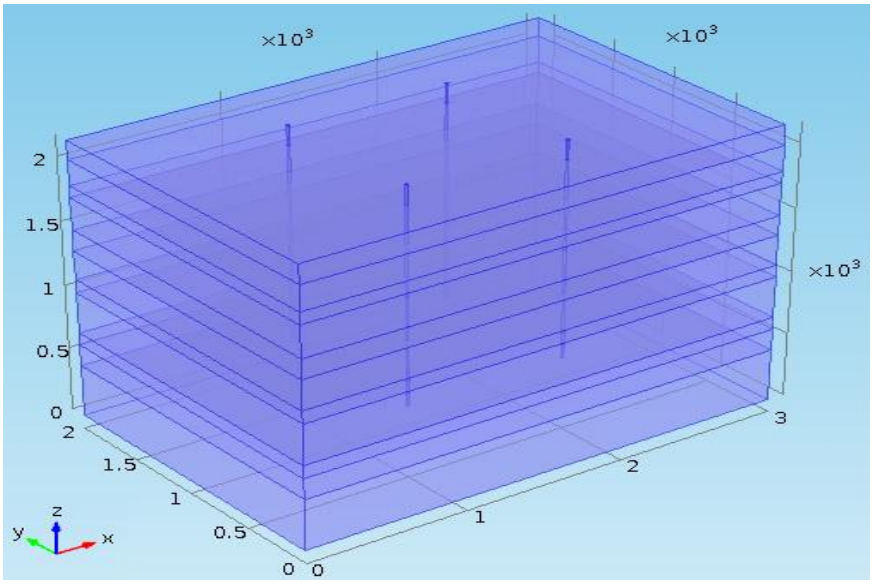

Figure 5.1 Simulation models for the Ghawar Arab-D carbonate petroleum reservoir undergoing CO_2 injection; (a) two wells, (b) three wells (triangular), (c) four wells (rectangular)

Table 5.1Formation properties for the simulation of CO_2 injection into carbonate reservoir [70, 72, 104-107]

Model Parameter	For Reservoir	For Caprock	For under burden layer
Rock Density, $\rho(Kg/m^3)$	2400	1870	2550
Young's Modulus, E (GPa)	48.5	37.05	53.5
Bulk Modulus, K (GPa)	39.24	23.75	34.5
Shear Modulus, G (GPa)	18.1	13.8	19.9
Initial porosity, $\emptyset_m$	0.13	0.01	0.10
Initial permeability, k_m (10^{-15} m^2)	0.6	0.00001	0.2
Biot Coefficient, α	0.8	0.2	0.4
Dynamic Viscosity, $\mu(10^{-5}Pa.s)$	1.84	1.84	1.84
Pressure wave velocity, Vp (m/sec)	5140	4750	4900
Shear wave velocity, Vs (m/sec)	2748	2720	2800

The overall simulation properties for CO_2 injection scenarios into the multi-layer 3D models for Ghawar location is given in Table 5.2.

Table 5.2 Overall simulation properties for CO_2 injection into Ghawar reservoir

CO_2 injection rate (kTons/Year)	1,000 (31.7 kg/sec)
CO_2 injection period (Years)	5
Overall model dimensions, length×width×height (m)	3,000 X 2,000 X 2,170

The following sections of the chapter discuss the effects of increasing the number of carbon dioxide injection wells on the pore-pressure buildup, ground uplift, maximum occupancy, and stability of the reservoir.

5.2 Various injection well arrangements with two injection wells

In the case of two injection wells the various discussed wells arrangements are in-line (injection wells placed along a line along the length of the reservoir passes through the center of the reservoir) wells arrangement type. With symmetric placement of the

injection wells along the centre line of the wells, the various arrangements of the injection wells are given in Table 5.3.

Table 5.3 Different in-line two-well arrangements

Arrangement	Well Spacing (m)
Case 1	600
Case 2	800
Case 3	1000
Case 4	1200

The following sections summarize the numerical simulation results for the two injection wells at 600, 800, 1000, and 1200 meters distance.

5.2.1 Pressure variation for various arrangements with two injection wells

For the case of two injection wells, as a starting point, the injection wells are placed along the centerline of the injection plane in the reservoir. Each well is at a distance of 300 meters from the center of the reservoir with a central distance of 600 meters between the two injection wells. After a five-year injection period, the pressure variation is shown in Figure 5.2. As shown in Figure 5.2, the pore pressure increases with carbon dioxide injection. The regions of the reservoir nearer to the injection wells are at higher pressure as compared to the areas far away from the wells. The pore pressure variation for various periods of carbon dioxide injection is shown in Figure 5.3. After five years of injection period, the pressure variation for the various arrangements with two injection wells is shown in Figure 5.4. As shown in Figure 5.4, the injection wells at 800 meters has the

lowest pore pressure build up value and the injection wells at 1200 meters has the maximum pressure build value. The pore pressure variation for the various arrangements of two injection wells is shown in Figure 5.5. As shown in Figure 5.5, the pore pressure variation is highly dependent on the arrangement of injection wells. The pressure build up is high for the injection wells nearer to each other during the initial period of carbon dioxide injection. The pressure built up for the injection wells nearer to the boundary surfaces of the reservoir is higher after almost three years of carbon dioxide injection.

The maximum pore pressure for various arrangements of two-injection wells is summarized in Figure 5.6. The case 1 is for two injection wells with a central distance of 600 meters and case 2 is for two injection wells with a central distance of 800 meters. Case 3 is for two injection wells with a central distance of 1000 meters and case 4 is for two injection wells with a central distance of 1200 meters. The pore pressure value for case 1 is more as compared to case 2 because the injection wells are nearer in case 1 and the pore pressure profiles interact and thus increase the overall pore pressure value. The pore pressure value of case 3 and case 4 are more as compared to case 1, although the injection wells in case 3 and 4 are far away from one another. The reason is that when the injection wells are nearer to the boundaries of the reservoir, the pressure buildup is more as compare to the case when the injection wells are nearer because the boundaries of the model are with no flow condition and will cause CO_2 accumulation. The maximum pressure buildup is for two injection wells at a central distance of 1200 meters and nearer to the reservoir boundaries.

(a)

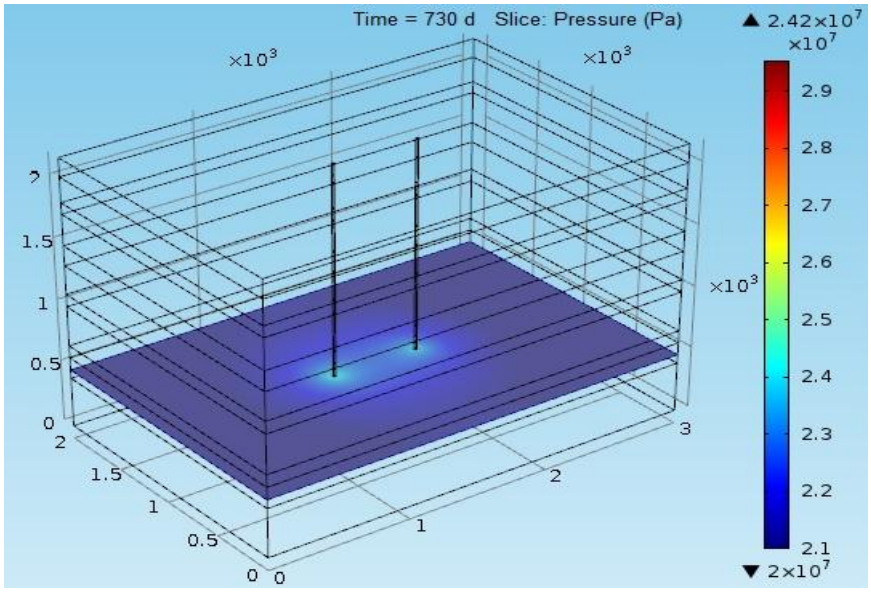
Time = 730 d Slice: Pressure (Pa)
▲ 2.42×10^7
×10^7
2.9
2.8
2.7
2.6
2.5
2.4
2.3
2.2
2.1
▼ 2×10^7
×10^3
×10^3
×10^3
0
0.5
1
1.5
2
0
0.5
1
1.5
2
0
1
2
3

(b)

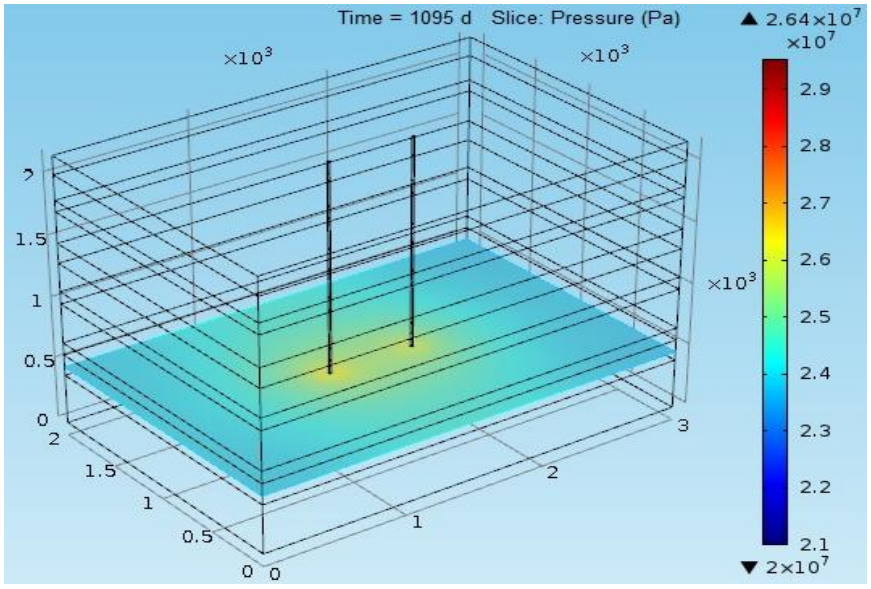
Time = 1095 d Slice: Pressure (Pa)
▲ 2.64×10^7
×10^7
2.9
2.8
2.7
2.6
2.5
2.4
2.3
2.2
2.1
▼ 2×10^7
×10^3
×10^3
×10^3
0
0.5
1
1.5
2
0
0.5
1
1.5
2
0
1
2
3

(c)

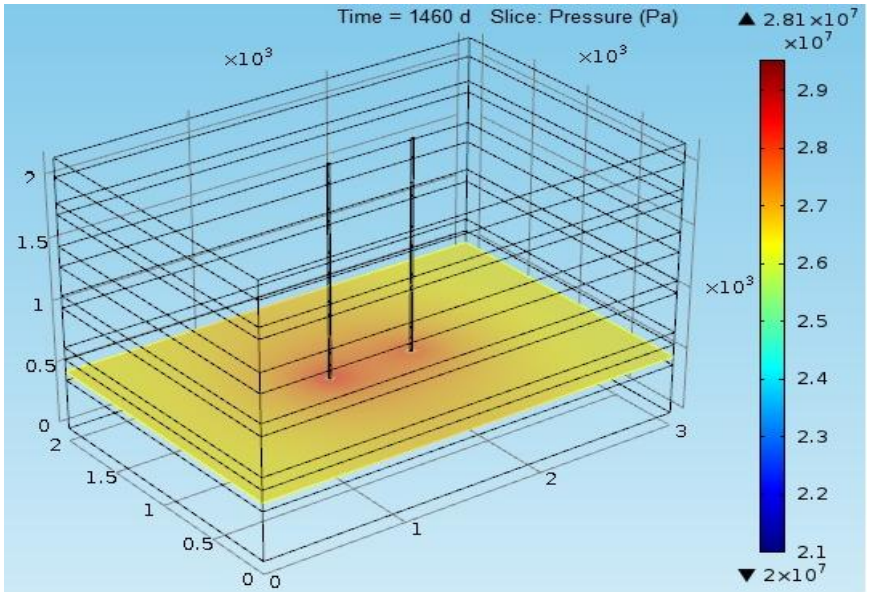

(d)

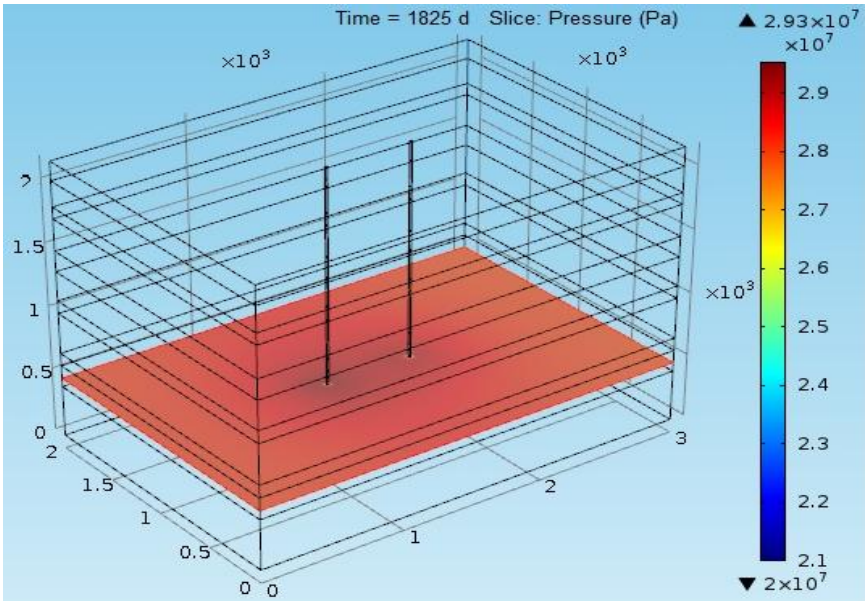

Figure 5.2 The pressure variation after five years of carbon dioxide injection using two injection wells at 600 meters

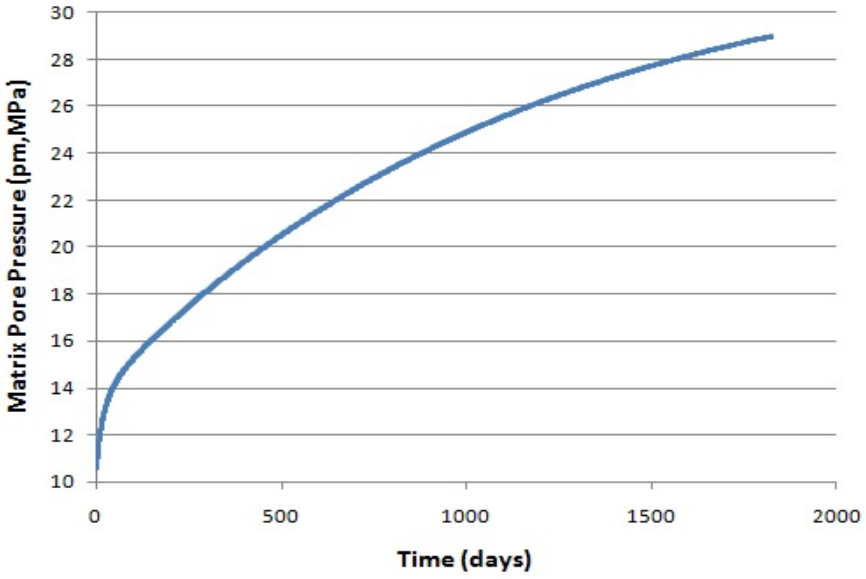

Figure 5.3 The pore pressure variations for various periods of carbon dioxide injection for two injection wells at 600 meters

(a)

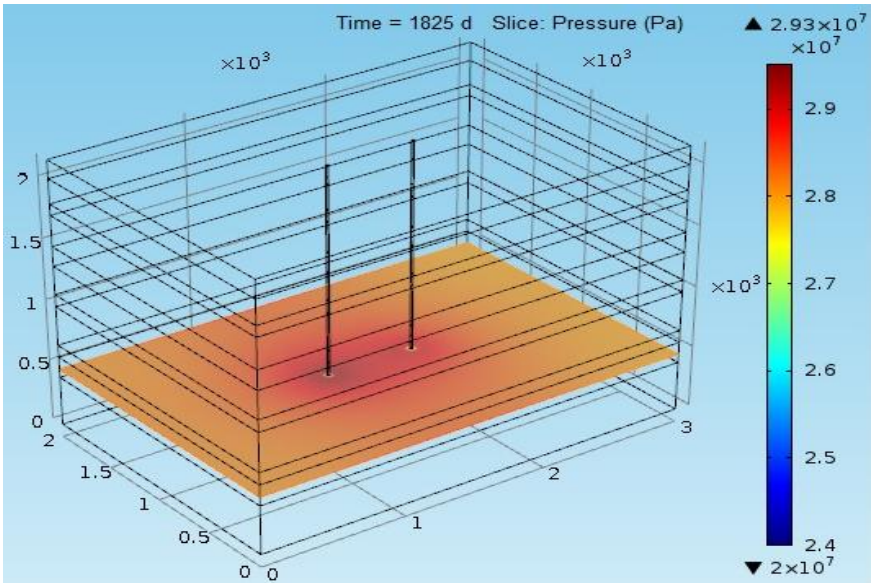

(b)

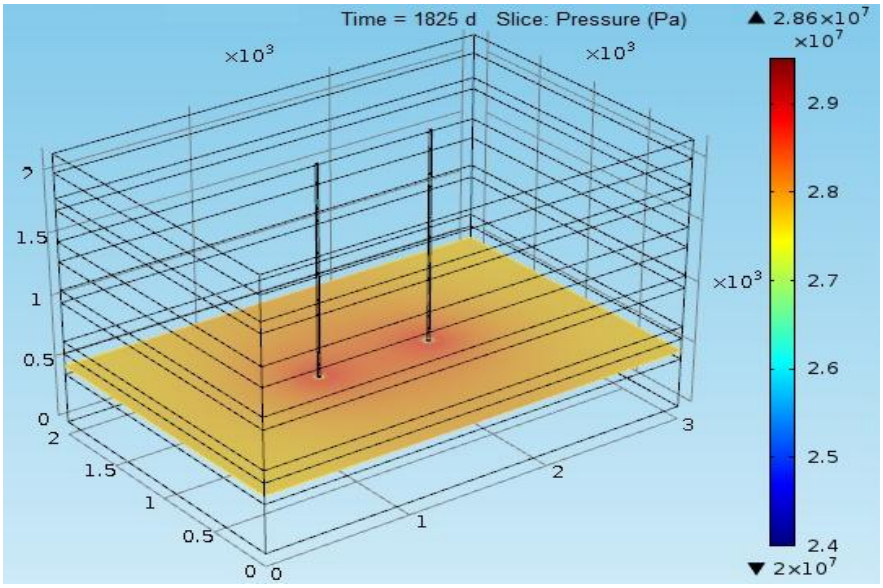
Time = 1825 d Slice: Pressure (Pa)
▲ 2.86×10^7
×10^7
2.9
2.8
2.7
2.6
2.5
2.4
▼ 2×10^7
×10^3
×10^3
×10^3
0
0.5
1
1.5
2
0
0.5
1
1.5
2
0
1
2
3

(c)

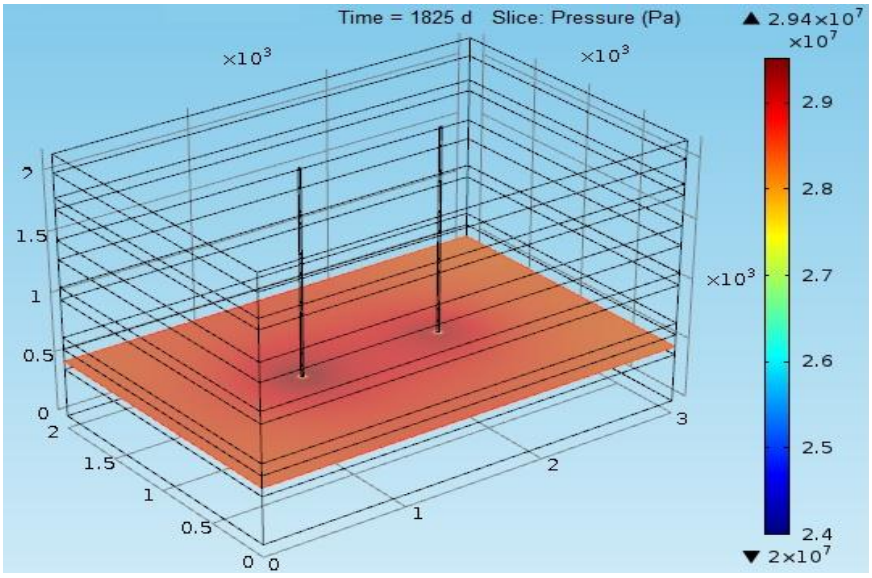
Time = 1825 d Slice: Pressure (Pa)
▲ 2.94×10^7
×10^7
2.9
2.8
2.7
2.6
2.5
2.4
▼ 2×10^7
×10^3
×10^3
×10^3
0
0.5
1
1.5
2
0
0.5
1
1.5
2
0
1
2
3

(d)

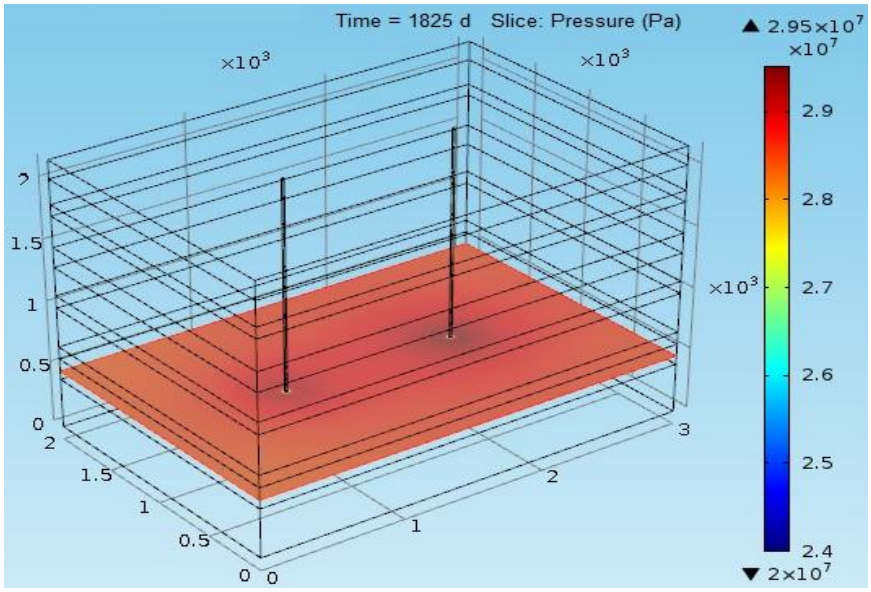

Figure 5.4 The pressure variation after five years of carbon dioxide injection using two injection wells; (a) At 600 meters, (b) At 800 meters, (c) At 1000 meters (d) At 1200 meters

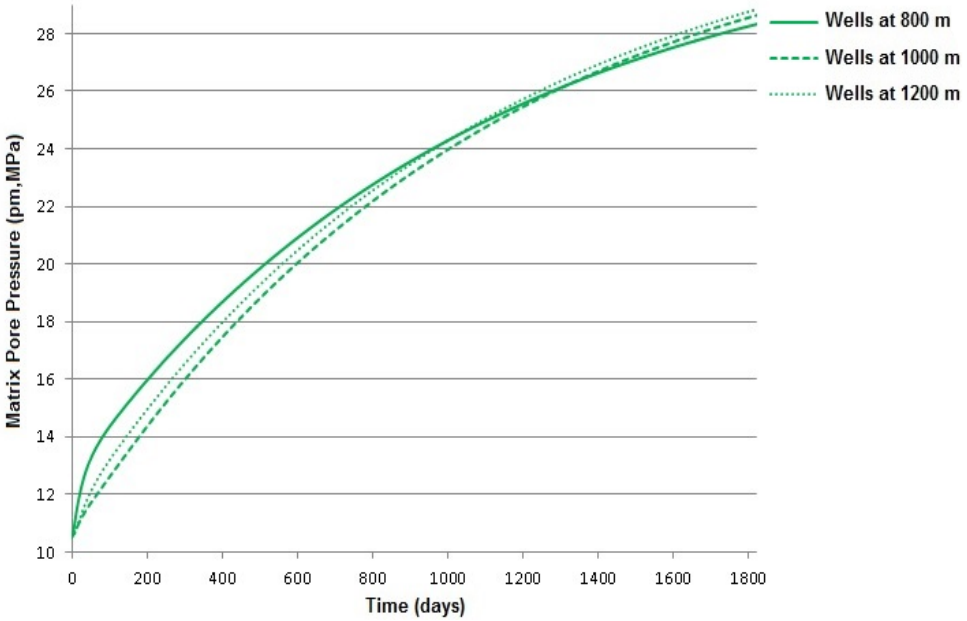

Figure 5.5 The pore pressure variations for CO_2 injection using two injection wells

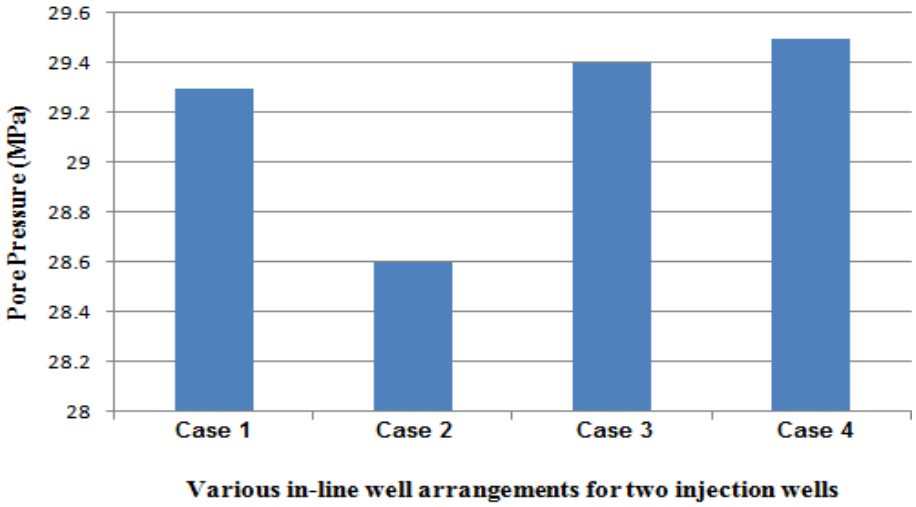

Figure 5.6 Maximum pore-pressure for various arrangements of two injection wells

5.2.2 Ground uplift for various arrangements with two injection wells

One of the key outputs of the geomechanical modeling procedure is the ground uplift during carbon dioxide injection into the reservoir. For the case of two injection wells at 600 meters, the vertical ground uplift after various injection periods is shown in Figure 5.7. The vertical ground uplift after five years of injection period for various arrangements with two injection wells is shown in Figure 5.8. Two wells at 600 meters distance has maximum vertical ground uplift of 24.4 mm, two wells at 800 meters distance has a maximum vertical uplift of 23.1 mm, two wells at 1000 meters distance has a maximum vertical uplift of 24.8 mm, and two wells at 1200 meters distance has a maximum vertical uplift of 25.1 mm.

For two injection wells case, the vertical ground uplift at various injection periods is shown in Figure 5.9. It can be seen from Figure 5.9 that the maximum ground uplift is for the two injection wells at a distance of 1200 meters from one another. One of the possible reasons for this huge ground uplift is that these two injection wells are very

nearer to the boundaries of the reservoir and thus the high value of the pressure buildup creates this huge ground uplift.

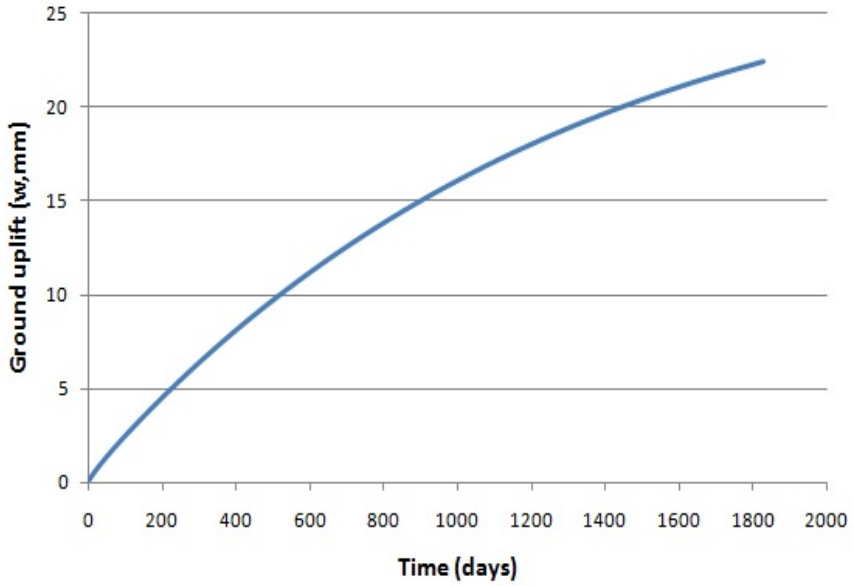

Figure 5.7 The vertical ground uplift after various injection periods for two injection wells at 600 meters

(a)

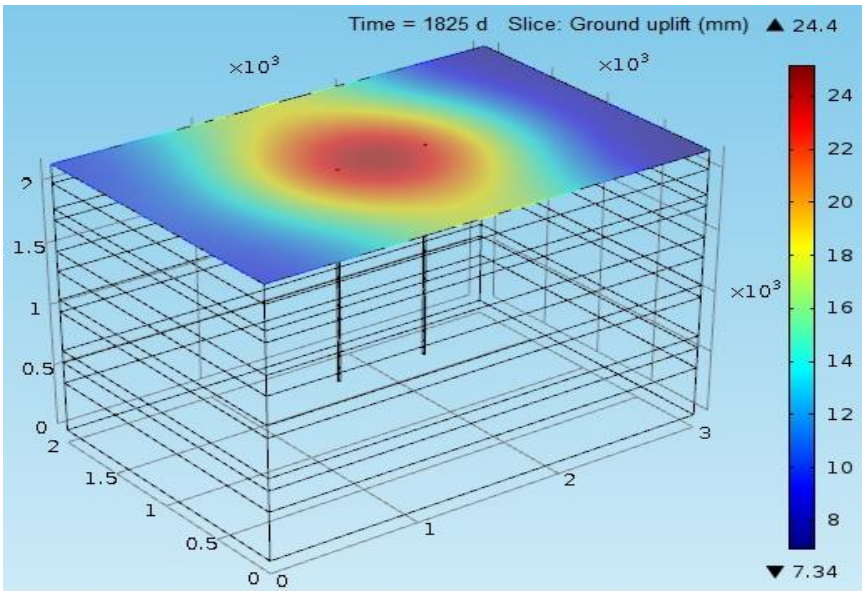

(b)

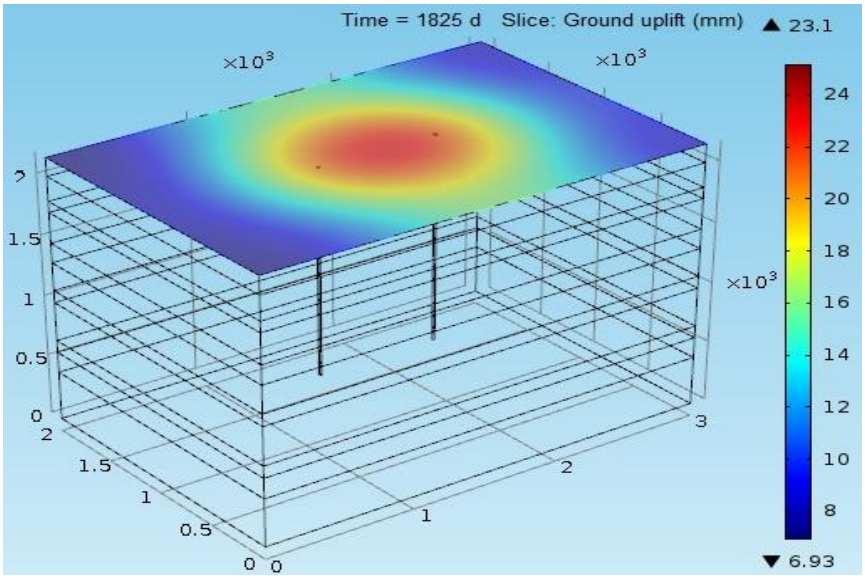
Time = 1825 d Slice: Ground uplift (mm)
▲ 23.1
▼ 6.93
×10³
×10³
×10³
24
22
20
18
16
14
12
10
8
0
0.5
1
1.5
2
3

(c)

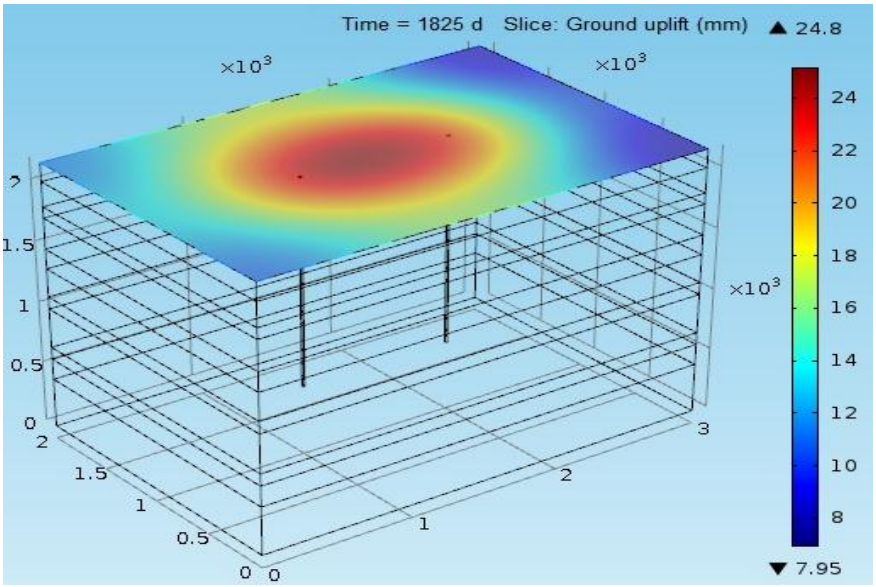
Time = 1825 d Slice: Ground uplift (mm)
▲ 24.8
▼ 7.95
×10³
×10³
×10³
24
22
20
18
16
14
12
10
8
0
0.5
1
1.5
2
3

(d)

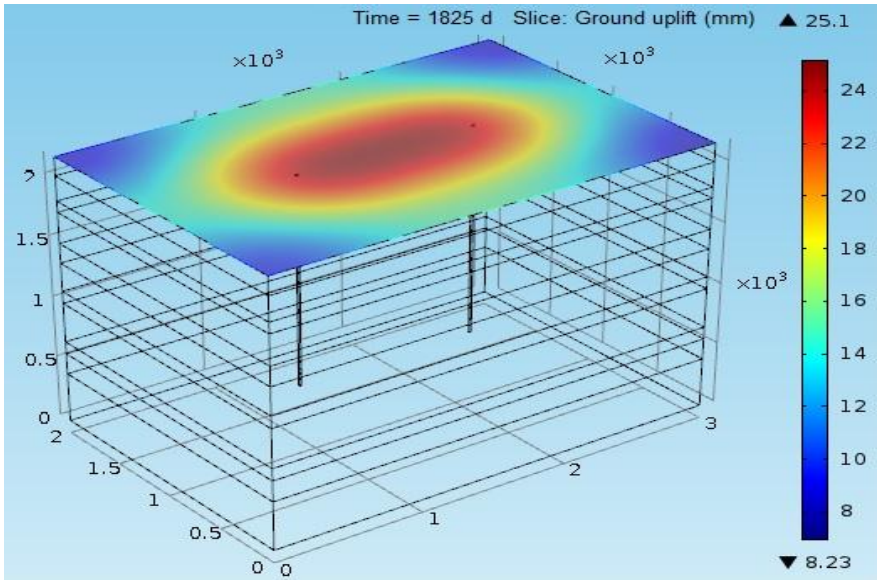

Figure 5.8 The vertical ground uplift after five years of CO2 injection for two injection wells; (a) At 600 meters, (b) At 800 meters, (c) At 1000 meters (d) At 1200 meters

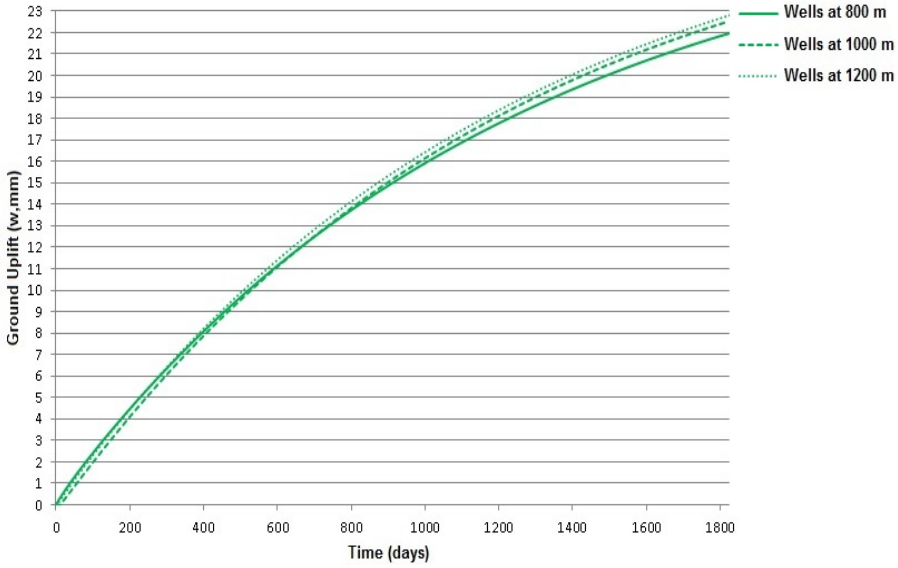

Figure 5.9 The ground uplift after various periods of carbon dioxide injection with two injection wells

5.3 Various injection well arrangements with three injection wells

For three injection wells, the various patterns, in which carbon dioxide injection is simulated, is given in Table 5.4. In the case of three injection wells the various discussed

wells arrangements are in-line, and central (equally spaced around the center of the well), wells arrangement types as shown in Figure 5.10. The selection of optimum well arrangement will depend on the dimensions of the reservoir. After observing the pore pressure increase for various cases of two injection wells, it can be concluded that for a reservoir with minimum width and thickness as compare to its length, the in-line well arrangements will be more suitable as compared to the central wells arrangements. However, if the width of the reservoir has almost equal value to the length of the reservoir, then the optimum central wells arrangements can keep the pore pressure value much less than the critical pore pressure for the reservoir. The maximum pore pressure for each pattern of three injection wells and its corresponding effects on the reservoir stability is explained in the following sections.

Table 5.4 Different cases of three-well arrangements

Arrangement	Spacing (m)
Case 1	Equilateral triangular arrangement; l = 300 m
Case 2	Equilateral triangular arrangement; l = 400 m
Case 3	Equilateral triangular arrangement; l = 500 m
Case 4	Equilateral triangular arrangement; l = 600 m
Case 5	In-line arrangement; l = 500 m
Case 6	In-line arrangement; l = 600 m
Case 7	In-line arrangement; l = 700 m
Case 8	In-line arrangement; l = 800 m

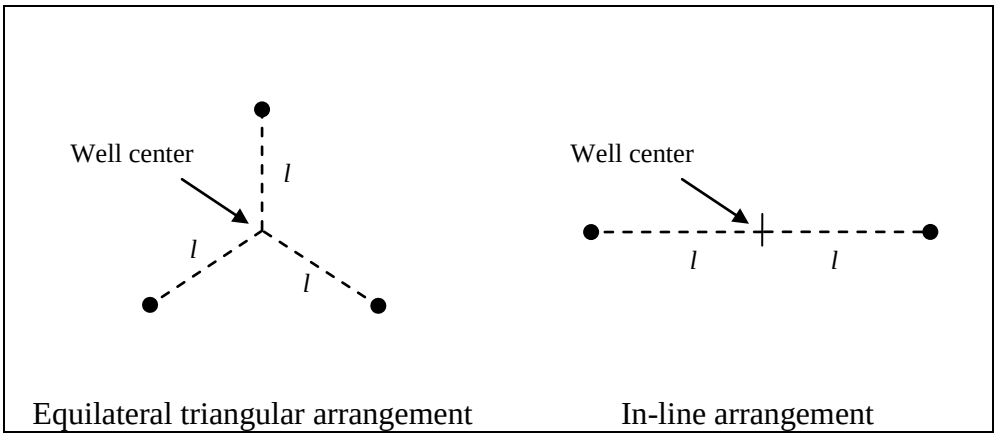

Figure 5.10 Different three-well arrangements

5.3.1 Pressure variations for various arrangements with three injection wells

After a five-year injection period, the pressure variation is shown in Figure 5.11, wherein the pore pressure is shown to increase with carbon dioxide injection. Moreover, the pore pressure variations for the triangular-injection and the in-line injection well arrangements for various periods of carbon dioxide injection are shown in Figures 5.12 and 5.13, respectively. Apparently, the pore pressure variation is shown to be highly dependent on the arrangement of injection wells. The pore pressure increase is more for the case of three injection wells at 600 meters distance from the reservoir center as compared to other three wells arrangements.

The maximum pore pressure for different three-injection well arrangements is summarized in Figure 5.14. The various cases shown in Figure 5.14 are explained in Table 5.4. Cases 1 to 4 are equilateral triangular arrangements, and cases 5 to 8 are in-line arrangements. Figure 5.14 shows that the equilateral triangular arrangements of the injection wells have more pressure buildup as compared to the in-line well arrangements. One of the reasons is that with equilateral triangular arrangements, the injection wells are more nearer to the reservoir boundary walls as compared to the in-line well arrangements.

Among the equilateral triangular arrangements the optimum arrangement with less pressure buildup is case 2 with three injection wells at a distance of 400 meters from the reservoir center. Among the in-line wells arrangements the optimum arrangement with less pressure buildup is case 6 with three injection wells placed in-line such that one of the well is at the reservoir center and the other two are at a distance of 600 meters from the central well.

(a)

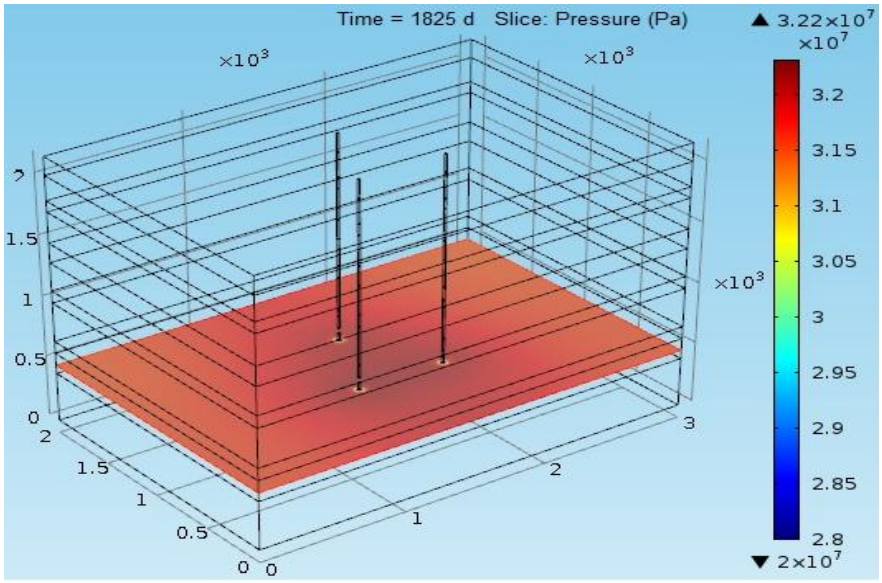

(b)

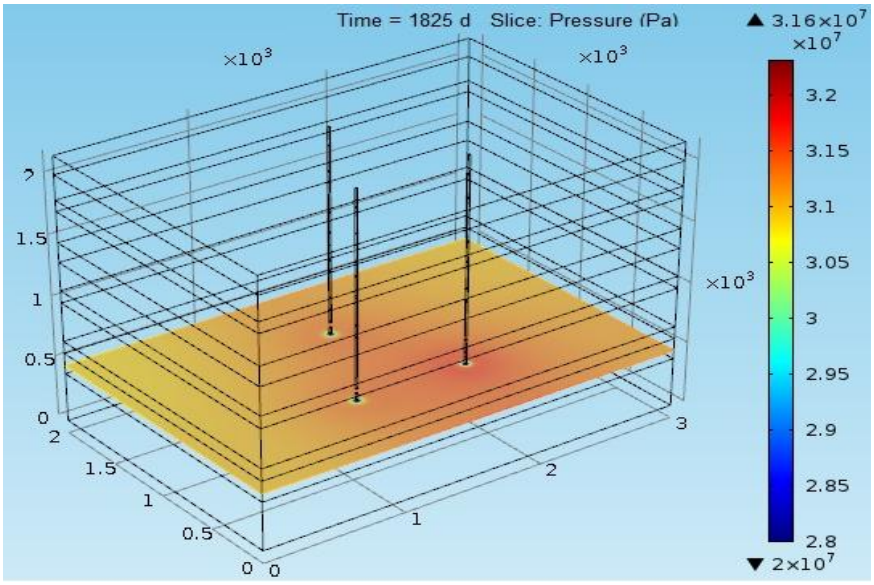
Time = 1825 d Slice: Pressure (Pa)
▲ 3.16×10^7
×10^7
3.2
3.15
3.1
3.05
3
2.95
2.9
2.85
2.8
▼ 2×10^7
×10^3
×10^3
×10^3
0
0.5
1
1.5
2
0
0.5
1
1.5
2
0
1
2
3

(c)

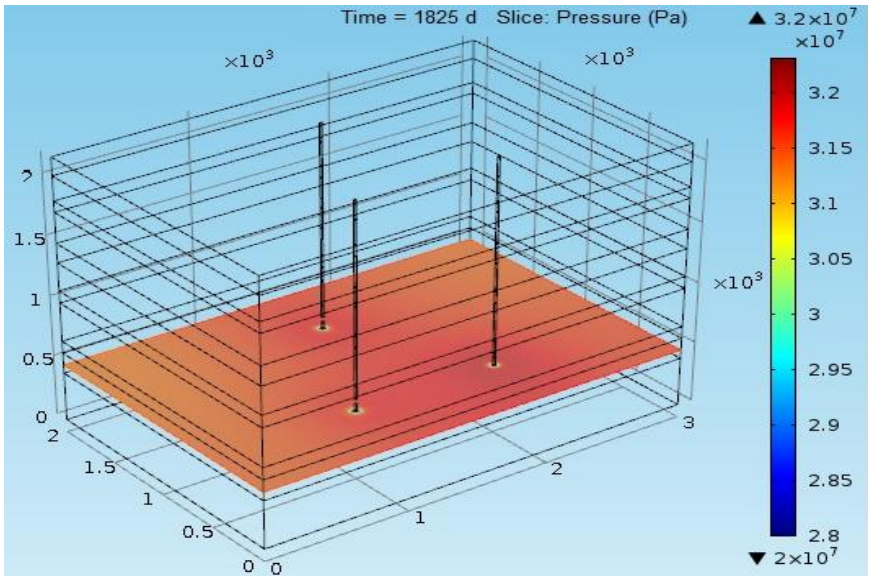
Time = 1825 d Slice: Pressure (Pa)
▲ 3.2×10^7
×10^7
3.2
3.15
3.1
3.05
3
2.95
2.9
2.85
2.8
▼ 2×10^7
×10^3
×10^3
×10^3
0
0.5
1
1.5
2
0
0.5
1
1.5
2
0
1
2
3

(d)

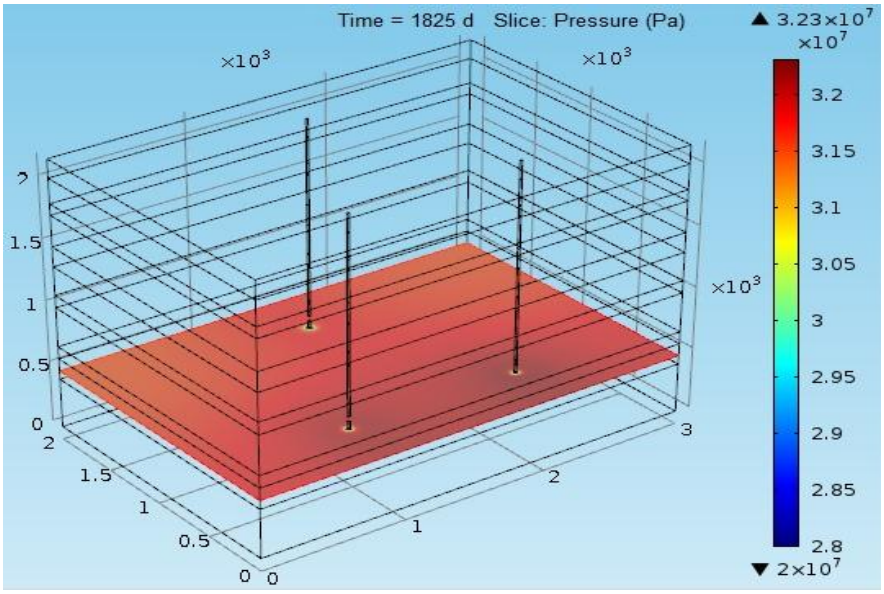
Time = 1825 d Slice: Pressure (Pa)
▲ 3.23×10^7
×10^7
3.2
3.15
3.1
3.05
3
2.95
2.9
2.85
2.8
▼ 2×10^7
×10^3
×10^3
×10^3
0
0.5
1
1.5
2
0
0.5
1
1.5
2
0
1
2
3

(e)

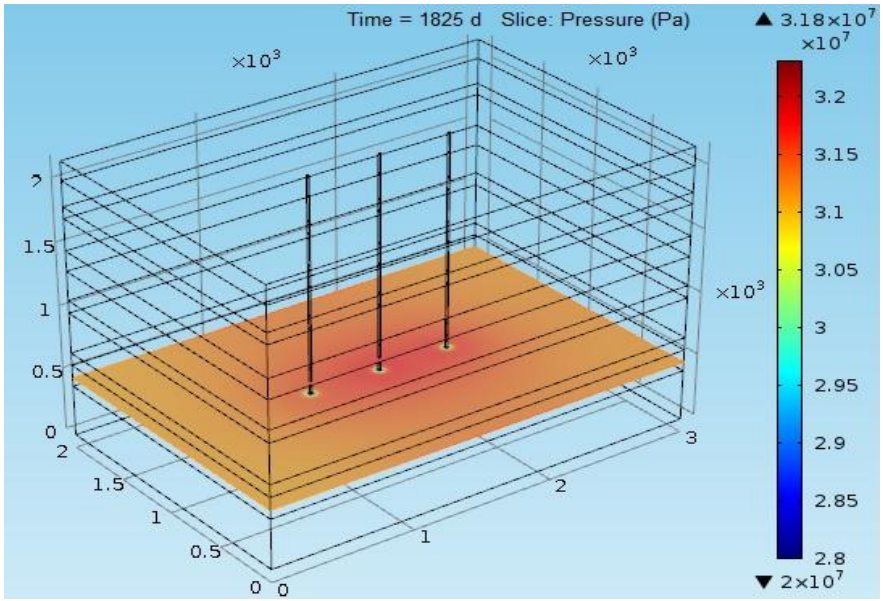
Time = 1825 d Slice: Pressure (Pa)
▲ 3.18×10^7
×10^7
3.2
3.15
3.1
3.05
3
2.95
2.9
2.85
2.8
▼ 2×10^7
×10^3
×10^3
×10^3
0
0.5
1
1.5
2
0
0.5
1
1.5
2
0
1
2
3

(f)

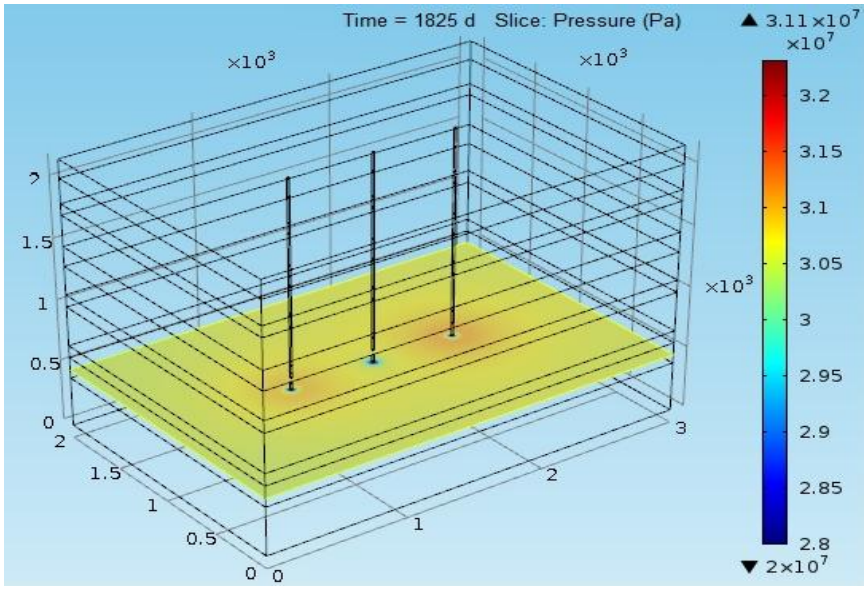
Time = 1825 d Slice: Pressure (Pa)
▲ 3.11×10^7
×10^7
3.2
3.15
3.1
3.05
3
2.95
2.9
2.85
2.8
▼ 2×10^7
×10^3
×10^3
×10^3
0
0.5
1
1.5
2
0
1
2
3

(g)

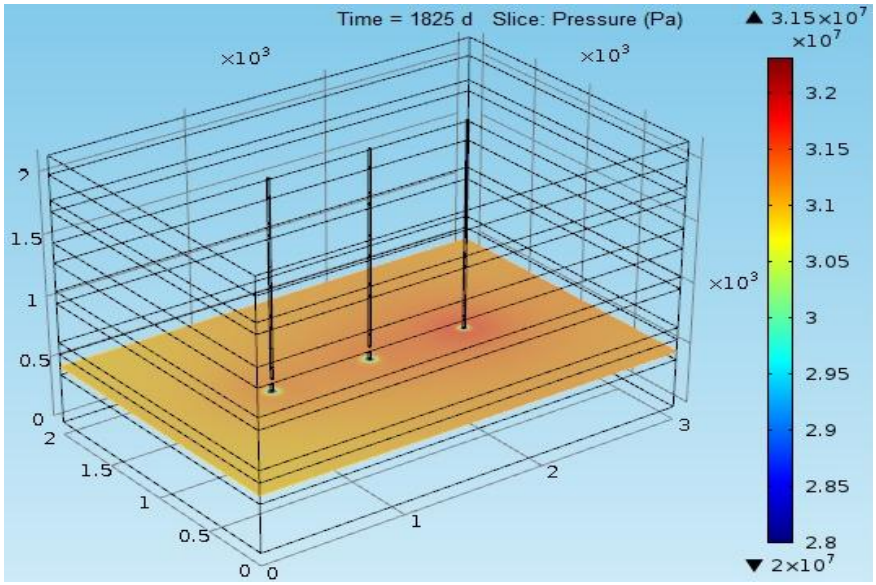
Time = 1825 d Slice: Pressure (Pa)
▲ 3.15×10^7
×10^7
3.2
3.15
3.1
3.05
3
2.95
2.9
2.85
2.8
▼ 2×10^7
×10^3
×10^3
×10^3
0
0.5
1
1.5
2
0
1
2
3

(h)

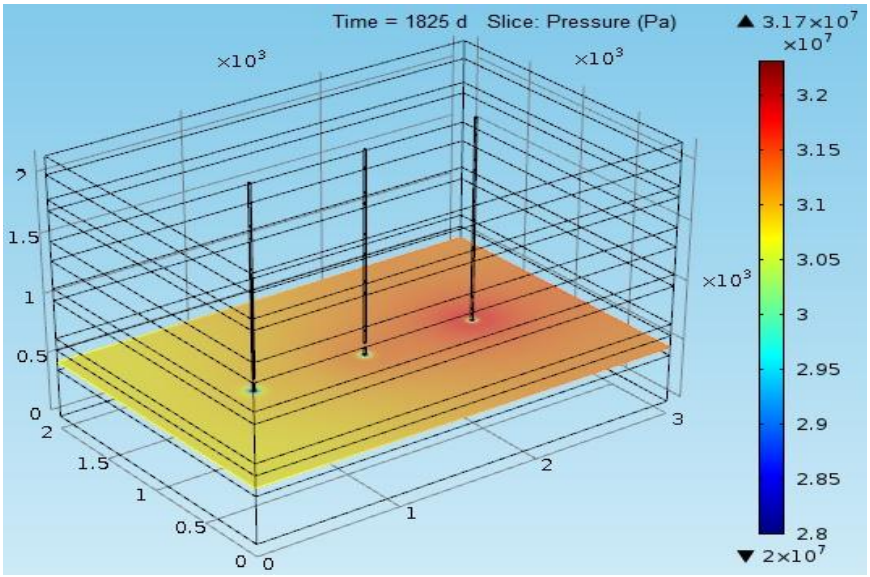

Figure 5.11 The pressure variation after five years of CO_2 injection using three injection wells; (a) At 300 m triangular, (b) At 400 m triangular, (c) At 500 m triangular (d) At 600 m triangular (e) At 500 m in-line (f) At 600 m in-line (g) At 700 m in-line (h) At 800 m in-line

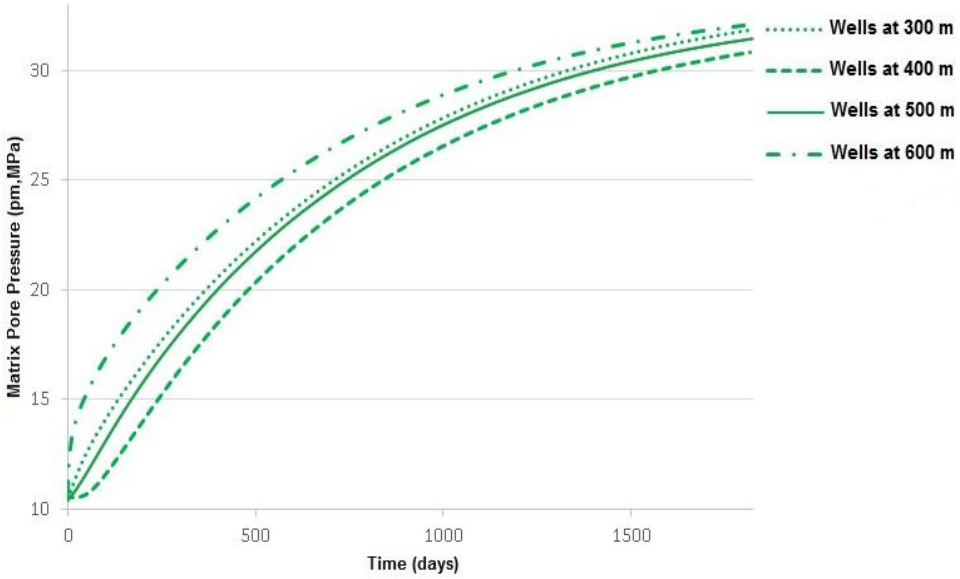

Figure 5.12 The pore pressure variations for various periods of carbon dioxide injection using three injection wells with triangular arrangement

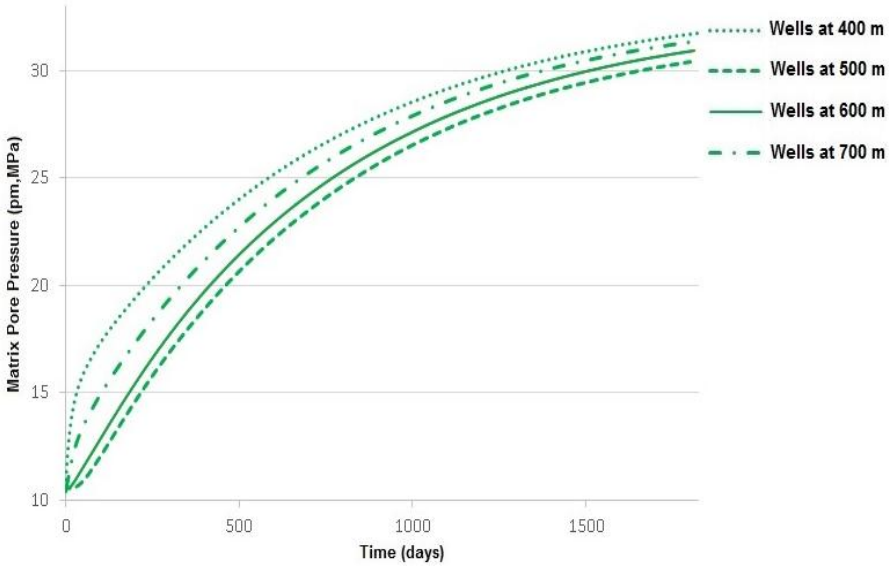

Figure 5.13 The pore pressure variations for various periods of carbon dioxide injection using three injection wells with in-line arrangement

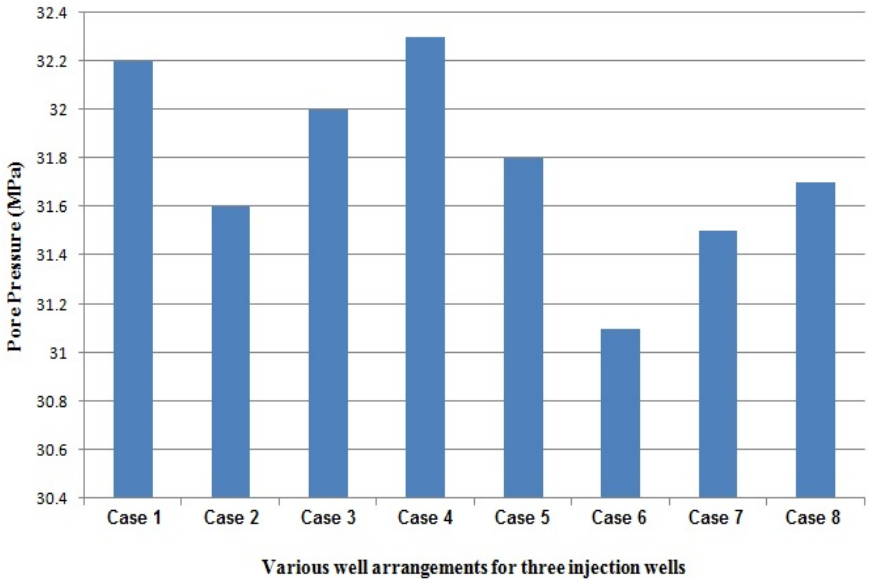

Figure 5.14 Maximum pore-pressure for various arrangements of three injection wells

5.3.2 Ground uplift with various arrangements for three injection wells

The vertical ground uplift after five years of injection period is shown in Figure 5.15. Three wells at 300 meters distance from reservoir center has maximum vertical ground uplift of 28.1 mm, three wells at 400 meters distance from reservoir center has maximum vertical ground uplift of 27.3 mm, three wells at 500 meters distance from reservoir

center has maximum vertical ground uplift of 27.8 mm, and three wells at 600 meters distance from reservoir center has maximum vertical ground uplift of 28.2 mm. Similarly, three wells with in-line arrangement at a distance of 500 meters has a vertical ground uplift of 27.6 mm, three wells with inline arrangement at a distance of 600 meters has a vertical ground uplift of 26.5 mm, three wells with in-line arrangement at a distance of 700 meters has a vertical ground uplift of 27.3 mm, and three wells with in-line arrangement at a distance of 800 meters has a vertical ground uplift of 27.5 mm. The corresponding vertical ground uplift for the aforementioned triangular and inline injection well arrangements for different injection periods is shown in Figures 5.16 and 5.17, respectively.

(a)

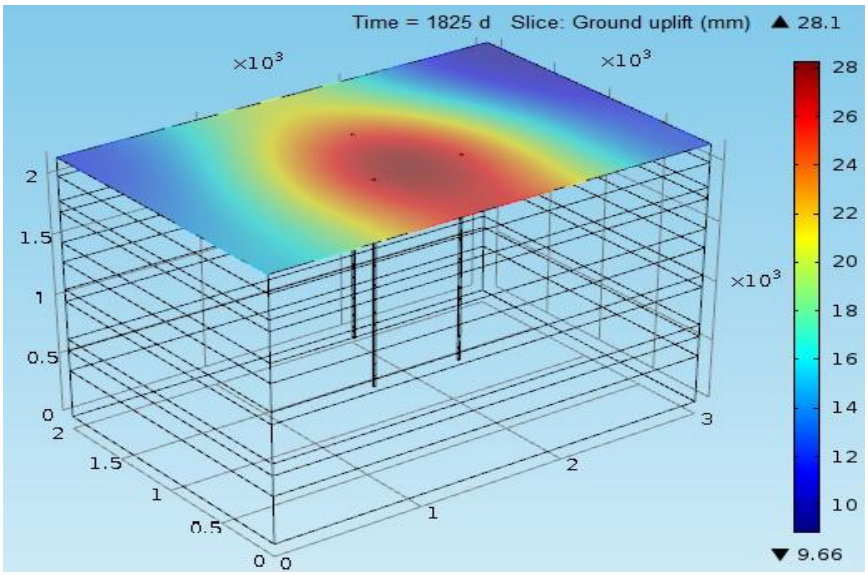

(b)

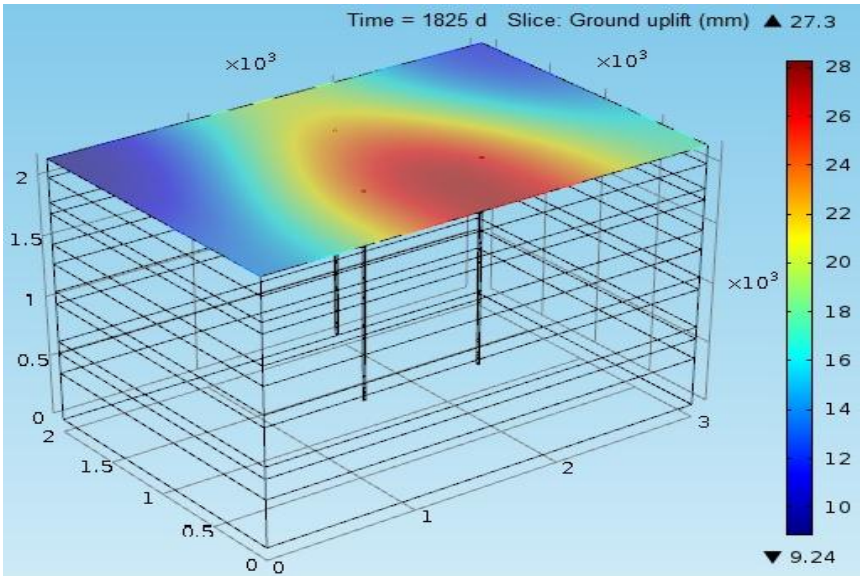
Time = 1825 d Slice: Ground uplift (mm)
▲ 27.3
▼ 9.24
×10³
×10³
×10³
28
26
24
22
20
18
16
14
12
10
2
1.5
1
0.5
0
0
1
2
3

(c)

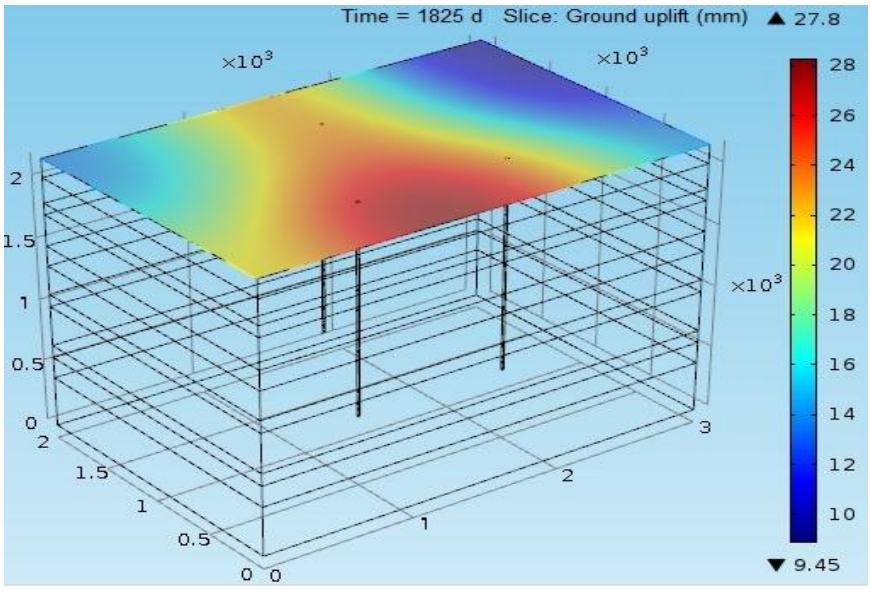
Time = 1825 d Slice: Ground uplift (mm)
▲ 27.8
▼ 9.45
×10³
×10³
×10³
28
26
24
22
20
18
16
14
12
10
2
1.5
1
0.5
0
0
1
2
3

(d)

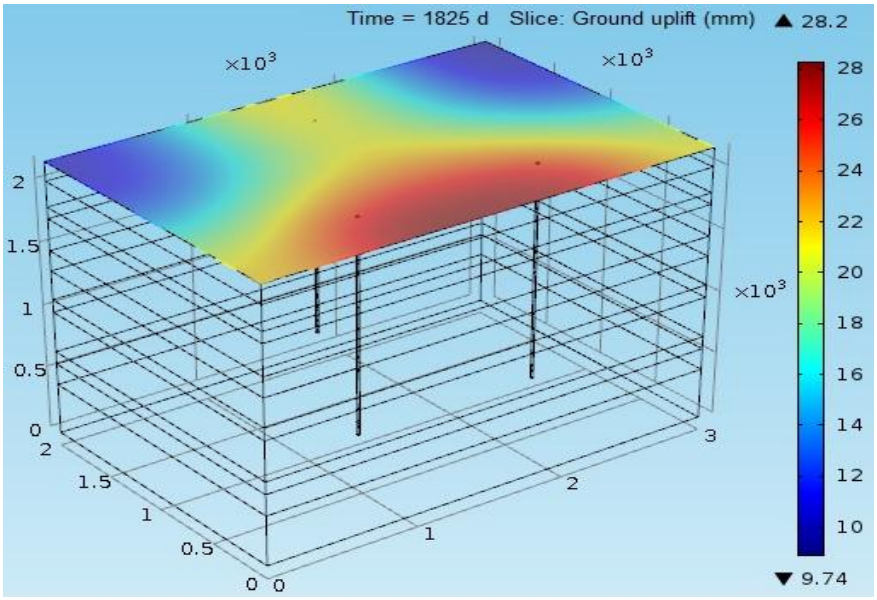
Time = 1825 d Slice: Ground uplift (mm) ▲ 28.2
×10³
×10³
×10³
28
26
24
22
20
18
16
14
12
10
▼ 9.74
2
1.5
1
0.5
0
0
0.5
1
1.5
2
3

(e)

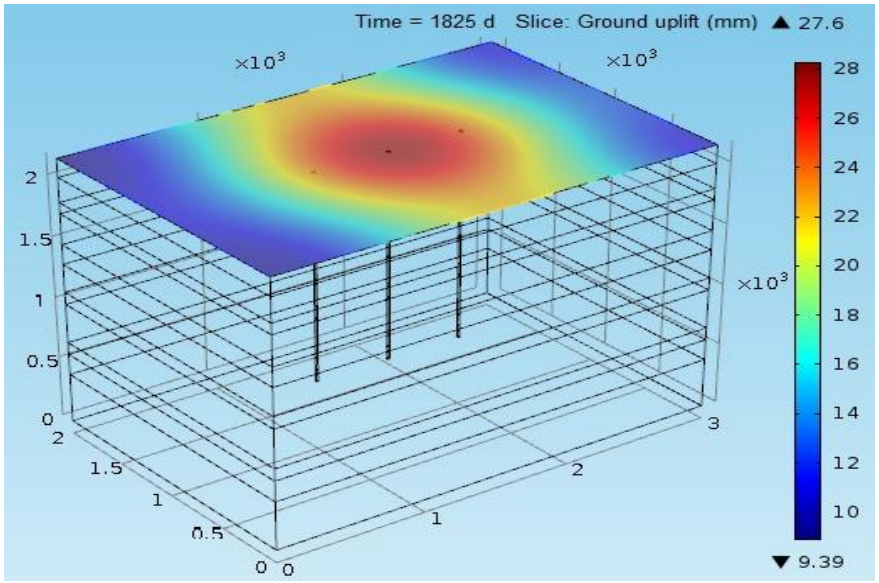
Time = 1825 d Slice: Ground uplift (mm) ▲ 27.6
×10³
×10³
×10³
28
26
24
22
20
18
16
14
12
10
▼ 9.39
2
1.5
1
0.5
0
0
0.5
1
1.5
2
3

(f)

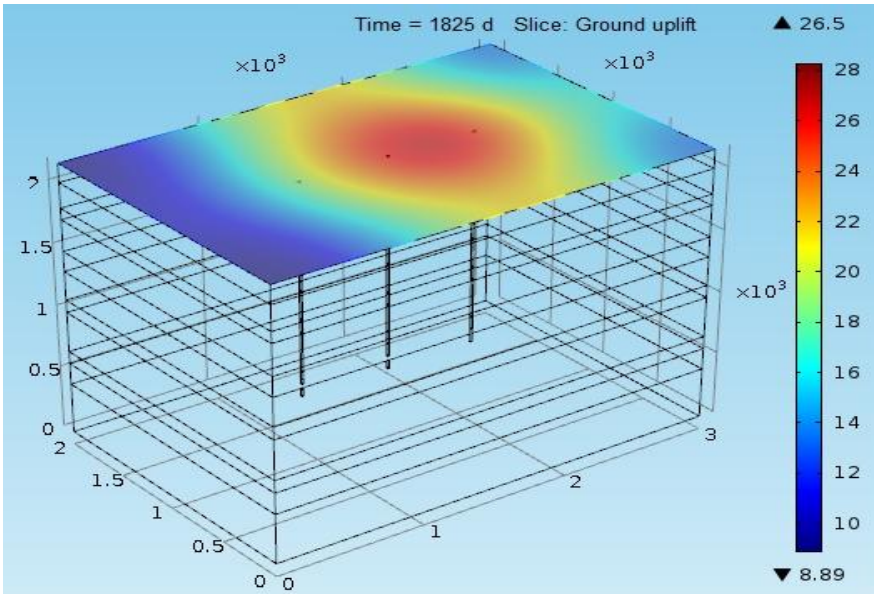
Time = 1825 d Slice: Ground uplift
▲ 26.5
×10³
×10³
×10³
28
26
24
22
20
18
16
14
12
10
▼ 8.89
0
0.5
1
1.5
2
0
1
2
3

(g)

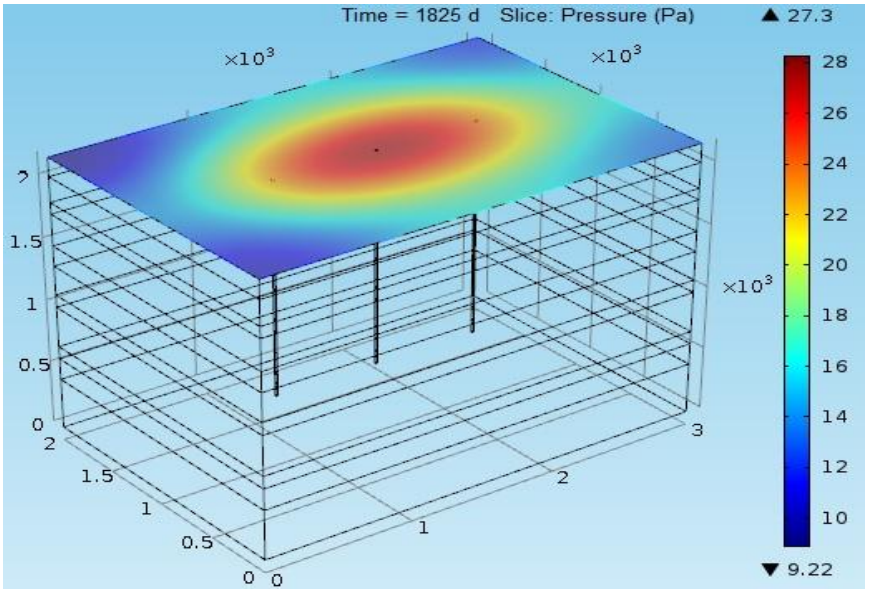
Time = 1825 d Slice: Pressure (Pa)
▲ 27.3
×10³
×10³
×10³
28
26
24
22
20
18
16
14
12
10
▼ 9.22
0
0.5
1
1.5
2
0
1
2
3

(h)

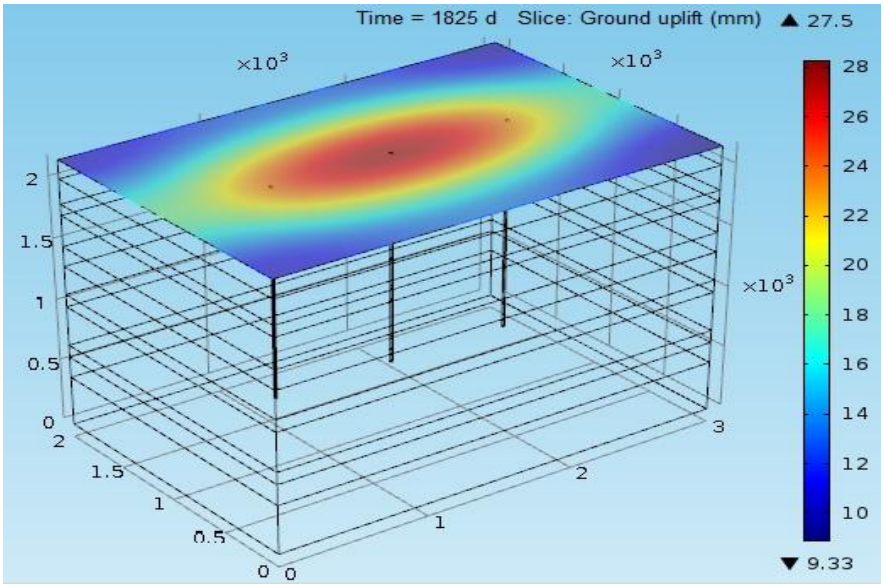

Figure 5.15 The vertical ground uplift after five years of CO_2 injection for two injection wells; (a) At 300 m triangular, (b) At 400 m triangular, (c) At 500 m triangular (d) At 600 m triangular (e) At 500 m in-line (f) At 600 m in-line (g) At 700 m in-line (h) At 800 m in-line

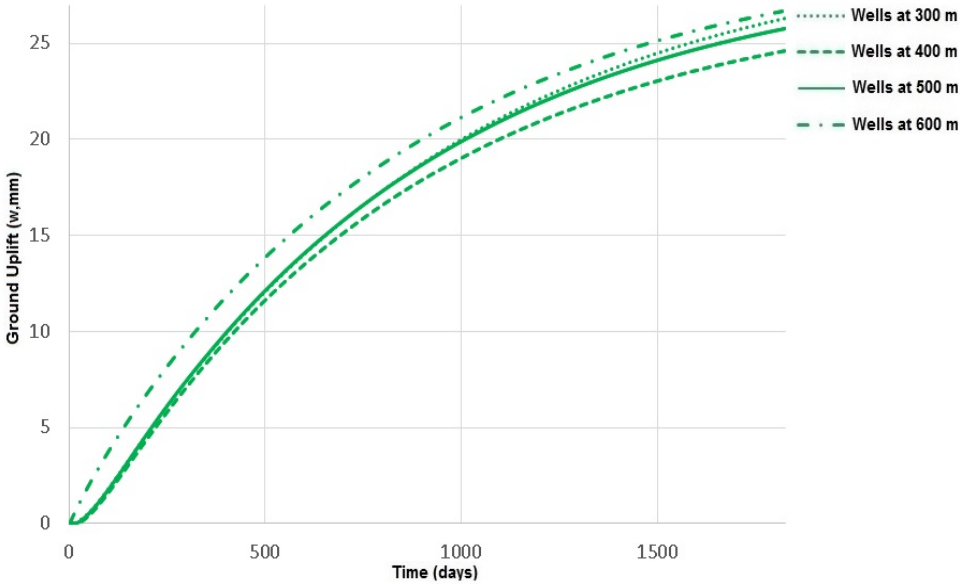

Figure 5.16 The ground uplift after various injection periods for three injection wells with triangular arrangement

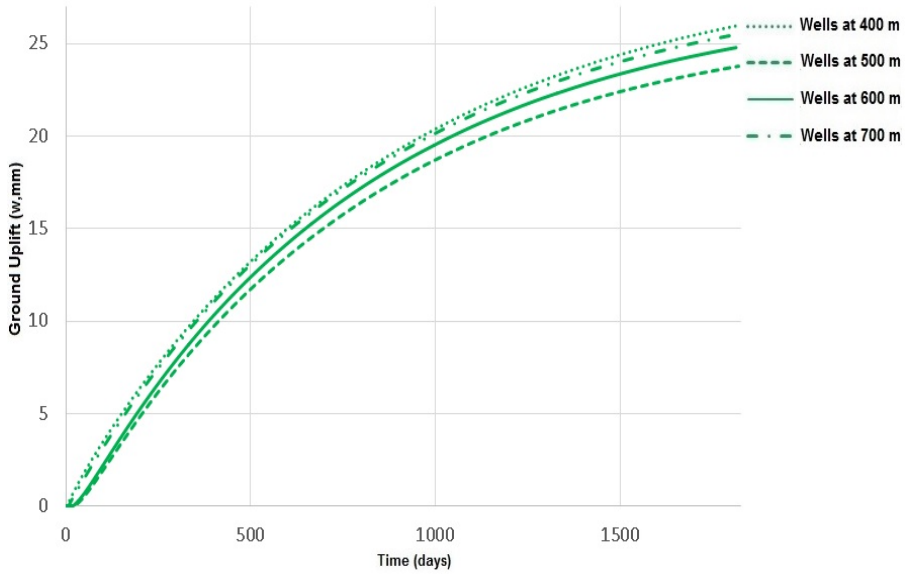

Figure 5.17 The ground uplift after various injection periods for three injection wells with in-line arrangement

5.4 Various injection well arrangements with four injection wells

For four injection wells, the various patterns, in which carbon dioxide injection is simulated, is given in Table 5.5. In the case of four injection wells, the different well arrangements that are equally spaced from the center of the well are considered. In the first three cases tabulated in Table 5.5, the four injection wells are arranged in the form of a square, with the center of the square coincident with the reservoir center. In the last case in Table 5.5, the four injection wells are arranged in the form of rectangle, with its center being coincident with the reservoir center. The maximum pore pressure for each pattern of four injection wells and its corresponding effects on the reservoir stability is also explained in the following sections.

Table 5.5 Various arrangements for four injection wells

Different Cases for 4 injection wells	Type of arrangement (meters)
Case 1 (central well arrangement)	All the four injection wells are at a distance of 400 meters from the reservoir center in the form of a square.
Case 2 (central well arrangement)	All the four injection wells are at a distance of 500 meters from the reservoir center in the form of a square.
Case 3 (central well arrangement)	All the four injection wells are at a distance of 600 meters from the reservoir center in the form of a square.
Case 4 (central well arrangement)	Four injection wells placed at a distance of 700 meters from the reservoir center in the form of a rectangle with a diagonal angle of 34.85 degrees with line passing through the reservoir center along the length of the reservoir.

5.4.1 Pressure variation for various arrangements with four injection wells

The following section summarizes the numerical simulation results for the four injection wells at 400, 500, 600, and 700 meters distance from the reservoir center. After five years of injection period, the pressure variation is shown in Figure 5.18. The pore pressure for various periods of CO_2 injection is shown in Figure 5.18. As shown in Figure 5.18 the pore pressure variation is highly dependent on the arrangement of injection wells. For four injection wells at 700 meters distance from the reservoir center, the pore pressure has a maximum increase as compared to the other four wells arrangements because the boundaries of the model are with no flow condition and will cause CO_2 accumulation.

Figure 5.19 shows the maximum pore pressure for various arrangements of four injection well arrangements. Table 5.5 discusses the various four wells arrangements in detail. Among the four cases, the minimum pore pressure buildup is for case 2 having four injection wells at a distance of 500 meters from the reservoir center. The maximum pressure buildup is for case 4 with four injection wells at a distance of 700 meters from

the reservoir center. In case 4 the value of the pore pressure after carbon dioxide injection is high due to the reason that the injection wells are much nearer to the boundary walls of the reservoir.

(a)

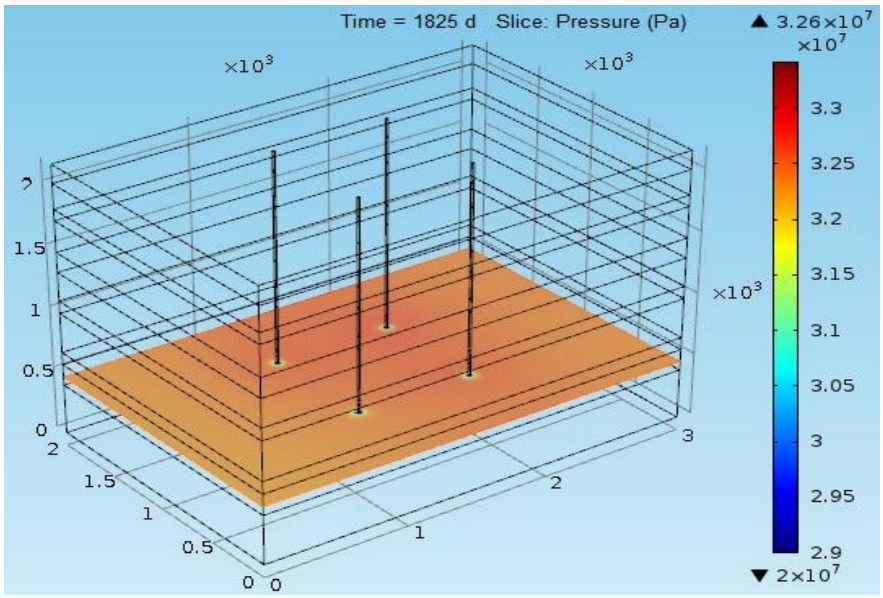

(b)

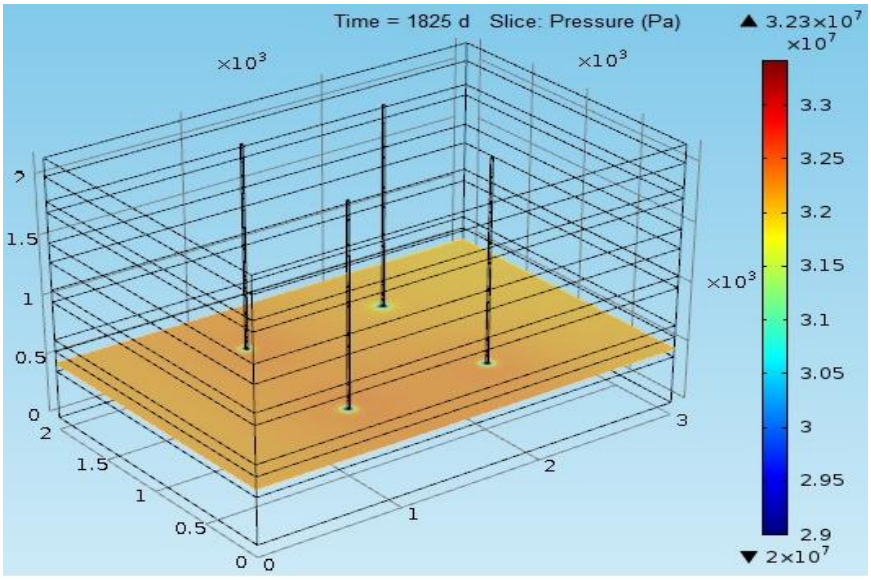

(c)

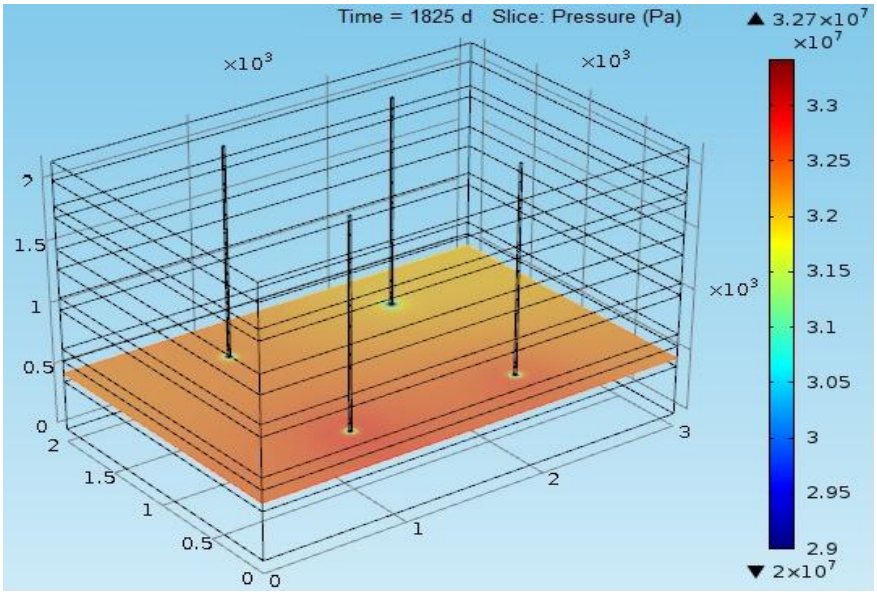

(d)

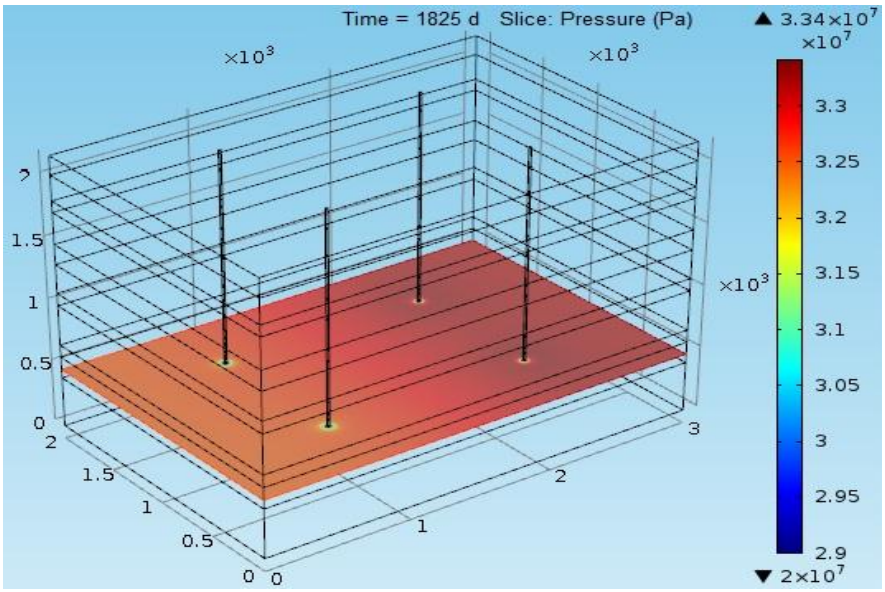

Figure 5.18 The pressure variation after five years of carbon dioxide injection using four injection wells; (a) At 400 meters, (b) At 500 meters, (c) At 600 meters (d) At 700 meters

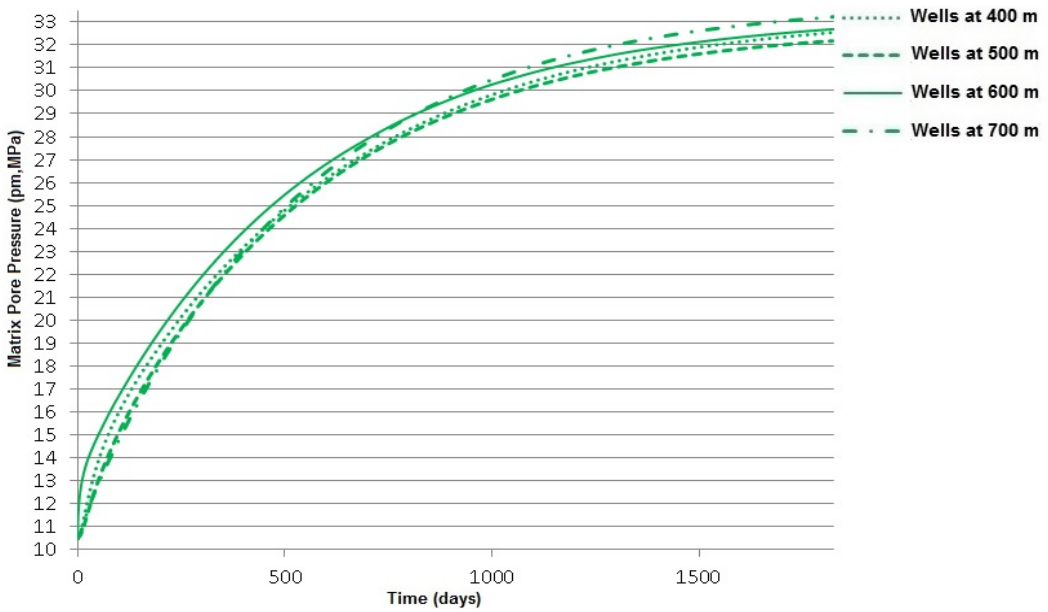

Figure 5.19 The pore pressure variations for various periods of carbon dioxide injection using four injection wells

5.4.2 Ground uplift for various arrangements with four injection wells

The vertical ground uplift measured near to the injection point after five years of injection period is shown in Figure 5.20. Four wells at 400 meters distance from the reservoir center has maximum vertical ground uplift of 28.9 mm, four wells at 500 meters distance from the reservoir center has maximum vertical ground uplift of 28.3 mm, four wells at 600 meters distance from the reservoir center has maximum vertical ground uplift of 29.1 mm, and four wells at 700 meters distance from the reservoir center has maximum vertical ground uplift of 30.2 mm. The corresponding vertical ground uplift at various periods of carbon dioxide injection is shown in Figure 5.21.

(a)

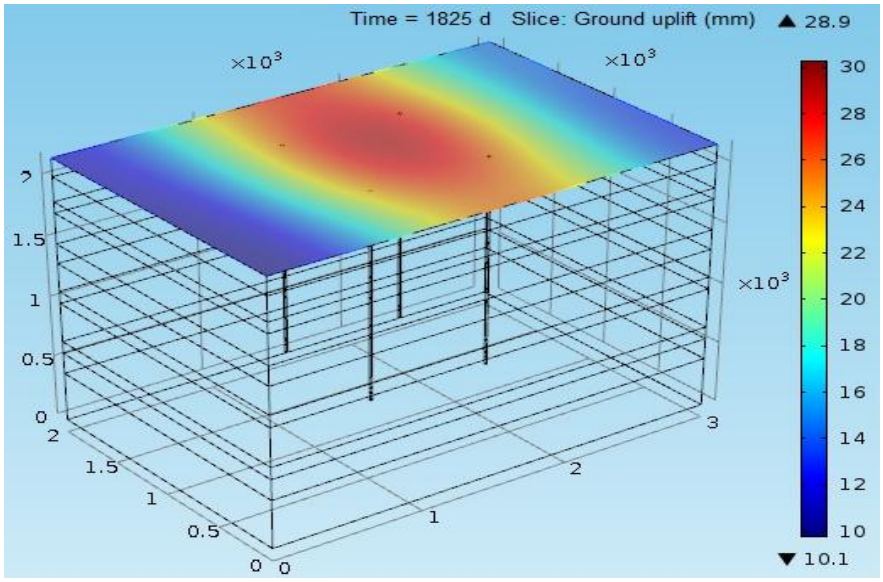
Time = 1825 d Slice: Ground uplift (mm)
▲ 28.9
▼ 10.1
×10³
30
28
26
24
22
20
18
16
14
12
10

(b)

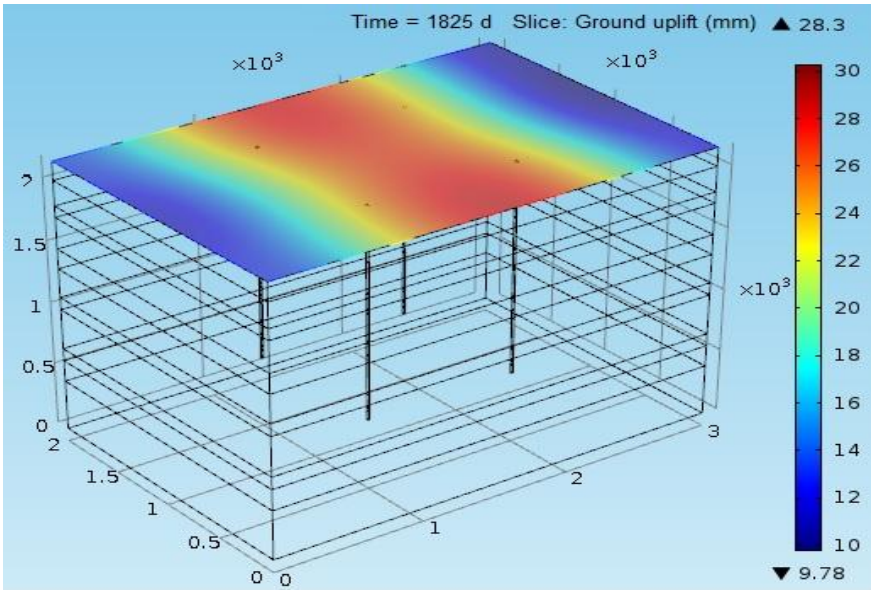
Time = 1825 d Slice: Ground uplift (mm)
▲ 28.3
▼ 9.78
×10³
30
28
26
24
22
20
18
16
14
12
10

(c)

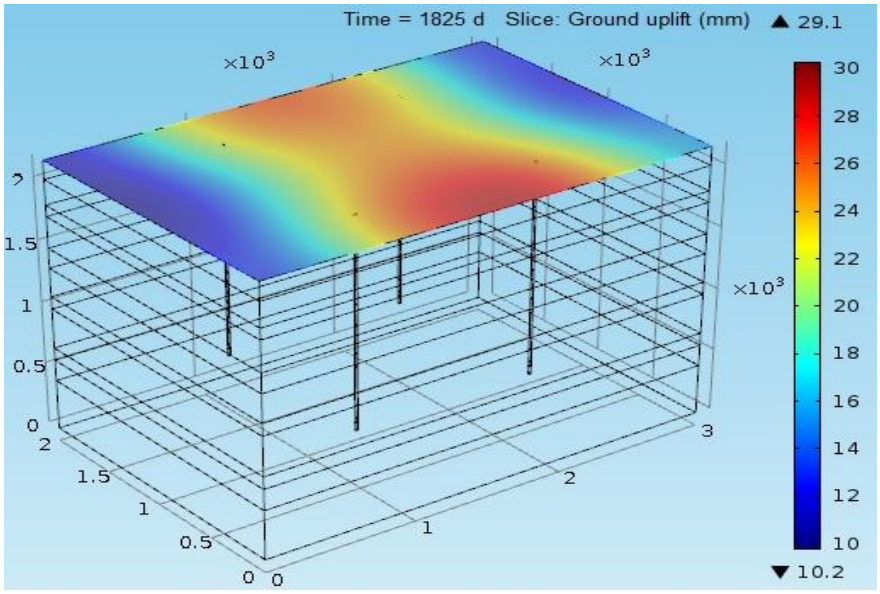

(d)

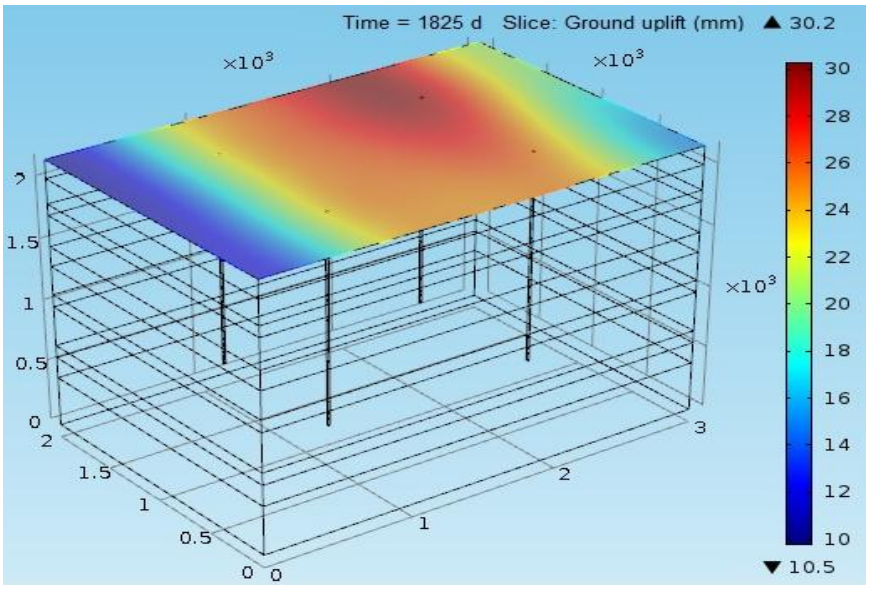

Figure 5.20 The vertical ground uplift after five years of CO_2 injection pressure for four injection wells; (a) At 400 meters, (b) At 500 meters, (c) At 600 meters (d) At 700 meters

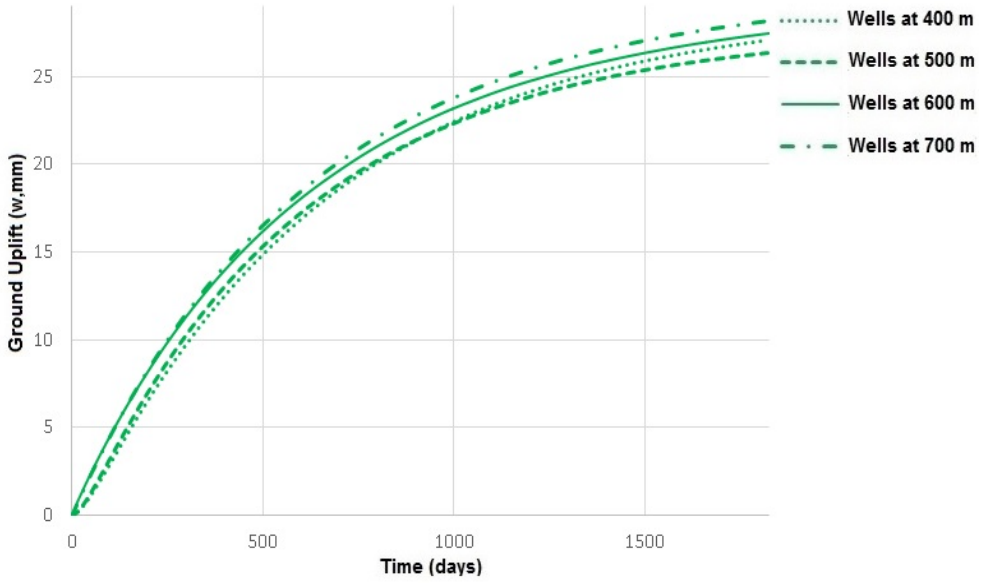

Figure 5.21 The ground uplift after various carbon dioxide injection periods with four injection wells

5.5 Maximum carbon dioxide occupancy for various numbers of injection wells

5.5.1 The case of two injection wells

With an initial volume of $1.6926 \text{ X } 10^9 m^3$ for the reservoir, the volume of carbon dioxide injected during five years of the injection period at ground level is $5.0504 \text{ X } 10^9 m^3$. Due to the high pressure at the reservoir depth of 1750 meters, the volume of the carbon dioxide will decrease with a volume factor of 0.00275 m^3/m^3 [86, 124]. The volume of carbon dioxide at the reservoir level will be $13.88 \text{ X } 10^6 m^3$, which is 0.82% of the available pore volume. With maximum occupancy limit of 3% of the total available volume the current injection scenario with two injection well is in the safe limits [30, 87, 88].

5.5.2 The case of three injection wells

With three injection wells the volume of carbon dioxide injected into the reservoir at the ground level is equal to $7.5756 \text{ X } 10^9 m^3$ for five years of injection period. Due to the

high pressure value of the reservoir, the volume of the injected carbon dioxide decreases to $20.83 \text{ X } 10^6 m^3$, which is 1.23 % of the available pore volume of the reservoir. Still with an occupancy of 1.23 %, the reservoir will be on safe side because this occupancy value is less than 3 % which is the maximum occupancy limit [30, 87, 88].

5.5.3 The case of four injection wells

When four injection wells were used for carbon dioxide injection into the reservoir, $10.1008 \text{ X } 10^9 m^3$ volume of carbon dioxide was injected into the reservoir at ground level. At the reservoir level of 1750 meters, the carbon dioxide is stored in a dense form with a volume of $27.77 \text{ X } 10^6 m^3$, with occupancy of 1.64% of the available pore volume. The maximum occupancy value for the reservoir is 3% of the total available volume, which shows that the current injection scenario with four injection wells is in the safe limits [30, 87, 88].

5.6 Reservoir stability analysis using Mohr-Coulomb criteria

The flow and transport of carbon dioxide along the reservoir is strongly dependent on the injection pressure. The more the injection pressure increases, the more the flow of carbon dioxide increases into the reservoir. For maximum storage capacity of carbon dioxide, it is desirable to increase the injection pressure. Yet, it is necessary to observe the estimated safe values of the injection pressure. The safe values of the injection pressure are obviously less than the critical pore pressures. The Mohr-Coulomb failure criterion for the compressional stress regime is used to analyze the effect of pore pressure variation on the reservoir stability. Either the increase or the decrease in the pore pressure can cause failure of the reservoir due to the subsequent changes in the magnitude of effective stresses in the reservoir [30, 84]. In this context, the Mohr-Coulomb failure criterion is

utilized to draw the failure envelope for the reservoir. As the pore pressure increases the effective stresses on the reservoir decreases and reservoir tends to move to a new stress condition that is nearer to the failure line as compared to the initial stress condition. The stability analysis in this part of the study also takes into account the change in the horizontal stresses due to pore pressure built up.

Figure 5.22 shows new stressed position of the reservoir due to the increase in the pore pressure. The increase in the pore pressure for the case of two injection wells at 1200 meters central distance is more as compared to the case of injection with single injection well. The Mohr's circle for the new stressed condition of the reservoir in Figure 5.22 is nearer to the failure line compared to the case of single injection well. Yet, the two-injection well scenarios considered in Table 5.3, the reservoir remains in the safe stable condition.

The pore pressure increase is more for the case of three injection wells at 600 meters distance from the reservoir center as compared to other three wells arrangements. Failure envelope is drawn for the case of three injection wells at 600 meters distance from the reservoir center in Figure 5.23. With three injection wells at 600 meters from the reservoir center, the reservoir is more nearer to the failure envelope as compared to the cases of single and two injection wells. However, the reservoir maintains the safe stable condition.

For four injection wells at 700 meters distance from the reservoir center, the pore pressure has a maximum increase as compared to the other four wells arrangements. The failure envelope for four injection wells at 700 meters distance from the reservoir center is shown in Figure 5.24. Due to the coupled geomechanical modeling the Mohr's circle

corresponding to the final stressed condition of the reservoir as shown in Figure 5.24 is bigger as compared to the circle corresponding to the initial stressed condition of the reservoir. Even with the high magnitude of increase in the pore pressure for four injection wells at 700 meters distance from the reservoir center, the reservoir is still on safe side.

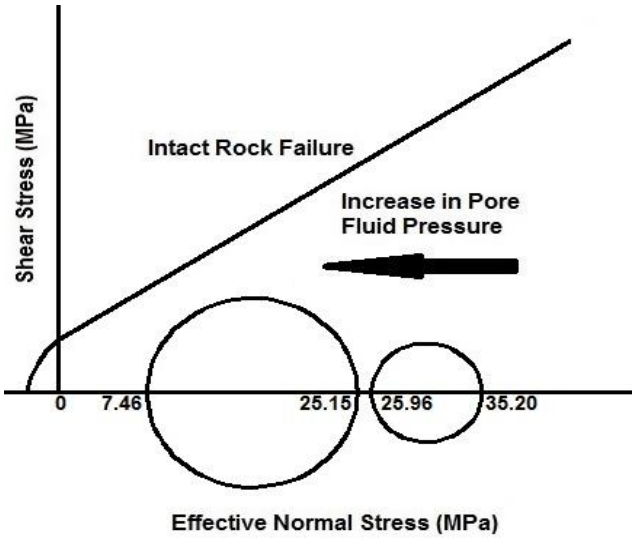

Figure 5.22 Effect of pore pressure variation on the stability of the carbonate reservoir in compressional stress regime for two injection wells at 1200 meter

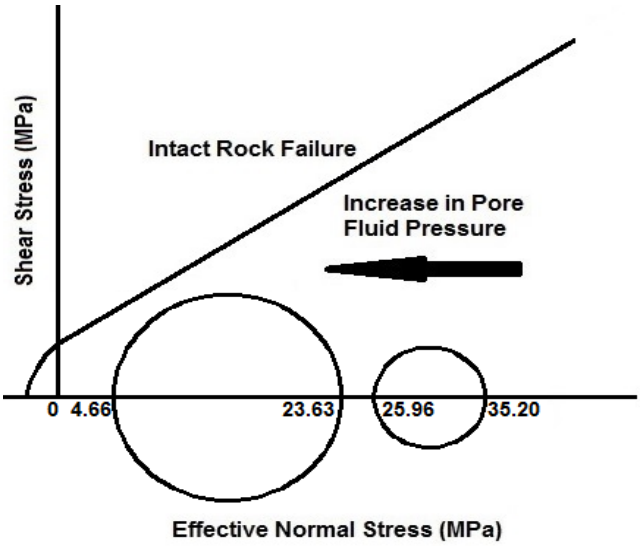

Figure 5.23 Effect of pore pressure variation on the stability of the carbonate reservoir in compressional stress regime for three injection wells at 600 meters distance from the reservoir center

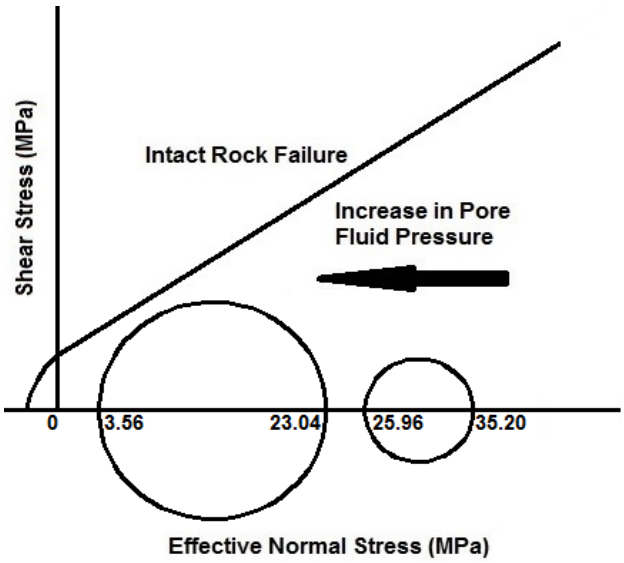

Figure 5.24 Effect of pore pressure variation on the stability of the carbonate reservoir in compressional stress regime for four injection wells at 700 meters distance from the reservoir center

It can be concluded from this chapter that increasing the number of injection wells causes an increase in the pore pressure, which significantly decreases the effective stresses at the reservoir and drives the reservoir to move towards the failure line. The failure envelope shows that increasing the number of injection wells and placing the injection wells closer to one another can lead to the failure of the reservoir. For the various injection scenarios discussed in this study, the reservoir remained at the safe stable condition. The four-injection well scenarios were closer to the failure line as compared to the other injection scenarios.

CHAPTER 6

CONCLUSIONS AND RECOMMENDATIONS

6.1 Conclusions:

In this investigation, a numerical modeling scheme has been developed using COMSOL Multiphysics finite element software for the geomechanical modeling of a single-porosity Biyadh sandstone reservoir and a naturally fractured Ghawar carbonate reservoir during the process of carbon dioxide injection.

6.1.1 Geomechanical modeling of a single-porosity Biyadh reservoir

Geomechanical modeling of Biyadh reservoir with single-phase flow

Here, the developed numerical model was validated via comparisons with some published results of different injection scenarios, which were obtained using different solution methods. The major findings are summarized as follows:

- The injection of carbon dioxide into the reservoir causes an increase in the pore pressure, which attains higher values closer to the injection port and decreases farther away from the injection point. It was also noted that the rate of pore pressure increase is higher during the first year of carbon dioxide injection, which is attributed to the higher potential for carbon dioxide flow due to the pressure difference between the injected carbon dioxide and the local reservoir pressure.

- The increase in the pore pressure causes a volumetric expansion of the reservoir and hence causes the ground surface to move in upward direction. The ground uplift reaches its maximum value near the injection well and extends over several kilometers around the injection point.

- The Mohr-Coulomb failure analysis revealed that the CO_2 injection induced increase in the pore pressure injection has caused the reservoir to assume a new stress condition closer to the failure condition. For both the coupled and uncoupled stability analyses, the considered injection scenario is at the safe side of the failure limit according to the Mohr-Coulomb criterion.
- The occupancy of the reservoir was 2.4 % of the available pore volume of the reservoir, which is less than the allowable 3 % for the closed reservoir condition. The maximum occupancy calculation showed that the adopted injection scenario of carbon dioxide is still at the safe side of the maximum occupancy limit.

Geomechanical modeling of Biyadh reservoir with two-phase flow

In this case, the coupled geomechanical analysis was performed using CMG-GEM software to evaluate the feasibility of Biyadh reservoir for CO_2 sequestration. The following was concluded:

- For the case of a non-fractured caprock, carbon dioxide is restricted by the caprock to spread only within the reservoir, while for the case of fractured caprock, carbon dioxide leaks into the overburden layers, as anticipated. Accordingly, the pressure buildup attains higher values in the case of non-fractured. On the other hand, for the case of fractured caprock the leakage of carbon dioxide tends to increase the local pore pressure of the overburden layers.
- The location of the fracture zone in the caprock was found to have an influence on the magnitude of the pore pressure in the overburden layers. It was observed that the pore pressure gets higher when the fractured zone draws closer to the injection well.

- For the case of non-fractured caprock, the ground vertical uplift reaches its highest value just above the injection point at the center of the reservoir, yet for the case of fractured caprock, the ground uplift is centered above the fractured zone. It is important to note that the increase in the ground uplift just above the fractured zone can be instrumental in the identification and localization of the fractured zone in the caprock.
- It is noteworthy to point out that the location of the fracture zone in the caprock will also influence the magnitude of the vertical ground displacement. The magnitude of the ground uplift gets higher as the fracture zone gets closer to the injection well.
- There is a significant influence of fractured zone permeability on the amount of CO_2 leakage to the overburden layers and hence on the vertical ground uplift. It was observed that the vertical ground displacement above the fractured zone decreases as the permeability of the fractured zone is decreased.
- The Mohr-Coulomb failure criterion was invoked to perform the coupled stability analysis of the reservoir during CO_2 injection. Due to leakage of CO_2 into the overburden layers in the case of fractured caprock, the pressure buildup in the reservoir did not reach high enough values to cause the failure of the reservoir structure. Even for higher values of pressure buildup, in the case of non-fractured caprock, the reservoir was found to maintain stability and stay in the safe side for the 10-year period of CO_2 injection.

6.1.2 Geomechanical modeling of a naturally fractured Ghawar reservoir

Geomechanical modeling of Ghawar reservoir with single-phase flow

In this portion of the study, numerical modeling techniques are used for the geomechanical modeling of a naturally fractured carbonate reservoir undergoing carbon dioxide injection. Single-phase flow is considered in the reservoir. The adopted poroelastic modeling accommodates the transport of carbon dioxide both in the matrix and the fractures, in addition to calculating the deformation of the reservoir due to the change in pore pressure. The major findings of the study are summarized as follows:

- The injection pressure has a significant influence on the amount of carbon dioxide storage and the spread of carbon dioxide in the reservoir. The larger the injection pressure, the larger the pore pressure, and conversely the smaller the effective stresses. Exceeding the maximum allowable value of the injection pressure can lead to failure of the reservoir structure. The results of Mohr-Coulomb failure criterion showed that even at the highest injection pressure used in this study the reservoir remains in a stable condition.
- The maximum occupancy of the reservoir is a major factor for determining the period of carbon dioxide injection. For the selected simulation and injection parameters during the selected injection period, the occupancy analysis was performed for the reservoir considering the formation volume factor at the depth of the reservoir. The analysis showed that the occupancy was 0.41 %, which is less than the allowable 3 % for the current reservoir conditions. The maximum occupancy analysis showed that the current carbon dioxide injection scenario is at the safe side of the maximum occupancy limit.

- The permeability of the reservoir is highly dependent on the change in the pore pressure. Moreover, the final value of the permeability depends on the adsorption induced strains in the reservoir. The permeability simulation results showed a sharp increase in the permeability with time, followed by a slower rate of decrease due to the adsorption induced strains. The adsorption-induced strains tend to decrease the permeability when large injection periods are considered. The initial increase in the permeability is pressure induced, while the adsorption induced strains result in a decrease in the permeability at later stages. The carbon dioxide mobility of the reservoir in the current study is relatively higher when compared to other sedimentary reservoirs due to the presence of fractures and smaller adsorption induced strains.
- The volumetric strain due to carbon dioxide injection is provoked by the adsorption-induced swelling of the reservoir matrix and the decrease in the effective stresses resulting from the increase in the matrix pore pressure. An increase in the pressure causes an increase in the adsorption-induced swelling, thus boosting the rate of increase of the volumetric strains in the reservoir matrix.
- The sensitivity of the model output to the input parameters has been evaluated by calculating the normalized sensitivity coefficients of the model parameters. The sensitivity analysis revealed that the calculated values of the pore pressure during carbon dioxide injection are highly sensitive to the initial reservoir permeability, initial reservoir porosity and poroelastic coefficient for the reservoir. Yet, the model predictions are shown to be reliable for the sensitivity measure of $\pm 10\%$ of the input parameters' base-values.

Geomechanical modeling of Ghawar reservoir with two-phase flow

In this portion of the study the two-phase fully coupled geomechanical analysis is performed using CMG-GEM software to evaluate the safe CO2 injection parameters for the selected sequestration site. The major findings of the study are summarized as follows:

- The injection of carbon dioxide causes an increase in the reservoir pore pressure however, adding a production well to the carbon dioxide injection and sequestration process will tends to decrease the overall pore pressure. The carbon dioxide saturation plots show that with production well in the system the potential of carbon dioxide flow is high through the reservoir. The magnitude of pore pressure after carbon dioxide injection is high for injection process with only injection well and no production well. When carbon dioxide injection and water production were carried out simultaneously for five years, the net effect was that the maximum value of the pore pressures was reduced but due to the production process, pressure depletion occurred near the production well.
- During the case of single injection well the pore pressure increases continuously to a maximum value till the end of injection period. During the case of simultaneous injection and production process the pore pressure increases continuously but the maximum value is less than that of the case of single injection well. During the case when carbon dioxide injection and water production was carried out in series, the output pressure response shows an increase in the pore pressure during the first 3 years of carbon dioxide injection, followed by a pressure reduction during the 3 years of water production, and at

the end again an increase in the pressure during the last 2 years of carbon dioxide injection. At the end of the process the final value of the pore pressure is minimum compared to the other injection scenarios.

- For the case of only injection well in the system, the ground vertical displacement is the maximum. Adding the production well to the reservoir helps in reducing the magnitude of ground vertical displacement. During the simultaneous carbon dioxide injection and water production process although the maximum value of the ground vertical uplift was reduced but the ground surface above the production well has a high value of subsidence due to the pore pressure reduction in the vicinity of the production well. When water production process was performed after the initial carbon dioxide injection the value of ground subsidence above the production well and the vertical ground displacement above the injection well was reduced.
- After five years of carbon dioxide injection the final stressed condition of the reservoir for the cases of single injection well and combined injection and production wells shows that even for high values of pressure buildup during the case of only injection well in the system, the reservoir is still on safe side for five years of carbon dioxide injection.

6.1.3 Geomechanical modeling for Ghawar carbonate reservoir undergoing carbon dioxide injection with multiple injection wells

In this portion of the study, the number of carbon dioxide injection wells is varied along with the distance between the injection wells. COMSOL Multi-physics finite element

software is utilized for the numerical modeling of different carbon dioxide injection scenarios. The major findings of the study are summarized as follows:

- The new methodology developed and discussed in this study will help in identifying proper number and placement of carbon dioxide injection wells that will help in increasing the reservoir storage capacity and stability. Increasing the number of injection wells causes an increase in the pore pressure, which significantly decreases the effective stresses at the reservoir and drives the reservoir to move towards the failure line. Arranging injection wells in various patterns also effect the pore pressure and hence the stability of the reservoir. For multiple injection wells, if the injection wells are closer to each other, the pore pressure will significantly increase during carbon dioxide injection. The failure envelope shows that increasing the number of injection wells and placing the injection wells closer to one another can lead to the failure of the reservoir. For the various injection scenarios discussed in this study, the reservoir remained at the safe stable condition. The four-injection well scenarios were closer to the failure line as compared to the other injection scenarios.
- The ground surface vertical uplift was evaluated during the injection period of carbon dioxide for the different arrangements of injection wells. For the naturally fractured reservoir considered in this study, the maximum ground vertical uplift was up to 17.1 mm for one injection well, 25.1 mm for two injection wells, 28.2 mm for three injection wells, and 30.2 mm for four injection wells for the five-year injection period. The ground vertical uplift was noted to increase significantly with increasing the number of injection wells. Although injecting

carbon dioxide through four injection wells did not exceed the maximum occupancy limit of the reservoir, it caused a significant reduction in the effective stresses. Consequently, the reservoir was driven towards the failure line, in addition to resulting in higher values of ground vertical uplift that extended several kilometers surrounding the injection wells.

- One of the key factors for deciding the optimum number of injection wells and the optimum wells arrangement is the accumulation of carbon dioxide during injection. It was observed that for three injection wells when the injection wells are placed in a non-symmetric central arrangement, carbon dioxide accumulation takes place that causes significant ground uplift above the accumulation region. It was noted that the accumulation can also occur when the injection wells are placed nearer to the closed boundary surfaces of the reservoir. The results from the numerical investigation methodology suggest that the injection wells should not be placed very near to each other and to the boundaries of the reservoir.
- Among the various arrangements of injection wells used for carbon dioxide injection in this study, the numerical methodology suggests the best possible arrangement. For maximum reservoir stability, maximum reservoir storage capacity and low values of the vertical ground uplift, it is recommended to use two injection wells placed at optimum distance with less pore pressure buildup. With three and four injection wells, the storage capacity will be more but comparatively less reservoir stability and high values of ground vertical uplift.
- The numerical investigation in this study focuses on developing a methodology for increasing the reservoir storage capacity and stability. The methodology

suggests the existence of an optimum injection well arrangement, at which the reservoir has the maximum accumulation of the injected carbon dioxide, while maintaining the best stability margin for the same given conditions of injection pressure and injection period. This finding opens the door for a challenging analytical investigation to find the optimum case of injection well arrangement for a given reservoir at specified injection conditions, as a future extension to this study.

6.2 Recommendations

The main objective of the current study was to perform geomechanical modeling of the single-porosity and naturally fractured reservoirs in order to facilitate safe carbon dioxide sequestration process in geological reservoir at Saudi Arabia. The following are the recommendations for future utilization and extension of the current investigation:

- The injection of carbon dioxide at high injection pressures may induce local seismicity events. If the reservoir contains conductive fractures or critically stressed faults, the injection of carbon dioxide can cause sliding of the geological layers and hence can cause local seismicity events. One of the potential extensions of the developed model is to account for normal stresses on the faults in order to avoid these seismicity events during carbon dioxide injection.
- In order to optimize of the carbon dioxide sequestration process, the numerical scheme can be extended to model the enhanced oil recovery (EOR) during the carbon dioxide sequestration process. Accordingly, the cost of the carbon dioxide sequestration can be partially recovered by the EOR.

- The developed model has been established for the carbon dioxide injection period. The model can be extended to include the post-injection geochemical modeling in order to study the interaction between the stored carbon dioxide and the reservoir's formation.

REFERENCES

[1] J. Gibbins and H. Chalmers, "Carbon capture and storage," *Energy Policy*, vol. 36, pp. 4317–4322, 2008.

[2] A. Witkowski, M. Majkut, and S. Rulik, "Analysis of pipeline transportation systems for carbon dioxide sequestration," *Arch. Thermodyn.*, vol. 35, pp. 117–140, 2014.

[3] B. Ashkan et al., "Simulation study of CO_2 sequestration potential of the Mary Lee coal zone, Black Warrior basin. *Environmental Earth Sciences*, vol. 70, pp. 2501–2509, 2013.

[4] S. P. Sung et al., "Numerical modeling of the tensile fracture reactivation under the effects of rockgeomechanical properties and heterogeneity during CO_2 storage." *Environmental Earth Sciences*, vol. 75, pp. 298-303, 2016.

[5] H. Zhangshuan et al. "Evaluating the impact of caprock and reservoir properties on potential risk of CO_2 leakage after injection. *Environmental Earth Sciences*, vol. 66, pp. 2403–2415, 2012.

[6] D. C. Thomas, and S. M. Benson, editors., "Carbon Dioxide Capture for Storage in Deep Geologic Formations-Results from the CO_2 Capture Project: Vol 2-Geologic Storage of Carbon Dioxide with Monitoring and Verification." *Elsevier*, 2015.

[7] H. J. Herzog, "Scaling up carbon dioxide capture and storage: From megatons to gigatons. *Energy Economics*, vol. 33(4), pp.597-604, 2011.

[8] B. Metz, editor. "Carbon dioxide capture and storage: special report of the intergovernmental panel on climate change." *Cambridge University Press*; 2005 Dec 19.

[9] K. A. Mumford, Y. Wu, K. H. Smith, and G. W. Stevens, "Review of solvent based carbon-dioxide capture technologies." *Frontiers of Chemical Science and Engineering*, vol. 9(2), pp.125-141, 2015.

[10] E. S. Fernandez, "Novel process designs to improve the efficiency of postcombustion carbon dioxide capture." *TU Delft, Delft University of Technology*; 2013.

[11] E. S. Fernandez, K. Heffernan, H. Ham, M. J. Linders, D. W. F. Brilman, E. L. Goetheer, and T. J. Vlugt, "Analysis of process configurations for CO_2 capture by

precipitating amino acid solvents." *Industrial & Engineering Chemistry Research*, vol. 53(6), pp.2348-2361, 2014.

[12] S. Hanson, editor, "Guidelines for carbon dioxide capture, transport and storage," *World Resources Institute, Washington, DC (United States)*, 2008.

[13] S. Holloway, A. Karimjee, M. Akai, R. Pipatti, and K. Rypdal, "Guidelines for National Greenhouse Gas Inventories," *Energy*, Vol. 2, 2006.

[14] D. A. Barnes, D. H. Bacon, and S. R. Kelley, "Geological sequestration of carbon dioxide in the Cambrian Mount Simon Sandstone: Regional storage capacity, site characterization, and large-scale injection feasibility, Michigan Basin. Environmental Geosciences, vol. 16(3), pp.163-183, 2009.

[15] O. Bogda, "Some Geomechanical Aspects of Geological CO_2 Sequestration." *KSCE Journal of Civil Engineering*, Vol. 13(4), pp. 225-232, 2009.

[16] A. Mazzoldi, A. P. Rinaldi, A. Borgia, and J. Rutqvist, "Induced seismicity within geological carbon sequestration projects: maximum earthquake magnitude and leakage potential from undetected faults." *Int. J. Greenhouse Gas Contr*., vol. 10, pp. 434–442, 2012.

[17] A. P. Rinaldi, J. Rutqvist, and F. Cappa, "Geomechanical effects on CO_2 leakage through fault zones during large-scale underground injection. *Int. J. of Greenhouse Gas Control*, vol. 20, pp. 117–131, 2013.

[18] J. Kaldi, and C. G. Poole, "Storage capacity estimation, site selection and characterization for CO_2 storage projects." *Report No: RPT08-1001*, CO_2 CRC, Canberra, ACT.

[19] R. L. Folk, P. B. Andrews, and D. W. Lewis, "Detrital sedimentary rock classification and nomenclature for use in New Zealand," New Zeal. J. Geol. Geophys., vol. 13, pp. 937–968, 1970.

[20] E. M. Winter and P. D. Bergman, "Availability of Depleted Oil and Gas Reservoirs for Disposal of Carbon Dioxide in the United States," *Energy Conversion & Management*, vol. 34, pp. 1177-1187, 1993.

[21] P. Bergman, E. M. Winter, and Z. Y. Chen, "Disposal of power plant CO_2 in depleted oil and gas reservoirs in Texas. *Energy Conver. Mgmt*., vol. 38, pp. 211-216, 1997.

[22] Z. Li, M. Dong, S. Li, and S. Huang, "CO_2 sequestration in depleted oil and gas reservoirs—caprock characterization and storage capacity," *Energy Conversion and Management*, vol. 47(11), pp. 1372-1382, 2006.

[23] M. S. Perera, P. G. Ranjith, D. W. Airey, and S. K. Choi, "Sub- and supercritical carbon dioxide flow behavior in naturally fractured black coal: An experimental study," *Fuel*, vol. 90, pp. 3390–3397, 2011.

[24] S. Reeves, "Geological sequestration of CO_2 in deep, unmineable coal beds: An integrated research and commercial-scale field demonstration project", *SPE 71749: Presented at SPE Annual Technical Conference and Exhibition*, New Orleans, Louisiana, 2001.

[25] S. H. Stevens, V. A. Kuskraa, J. J. Gale and D. Beecy, "CO_2 injection and sequestration in depleted oil and gas fields and deep coal seams: Worldwide potential and costs", AAPG Bulletin, vol. 84, pp. 1497–1498, 2000.

[26] H. Xu, et al., "Bioherm petroleum reservoir types and features in main sedimentary basins of the South China Sea," *Journal of Earth Science*, vol. 23(6), pp. 828–841, 2012.

[27] J. E. Streit and A. F. Siggins, "Predicting, monitoring and controlling geomechanical effects of CO_2 injection," *Greenh. Gas Control Technol.*, vol. 2, pp. 643–651, 2005.

[28] I. Arshad, and S. Antonin, "Injection Modeling and Shear Failure Predictions in Tight Gas Sands — A Coupled Geomechanical Simulation Approach," *Effective and Sustainable Hydraulic Fracturing*, DOI: 10.5772/56312, 2013.

[29] L. Ji, A. T. Settari, R. B. Sullivan, and D. Orr, "Methods For Modeling Dynamic Fractures InCoupled Reservoir And Geomechanics Simulation," *Society of Petroleum Engineers*, doi:10.2118/90874-MS, 2004.

[30] J. E. Streit and R. R. Hillis, "Estimating fault stability and sustainable fluid pressures for underground storage of CO_2 in porous rock," *Energy*, vol. 29, pp. 1445–1456, 2004.

[31] C. M. Gibson-Poole, R. S. Root, S. C. Lang, J. E. Streit, A. L. Hennig, C. J. Otto, & J. R. Underschultz, "Conducting comprehensive analyses of potential sites for geological CO_2 storage," *Greenhouse Gas Control Technologies*, vol. 1, pp. 673–681, 2005.

[32] J. G. Berryman, “Effective stress for transport properties of inhomogeneous porous rock,” *J. Geophys. Res.*, vol. 97, p. 17409-17424, 1992.

[33] J. B. Altmann, “Poroelastic effects in reservoir modeling,” (Doctoral Dissertation).Universität Karlsruhe. Retrieved from http: //digbib.ubka.uni - karlsruhe.de /volltexte /documents/1553630, 2010.

[34] A. F. Siggins, “Saturation, pore pressure and effective stress from sandstone acoustic properties,” *Geophys. Res. Lett.*, vol. 30, pp. 10–13, 2003.

[35] F. Santarelli and J. Tronvoll, “Reservoir stress path: the depletion and the rebound,” *SPE/ISRM 47350 proc. EUROCK ’98 Norway*, pp. 1–7, 8-10 July 1998.

[36] M. H. H. Hettema and C. J. de Peter, “The Poromechanical behaviour of Felser sandstone: Stress- and Temperature-Dependent,” *Proc. SPE/ISRM 47270 proc. EUROCK ’98 Norway*, 1-9, 8-10 July 1998.

[37] L. W. Teufel, D. W. Rhett, and H. E. Farrell, “Effect of reservoir depletion and pore pressure drawdown on in situ stress and deformation in the Ekofisk field, north sea,” *32nd U.S. Symp. Rock Mech.*, pp. 63–72, 1991.

[38] J. B. Altmann, T. M. Müller, B. I. R. Müller, M. R. P. Tingay, and O. Heidbach, “Poroelastic contribution to the reservoir stress path,” *Int. J. Rock Mech. Min. Sci.*, vol. 47, pp. 1104–1113, 2010.

[39] J. P. Johnson, D. W. Rhett, and W. T. Siemers, “Rock mechanics of the Ekofisk reservoir in the evaluation of subsidence,” *J. Pet. Technol.*, vol. 41, pp. 1-12, 1989.

[40] P. Segall, “Earthquakes triggered by fluid extraction,” *Geology*, vol. 17, pp. 942 – 946, 1989.

[41] A. Yudovich, L. Y. Chin, and D. R. Morgan, “Casing deformation in Ekofisk,” *J. Pet. Technol.*, vol. 41, pp. 729–734, 1989.

[42] J. Rutqvist, D. W. Vasco, and L. Myer, “Coupled reservoir-geomechanical analysis of CO_2 injection and ground deformations at In Salah, Algeria,” *Int. J. Greenh. Gas Control*, vol. 4, no. 2, pp. 225–230, 2010.

[43] R. M. Bustin, and C. R. Clarkson, “Geological controls on coal bed methane reservoir capacity and gas content”. *Int. J. Coal Geol*., vol. 38, pp. 3-26, 1998.

[44] J. W. Larsen, "The effects of dissolved CO_2 on coal structure and properties". *Int. J. Coal Geol.* vol. 57, pp. 63-70, 2004.

[45] T. Engelder, and M. P. Fischer, "Influence of poroelastic behavior on the magnitude of minimum horizontal stress, Sh, in over pressured parts of sedimentary basins", *Geology*. vol. 22, pp. 949–952, 1994.

[46] F. Cappa, and J. Rutqvist, "Modeling of coupled deformation and Permeability evolution during fault reactivation induced by deep underground injection of CO_2," *International Journal of Greenhouse Gas Control*, vol. 5, pp. 336–346, 2011.

[47] J. Rutqvist, Y. S. Wu, C. F. Tsang, G. Bodvarsson, "A modeling approach for analysis of coupled multiphase fluidflow, heat transfer, and deformation in fractured porous rock. *International Journal of Rock Mechanics and Mining Sciences*. vol. 39, pp. 429–442, 2002.

[48] Z. Zhang, and R. Agarwal, "Numerical simulation and optimization of CO_2 sequestration in saline aquifers," *Computers & Fluids*, vol. 80, pp.79-87, 2013.

[49] D. X. Yang, R. S. Zeng, Y. Zhang, Z. Q. Wang, S. Wang, and C. Jin, "Numerical simulation of multiphase flows of CO_2 storage in saline aquifers in Daqingzijing oilfield, China," *Clean Technologies and Environmental Policy*, vol. 14(4), pp.609-618, 2012.

[50] K. Pruess, and N. Muller, "Formation dryout from CO_2 injection into saline aquifers: 1. Effects of solids precipitation and their mitigation," *Water Resources Research*, vol. 45(3), 2009.

[51] S. Vidal-Gilbert, J. F. Nauroy, and E. Brosse, "3D geomechanical modelling for CO_2 geologic storage in the Dogger carbonates of the Paris Basin," *Int. J. Greenh. Gas Control*, vol. 3, pp. 288–299, 2009.

[52] R. Masoudi, M. A. A. Jalil, D. Press, K.-H. Lee, C. P. Tan, L. Anis, N. Darman, and M. Othman, "An Integrated Reservoir Simulation-Geomechanical Study on Feasibility of CO_2 Storage in M4 Carbonate Reservoir, Malaysia," *Int. Pet. Technol. Conf. 7-9 Febr. 2012, Bangkok, Thail.*, 2011.

[53] L. André, P. Audigane, M. Azaroual, and a. Menjoz, "Numerical modeling of fluid-rock chemical interactions at the supercritical CO2-liquid interface during CO_2 injection into a carbonate reservoir, the Dogger aquifer (Paris Basin, France)," *Energy Convers. Manag.*, vol. 48, pp. 1782–1797, 2007.

[54] F. Cappa, Y. Guglielmi, P. Fénart, V. Merrien, and A. Thoraval, "Hydromechanical interactions in a fractured carbonate reservoir inferred from hydraulic and mechanical measurements," *Int. J. Rock Mech. Min. Sci.*, vol. 42, pp. 287–306, 2005.

[55] L. S. K. Fung, U. Middya, A. H. Dogru, and S. Aramco, "SPE 142296 Numerical Simulation of Fractured Carbonate Reservoirs with the M_1 Bimodal Pore System," pp. 1–13, 2011.

[56] A. N. Beni, M. Kühn, R. Meyer, and C. Clauser, "Numerical Modeling of a Potential Geological CO_2 Sequestration Site at Minden (Germany)," *Environ. Model. Assess.*, vol. 17, pp. 337–351, 2012.

[57] C. Coelho, A. C. Soares, and N. F. F. Ebecken, "Modelling mechanical behaviour of limestone under reservoir conditions," *Int. J. Numer. Anal. Methods Geomech.*, no. August, pp. 1477–1500, 2006.

[58] D. Grgic, "Influence of CO_2 on the long-term chemomechanical behavior of an oolitic limestone," *J. Geophys. Res. Solid Earth*, vol. 116, no. July, pp. 1–22, 2011.

[59] M. S. A. Perera et al., "Effects of Seam Conditions, Injection Pressure and Gas Composition on CO_2 Sequestration in Coal" *ASCE Geotechnical Special Publication no. 217*, pp. 2–7, 2011.

[60] J. E. Warren and P. J. Root "The Behavior of Naturally Fractured Reservoirs. *Soc. Pet. Eng. J*, vol. 3, 245-255, 1963.

[61] J. A. Hudson, E. Liu and S. Crampin, "The mechanical properties of materials withinterconnected cracks and Pores" *Geophys. J. Int*, vol. 124, pp. 105-112, 1996.

[62] M. A. Abdulkader, "Ghawar: The Anatomy of the World's Largest Oil Field," *Saudi Aramco Search and Discovery Article#20026*, 2005.

[63] M. Godec, G. Koperna, R. Petrusak, and A. Oudinot, "Assessment of Factors Influencing CO_2 Storage Capacity and Injectivity in Eastern U.S." *Gas Shale Energy Proceeding*, vol. 37, pp. 6644– 6655, 2013.

[64] C. Guo, M. Wei, H. Chen, H. Xiaoming, and B. Bai, "Improved Numerical Simulation for Shale Gas Reservoirs," *Paper OTC-24913 presented at Offshore Technology Conference, Kuala Lumpur, Malaysia*. pp. 1-17, 2014.

[65] E. Susan, A. Minkoff, S. Mike, B. Steve, P. Malgorzata, and F. Mary, "Coupled fluid flow and geomechanical deformation modeling." *Journal of Petroleum Science and Engineering*. vol. 38, pp. 37-56, 2013.

[66] B. Kvamme, and S. Liu, "Reactive transport of CO_2 in saline aquifers with implicit geomechanical analysis," *Energy Procedia*, vol. 1(1), pp. 3267-3274, 2009.

[67] E. Holzbecher, "Poroelasticity Benchmarking for FEM on Analytical Solutions." *Excerpt from the Proceedings of the COMSOL Conference Rotterdam*, pp. 1-7, 2013.

[68] J. Rutqvist, J. T. Birkholzer, F. Cappa, and C. Tsang, "Estimating maximum sustainable injection pressure during geological sequestration of CO_2 using coupled fluid flow and geomechanical fault-slip analysis." *Energy Conversion and Management*. vol. 48, pp. 1798–1807, 2007.

[69] B. Tore, A. Eyvind, and S. Elin, "Safe Storage Parameters during CO_2 Injection Using Coupled Reservoir Geomechanical Analysis." *Excerpt from the Proceedings of the COMSOL Conference Milan*, pp. 1-7, 2009.

[70] A. A. Al-Shuhail, A. A. Alshuhail, and Y. A. Khulief, "CO_2 Leakage Detection using Geophysical Methods under Arid Near-surface Conditions": *Progress Report of KACST TIC-CCS Project number TIC-CCS-1*, pp. 1-47, 2014.

[71] H. H. Mohammed, R. S. Mohamed, and W. H. Abdullah, "Diagenetic characteristics and reservoir quality of the Lower Cretaceous Biyadh sandstones at Kharir oilfield in the western central Masila Basin, Yemen." *Journal of Asian Earth Sciences*, vol. 51, pp. 109-120, 2012.

[72] X. Tan, and K. Heinz, "Numerical study of variation in Biot's coefficient with respect to microstructure of rocks." *Tectono-physics*, vol. 61,pp. 159–171, 2014.

[73] A. Z. Martin, "Late Permian to Holocene Paleofacies Evolution of the Arabian Plate and its Hydrocarbon Occurrences." *Geo Arabia* , vol. 6, pp. 445-504, 2001.

[74] O. Heidbach, et al., "The World Stress Map based on the database release 2008", *equatorial scale 1:46,000,000, Commission for the Geological Map of the World, Paris, doi:10.1594/GFZ.WSM.Map*, 2009.

[75] B. Robert, et al. "Regional Depositional History, Stratigraphy and Palaeo geography of the Shu'aiba." *GeoArabia*, vol. 12, pp. 135-152, 2007.

[76] T. Buchmann, and P. Connolly, "Contemporary kinematics of the Upper Rhine Graben: A 3D finite element approach." *Global and Planetary Change*, vol. 58, pp. 287-309, 2007.

[77] A. Eckert, and A. Connolly, "Stress and fluid-flow interaction for the Geothermal Field derived from 3D numerical models." *GRC Transactions*. pp. 385–390, 2007.

[78] T. Hergert, and O. Heidbach, "Geomechanical model of the Marmara Sea region-II. 3-Dcontemporary Background stress field." *Geophys. J. Int*. vol. 185, pp. 1090–1120, 2011.

[79] J. Rudnicki, "Fluid mass sources and point forces in linear elastic diffusive solids," *Mechanics of Material*, vol. 5, pp. 383–393, 1986.

[80] A. Amirlatifi, "Coupled Geomechanical Reservoir Simulation". Dissertation, Missouri University of Science and Technology, Print, 2013.

[81] S. A. Haidary, H. A. Shehri, A. Abdulraheem, et al., "Wellbore stability analysis for trouble free drilling." *Presented at SPE Kuwait oil and gas show and conference, 11-14 October. SPE-175170-MS*, 2015.

[82] J. Byerlee, "Friction of rocks." *Pure and Applied Geophysics*, vol. 116, pp. 615–626, 1978.

[83] M. Paradeis, A. Eckert, and X. Liu, "Influences of Anticline Reservoir Geometry on Critical Pore Pressures Associated With CO_2 Sequestration." *46th U.S. Rock Mechanics Symposium, Chicago, Illinois. Chicago, IL*; pp. 201–319, 2012.

[84] E. S. Jtirgen, F. A. Siggins, and J. E. Brian, "Predicting and Monitoring Geomechanical effects of CO_2 injection." *Carbon Dioxide Capture for Storage in Deep Geologic Formations*, vol. 2, pp. 751-766, 2005.

[85] P. Papanastasiou, and M. Thiercelin, "Modeling Borehole Perforation Collapse with the Capability of Predicting the Scale Effect." *International journal of geomechanics*, 10.1061/(ASCE)GM.1943-5622.0000013, pp. 286-293, 2011.

[86] Z. H. Hassan, P. D. Mehran, A. M. Elsharkawy, W. K. David, and Y. Leonenko, "Predicting PVT data for CO_2–brine mixtures for black-oil Simulation of CO_2 geological storage." *International journal of Greenhouse gas control*, vol. 2, pp. 65–77, 2008.

[87] S. Bachu, "Comparison between Methodologies Recommended for Estimation of CO_2 Storage Capacity In Geological Media." *CSLF-T-2008-04*, pp. 1-21, 2008.

[88] J. Kaldi, C. G. Poole, "Storage capacity estimation, site selection and characterization for CO_2 storage projects." *Report No: RPT08-1001, CO_2 CRC, Canberra, ACT*, 2008.

[89] GEM Advanced Compositional Reservoir Simulator, Version 2012 User Guide. 2012. Calgary, Alberta: CM

[90] K. Anjani, and P. Varun, "The role of coupled geomechanical modeling in reservoir simulation Calgary, Alberta: CMG".

[91] J. S. Curnow, "Coupled geomechanics and fluid flow model for production optimization in naturally fractured shale reservoirs", 2007.

[92] H. Kazemi, C. R. Vestal, and D. G. Shank, "An efficient multi component numerical simulator," *Society of Petroleum Engineers Journal*, vol. 18(05), pp. 355-368, 1978.

[93] D. Tran, W. L. Buchanan, and L. X. Nghiem, "Improved gridding technique for coupling geomechanics to reservoir flow," *SPE Journal*, vol. 15(01), pp. 64-75, 2010.

[94] M. Sahimi, "Flow and transport in porous media and fractured rock: from classical methods to modern approaches," *John Wiley & Sons*, 2011.

[95] C. A. Barton, M. D. Zoback, and D. Moos, "Fluid flow along potentially active faults in crystalline rock," *Geology*, vol. 23(8), pp.683-686, 1995.

[96] Q. Tao, "Numerical modeling of fracture permeability change in naturally fractured reservoirs using a fully coupled displacement discontinuity method (Doctoral dissertation, Texas A&M University)", 2010.

[97] Z. Chen, G. Huan, and Y. Ma, "Computational methods for multiphase flows in porous media (Vol. 2). Siam, pp. 1-569, 2006.

[98] D. Tran, L. Nghiem, and L. Buchanan, "An overview of iterative coupling between geomechanical deformation and reservoir flow," *In SPE International Thermal Operations and Heavy Oil Symposium. Society of Petroleum Engineers*, 2005.

[99] G. T. Thomas Mase, G. E. Mase, "Continuum mechanics for engineers," 2nd edition.

[100] G. E. Mase, "Theory and problems of continuum mechanics, Schaum's outline series".

[101] N. S. Ottosen, and M. Ristinmaa, "The mechanics of constitutive modeling. Elsevier," 2005.

[102] W. F. Chen, & A. F. Saleeb, A.F., "Constitutive equations for engineering materials," *New York, Wiley*, 1982.

[103] Y. Wu, J. Liu, and D. Elsworth, "Dual poroelastic response of a coal seam to CO_2 injection," *Int. J. Green h. Gas Control*, vol. 4, pp. 668-678, 2010.

[104] M. S. Ameen, et al., "Predicting rock mechanical properties of carbonates from wireline logs (A case study: Arab-D reservoir, Ghawar field, Saudi Arabia). Mar Petrol", *Geology*, vol. 26, pp. 430-444, 2009.

[105] K. Eshiet, and Y. Sheng, "Investigation of geomechanical responses of reservoirs induced by CO_2 storage," *Environmental Earth Sciences*, vol. 71, pp. 3999–4020, 2014.

[106] M. Gameil, and S. Abdelbaset, "Gastropods from the Campanian Maastrichtian Aruma Formation, Central Saudi Arabia," *Journal of African Earth Sciences*, vol. 103, pp. 128-139, 2015.

[107] H. Robert, and Z. Mark, "Adsorption of methane and carbon dioxide on gas Shale and pure mineral samples" Journal of Unconventional Oil and Gas Resources, vol. 8, pp. 14–24, 2014.

[108] B. Bennion, and S. Bachu, "Relative permeability characteristics for supercritical CO_2 displacing water in a variety of potential sequestration zones," *In SPE Annual Technical Conference and Exhibition. Society of Petroleum Engineers*, 2005.

[109] D. B. Bennion, and Bachu, "Dependence on temperature, pressure, and salinity of the IFT and relative permeability displacement characteristics of CO_2 injected in deep saline aquifers," *In SPE Annual Technical Conference and Exhibition. Society of Petroleum Engineers*, 2006.

[110] H. B. Zhang, J. Liu, and D. Elsworth, "How sorption-induced matrix deformation affects gasflow in coal seams: a new FE model," *Int. J.Rock Mech. Mining Sci.*, vol. 45, pp. 1226-1236, 2008.

[111] X. Cui and R. M. Bustin, "Volumetric strain associated with methane desorption and its impact on coal bed gas production from deep coal seams," *AAPG Bull*, vol. 89, pp. 1181–1202, 2005.

[112] J. Liu, and D. Elsworth, "Evaluation of pore water pressure fluctuation around an advancing long wall panel," *Adv. Water Res*, vol. 22, pp. 633-644, 1999.

[113] E. C. Robertson and L. Richard L, "A permeability model for coal and other fractured sorptive-elastic media," *Paper SPE 104380, In: Proceedings of the SPE Eastern Regional Meeting, Ohio*, 2006.

[114] M. Masi, S. Fogliani, S. Carra, S, "Sensitivity analysis on indiumphosphide liquid encapsulated Czochralski growth," *Crystal Researchand Technology*, vol. 34, pp. 1157–1167, 1999.

[115] H. Jabbari, Z. Zeng, and N. A. Dakota, "Three-Parameter Dual-Porosity Model for Naturally Fractured Reservoirs," *SPE 144560*, vol. 20, pp. 7-11, 2011.

[116] Q. Zheng, and B. Yu, "A fractal permeability model for gas flow through dual-porosity media," *Journal of Applied Physics*, vol. 111(2), pp. 1-7, 2012.

[117] D. Jim and A. Todd, "Dual-Porosity Models for Flow in Naturally Fractured Reservoirs," *Academic Press, London*, pp. 177-221, 1990.

[118] B. Gong, "Effective models of fractured systems," *Dissertation, Stanford University*, 2007.

[119] Advanced Compositional and GHG Reservoir Simulator. User's Guide, Computer Modeling Group Ltd, 2010.

[120] M. Gutierrex, andR. W. Lewis, "The role of geomechanics in reservoir simulation," *In SPE/ISRM 47392 Rock Mechanics in Petroleum Engineering 1998 Jan 1*. Society of Petroleum Engineers.

[121] T. Qingfeng, "Numerical Modeling of Fracture Permeability Change in Naturally Fractured Reservoirs Using a Fully Coupled Displacement Discontinuity Method," *Dissertation China University of Geosciences*, 2010.

[122] S. C. Jennifer, “Coupled geomechanics and fluid flow model for production optimization in naturally fractured shale reservoirs,” *Dissertation,Colorado School of Mines*, 2015.

[123] J. R. Gilman, “An efficient finite-difference method for simulating phase segregation in the matrix blocks in double-porosity reservoirs,” *SPE Reservoir Engineering*, vol. 1, pp. 403-413, 1986.

[124] B. Sally, and C. Peter, “Underground geological storage,” Cambridge University press, New York, 2005.

VITA

Name:	SIKANDAR KHAN
Place of Birth:	Mardan, Pakistan
Nationality:	Pakistani
Permanent Address:	District and Tehsile Mardan Post Office Garhi Garhi kapura, village Garhi ismail zai, KPK, Pakistan
Telephone:	+92-3326515086, +966-592135663
Email Address:	sikandarkhan@kfupm.edu.sa
Education Qualification:	MSc (Mechanical Engineering) January, 2013 Department of Mechanical Engineering University of Engineering and Technology, Peshawar, Pakistan BSc (Mechanical Engineering) August, 2009 Department of Mechanical Engineering University of Engineering and Technology, Peshawar, Pakistan

Publications:

1. Sikandar Khan, A.A Al-Shuhail, Y.A. Khulief. "Numerical modeling of the geomechanical behavior of Ghawar Arab-D carbonate petroleum reservoir undergoing CO_2 injection" *Journal of Environmental Earth Sciences*, (2016) 75:1499, DOI 10.1007/s12665-016-6122-3, (**Published**)

2. Sikandar Khan, Y.A. Khulief, A.A Al-Shuhail "The effect of injection well arrangement on CO_2 injection into carbonate petroleum reservoir: A case study from Saudi Arabia", *International Journal of Global Warming*, (**Accepted**)

3. Sikandar Khan, Y.A. Khulief, A.A Al-Shuhail "Numerical modeling of the geomechanical behavior of Biyadh reservoir undergoing CO_2 injection", *International Journal of Geomechanics*, (**Accepted**)